

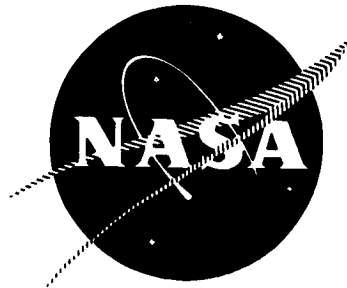
FACILITY FORM 802

N 68-23432	(THRU)
(ACCESSION NUMBER)	1
266	(CODE)
(PAGES)	28
CR-72303	(CATEGORY)
(NASA CR OR TMX OR AD NUMBER)	

NASA CR-72303

R-7199

33



## TWO-STAGE BIPROPELLANT INJECTION SYSTEM STUDIES

GPO PRICE \$ \_\_\_\_\_

by

CFSTI PRICE(S) \$ \_\_\_\_\_

P. F. Mehegan

Hard copy (HC) 3.00

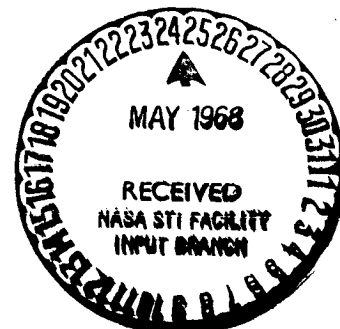
Microfiche (MF) .65

ff 653 July 65

prepared for

NATIONAL AERONAUTICS AND SPACE ADMINISTRATION

CONTRACT NAS3-7962



**ROCKETDYNE**

A DIVISION OF NORTH AMERICAN AVIATION, INC.  
6633 CANOGA AVENUE, CANOGA PARK, CALIFORNIA

#### NOTICE

This report was prepared as an account of Government sponsored work. Neither the United States, nor the National Aeronautics and Space Administration (NASA), nor any person acting on behalf of NASA:

- A.) Makes any warranty or representation, expressed or implied, with respect to the accuracy, completeness, or usefulness of the information contained in this report, or that the use of any information, apparatus, method, or process disclosed in this report may not infringe privately owned rights; or
- B.) Assumes any liabilities with respect to the use of, or for damages resulting from the use of any information, apparatus, method or process disclosed in this report.

As used above, "person acting on behalf of NASA" includes any employee or contractor of NASA, or employee of such contractor, to the extent that such employee or contractor of NASA, or employee of such contractor prepares, disseminates, or provides access to, any information pursuant to his employment or contract with NASA, or his employment with such contractor.

Requests for copies of this report should be referred to

National Aeronautics and Space Administration  
Office of Scientific and Technical Information  
Attention: AFSS-A  
Washington, D.C. 20546

NASA CR-72303  
R-7199

FINAL REPORT

TWO-STAGE BIPROPELLANT INJECTION SYSTEM STUDIES

by

P. F. Mehegan

prepared for

NATIONAL AERONAUTICS AND SPACE ADMINISTRATION

30 August 1967

CONTRACT NAS3-7962

Technical Management  
NASA Lewis Research Center  
Cleveland, Ohio  
Liquid Rocket Technology Branch  
T. Male

ROCKETDYNE  
A Division of North American Aviation, Inc.  
Canoga Park, California

PRECEDING PAGE BLANK NOT FILMED.

#### FOREWORD

This is the final report documenting a 1-year program to investigate large-thrust-per-element injector concepts employing the two-stage injection principle. The program was conducted under NASA Contract NAS3-7962 and was instituted by the National Aeronautics and Space Administration, Lewis Research Center under the direction of T. Male, Technical Program Manager. This report was prepared under G.O. 08864 in compliance with Paragraph C of Exhibit B, Contract NAS3-7962.

#### ACKNOWLEDGMENTS

The author gratefully acknowledges the valuable technical, literary and management contributions of the following people: W. Anderson and H. Burge for their overall program direction; J. Watkins, E. Appling, and R. Sorensen for their hardware design contributions; E. Eberle, D. Campbell, and P. Combs for the performance analysis contributions; G. Haroldsen, F. Hoehn, and S. Clapp for their part in the cold-flow studies; R. Cook, the CTL-3 test personnel, and, in particular, J. Button and W. Ingle for their support in conducting the hot-firing test program.

## ABSTRACT

The Two-Stage Bipropellant Injection System Program was initiated to investigate hot-gas injection in combination with large-thrust-per-element injector concepts. Analyses and cold-flow experiments were used to guide the selection of injector concepts to be evaluated during hot-firing tests. Twenty hot-firing tests were conducted to evaluate the performance and stability of four different injectors. The test results proved feasibility of the principle and also demonstrated that stable operation and high combustion efficiencies of at least 97.5 percent were possible with a single-element 20,000-pound-thrust injector.

## CONTENTS

	Page No.
Foreword . . . . .	iii
Acknowledgments . . . . .	iii
Abstract . . . . .	iv
Introduction . . . . .	1
Summary . . . . .	3
Conclusions and Recommendations . . . . .	13
Two-Stage Injection . . . . .	13
Performance . . . . .	13
Stability . . . . .	14
Design Feasibility . . . . .	14
General Approach . . . . .	17
<u>Task I</u>	
Analysis . . . . .	21
Concept Selection . . . . .	21
Design Analysis . . . . .	27
Performance Analysis . . . . .	47
Injector Rating and Selection . . . . .	71
<u>Task II</u>	--
Cold-Flow Studies . . . . .	77
Cold-Flow Apparatus . . . . .	79
Cold-Flow Simulation . . . . .	99
Test Results and Discussion . . . . .	110
Summary of Cold-Flow Results . . . . .	142
<u>Task III</u>	
Hot-Fire Testing . . . . .	145
Test Hardware . . . . .	147
Test Facility . . . . .	167
Test Procedures . . . . .	173
Test Results . . . . .	192

	Page No.
Discussion of Test Results . . . . .	214
References . . . . .	225
Nomenclature . . . . .	227
<u>Appendix A</u>	
Tricentric Injector Atomization Analyses . . . . .	A-1
LOX Central Core . . . . .	A-1
LOX Annulus . . . . .	A-4
Discussion . . . . .	A-8
<u>Appendix B</u>	
Cold Flow Sampling Probe Results . . . . .	B-1
<u>Appendix C</u>	
Heat Transfer Operating Conditions, Properties, and Design	C-2
Equations for Hardware Design . . . . .	C-1
Low-Mixture-Ratio Gases to Injector . . . . .	C-1
Properties for Copper . . . . .	C-1
Nominal Chamber Conditions Used for Thermal Design . . . . .	C-1
Equations . . . . .	C-2
<u>Appendix D</u>	
Report Distribution List For Contract No. NAS3-7962 . . . . .	D-1

## ILLUSTRATIONS

Fig. No.	Page No.
1. Summary of Major Program Tasks . . . . .	19
2. Summary of Task I Analysis Effort . . . . .	22
3. Candidate Commercial Nozzles Selected for Preliminary Water-Flow Tests . . . . .	36
4. 1000K Injector Concept Using Configuration 1A Elements (20K Thrust per Element) . . . . .	40
5. Analytical Spray Characteristics of Configuration 2A Element (20K Thrust) . . . . .	44
6. Analytical Spray Characteristics of Configuration 2C Element (20K Thrust) . . . . .	45
7. Comparison of Analytical and Actual Spray Vectors . . . . .	46
8. Front View of 20K Tricentric Injector Configuration 1A . . . . .	81
9. Side View of 20K Tricentric Injector Configuration 1A . . . . .	82
10. Tricentric Injector Exit Configurations . . . . .	83
11. 20K Tricentric Injector Configuration 1A With Three 1-Inch Plugs Installed in Water Annulus . . . . .	84
12. 20K Tricentric Injector Configuration 1A With Six 1/4-Inch Plugs Installed in Water Annulus and Recessed 1/4-Inch From Injector Face . . . . .	85
13. 20K Biplanar Impingement Injector Configuration 2A . . . . .	87
14. 20K Biplanar Impingement Injector Configuration 2C . . . . .	88
15. 20K Impinging Coaxial Injector Configuration 9A With no Cylindrical Portion on Cup . . . . .	90
16. 20K Commercial Nozzle Injector Configuration 11A . . . . .	91
17. Cold-Flow Test System With Tricentric Injector Configuration 1A in Position for Liquid Mass Distribution Test . . . . .	93
18. Cold-Flow Test System Schematic . . . . .	94

Fig. No.	Page No.
19. Simple Impinging Doublet Injector Model Used to Produce a Reference Spray Field Characterized by 200-Micron Mean Droplet Size . . . . .	96
20. Liquid Mass Distribution Collection Apparatus . . . . .	98
21. Spray Field Characteristics of Standard Doublet Injector . . . . .	111
22. Spray Field Characteristics of 20K Tricentric Injector Configuration 1A With Outside Tube Extended 1-1/2 Inches . . .	115
23. Liquid Mass Distribution of 20K Tricentric Injector Configuration 1A . . . . .	116
24. Spray Field Pattern of 5K Tricentric Injector Configuration 1A With Three Exit Nozzle Configurations . . . . .	118
25. Spray Fields of 5K and 20K Tricentric Injector Configura- tions 1A Modified With Three Plugs in the Water Annulus . . .	120
26. Liquid Mass Distribution Modified 20K Injector Configuration 1A . . . . .	121
27. Fan-Edge View of Spray From 20K Biplanar Impingement Injector Configuration 2A . . . . .	123
28. Liquid Mass Distribution of 20K Biplanar Impingement Injector Configuration 2A With Water Only Flowing . . . . .	124
29. Liquid Mass Distribution for 20K Biplanar Impingement Injector Configuration 2A With Water and Nitrogen Flowing . . . . .	125
30. Liquid Mass Distribution for 20K Biplanar Impingement Injector Configuration 2A With All Simulants Flowing . . . . .	126
31. Liquid Mass Distribution of 5K Injector Configuration 2A With All Simulants Flowing . . . . .	128
32. Fan-Edge View of Spray From 20K Biplanar Impingement Injector Configuration 2C . . . . .	129
33. Liquid Mass Distribution of 20K Biplanar Impingement Injector Configuration 2C With All Simulants Flowing . . . . .	131

Fig. No.	Page No.
34. Spray Field Characteristics of 20K Impinging Coaxial Injector Configuration 9A With Recessed Cup . . . . .	132
35. Liquid Mass Distribution of 20K Impinging Coaxial Injector Configuration 9A . . . . .	133
36. Spray Field Characteristics of Modified 20K Impinging Coaxial Injector Configuration 9A . . . . .	135
37. Liquid Mass Distribution of Modified 20K Impinging Coaxial Injector Configuration 9A . . . . .	136
38. Spray Field Characteristics of 20K Commercial Nozzle Injector Configuration 11A With Normal Water Flowrate . . . .	137
39. Liquid Mass Distribution of 20K Commercial Nozzle Injector Configuration 11A With Normal Water Flowrate . . . .	139
40. Spray Field Characteristics of 20K Commercial Nozzle Injector Configuration 11A at Twofold Increase in Water Flowrate . . . . .	140
41. Liquid Mass Distribution of 20K Commercial Nozzle Injector Configuration 11A at Twofold Increase in Water Flowrate . . . . .	141
42. 20K Tricentric Injector Configuration 1A Mounted in Thrust Chamber . . . . .	149
43. Front View of 5K Tricentric Injector Configuration 1A . . . .	151
44. Rear View of 5K Tricentric Injector Configuration 1A . . . .	152
45. Front View of 20K Impinging Coaxial Injector Configura- tion 9A . . . . .	154
46. Rear View of 20K Impinging Coaxial Injector Configura- tion 9A . . . . .	155
47. Front View of 5K Impinging Coaxial Injector Configuration 9A . . . . .	157
48. Isometric View of Workhorse Thrust Chamber Used for Hot-Firing Tests . . . . .	159

Fig. No.	Page No.
49. Transient Heating of a Solid Copper Wall Without Convective Cooling . . . . .	162
50. Workhorse Thrust Chamber Assembly and Spare Parts . . . . .	164
51. Gas Generator Assembly for J-2 Engine . . . . .	166
52. Schematic of Two-Stage Injector Test System . . . . .	169
53. Test Operating Sequence . . . . .	174
54. 20K Tricentric Injector Configuration 1A After Test 004 . . . . .	181
55. 5K Impinging Coaxial Injector Configuration 9A After Test 011 . . . . .	185
56. Modified 20K Tricentric Injector Configuration 1A Prior to Test 015 . . . . .	187
57. Modified 20K Tricentric Injector Configuration 1A After Test 015 . . . . .	188
58. Rear View of Test Facility . . . . .	196
59. Boundary Layer Losses vs Chamber Length . . . . .	199
60. Nozzle Discharge Coefficient vs Chamber Length . . . . .	204
61. Brush Recording of Photocon and Accelerometer Data From Test 004 . . . . .	208
62. Total Gas Momentum Effect on Injector Performance . . . . .	219
A-1. Atomization of LOX Jet by Surrounding Gas . . . . .	A-3
A-2. Atomization of Annular LOX Jet . . . . .	A-6
B-1. Schematic of Sampling Probe . . . . .	B-2
B-2. Droplet Photograph Obtained With Sampling Probe . . . . .	B-3

## TABLES

Table No.	Page No.
1. Candidate Injector Concepts . . . . .	25
2. Characteristics of Candidate Commercial Nozzles Selected for Preliminary Water-Flow Tests . . . . .	37
3. Results of Preliminary Water-Flow Tests With Commercial Nozzles . . . . .	38
4. Predicted Injector Performance . . . . .	64
5. Injector Performance Rating Criteria . . . . .	72
6. Injector Ratings . . . . .	73
7. Major Characteristics of Four Injector Concepts Selected for Cold-Flow Studies . . . . .	75
8. Cold-Flow Test Matrix . . . . .	78
9. Cold-Flow Simulation of Hot-Firing Conditions for Injector Configuration 1A at 15-Percent Hot-Gas Flow . . . .	104
10. Cold-Flow Simulation of Hot-Firing Conditions for Injector Configuration 2A at 15-Percent Hot-Gas Flow . . . .	105
11. Cold-Flow Simulation of Hot-Firing Conditions for Injector Configuration 2C at 15-Percent Hot-Gas Flow . . . .	106
12. Cold-Flow Simulation of Hot-Firing Conditions for Injector Configuration 9A at 15-Percent Hot-Gas Flow . . . .	108
13. Cold-Flow Simulation of Hot-Firing Conditions for Injector Configuration 11A at 15-Percent Hot-Gas Flow . . . .	109
14. Summary of Injector Cold-Flow Test Results . . . . .	112
15. Main Thrust Chamber Operating Parameters Using 5K and 20K Injectors . . . . .	146
16. Primary Instrumentation Used During Hot-Fire Tests . . . .	171
17. Summary of Hot-Fire Test Results . . . . .	178
18. Summary of Performance Results . . . . .	223
19. Nozzle Heat Transfer Results . . . . .	211
20. Summary of Select Hot-Fire Test Results . . . . .	215

## INTRODUCTION

The Two-Stage Bipropellant Injection System Program was instituted by NASA, Lewis Research Center, for the purpose of investigating hot-gas injection in conjunction with relatively-large-thrust-per-element injector concepts. Hot gas was used in combination with commonly used liquid injection systems to promote atomization, vaporization, and mixing of the propellants. The primary objectives of the program were to investigate the gaseous injection concept to determine its effect on performance and stability of the large-thrust-per-element injectors and to determine design variables for optimizing the injector and hot-gas flowrate. Potential benefits to be realized from this program include reduced injector fabrication costs, increased throttling capability without performance loss, and reduced injector pressure losses.

Three separate tasks were formulated to aid in accomplishing the program objectives. The first task was a design analysis to study the many possible injector concepts and select the most promising concepts for cold-flow studies (the second task). The primary purpose of the cold-flow studies was to experimentally determine the flow characteristics of the select injector concepts using inert fluids to simulate hot-firing propellants. The third task was hot-fire testing to evaluate experimentally the performance and stability of the most promising injector concepts. A nominal 20,000-pound thrust and 500-psia chamber pressure were selected as the operating level for the hot-fire testing. Liquid oxygen, hydrogen, and hot gas (1200 F temperature) were the propellants. These three tasks were scheduled to be accomplished during a 12-month period beginning 30 June 1966.

Data generated during this program may be used for the design of larger-thrust-per-element injectors while providing design criteria for high combustion efficiency and stable combustion. These data are of major interest from the standpoint of reduced engine system pressure losses and deep throttling potential without performance loss. Also of major importance is the fact that substantial engine cost savings may be realized from the use of high-thrust-per-element injection schemes.

## SUMMARY

The Two-Stage Bipropellant Injection System Program was designed to investigate highly energetic hot-gas injection in conjunction with large-thrust-per-element (up to 20,000-pound-thrust per element) injector concepts. Hot gas was employed to promote efficient atomization, vaporization and mixing of liquid oxygen/hydrogen propellants injected by commonly used techniques. The primary objectives were to evaluate performance and stability of various injector concepts. To accomplish these objectives, the program was divided into three tasks.

The first task was a design and analytical evaluation of 20 different candidate injector concepts. These concepts were basically the coaxial type or some version of the impinging stream type of concept. The main purpose of this first task was to provide the foundation analysis for selecting the four most promising injector concepts for subsequent cold-flow studies.

The second task, the cold-flow study phase of the program, was designed to experimentally determine the flow characteristics of the four injector concepts. Water, gaseous nitrogen, and helium were used as inert fluids to simulate liquid oxygen, gaseous hydrogen, and hot gas, respectively, during the cold-flow experiments. The results of these cold-flow studies were the basis for selecting two injector concepts for hot-firing evaluation.

The third task was the hot-firing phase of the program, directed toward performance and stability evaluation of the two select injector concepts.

At the onset of Task I, many injector concepts were screened and 20 were selected along with the basic design and operating characteristics of the concept. Each of the 20 injector concepts was subjected to extensive

design and performance analyses. The objective of the design analysis was to study the practical aspects of the various injector concepts, such as fabrication, cost, packaging, manifolding, etc., and to generate the physical dimensions necessary to support the performance analysis. Design layouts were made for most of the injector concepts showing a single element sized for 20,000 pounds of thrust. These layouts were then used to determine the most promising injector concepts from the fabrication standpoint.

The performance analysis was conducted concurrently with the design studies during Task I. The approach used during the performance analysis was first to predict the location of the primary LOX atomization and initial drop size distribution. The effects of spray droplet heating, acceleration, evaporation, and secondary breakup were then evaluated to a point where the beginning of combustion was predicted. Performance was calculated based on the computed spray and gas stream parameters.

The performance analysis singled out the concepts which appeared to offer effective atomization, gas-phase mixing, and potentially good performance. Gas-phase mixing limited the performance of several of the potential injector types and, in general, presented more of a problem with large-thrust-per-element injectors than atomization. For example, the simple tricentric injector with hot gas inside LOX and fuel annulii (Type 1A) could perform well provided positive means could be devised to aid the mixing of the fuel ( $\text{GH}_2$ ) with the hot-gas/LOX spray mixture generated within the annular LOX jet.

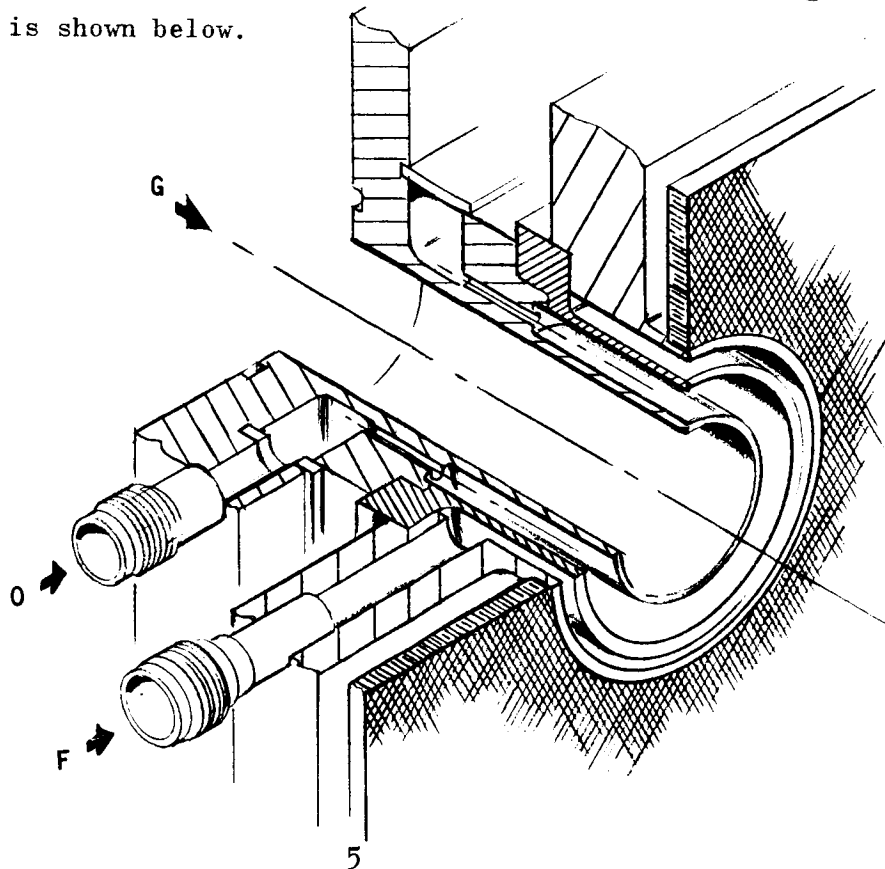
At the conclusion of Task I, the results of the design studies and the performance analysis were combined to guide the selection of four injector concepts for cold-flow studies. The four concepts selected were as follows:

1. The tricentric injector type 1A (hot gas inside LOX and fuel annulii)

2. The impinging jet injectors (Types 2A and 2C) where one pair of self-impinging streams contained LOX, another pair contained hot gas (Type 2A) or fuel (Type 2C) and these streams impinged with a central showerhead stream containing either fuel or hot gas, respectively
3. The coaxial impinging recessed-cup injector (Type 9A) where four coaxial LOX/fuel streams impinged with a central hot-gas stream inside a recessed cup
4. The commercial nozzle injector (Type 11A) where the LOX was injected through a central commercial spray nozzle surrounded by annulii of hot gas and fuel.

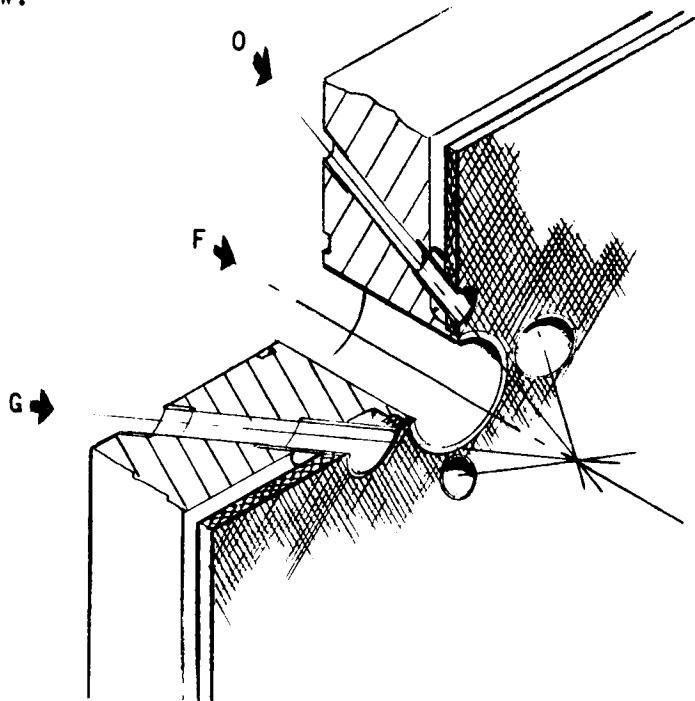
The objective of the cold-flow studies was to evaluate the flow characteristics of the four large-thrust-per-element injector concepts using experimental screening techniques. Each of the four selected injector concepts were represented by two flow models, one simulating a 5,000-pound-thrust element and one simulating a 20,000-pound-thrust element. The screening process was accomplished by comparing high-speed motion pictures of the spray fields and by analysis of the collected liquid mass distribution data.

The first configuration tested was a tricentric element (Type 1A) which extended the familiar coaxial injector concept to include the hot gas. This configuration is shown below.



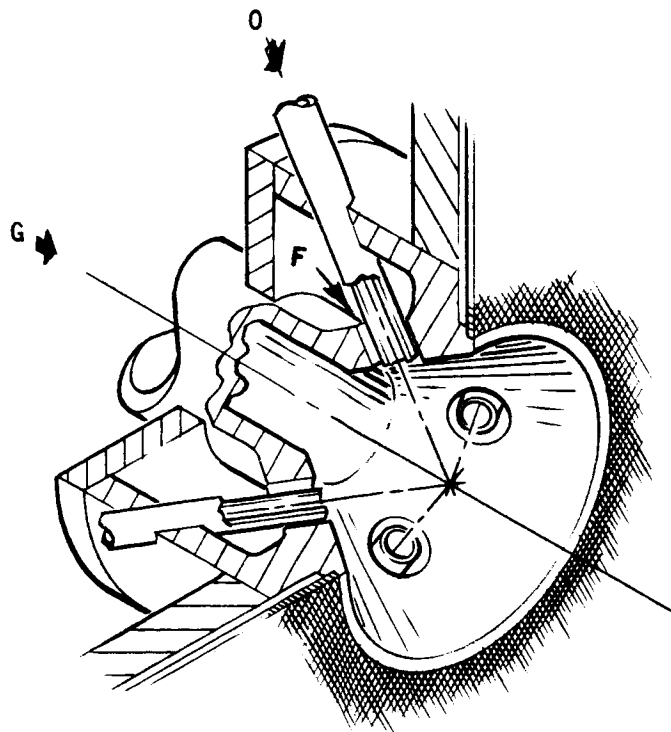
The mass distribution and atomization test results for this configuration were satisfactory. It was observed during the cold-flow studies that the tricentric model 1A was susceptible to pulsating flow conditions. The phenomenon was attributed to reduced velocity of sound propagation through the homogeneous two-phase flow mixture of dispersed liquid and gas. The degree of pulsation was greatly influenced by the exit geometry of the tricentric elements. Two modifications were determined to be effective in eliminating flow pulsations: (1) partial restriction of the annular water (LOX simulant) flow passages, and (2) extension of the inner hot-gas (helium simulant) tube. Both "fixes" decreased the uniform intimate contact between the water and helium (LOX and hot-gas simulants) streams and thereby influenced the quality of the two-phase mixture.

The second configuration tested was an impinging jet injector (Types 2A and 2C). One pair of impinging streams contained water (LOX simulant), and the other pair contained either helium (hot-gas simulant) or nitrogen (fuel simulant). The large center showerhead orifice contained either, nitrogen (Type 2A) or helium (Type 2C). This configuration (Type 2A) is shown below.



Cold-flow results with the impinging jet injectors indicated ineffective utilization of the gas doublet momentum. A satisfactory liquid mass distribution was obtained with both configuration (2A and 2C) with the center gas flowing. The introduction of either gas through the doublet elements caused immediate separation of the liquid spray. It follows that further effort on this pattern should include evaluation of a logical location for the injection of both gases (e.g.; through a central coaxial element) or for one gas species (e.g.; through a single element).

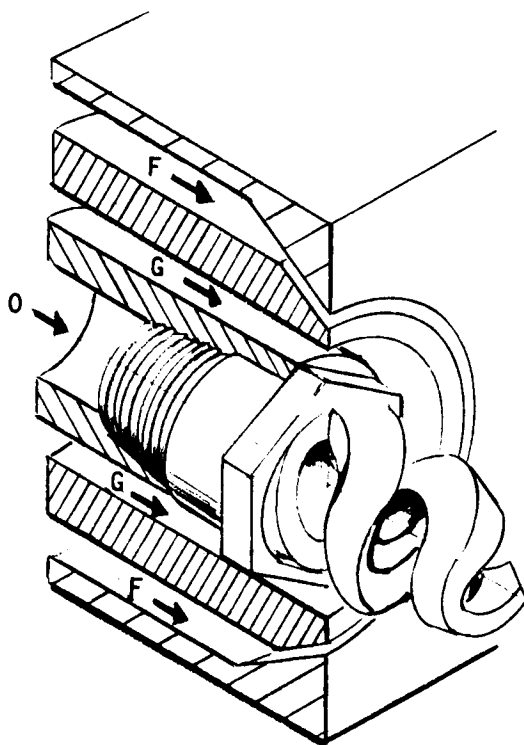
The third configuration tested was an impinging coaxial injector with a recessed cup (Type 9A). This configuration is shown below.



The original 9A concept was designed such that the four coaxial elements impinged within a recessed cup upstream of the injector face. However, because of potential heat transfer problems associated with this precombustor design,

a portion of the cup was removed during the cold-flow studies. Cold-flow characterizations were obtained with both the original and the modified configurations. All Type 9A injector model tests produced favorable atomization and liquid mass distribution results.

The final configuration tested contained a commercial-type of helical spray nozzle for water (LOX simulant) injection. This configuration (11A) is shown below.



During the 11A cold-flow tests using water only, the centrifugal spray nozzle produced a uniform cone-shaped spray field. With the introduction of helium (hot-gas simulant) flow through the annulus surrounding the nozzle, the liquid spray field was reduced to an unacceptable, very narrow distribution pattern. The data indicated quite clearly that this concept would not produce acceptable performance during hot-firing tests.

In general, the photographic results indicated adequate spray atomization with each injector configuration, but no significant difference was evident in the degree of atomization achieved during the cold-flow experimentation. By contrast, the liquid mass distribution tests brought to light significant differences. Configurations 2A, 2C, and 11A showed unacceptable mass distribution, and accordingly were eliminated as candidates for the hot-firing tests. Configurations 1A and 9A were logical choices, based upon their good liquid mass distribution characteristics. The modified 9A version, with the cylindrical portion of the cup removed, showed qualitatively even better flow characteristics than the unmodified model. Consequently, the modified version was selected for the hot-firing program. Similarly, on the basis of relatively good mass distribution data and manufacturing simplicity, the tricentric 1A design, suitably modified to minimize pulsing, was the other concept selected.

Two versions of each injector concept were used for the hot-firing tests, giving a total of four injectors. These injectors were the four-element (5000-pound-thrust per element) and the one element (20,000-pound-thrust per element) versions of the tricentric (1A) and coaxial impinging recessed cup (9A) configurations. A workhorse thrust chamber was designed and fabricated to support the injector evaluations and the hot gas was supplied by a gas generator used for the J-2 engine program.

Twenty mainstage tests were conducted at CTL-3, Cell 18B, of the Rocketdyne Santa Susana Field Laboratory to evaluate the high-thrust-per-element injectors. Each of the four injectors was tested to characterize performance and stability with respect to the quantity (up to 15 percent of the total propellant flow) of hot gas used. During these initial characterization tests, the chamber pressure, mixture ratio, and hot-gas temperature were maintained at or near the nominal design values (i.e.; 500-psia chamber pressure, 5 mixture ratio, and 1200 F hot-gas temperature). The fuel temperature was varied radically in a few tests.

After completion of the initial characterization tests, the 1A and 9A configurations of the 20,000-pound-thrust-per element injectors were selected for further evaluation. The tricentric (1A) injector was modified to improve performance and was then subjected to two evaluation tests. The coaxial impinging (recessed-cup) injector (9A) was selected for additional performance and stability tests at off-design conditions of low chamber pressures (to 50 psia), low fuel temperatures (near 50 R) and increased chamber  $L^*$  (to 70 inches).

Performance of the 9A configuration with a single 20,000-pound-thrust element was the highest of the four injectors tested. The combustion efficiency was approximately 95 percent with a 30-inch  $L^*$  chamber, and 97.5 percent with a 43.5 inch  $L^*$  chamber. No further increase (above 97.5 percent) was observed with a 70-inch  $L^*$  chamber. The combustion efficiency of the injector decayed when the quantity of hot gas was decreased, when the fuel temperature was reduced to about 50 R, and when the chamber pressure was reduced to 200 and to 50 psia. Performance improvement is predicted at these off-design conditions if the injector design is tailored accordingly.

Performance of the 1A configuration with a single 20,000-pound-thrust element was low, approximately 77 percent. The performance analysis conducted in Task I suggested that this low performance was caused by poor mixing of the fuel with the hot-gas/LOX mixture. The injector was subjected to minor modifications to improve mixing and performance. Combustion efficiency was significantly increased (approximately 8 percent) as a result of the modification.

Performance of the 9A configuration with four 5000-pound-thrust elements was slightly lower than the 9A configuration with a single 20,000-pound-thrust element, contrary to expectations. The combustion efficiency of the four-element 9A injector was about 95 percent at the highest hot-gas flowrates and it also decreased with a decrease in the quantity of hot-gas flow.

Performance of the 1A configuration with four 5000-pound-thrust elements was approximately 91 percent, which was about 14 percent higher than the 1A configuration with a single 20,000-pound-thrust element. This performance difference suggests that the size of the element has a significant influence on performance of the tricentric injector concept.

The performance of each hot-firing injector decayed as the quantity of hot gas was reduced, more with some injectors than with others. The highest performance occurred where the quantity of hot gas and the fuel temperature were the greatest; i.e., with hot-gas flows equal to 12 to 14 percent of the total propellant flow with fuel temperatures near 250 R. In addition, the performance appeared to be a strong function of the total gas momentum (hot gas plus fuel), suggesting that for design and operating simplicity, the two gas species might be combined into one.

Stability of each injector configuration was good throughout the hot-firing test program. No significant change in stability was noted at the off-design fuel temperature of 50 R, chamber pressure of 50 psia, or  $L^*$  of 70 inches.

Durability of each injector was satisfactory. Minor erosions were observed on the four-element 9A and one-element 1A injectors, but these erosions proved to be insignificant.

The merits of the two-stage injection principle were conclusively demonstrated during the hot-firing test program, and were supported by the analysis and cold-flow studies. Also, the high-thrust-per-element injector concept was proved feasible when used in conjunction with two-stage injection

## CONCLUSIONS AND RECOMMENDATIONS

### TWO-STAGE INJECTION

The two-stage injection principle (the use of highly energetic gas to augment atomization) was conclusively demonstrated during the hot-fire testing. The merits of this principle were also supported by the analysis and cold-flow studies.

The test results proved that high-thrust-per-element injectors are feasible and have good potential when used in conjunction with high-energy gases.

It is recommended that for peak performance with the LOX/hydrogen propellant combination, further optimization should be conducted with regard to the injector and chamber geometry and the quantity, temperature, and type of gas used.

It is also recommended that the two-stage injection principle be applied to other propellant combinations.

### PERFORMANCE

Results of the analytical studies indicated that several injector concepts could produce high performance.

Results obtained from the analyses and cold-flow studies provided useful and comparatively inexpensive information. The relative fabrication ease, atomization, and performance were determined. In addition, the cold-flow studies revealed characteristics that might never be identified by theoretical analysis alone, such as maldistribution of the propellants and flow instabilities.

The 20,000-pound-thrust-per-element version of the 9A coaxial impinging injector (recessed cup) showed the most promise during the hot-fire testing. Combustion efficiency with this injector was 97.5 percent with a 43.5-inch  $L^*$  chamber.

Performance analysis and hot-fire testing indicated that the combustion efficiency of the 20,000-pound-thrust-per-element tricentric (1A) injector configuration was greatly affected by the degree of mixing between the  $\text{GH}_2$  and the core of LOX-rich combustion gases. High performance may be possible if the mixing is sufficiently improved.

The performance of each injector appeared to be a strong function of the total gas momentum (fuel and hot-gas momentum), thereby suggesting that the fuel and the hot gas might be combined into one high-energy gas species. Thus, the injection principle would be better suited to a wide range of future applications.

The 20,000-pound-thrust-per-element coaxial recesses-cup (9A) injector configuration was successfully tested over a wide range of operating conditions. Performance reduction at off-design conditions indicates a need for further studies to tailor the injector for off-design operation.

#### STABILITY

Stability of each injector concept was good throughout the test program even at the off-design fuel temperatures of approximately 50 R.

#### DESIGN FEASIBILITY

Durability of each injector proved to be satisfactory during the hot-firing tests, and no significant damage occurred.

Injector design simplicity and low fabrication costs were demonstrated during this program. Simple, low-cost, large rocket engine injectors appear feasible using the large-thrust-per-element two-stage injector principle.

## GENERAL APPROACH

The ultimate use of large-thrust-per-element injectors is predicated upon demonstration of high performance, stability, and substantial fabrication cost reductions. With regard to obtaining high performance, it is well known that for most propellant systems the three factors of atomization, mixture ratio distribution, and mass distribution must be combined in a near-optimum manner for peak performance. This is usually accomplished with a fineness of element to promote atomization, a match of momentum ratios to provide uniform mixture ratio, and uniform equal-area injection density to achieve maximum uniformity of mass distribution. The large-thrust-per-element concept results in a degradation of these design principles. For this reason, the two-stage injection system incorporates supplementary hot-gas injection to promote atomization, vaporization, and mixing of the propellants. The amount of hot gas required and its placement within the various injector elements relative to atomization, mass, and mixture ratio distribution was a primary concern of the overall program effort.

The program was divided into three tasks, each of which provided partial evaluation of the potential injector concepts. The flow diagram presented in Fig. 1 illustrates the overall program structure and the interrelationship between the various tasks.

The Task I analysis phase of the program consisted of the design and analytical evaluation of 20 different candidate injector concepts. The elements were of the coaxial-type or some adaptation of the impinging-stream concept. The main purpose of the analyses was to aid in the selection of the four most promising injector element types from the standpoint of probable performance using LOX/gaseous hydrogen/hot gas propellants.

The primary purpose of the cold-flow studies (Task II) was to determine experimentally the flow characteristics of the four injector concepts selected in Task I. These studies were directed toward evaluating the propellant mass distribution and the relative degree of liquid atomization. All the experiments were conducted using water, gaseous nitrogen, and helium to simulate the liquid oxygen, gaseous hydrogen, and hot gas, respectively. Eight single-element injector models were used simulating two different thrust-per-element sizes (5000- and 20,000-pound thrust) for each of the four injector concepts. The experimental results of these cold-flow studies were used as the basis for selecting two concepts for hot-firing evaluation.

Task III, the hot-firing tests, was essentially for performance and stability evaluation of the two select injector concepts. Four injectors were evaluated; i.e., two (one of each concept) containing four 5000-pound-thrust (5K) elements and two (one of each concept) with a single 20,000-pound-thrust (20K) element. Hot-gas flowrate and fuel temperature were the main variables investigated in conjunction with the injector evaluations. In selected tests, the chamber characteristic length ( $L^*$ ) and the chamber pressure were varied, again with performance and stability evaluations in mind. A detailed discussion of each of these three tasks is given in the following sections of this report.

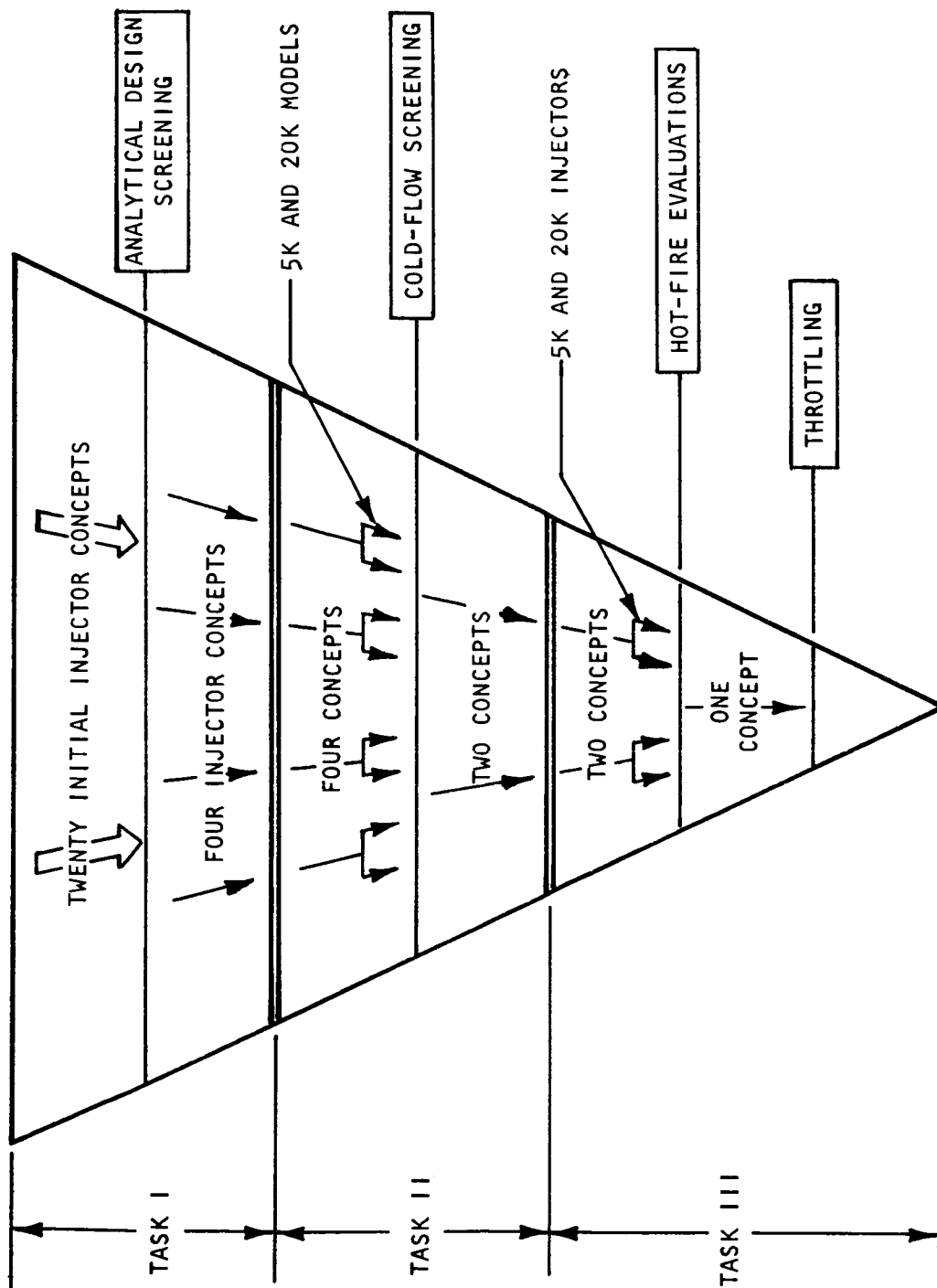


Figure 1. Summary of Major Program Tasks

## TASK I

### ANALYSIS

The analysis phase of the program was an analytical/design evaluation of the candidate injector concepts. As a result of this evaluation, the most promising concepts were selected for Task II cold-flow testing. The approach that was followed during the analysis phase is presented in Fig. 2, beginning with selection of the candidate injector concepts for investigation, and the selection of design and operating characteristics for the various concepts. When these concepts were selected, each was subjected to design and performance analyses as shown in Fig. 2. Following the analyses, the injector concepts were rated and the four most promising concepts were selected for experimental cold-flow studies. A detailed discussion of the analysis is presented in the following sections.

### CONCEPT SELECTION

Elemental injection configurations selected for investigation were divided into four categories: (1) tricentric, (2) impingement, (3) splash plate, and (4) two-stage. Candidate concepts from each category were subjected to preliminary analyses at the 5000- and 20,000-pound-thrust-per-element level to provide input for establishing the basic design and operating characteristics. The preliminary analyses were predicated upon injector propellant pressure drops ( $\Delta P$ ) which reflect consideration for engine system integration, throttling requirements, and the performance and stability goals. The selected injector  $\Delta P$  values are listed as follows along with the corresponding maximum flowrates anticipated.

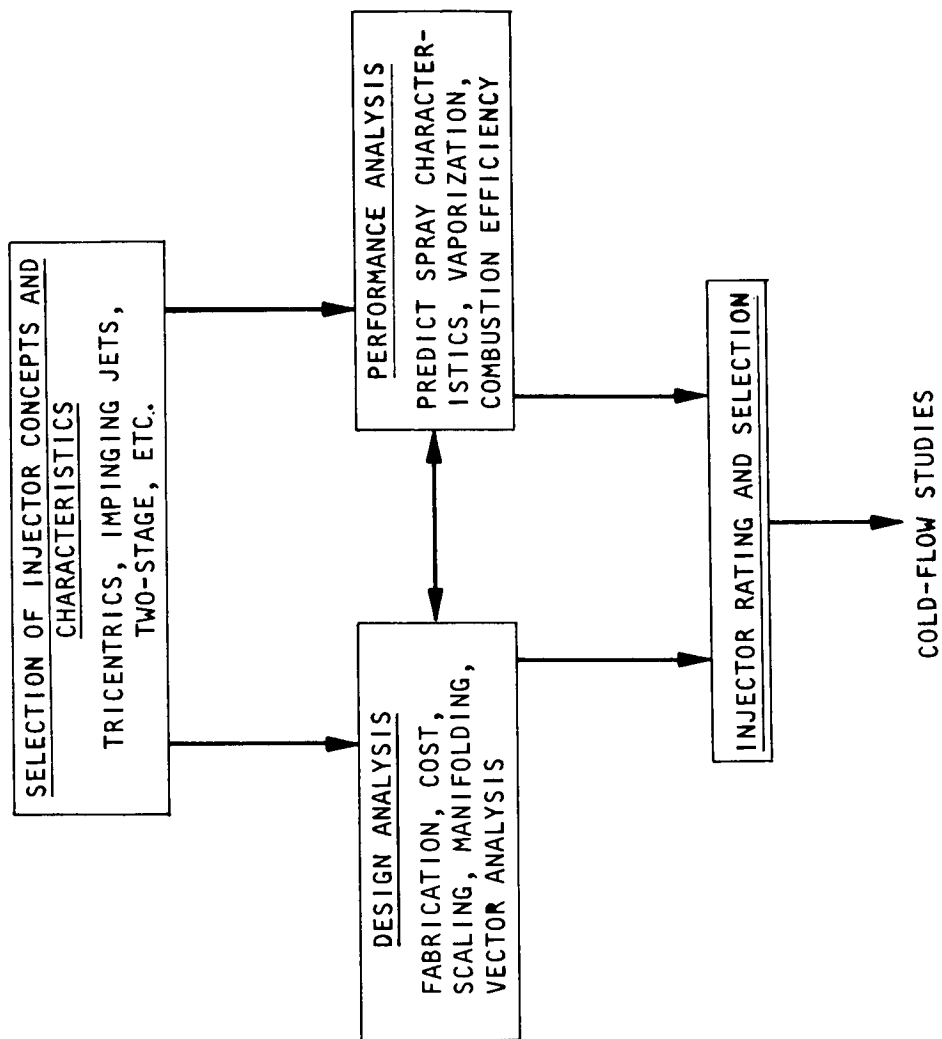


Figure 2. Summary of Task I Analysis Effort

Fuel Side: 100-psi  $\Delta P$  at 8.43 lb/sec flowrate using 150 R  
gaseous hydrogen

Oxidizer Side: 150-psi  $\Delta P$  at 49.31 lb/sec flowrate using liquid  
oxygen

Hot-Gas Side: 250-psi  $\Delta P$  at 9.13 lb/sec flowrate using 1200 F  
hot gas

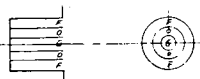
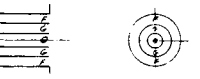
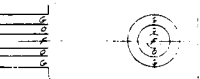
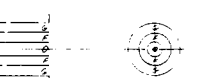
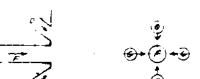
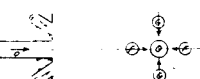
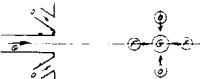


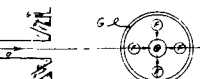

Primary injector characteristics which were considered during the preliminary design analysis were manifolding, propellant positioning, injection velocities, orifice geometry, nature of the spray, recess depth or contour, and adaptability of commercial spray nozzles. The preliminary analysis consisted of calculations to establish the operating characteristics of the various injectors; i.e., the velocities, pressure drops, injection areas, momentum ratios, etc. In addition, sketches of each injector concept were generated to support the design analysis. These sketches served as a visual aid for studying some of the practical aspects of the candidate concepts, such as fabricability, chamber and injector burning, distribution, atomization, cost, and scalability. The practical aspects of each injector configuration was one criterion for accepting concepts for further analysis or for rejecting them.

Twenty injector configurations were initially selected. A single element of each is shown in Table 1. The first group of four configurations (1A through 1D) represents different versions of the "tricentric," or coaxial, injector element with each one containing a different propellant orientation (fuel/oxidizer/hot gas) with respect to the other three. The second

group of three configurations (2A through 2C) contains four jets and two of the propellants impinging with a single, central, third propellant jet. Again, the propellants are oriented differently for each configuration. The third group of four configurations (3A through 3D) utilizes the impinging jet feature for two of the propellants and an annular slot for injecting the third propellant. Element configurations 4A through 12A represent a variety of individual impinging jet, two-stage, and splash plate injector element concepts. In addition to the basic injector element configurations, many auxiliary injection features and/or variables were considered. Some of these features are listed in Table 1.

A 20,000-pound thrust level, an overall mixture ratio of 5, and the quantity of hot gas (5, 10, and 15 percent) were the parameters used to establish the propellant flowrates shown in Table 1. As previously mentioned, the pressure drops were selected considering engine system integration and throttling requirements. Injection velocities and injection areas were calculated for each injector configuration as shown in Table 1. The oxidizer injection velocities for the nonimpinging (tricentric) configurations were somewhat lower than for the impinging jet configurations, thereby creating a more favorable shearing force between the liquid oxidizer and the high-velocity gases. Injection momentum, momentum flux, and the dynamic flow parameters were computed to indicate available energy of the propellants; these parameters subsequently were used in the spray and performance analyses.

Prior to a detailed analysis, each candidate configuration was subjected to a superficial "practicability" survey involving fabricability, injector/chamber burning, mass/mixture ratio distribution, atomization, cost, and scalability. The results of this survey are summarized in the "Remarks" column of Table 1.

Element Configuration	Hot-Gas Flow Condition, percent of total thrust chamber propellant	Propellant Flowrate, lb/sec			Total Injector $\Delta P$ , psi			Injection Velocity, ft/sec			Injection sq in. <sup>(1)</sup>		
					Fuel at 150 R Temperature	Oxidizer at 170 R Temperature	Hot Gas at 1200 F Temperature						
		Fuel	Oxidizer	Hot Gas	Fuel	Oxidizer	Hot Gas	Fuel	Oxidizer	Hot Gas	Fuel	Oxidizer	
Tricentric 1A Fuel (outer) Oxidizer (middle) Hot-Gas (inner)		5	8.43	49.31	3.04	≤100	≤150	≤30	≤1060	≤50.0	≤1375	≥1.66	≥2.07
Tricentric 1B Fuel (outer) Hot-Gas (middle) Oxidizer (inner)		10	6.93	47.77	6.08	≤67	≤141	≤110	≤870	≤48.5	≤2750		
Tricentric 1C Hot-Gas (outer) Oxidizer (middle) Fuel (inner)		15	5.33	46.32	9.13	≤40	≤133	≤250	≤670	≤47.0	≤4125		
Tricentric 1D Hot-Gas (outer) Fuel (middle) Oxidizer (inner)													
Impingement 2A									≤123 ≤119 ≤116			≥0.81 ≥0.81 ≥0.81	
Impingement 2B									≤50.0 ≤48.5 ≤47.0			≥2.03 ≥2.03 ≥2.03	
Impingement 2C									≤123 ≤119 ≤116			≥0.81 ≥0.81 ≥0.81	
Impingement 3A													
Impingement 3B													
Impingement 3C									≤50.0 ≤48.5 ≤47.0			≥2.03 ≥2.03 ≥2.03	
Impingement 3D													

NOTES: 20K total thrust  
500-psia chamber pressure  
60.8-lb/sec total propellant flow  
Transpiration-cooled injector face plate; ~7 percent fuel

① Based on a 20K element  
② Distance from bottom of cup  
③ Assumed cup  $\Delta P$  = 30 psi

④ Commercial spray nozzle  
⑤ Undetermined

FOLDOUT FRAME

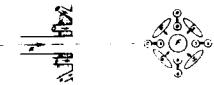
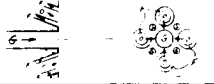
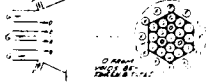

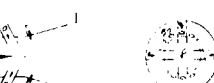
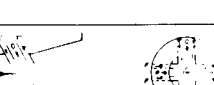
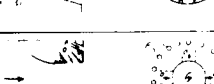
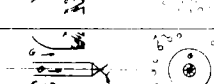
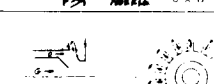
**TABLE 1**  
**CANDIDATE INJECTOR CONCEPTS**

Area, sq ft	Injection Momentum, $(\frac{\dot{w}V}{g})$ , pounds			Injection Momentum Flux $(\frac{\dot{w}V}{gA})$ , psi			Dynamic Flow Parameter $(\frac{\dot{w}}{\dot{w}_f V_f + \dot{w}_o V_o + \dot{w}_{HG} V_{HG}})$ , sec/ft	Impingement Angle, degrees			Impingement Distance, inches <sup>(1)</sup>			Notes	
	Hot Gas	Fuel	Oxidizer	Hot Gas	Fuel	Oxidizer	Hot Gas	Fuel	Oxidizer	Hot Gas	Fuel	Oxidizer	Hot Gas		
1	≥ 3.00	≤ 260	≤ 76.5	≤ 130	≤ 156	≤ 37.7	≤ 43.3	≥ 3.28 x 10 <sup>-3</sup>	0	0	0	∞	∞	∞	• Contour divergent
		≤ 174	≤ 71.8	≤ 520	≤ 105	≤ 35.4	≤ 173	≥ 1.94 x 10 <sup>-3</sup>							
		≤ 103	≤ 67.6	≤ 170	≤ 62	≤ 33.	≤ 390	≥ 1.07 x 10 <sup>-3</sup>							
2															• Contour divergent
3															• Recession
4															• Intersecting annular
5			≤ 188			≤ 231		≥ 2.66 x 10 <sup>-3</sup>		90	120		2.5	4.5	• Extension
		≤ 176				≤ 216		≥ 1.71 x 10 <sup>-3</sup>							
		≤ 167				≤ 206		≥ 1.00 x 10 <sup>-3</sup>							
6		≤ 76.5			≤ 37.7			≥ 3.28 x 10 <sup>-3</sup>	90	0	90	2.5	∞	2.8	• Extension
		≤ 71.8			≤ 35.4			≥ 1.94 x 10 <sup>-3</sup>							
		≤ 67.6			≤ 33.4			≥ 1.07 x 10 <sup>-3</sup>							
7		≤ 188			≤ 231			≥ 2.66 x 10 <sup>-3</sup>	60	60	0	4.5	4.5	∞	• Extension
8		≤ 176			≤ 216			≥ 1.71 x 10 <sup>-3</sup>							
9		≤ 167			≤ 206			≥ 1.00 x 10 <sup>-3</sup>							
10									≤ 90	90		—	2.4		• Injection orifice
11									0		≤ 90	∞	2.1	—	• Extension
12		≤ 76.5			≤ 37.7			≥ 3.28 x 10 <sup>-3</sup>	90	0		2.4	∞		• Extension
		≤ 71.8			≤ 35.4			≥ 1.94 x 10 <sup>-3</sup>							• Biplanar
		≤ 67.7			≤ 33.4			≥ 1.07 x 10 <sup>-3</sup>							• "Offset"
13									≤ 90		90	—		2.4	• Injection orifice
14															

FOLDOUT FRAME 2

Injection Distance, inches ①		Potential Auxiliary Injection Features and/or Variables				Remarks
Oxidizer	Hot Gas	Fuel	Oxidizer	Hot Gas	General	
0.8 ↓	3.9 ↓	• Extension tube	• Two-on-one	• Extension tubes • Orifice shape	• Reverse fuel and hot gas • "Cup" contour	• Moderate fabrication problem • Good injector/chamber cooling • Good atomization potential • Good scaling features
2.6 ↓	∞	• Contoured divergence • Extension tubes	• Recessed	• Extension tubes • Number of orifices	• Reverse fuel and hot gas • "Cup" contour • "Offset" injection • Two-on-one	• Moderate fabrication problem • Good injector/chamber cooling • Good atomization potential • Good scaling features
∞ ↓		• Number of orifices	• Number of orifices • Swirler (tubular passages only)	• Number of orifices	• "Cup" contour	• Difficult fabrication problem • Possibility of injector/chamber burning problem • Cannot get sufficient LOX area unless at least three "gas tubes" are used for LOX • Good LOX/hot-gas exposure
— ↓		• Number of orifices	• Number of orifices	• Injection orifice shape		• Difficult fabrication problem (especially with 5K element) • Many orifices should provide good atomization • Good scaling features
1.4 <sup>②</sup> ↓		• Number of orifices	• Extension tubes • "Offset" injection • Injection location		• "Cup" contour	• Moderate fabrication problem • Possible injector burning problem • Good oxidizer atomizing potential • Film cooling of "premix" chamber may not provide good oxidizer/fuel mixing • Poor ΔP prediction • Good scaling features
1.7 <sup>②</sup> ↓		• Extension tubes	• Recessed		• "Cup" contour • "Offset" injection	• Difficult fabrication problem • Possible injector burning problem • Good atomization potential • Poor ΔP prediction • Good scaling features
0 ↓		• Number of orifices	• Injection location • Extension tubes • "Offset" injection			• Moderate fabrication problem • Good injector/chamber cooling • Good atomization potential • Good scaling features
— ↓		• Number of orifices	• Commercial nozzle configuration • Commercial nozzle location			• Easily fabricated • Possibility of spray nozzle burning • Good atomization potential • Good scaling features
— ↓		• Number of orifices	• Number of orifices		• "Cup" contour	• Difficult fabrication problem • Possible injector burning problem • Good atomization potential • Poor ΔP prediction • Starting/stopping transient problem • Good scaling features

POUPOUT FRAME 3

Element Configuration	Hot-Gas Flow Condition, percent of total thrust chamber propellant	Propellant Flowrate, lb/sec			Total Injector $\Delta P$ , psi			Injector	
		Fuel	Oxidizer	Hot Gas	Fuel at 150 R Temperature	Oxidizer at 170 R Temperature	Hot Gas at 1200 F Temperature	Fuel	Oxidizer
Impingement 4A 	5	8.43	49.31	3.04	≤100	≤150	≤30	≤1060	≤870
	10	6.93	47.77	6.08	≤67	≤141	≤110	≤870	≤870
	15	5.33	46.32	9.13	≤40	≤133	≤250	≤670	≤670
Impingement 5A 									
Two-Stage 6A 									
Two-Stage 7A 									
Two-Stage 8A 					③	③	③	≤ 860 ≤ 705 ≤ 540	≤ 870 ≤ 870 ≤ 870
Two-Stage 9A 					③	③	③		
Two-Stage 10A 								≤ 1060 ≤ 870 ≤ 670	≤ 870 ≤ 870 ≤ 870
Two-Stage 11A 									
Splash Plate 12A 					③	③	③	≤ 860 ≤ 705 ≤ 504	≤ 870 ≤ 870 ≤ 870

NOTES: 20K total thrust  
500-psia chamber pressure  
60.8-lb/sec total propellant flow  
Transpiration-cooled injector face plate; ~7 percent fuel

① Based on a 20K element      ④ Commercial spray nozzle  
② Distance from bottom of cup      ⑤ Undetermined  
③ Assumed cup  $\Delta P = 30$  psi

TABLE 1  
(Concluded)

Injection Velocity ft/sec	Hot Gas	Injection Area, sq in (1)			Injection Momentum ( $\frac{WV}{g}$ ), pounds			Injection Momentum Flux ( $\frac{WV}{gA}$ ), psi			Dynamic Flow Parameter ( $\frac{w_f V_f + w_o V_o + w_{HG} V_{HG}}{\text{sec/ft}}$ )	Impingement Angle, degrees			Impingement Angle, degrees
		Fuel	Oxidizer	Hot Gas	Fuel	Oxidizer	Hot Gas	Fuel	Oxidizer	Hot Gas		Fuel	Oxidizer	Hot Gas	
123	≤ 1375	≥ 1.66	≥ 0.813	≥ 3.00	≤ 260	≤ 188	≤ 130	≤ 156	≤ 231	≤ 43.3	≥ 2.66 × 10 <sup>-3</sup>	90	45	60	∞
119	≤ 2750	≥ 1.66	≥ 0.813	≥ 3.00	≤ 174	≤ 176	≤ 520	≤ 105	≤ 216	≤ 173	≥ 1.71 × 10 <sup>-3</sup>	↓	↓	↓	↓
116	≤ 4125	≥ 1.66	≥ 0.813	≥ 3.00	≤ 103	≤ 167	≤ 1170	≤ 62	≤ 206	≤ 390	≥ 1.00 × 10 <sup>-3</sup>	↓	↓	↓	↓
97.5			1.04			150			144		2.94 × 10 <sup>-3</sup>	90	90	0	2.6
94.5			1.04			140			135		1.78 × 10 <sup>-3</sup>	↓	↓	↓	↓
92.0			1.04			132			127		1.02 × 10 <sup>-3</sup>	60	0		3.1
						≤ 188			≤ 231		≥ 2.66 × 10 <sup>-3</sup>	↓	↓	↓	↓
						≤ 176			≤ 216		≥ 1.77 × 10 <sup>-3</sup>	↓	↓	↓	↓
						≤ 167			≤ 206		≥ 1.00 × 10 <sup>-3</sup>	↓	↓	↓	↓
110	≤ 1220	≥ 1.94	0.91	≥ 3.20	≤ 210	≤ 168	≤ 115	≤ 108	≤ 185	≤ 36.0	≥ 3.11 × 10 <sup>-3</sup>	↓	↓	↓	2.9
107	≤ 2440	≥ 1.94	0.91	≥ 3.20	≤ 141	≤ 159	≤ 460	≤ 72.7	≤ 175	≤ 144	≥ 2.33 × 10 <sup>-3</sup>	120	90		↓
103	≤ 3650	≥ 1.94	0.91	≥ 3.20	≤ 83	≤ 148	≤ 1030	≤ 42.8	≤ 163	≤ 32.2	≥ 1.13 × 10 <sup>-3</sup>	↓	↓	↓	↓
												120			1.7
123	≤ 1375	≥ 1.66	≥ 0.813	≥ 3.00	≤ 260	≤ 188	≤ 130	≤ 156	≤ 231	≤ 43.3	≥ 2.66 × 10 <sup>-3</sup>	↓	↓	↓	1.5
119	≤ 2750	≥ 1.66	≥ 0.813	≥ 3.00	≤ 174	≤ 176	≤ 520	≤ 105	≤ 216	≤ 173	≥ 1.71 × 10 <sup>-3</sup>	↓	↓	↓	↓
116	≤ 4125	≥ 1.66	≥ 0.813	≥ 3.00	≤ 103	≤ 167	≤ 1170	≤ 62	≤ 206	≤ 390	≥ 1.00 × 10 <sup>-3</sup>	↓	↓	↓	↓
④			④			⑤			⑦		⑨	60	100		—
110	≤ 1220	≥ 1.94	≥ 0.91	≥ 3.20	≤ 210	≤ 168	≤ 115	≤ 108	≤ 185	≤ 36.0	≥ 3.11 × 10 <sup>-3</sup>	↓	↓	↓	↓
107	≤ 2440	≥ 1.94	≥ 0.91	≥ 3.20	≤ 141	≤ 159	≤ 460	≤ 72.7	≤ 175	≤ 144	≥ 2.33 × 10 <sup>-3</sup>	↓	↓	↓	↓
103	≤ 3650	≥ 1.94	≥ 0.91	≥ 3.20	≤ 83	≤ 148	≤ 1030	≤ 42.8	≤ 163	≤ 32.2	≥ 1.13 × 10 <sup>-3</sup>	↓	↓	↓	↓

Potential Auxiliary Injection Features and/or Variables				Remarks
Fuel	Oxidizer	Hot Gas	General	
Recessed annulus	<ul style="list-style-type: none"> <li>• Recessed</li> <li>• Multihole orifice disk</li> <li>• Interrupted annulus</li> </ul>	<ul style="list-style-type: none"> <li>• Recessed</li> </ul>		<ul style="list-style-type: none"> <li>• Easily fabricated</li> <li>• Good injector/chamber cooling</li> <li>• Good atomization potential with proper combination of auxiliary features</li> <li>• Good scaling features</li> </ul>
Recessed annulus	<ul style="list-style-type: none"> <li>• Recessed</li> <li>• Multihole orifice disk</li> <li>• Swirler</li> <li>• Castellated tip</li> </ul>	<ul style="list-style-type: none"> <li>• Interrupted annulus</li> </ul>		<ul style="list-style-type: none"> <li>• Easily fabricated</li> <li>• Good injector/chamber cooling</li> <li>• Large oxidizer core may be difficult to atomize (swirler may help)</li> <li>• Fuel removed from oxidizer</li> <li>• Probably poor scaling (large LOX diameter)</li> </ul>
Recessed annulus	<ul style="list-style-type: none"> <li>• Recessed</li> <li>• Multihole orifice disk</li> <li>• Interrupted annulus</li> </ul>	<ul style="list-style-type: none"> <li>• Contoured divergence</li> </ul>		<ul style="list-style-type: none"> <li>• Fabrication more difficult because of special face-cooling requirements with hot gas on outside</li> <li>• Good injector/chamber cooling</li> <li>• Less effective use of hot gas for oxidizer atomization</li> </ul>
Recessed annulus	<ul style="list-style-type: none"> <li>• Recessed</li> <li>• Multihole orifice disk</li> <li>• Swirler</li> <li>• Castellated tip</li> </ul>	<ul style="list-style-type: none"> <li>• Contoured divergence</li> </ul>		<ul style="list-style-type: none"> <li>• Fabrication more difficult because of special face-cooling requirements with hot gas on outside</li> <li>• Good injector/chamber cooling</li> <li>• Less effective use of hot gas for LOX atomization</li> <li>• Probably poor scaling</li> </ul>
Extension tubes	<ul style="list-style-type: none"> <li>• Multihole orifice disk</li> </ul>	<ul style="list-style-type: none"> <li>• Extension tubes</li> </ul>	<ul style="list-style-type: none"> <li>• Biplanar injection</li> <li>• "Offset" injection</li> <li>• "Cup" contour</li> </ul>	<ul style="list-style-type: none"> <li>• Moderate fabrication problem</li> <li>• Possibility of injector/chamber burning problem</li> <li>• Good atomization potential</li> <li>• Good scaling features</li> </ul>
Extension tubes	<ul style="list-style-type: none"> <li>• Multihole orifice disk</li> </ul>	<ul style="list-style-type: none"> <li>• Extension tubes</li> </ul>	<ul style="list-style-type: none"> <li>• Biplanar injection</li> <li>• "Offset" injection</li> <li>• "Cup" contour</li> </ul>	<ul style="list-style-type: none"> <li>• Moderate fabrication problem</li> <li>• Possibility of injector/chamber burning problem</li> <li>• Large LOX core may be difficult to atomize</li> <li>• Probably poor scaling (large LOX diameter)</li> </ul>
Extension tubes	<ul style="list-style-type: none"> <li>• Multihole orifice disk</li> </ul>	<ul style="list-style-type: none"> <li>• Extension tube</li> </ul>	<ul style="list-style-type: none"> <li>• Biplanar injection</li> <li>• "Offset" injection</li> <li>• "Cup" contour</li> </ul>	<ul style="list-style-type: none"> <li>• Moderate fabrication problem</li> <li>• Possibility of injector/chamber burning problem</li> <li>• Poor LOX-to-hot-gas diameter ratio</li> <li>• Does not utilize hot gas effectively</li> </ul>
Extension tubes	<ul style="list-style-type: none"> <li>• Biplanar injection</li> <li>• "Offset" injection</li> <li>• Two-on-one</li> </ul>	<ul style="list-style-type: none"> <li>• Extension tube</li> </ul>	<ul style="list-style-type: none"> <li>• "Cup" contour</li> </ul>	<ul style="list-style-type: none"> <li>• Moderate fabrication problem</li> <li>• Good injector/chamber cooling</li> <li>• Poor LOX-to-hot-gas diameter ratio may be counter-acted with proper combination of auxiliary features</li> </ul>
Extension tubes	<ul style="list-style-type: none"> <li>• Biplanar injection</li> <li>• "Offset" injection</li> <li>• Two-on-one</li> </ul>	<ul style="list-style-type: none"> <li>• Injection orifice shape</li> </ul>	<ul style="list-style-type: none"> <li>• "Cup" contour</li> </ul>	<ul style="list-style-type: none"> <li>• Difficult fabrication problem especially with angled hot-gas slot</li> <li>• Good injector/chamber cooling</li> <li>• Good atomization potential with proper combination of auxiliary features</li> <li>• Good scaling features</li> </ul>
Extension tubes	<ul style="list-style-type: none"> <li>• Multihole orifice disk</li> <li>• Swirler</li> </ul>	<ul style="list-style-type: none"> <li>• Injection orifice shape</li> </ul>	<ul style="list-style-type: none"> <li>• "Cup" contour</li> </ul>	<ul style="list-style-type: none"> <li>• Difficult fabrication problem especially with angled hot-gas slot</li> <li>• Good injector/chamber cooling</li> <li>• Large LOX core may be difficult to atomize</li> <li>• Probably poor scaling (large LOX diameter)</li> </ul>
Extension tubes	<ul style="list-style-type: none"> <li>• Multihole orifice disk</li> <li>• Swirler</li> </ul>	<ul style="list-style-type: none"> <li>• Extension tubes</li> <li>• Biplanar injection</li> <li>• "Offset" injection</li> <li>• Two-on-one</li> </ul>	<ul style="list-style-type: none"> <li>• "Cup" contour</li> </ul>	<ul style="list-style-type: none"> <li>• Moderate fabrication problem</li> <li>• Good injector/chamber cooling</li> <li>• Large LOX core may be difficult to atomize</li> <li>• Probably poor scaling (large LOX diameter)</li> </ul>

FOLDOUT FRAME 3

## DESIGN ANALYSIS

A more detailed analysis was undertaken to evaluate and narrow the 20 candidate concepts to 4. Design and performance analyses were used to guide the evaluation and selection. The objective of the design analysis was to study the practical aspects of the various injector concepts, such as fabrication, cost, packaging, manifolding, etc., and to generate physical dimensions necessary to support the performance analysis. Design layouts for most of the injector concepts were made showing a single 20K element and, in some cases, showing 5K elements positioned to fit within the selected chamber diameter of 8.55 inches.

The approach used for the layouts of the various concepts was based on ease of fabrication, low cost, no interpropellant welds if possible, external propellant manifolding, and most effective use of the available injection area. The selected chamber diameter (8.55 inches) in some cases caused packaging problems resulting in unequal injection density and/or a compromise in the element geometry for the four 5K element configurations. Parameters such as orifice angle, location, impingement distance, and number of orifices were some of the features studied in connection with the design analysis. Other auxiliary features or variables investigated to a limited degree during the design analysis included swirl devices, off-center impinging streams, vanes, castellations, and other devices to induce breakup of the liquid-propellant streams to increase atomization. In addition, commercial nozzles were investigated for potential atomization and reduced cost.

### Tricentric Injector Configurations 1A through 1D

Tricentric injector configurations 1A through 1D each contained the same basic design features which, in essence, were three tubes of different diameters positioned coaxially. The three propellants passed through the center tube and the two annular passages surrounding the center tube. Small changes in diameter or material (wall) thickness between propellants had little effect on the injector operating characteristics, but concentricity errors in either of the annular passages were undesirable. Therefore, dividers or spacers were placed in the annular passages to ensure concentricity. Propellant positioning, injection velocities, recessed or extended passages, swirl inducers, interruptions in the flow annuli, contoured exits, passage lengths, and length-to-diameter (L/D) ratios were among the variables considered during the tricentric injector design studies.

From a fabrication and packaging standpoint, each of the four basic tricentric configurations (1A through 1D) was attractive. However, auxiliary features such as swirls or other mechanical devices decreased the advantage of a tricentric configuration. The 1B and 1D configurations with the central LOX core require such devices to be competitive in the areas of atomization and scaling. Injector face and chamber cooling characteristics of the 1A and 1B configurations (with fuel in the outer annulus) are more desirable than those of the 1C and 1D configurations (with hot gas in the outer annulus) because the cooler fuel is the better coolant, manifolding the outer fuel coolant to other areas of the injector is easier, and the variable hot-gas flow requirement of this program is a disadvantage from the cooling standpoint.

### Impinging Jet Injector Configurations 2A Through 2C

The impinging jet injector configurations 2A through 2C were characterized by two sets of impinging streams with two of the propellants impinging on a single central stream containing the third propellant (four on one).

Fuel, oxidizer, and hot gas were designated for injection through the central jet in the 2A, 2B, and 2C configurations, respectively. Primary variables investigated during the design studies included the impingement angle of the jets (between 60- and 90-degree included angle), biplanar impingement, impingement distance from the injector face, manifolding, and packaging.

Fabrication of the impinging jet configurations would be relatively simple, although some manifolding difficulties (dimensional limitations) were experienced during the design studies when the four elements were packaged into the 8.55-inch-diameter chamber. Again, swirl devices would be required to break up the large central LOX core in the 2B configuration, detracting from the fabrication advantages. As mentioned in connection with the tri-centric injectors, fuel is a better propellant than the oxidizer or hot gas for injector face and chamber cooling. The fuel in the central jet of the 2A configuration would be somewhat undesirable from the standpoint of manifolding and cooling.

### Injector Configuration 3A Through 3D

Injector configurations 3A through 3D were composed of a central shower-head jet surrounded by four impinging jets which were surrounded by an annular jet. Each of the four configurations contained a different fuel/oxidizer/hot gas propellant arrangement: one through the central jet, a second through the four impinging jets, and the third through the outer

annulus. Impingement distance, impingement angle, slot or annular jet angle, swirl devices, offset injection, and manifolding were the main variables or auxiliary features studied during the design analysis.

Fabrication of this type of injector configuration would be moderately more difficult than the series 1 and 2 configurations. Areas of concern are in maintaining a concentric or constant-width annular slot, packaging, and manifolding. Also, swirl devices are necessary to help break up the large central LOX core in the 3C and 3D configurations, thereby creating more fabrication problems. When packaging four 5K elements within the 8.55-inch chamber diameter, the orifice and slot impingement angles must be minimized. From the cooling standpoint, the 3A and 3D configurations are the most attractive because of the cooled fuel on the outside of the element.

#### Injector Configuration 4A

This injector configuration contains a series of hot-gas jets and a series of impinging oxidizer jets all impinging on a central fuel jet. The number and shape of the orifices, the impingement angle, and manifolding were the primary variables for consideration during the design studies. In addition, another variable for consideration was to reverse the fuel and hot-gas injection.

Fabrication and manifolding of this injector configuration is more difficult because of the number and location of the injector orifices. Packaging of four 5K elements further complicates the manifolding and fabrication problems. Decreasing the number of injection orifices would simplify the fabrication; however, the configuration would then approach that of the 2A configuration.

### Injector Configurations 5A and 5B

Basically, the 5A injector configuration contains four coaxial fuel/oxidizer jets impinging on a central hot-gas jet. The fuel is injected through annulii surrounding the oxidizer jets. An alternate arrangement (the 5B configuration) was investigated, calling for fuel through the center jet impinging with the four coaxial oxidizer/hot-gas jets with the oxidizer around the hot gas. Other significant features investigated during the design studies were the impingement angle of the coaxial jets, the manifolding, and the packaging of four 5K elements. Like the trisentric configurations, spacers or dividers would be required to maintain a constant-width annulus in each of the coaxial impinging jets. Four auxiliary hot-gas feed holes are shown in the sketch in Table 1; however, these holes were discarded during the design studies.

Fabrication of this type of injector configuration would be moderately more difficult than the first two series of injector configurations. The number of injection ports, the coaxial elements, and the manifolding of the coaxial elements contribute to the fabrication complexity. Packaging of the four 5K elements presents a clearance problem in addition to manifolding complexity. A compromise (a decrease) in the impingement angle and selective rotation or positioning of the elements is required to prevent interference between elements.

### Injector Configuration 6A

Injector configuration 6A is composed of a bundle of parallel tubes which serve as the hot-gas injector orifices. Oxidizer is injected through the open areas between the tubes, and the fuel is directed into the hot-gas/oxidizer mixture from peripheral orifices angled inward. As shown on the

sketch in Table 1, some of the hot gas tubes were eliminated to give the required area for the oxidizer flow. Also, the injection ports are shown positioned in a recessed cup. The recessed cup shape, depth, and the number of injection orifices were the main variables considered during the design analysis.

As the number of hot-gas tubes or orifices is increased, greater oxidizer/hot-gas exposure and, consequently, higher performance is possible. However, fabrication of the multiorificed configuration is rather complex, primarily because of the oxidizer and hot-gas manifolding. Welding or brazing should be avoided between the oxidizer and the hot-gas (or fuel) manifolds, which further complicates this injector configuration.

#### Injector Configuration 7A

Injector configuration 7A is characterized by a tubular ring of fuel inside a tubular ring of oxidizer, with the hot gas passing through the slot (opening) between the two rings. Orifices are drilled in the oxidizer and fuel rings, directing these propellants toward each other and into the annulus of hot gas. Atomization and performance of this configuration is a strong function of the number of fuel and oxidizer orifices. A large number of orifices defeats the large-thrust-per-element principle and effectively creates many small elements.

Fabrication of this concept becomes more complex as the number of orifices is increased. Control of the hot-gas flow area (a narrow annular slot) could also present a problem. The design analysis suggested that it was not practical to package four 5K elements together; i.e., one 20K element is more advisable.

### Injector Configuration 8A

Injector configuration 8A contains a central hot-gas jet surrounded by and impinging with four oxidizer jets on one plane. Further downstream, the resulting mixture impinges with a series of fuel streams. All the orifices are positioned inside a recessed cavity or cup. The number of fuel and oxidizer orifices, orifice angles, cup geometry, and manifolding were of primary concern during the design analysis. The main purpose for the recessed cup is to utilize more of the high-energy hot gas to atomize the oxidizer before the gas energy is dissipated in the open chamber. The cup also permits a shorter impingement distance for the oxidizer and fuel streams, resulting in better atomization and mixing.

Fabrication of this type of injector configuration would be moderately difficult, similar to that of the Group 3 configurations. With the recessed cup concept, better packaging can be realized compared to a similar flat-face injection scheme because the recessed element can be contained within a smaller diameter. Recessed cup cooling was singled out as one of the potential problem areas with this configuration; thus, extra features may be required to cool the cup.

### Injector Configuration 9A

Injector configuration 9A is composed of an injection scheme similar to that of the 5A configuration but placed inside a recessed cup like the 8A configuration. Impingement angles, manifolding, packaging, and cup geometry were considered during the design studies. As in the 5A configuration, spacers or dividers would be required to maintain a consistent fuel annulus in the coaxial impinging jets. Shorter impingement distances and better atomization potential are possible because of the recess feature.

Fabrication of this configuration would be similar to that of the 5A configuration. Packaging would be somewhat easier because each element can be fit into a smaller diameter. Recessed cup cooling could be a problem depending on the cup geometry and the protective effectiveness of the fuel.

#### Injector Configuration 10A

Injector configuration 10A is identical to the 8A configuration except for the depth of the recessed cup; i.e., a shallower cup is used for the 10A configuration. Fabrication, manifolding, packaging, etc. would be similar for the two configurations. However, cup cooling would be less problematic for the 10A configuration.

#### Commercial Nozzle Injector Configuration 11A

The commercial nozzle configuration in principle is similar to the 1B tricentric injector configuration; i.e., the oxidizer is injected through the center, the hot gas through an annulus around the oxidizer, and the fuel from an annulus or a series of holes around the hot gas. The commercial nozzle is used as a swirl or atomizing device to break up the large central oxidizer core.

Several commercial spray nozzles were investigated for use with the 11A injector configuration. Items considered during the investigation were mounting, envelope dimensions, atomization potential over the throttling range (constant spray angle), and cooling capability. The investigation was limited to nozzles which give full-cone spray patterns because previous related experience with hollow-cone patterns indicated a high risk

of burning. Three nozzle types were screened, i.e., nozzles with internal turbine cores, nozzles with internal deflection vanes, and nozzles with external spirals. The most promising nozzle configuration from each type was obtained (Fig. 3), sized for the 5K and 20K flowrate capacity.

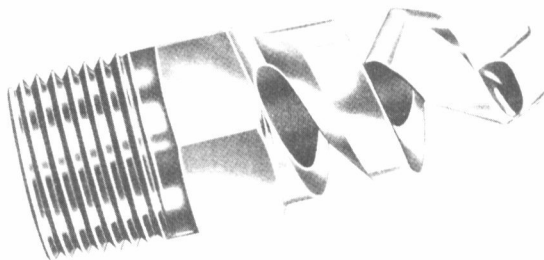
Prior to incorporating a potential commercial nozzle into the complete injector configuration 11A, the selected nozzles were water flow tested to visualize the flow distribution and to compare the flowrate and pressure drop characteristics with those predicted by the manufacturers. The nozzles tested and their characteristics are summarized in Table 2. Flowrate data were obtained by a direct-readout instrument coupled with an in-line turbine-type flowmeter. Pressure readings were taken from a Heise gage. To obtain the calibration data, the pressure readings were set and the flowrate was recorded. Flowrates of 330 gpm (rated thrust) and 130 gpm (throttled condition) were targeted for the 20K nozzles, and 83 and 33 gpm were targeted for the 5K nozzles. Table 3 shows pressure drop vs flowrate for select conditions. For comparison purposes, the manufacturer's flowrate vs pressure drop is also shown. Still photographs were taken at or near the targeted flowrates for each nozzle to show the spray characteristics.

In rating the commercial nozzles, the Spraco and the Bete "Tu-Cone" received first consideration. The Bete nonclogging nozzles were rated the lowest because they exhibited the poorest atomization and most severe streaking tendencies. The atomization characteristics for the different nozzles were evaluated at equivalent flowrates but not at the same  $\Delta P$ . It may be postulated that the atomization characteristics would tend to approach one another if the pressure drops were equal. A significant reason for the differences in pressure drop was because of the large discrepancy

INTERNAL TURBINE  
CORE TYPE



EXTERNAL SPIRAL  
TYPE



INTERNAL DEFLECTION  
VANE TYPE



- SPRACO CENTER JET SPRAY NOZZLE  
20K CAPACITY: NOZZLE NO. 12E;  
 $\Delta P = 130$  PSI  
5K CAPACITY: NOZZLE NO. 10D;  
 $\Delta P = 110$  PSI

- BETE WHIRL NOZZLE  
20K CAPACITY: NOZZLE NO. NC2570W;  
 $\Delta P = 160$  PSI  
5K CAPACITY: NOZZLE NO. NC1524W;  
 $\Delta P = 100$  PSI

- BETE "TU-CONE" SPIRAL NOZZLE  
20K CAPACITY: NOZZLE NO. N10W;  
 $\Delta P = 150$  PSI  
5K CAPACITY: NOZZLE NO. N6W;  
 $\Delta P = 150$  PSI

Figure 3. Candidate Commercial Nozzles Selected for Preliminary Water-Flow Tests

TABLE 2  
CHARACTERISTICS OF CANDIDATE COMMERCIAL NOZZLES SELECTED  
FOR PRELIMINARY WATER-FLOW TESTS

Nozzle Number	Nozzle Material	Nozzle Dimensions				Spray Characteristic	Spray Angle, degrees	Applicable Thrust Level, pounds
		Orifice Diameter, inches	Pipe Size	Length, inches	Hex Size, inches			
Bete N6W** Bete N10W**	316 CRES 316 CRES	1/2 1	1 MPT 1-1/2 MPT	3-1/2 4	1-1/8 2	Spiral shear "Tu-Cone" with an wide-angle outer cone and a narrower inner cone which combines to give a full-cone effect	100 100	5K 20K
Bete NC1524W** Bete NC2570W**	Cast Bronze Cast Bronze	23/32 1-1/4	1-1/2 FPT 2-1/2 FPT	4-1/8 5-3/4	2-1/4 3-1/4	Nonclogging full-cone wide angle	125 125	5K 20K
Spraco 10D* Spraco 12E*	Cast Iron Cast Iron	9/16 1-1/16	1-1/2 FPT 2-1/2 FPT	4-5/16 6	2-3/16 3-1/4	Full-cone medium angle	90 90	5K 20K

NOTE: Spray angles are approximate values, and may vary with pressure

\*Spray Engineering Company, Burlington, Mass.

\*\*Bete Fog Nozzle Inc., Greenfield, Mass.

TABLE 3

## RESULTS OF PRELIMINARY WATER-FLOW TESTS

## WITH COMMERCIAL NOZZLES

Nozzle Number	Nozzle $\Delta P$ , psi	Predicted Flowrate, gpm*	Actual Flowrate, gpm	Comments
<u>5K Thrust Nozzles</u>				
Bete N6W	150	81	103	• Flow streaking visible
	100	67	83	• Injection pattern not symmetrical (due to spiral)
	15	26	33	• Wide angle of injection
Bete NC1524W	150	104	119	• Good atomization at high injection pressure
	70	72	83	• Spiral sheet of fluid at low injection pressure
	8.5	27	33	• Nonuniform distribution of fluid
Spraco 10D	200	--	83	• Hollow cone injection pattern
	150	95	72	• Angle of injection decreased slightly as pressure increased
	26	41	33	• Circumference of injection pattern not uniform
20K Thrust Nozzles	174	--	83	• Least desirable for atomization
	150	334	72	• Streaking at all flowrates
	31	150	33	• Full cone flow more apparent than in other nozzles
Bete NC2570W	180	--	289	• Atomization and distribution good
	150	326	269	• Some streaking visible
	48	184	130	• Flow injection angle decreases as pressure increases
Spraco 12E	176	--	247	• Narrow injection angle
	150	350	224	• Spray characteristics similar to 5K nozzles
	20	135	130	• Desired flow not obtained, limited by safe operating pressure level of test area
Bete N10W	174	--	289	• Desired flow not obtained, limited by safe operating pressure level of test area
	150	334	269	• Spray characteristics similar to 5K nozzle
	31	150	130	• Spray characteristics similar to 5K nozzle

\*Published or extrapolated value from manufacturer's date

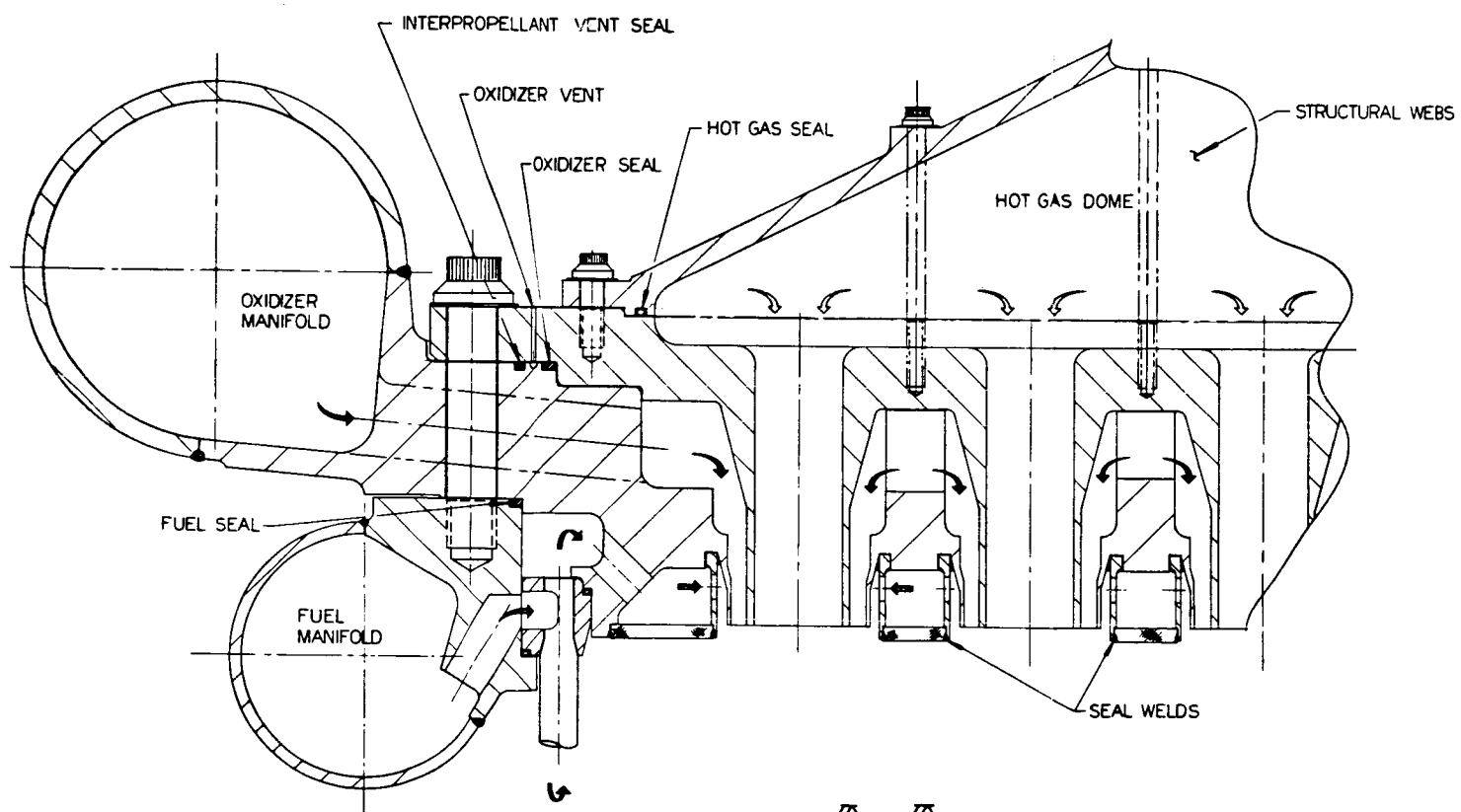
between the actual vs predicted (by manufacturers) pressure drop characteristics; thereby suggesting poor repeatability. Questionable repeatability and streaking were traits which could adversely influence the selection of a commercial nozzle concept for future testing.

#### Injector Configuration 12A

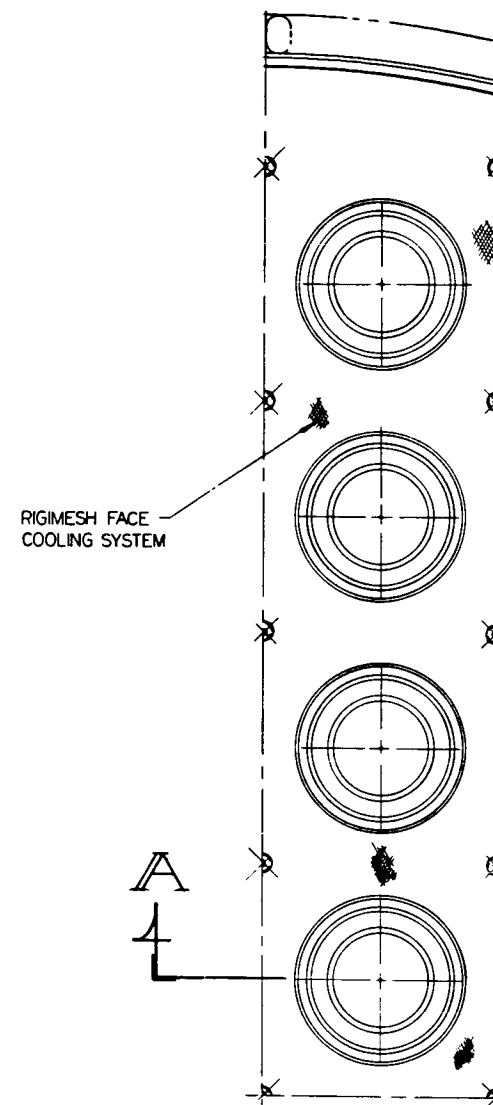
Injector configuration 12A is a splash plate element with hot gas through the center jet, oxidizer through an annulus around the hot gas deflecting from a splash plate into the hot gas, and fuel injected from a series of orifices parallel to the splash plate. The design studies were limited for this configuration because of the potential fabrication and cooling problems.

#### 1000K Design Studies

Conceptual designs for 1000K injectors were prepared using the 20K element size of three promising concepts--the 1A tricentric, the 2C impinging jet, and the 11A commercial nozzle. These conceptual design layouts were to point out the potential problem areas and solutions for packaging, manifolding and fabrication applicable to a full-scale 1000K injector. Element packaging to achieve uniform injection density resulted in 52 elements placed within 42-inch diameter envelope for the 1A and 11A patterns, but required a 52-inch diameter for the 2C impinging jet pattern. In all cases, the injectors were designed around the same basic ground rules; therefore, a close look at one (Fig. 4) is indicative of all configurations.



SECTION A-A



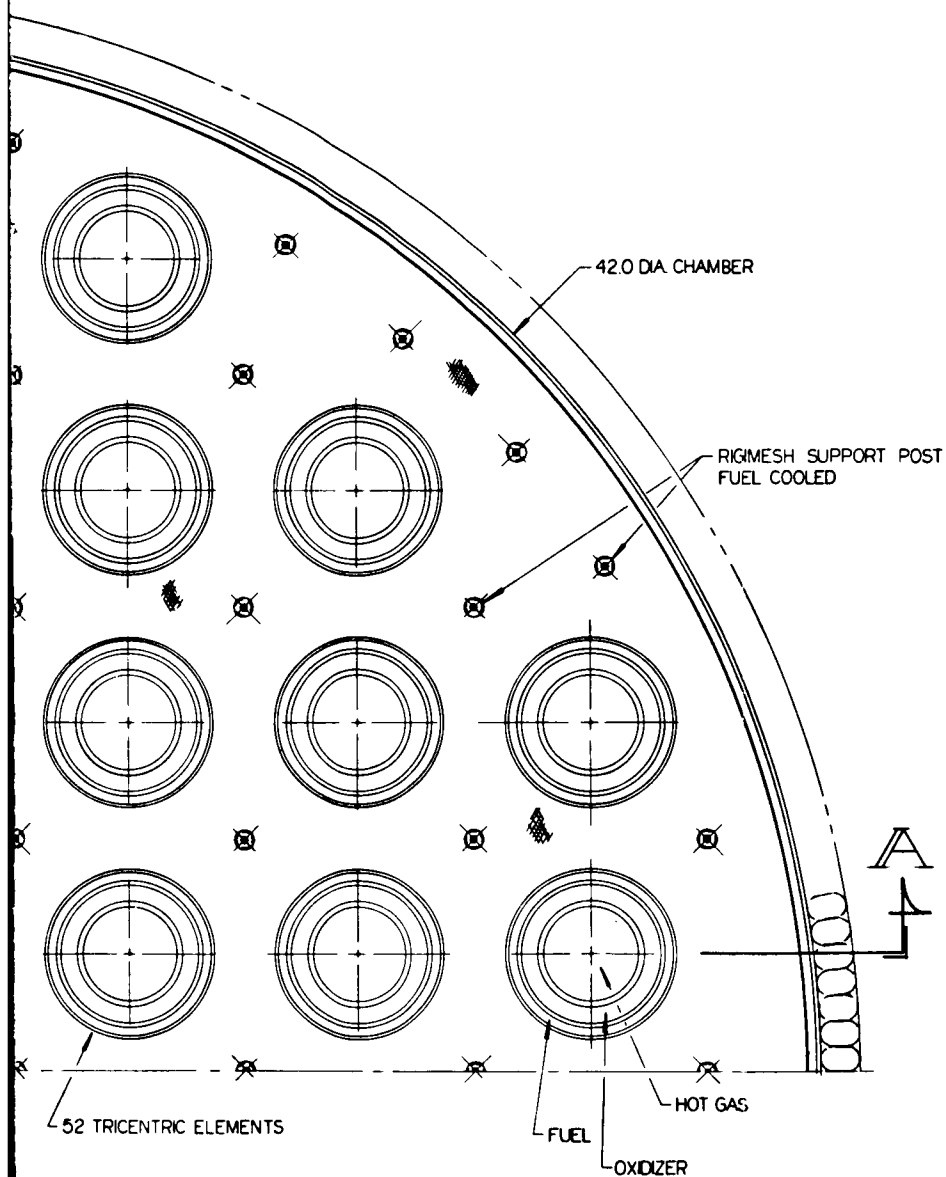


Figure 4. 1000K Injector Concept  
Using Configuration 1A  
Elements

A large casting is the simplest means of providing the main sections of the 1000K injector, but the possibility of porosity, inclusions, or cracks could eliminate this method of approach. Therefore, the backbone section would probably be fabricated from a single forged plate to eliminate the interpropellant welding and to provide a means of structural support. Injection ports, cross-feed manifolding, and attachments for the propellant inlet manifolding would be integrated with the main backbone section. The chamber side of the injector would have full fuel cooling through a Rigimesh face. The back side of the injector would contain a propellant manifold and possibly supports for gimbaling.

Conventional machining techniques and materials could be used to fabricate this type of injector. Fabrication cost estimates were not obtained during these 1000K design studies; however, the costs should be significantly less than similar configurations with many injection orifices.

### Vector Analysis

A momentum vector analysis was conducted to uncover instances of gross momentum flux unbalance with injection concepts employing jet impingement. Momentum unbalance with impinging jets can result in poor atomization, mixing, distribution, and a high risk of injector and/or chamber burning. The observations of this study played an important role during the final stages of the Task I concept screening and provided initial design criteria for the impingement jet patterns evaluated during the Task II cold-flow studies. The analysis included variation of the hot-gas flowrate (i.e., 5, 10, and 15 percent of the total propellant) at rated chamber pressure (500 psia) and throttled (200 psia) conditions. The momentums for this analysis are those given in Table 1 for the 500-psia case, and were

reduced accordingly for the 200-psia case. Results of the analysis were prepared in graphic form so that a greater appreciation can be had for the conditions affecting atomization, mixture ratio, and mass distribution.

Items which were observed during this study, along with an interpretation of their influence on spray characterization, are included below:

1. Momentum relationship of the liquid oxygen with the gaseous fuel and/or hot gas: Careful matching of the momentum ratios is necessary if high performance is to be achieved with large-thrust-per-element loading. Gross momentum unbalance will result in one jet being swept aside by the other, thus precluding uniform mixture ratio and mass distribution.
2. Variability of momentum ratios during throttling: Large excursions in momentum ratios of the impinging jets during throttling are undesirable because this condition is prone to performance and heat transfer variations.
3. Geometrical relationships of the impinging jets: Injection combinations should be avoided which do not permit effective use of the hot-gas force for atomization and mixing because of velocity dissipation or area limitation. Advantageous use of the hot-gas energy is an absolute requirement if performance goals are to be achieved.
4. Approximate jet spray envelope: The resultant primary spray envelope is a useful "tool" for predicting injector face and/or chamber burning potential. Impingement combinations should be rejected which have a high risk for recirculation of oxidizer-rich combustion products across the injector face or chamber walls.

5. Jet diameter relationships: Impinging jets with large diameter ratios do not provide well-developed spray fans because the wider stream tends to overpower the narrow one. This condition should be avoided because of its spray pattern unpredictability and the ineffective use of the jet energy of the large-diameter stream.

To demonstrate the utility of this study, typical graphic displays for element configurations 2A and 2C are included in Fig. 5 and 6, respectively. Figure 7 was taken from an early cold-flow test conducted with water and  $\text{GN}_2$  for a simulated large-thrust-per-element injector. Shown superimposed on the picture are the calculated vector analysis results, indicating remarkably close agreement between the vector analysis employed in this study and experiment.

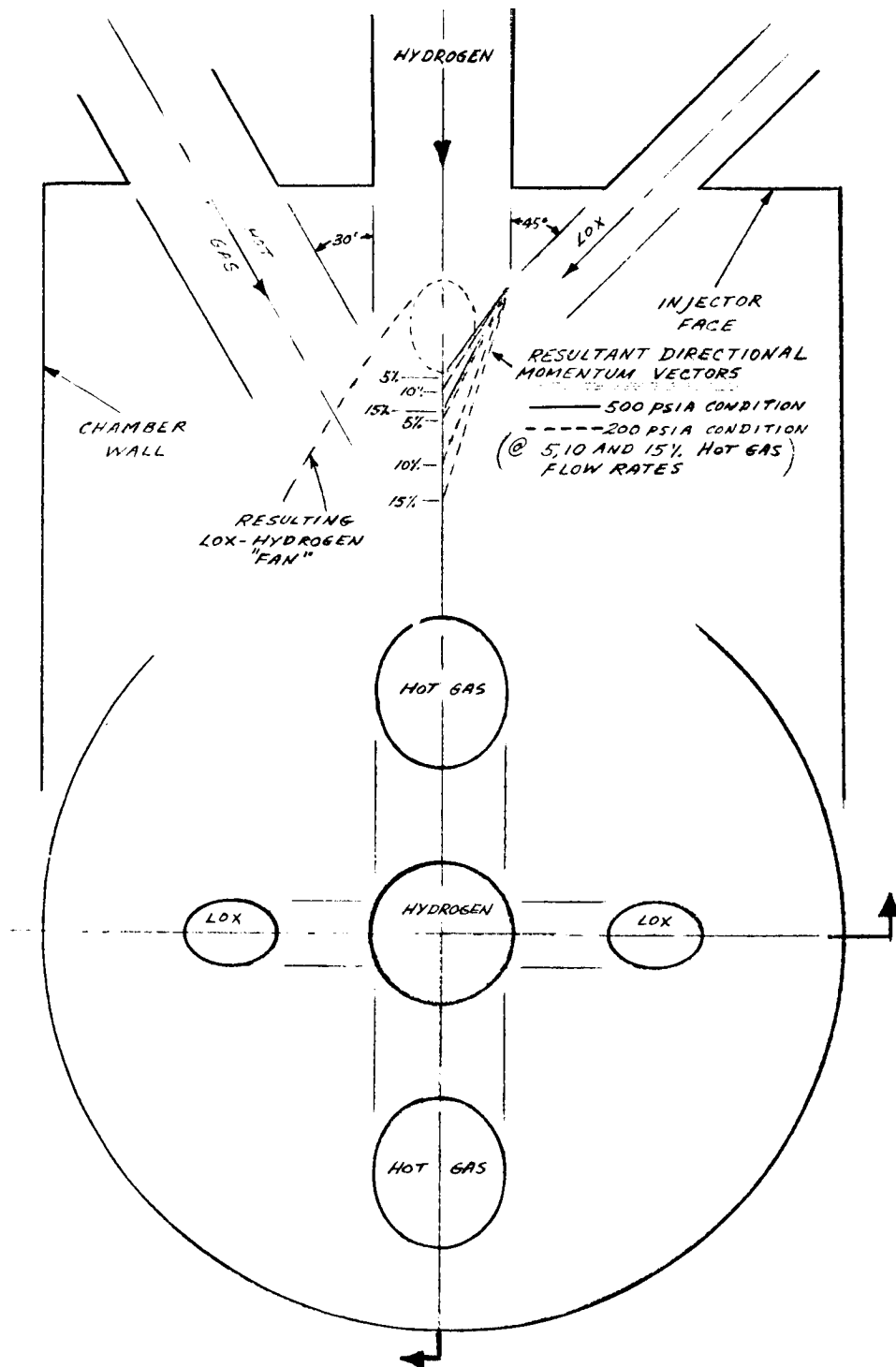


Figure 5. Analytical Spray Characteristics of Configuration 2A Element (20K Thrust)

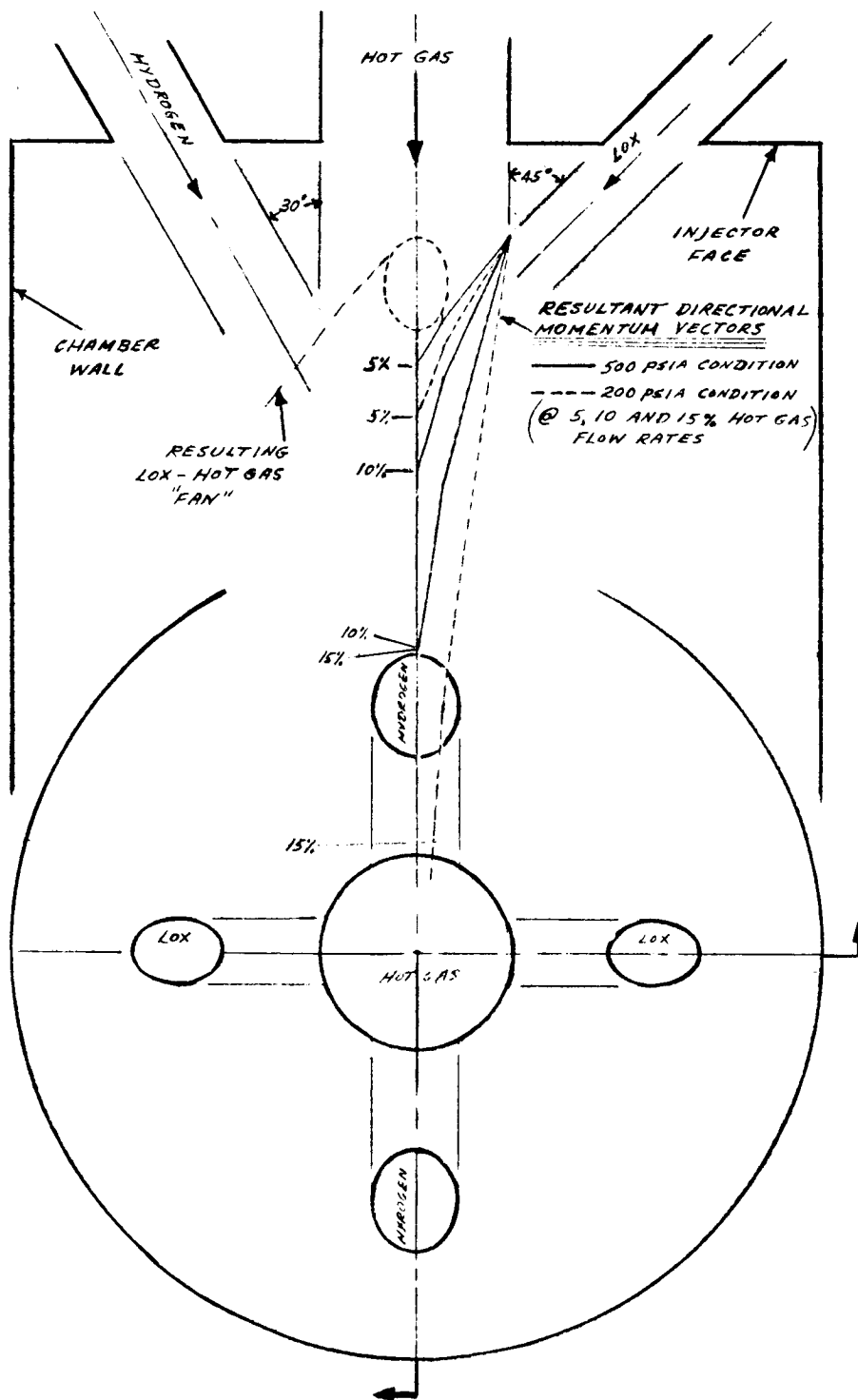


Figure 6. Analytical Spray Characteristics of Configuration 2C Element (20K Thrust)

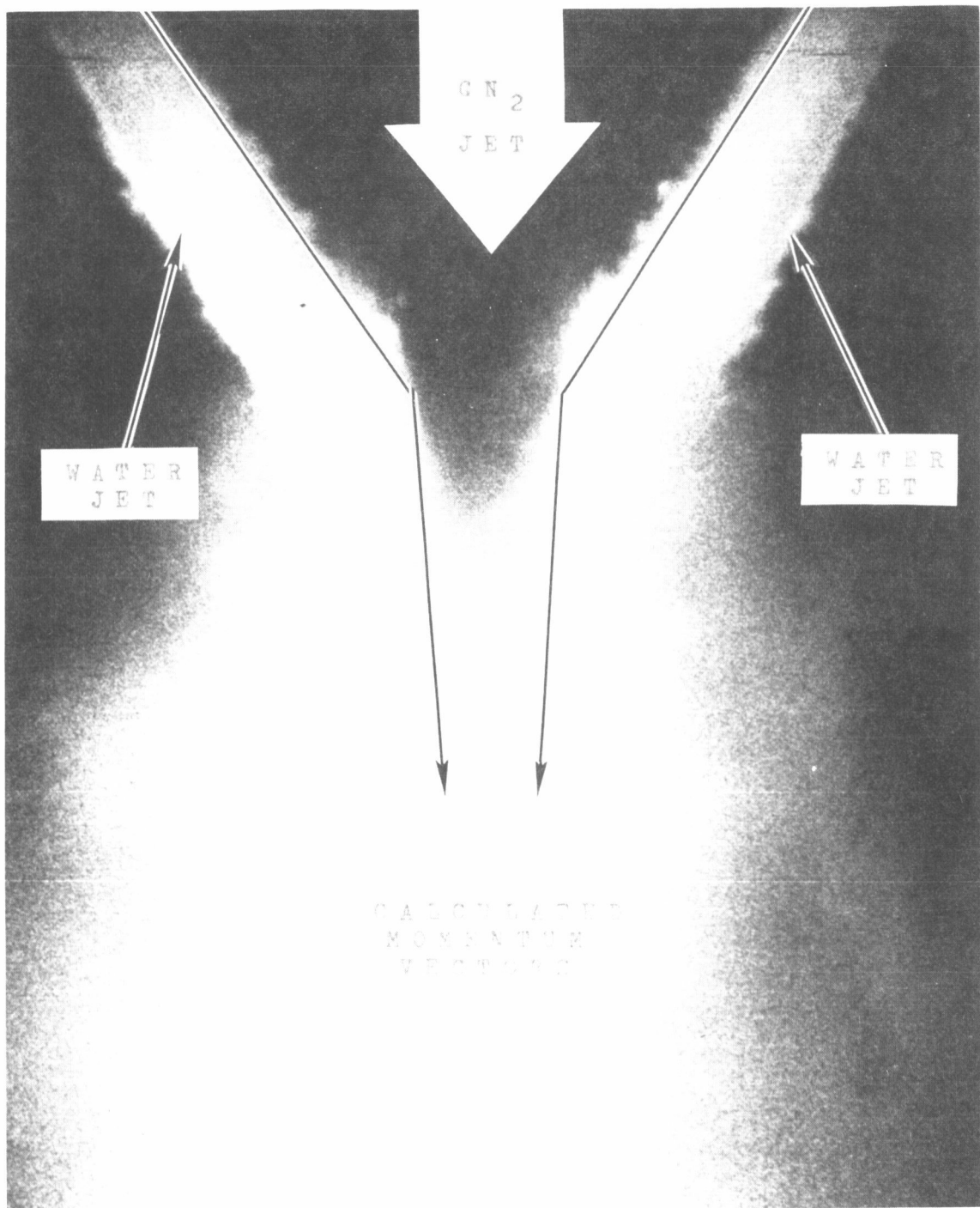


Figure 7. Comparison of Analytical and Actual Spray Vectors

## PERFORMANCE ANALYSIS

Performance analyses were performed during Task I to aid in selecting the types of high-thrust-per-element injectors to be used in succeeding phases of the program. Twenty types of elements were selected initially for consideration (Table 1). General types were as follows:

1. Tricentric elements (Group 1) which extended the familiar coaxial injector concept to include the hot gas
2. Pentad impinging jet elements (Groups 2 and 3)
3. More complex impingement types (4A and 5A)
4. Recessed cup ("two-stage") types (6A, 8A, 9A, and 10A)
5. An annular ring element type (7A)
6. An element using a commercial centrifugal pressure nozzle (11A).

Element 5A was replaced in the analysis by 5B, in which LOX was injected through four annular openings with hot gas in the center of each annulus and fuel in a large central orifice.

The basic approach was to first predict the location or region in the chamber where the LOX stream atomization was accomplished and to predict a corresponding initial droplet size distribution for the resultant LOX spray. Heating, acceleration, evaporation, and, where applicable, secondary breakup of the spray droplets were then considered downstream to a point where the combustion zone was assumed to begin. At this point the performance computer program "CAM"\* was initiated using spray and gas stream parameters calculated at that point. Combustion was considered to be controlled by

---

\*A combustion and mixing program developed previously at Rocketdyne to compute performance.

the LOX vaporization rate. In the "combustion zone" it was postulated that the bulk gas consisted of the thermodynamic equilibrium combustion products with a stagnation temperature equal to the adiabatic flame temperature.

### Primary Atomization

Tricentric Elements. Initial atomization for the tricentric elements and for types 5B and 6A should occur by shearing of droplets from the LOX jet by hot gas. A capillary wave mechanism as used by Mayer (Ref. 1) and discussed by Dickerson and Schuman (Ref. 2) was assumed. This was applied to cylindrical jets or annular jets. The stripping rate per unit area is

$$\dot{w}/A_s = C_A \left( \frac{\mu_\ell \rho_\ell}{\sigma} \right)^{1/3} \left( \rho_g U_r^2 \right)^{2/3} = K_A \left( \rho_g U_r^2 \right)^{2/3} \quad (1)$$

The coefficient  $K_A$ , which depends only on liquid properties, was obtained from an experimental/analytical investigation of another program at Rocketdyne using a LOX/GH<sub>2</sub> engine under conditions similar to those contemplated in this program.

Equation 1 was applied to determine the amount of atomization over a succession of axial increments designated as  $\Delta x$ . The mean diameter of the droplets being formed over each increment was obtained from the equation

$$D \text{ (microns)} = 2.07 \times 10^9 \left( \frac{\mu_l^2 \sigma_l}{\rho_l} \right)^{1/3} \left( \rho_g U_r^2 \right)^{-2/3} \quad (2)$$

Like Eq. 1 this is based on a capillary wave type of atomization. The critical step in successful application of Eq. 1 and 2 to describe the atomization process was to obtain the correct description of the gas velocity profile. This is discussed later in more detail. The atomization calculations for the tricentric elements are described in Appendix A.

Impinging Elements. The equation developed by Ingebo (Ref. 3) to calculate droplet diameters for impinging jets where the point of impingement occurs within a high-velocity gas stream is

$$D_j/D_{30} = 2.64 \sqrt{D_j U_j} + 0.97 D_j U_r \quad (3)$$

where  $D_j$  is expressed in inches and  $U_j$  and  $U_r$  are expressed in ft/sec.

Although the equation was developed for n-heptane it has been found to be qualitatively correct for most propellants. A simple parametric analysis indicates that key physical property ratios (e.g.,  $\sqrt{\sigma/\rho}$ ,  $\left(\frac{\mu}{\sqrt{\rho\sigma}}\right)^{1/2}$ , etc.) for LOX at 185 R temperature do not differ appreciably from those of ambient-temperature n-heptane. Therefore Eq. 3 was used to calculate the volume mean diameter of the sprays formed for the impingement-type injectors Groups 2 and 3, and element type 4A; for element type 7A, and for recessed

impingement-type injectors 8A, 9A, and 10A. When the volume mean droplet size,  $D_{30}$ , was calculated the spray distribution was described by the Nukiyama-Tanasawa distribution

$$\frac{dv}{dD} = \left( \frac{3.915}{D_{30}} \right)^6 \left( \frac{D}{120} \right)^5 e^{-3.915D/D_{30}} \quad (3A)$$

where  $v$  is the volume fraction of droplets with diameter between  $D$  and  $D + dD$ . The maximum droplet size was assumed to be about  $3.5 \times D_{30}$ . However, this assumption may be somewhat conservative; i.e.,  $D_{\max}$  may not be quite this large. In unpublished data Ingebo found  $D_{\max}$  to be 2.25 to  $2.9 \times D_{30}$ . Tanasawa and Tesima (Ref. 4) reported  $D_{\max}$  of 2.56 to  $3.2 \times D_{30}$ .

To apply Eq. 3 and 3A, it was necessary to know how far down the chamber the sheets, ligaments, and globs initially break into LOX droplets. Clarke (Ref. 5) was successful in correlating the degree of breakup of a liquid jet (water) in a gas cross stream by a dimensionless group  $\epsilon$  where

$$\epsilon = \frac{\rho_g}{\rho_l} \left( \frac{Vt}{D_j} \right)^2 \quad (4)$$

where  $V$  is the magnitude of the vector difference between the gas and liquid velocities and  $t$  is the time of exposure. For complete disintegration of the jet into spray,  $(\epsilon)^{1/2}$  was found to be about 4 (Ref. 5). To apply Eq. 4 to predict the "breakup location," the time  $t$  was replaced by breakup distance  $L_B$  divided by the axial component of the liquid jet velocity, so

$$L_B/D_j = \epsilon^{1/2} (\rho_l/\rho_g)^{1/2} (U_l \cos \theta) / |U_g - U_l| \quad (5)$$

For the subject analysis it was assumed that Eq. 5 was valid; however, the coefficient  $(\epsilon)^{1/2}$  was re-evaluated after reviewing unpublished Rocketdyne data (from another program) taken from high-speed photographs of liquid jets impinging in high-velocity gas streams. Gas velocities ranged from 800 to 1100 ft/sec with liquid velocities of 15 to 25 ft/sec (Clarke's (Ref. 5) maximum gas velocity was 430 ft/sec). The value of  $\epsilon^{1/2}$  thus obtained by applying Eq. 4 was 7.5. Further examination of the unpublished data revealed that breakup was appreciably slower under conditions where the gas stream momentum was so much greater than the liquid jet momentum that liquid-liquid impingement was prevented from occurring. For these extreme conditions, the value of  $(\epsilon)^{1/2}$  was about 20. During another program, criterion for a satisfactory momentum ratio was developed as:

$$\frac{\left(D_j \rho U^2\right)_{\text{gas}}}{\left(D_j \rho U \cos \theta/2\right)_{\text{liq.}}^2} \leq 4.47 \quad (6)$$

where  $\theta$  is the included angle between the liquid jets. Application of Eq. 6 led to a preference for 10 percent (rather than 15 percent) hot gas in element type 2C. The results of Eq. 6 tended to agree with the vector analysis previously discussed.

Commercial Spray Nozzles. Nelson and Stevens (Ref. 6) were successful in correlating spray distribution for commercial centrifugal pressure nozzles. Assuming a square root normal distribution, they empirically correlated the volume median diameter  $\tilde{D}$  and the standard deviation  $s$  by log-log plots of:

$$\left(\tilde{D}/D_o\right) \text{ vs } \left[Re (We/Re)^{0.55} (\tan \phi_m/2)^{1.2}\right]$$

and

$$\left( \frac{s}{\sqrt{D_o}} \frac{We}{Re} \right) \text{ vs } \left[ \left( \frac{W}{Re} \right) Re^{1/2} \right]$$

where  $\phi$  is the experimentally observed maximum included angle of the spray. The Reynold's and Weber's numbers are based on the average axial velocity of the liquid as it leaves the orifice. To calculate this velocity it is necessary to subtract the air core area from the geometrical orifice area. Nelson and Stevens (Ref. 6) presented an empirical correlation of:

$$D_a/D_o \text{ vs } \phi_m$$

where  $D_a$  is the diameter of the air core. The average axial velocity then is obtained by

$$\bar{U}_{l,x} = \frac{\dot{w}}{\rho \pi (D_o^2 - D_a^2)} \quad (7)$$

where  $D_o$  is the diameter used in calculating  $Re$  and  $We$ . The volume median diameter  $\tilde{D}$  and the standard deviation  $s$  when applied in the square root normal distribution, completely describe (Ref. 6) the spray droplet sizes. For convenience, a graphic correlation was presented in Ref. 6 to compare the Santer mean diameter of  $D_{32}$  with  $\tilde{D}$  and  $s$ .

For the subject analysis of element type 11A, the correlations of Ref. 6 were used. For easier application, the volume mean diameter was assumed to be approximately equal to  $D_{32}$  and the Nukiyama-Tanasawa distribution was used. Because of the high injection velocities, the median droplet

sizes were smaller than those observed in Ref. 6 and it was necessary to extrapolate their correlating curves to higher Reynolds numbers.

It was also necessary to determine where the sheets and ligaments emanating from the centrifugal nozzle would be broken into drops. To do so, the dimensionless group given by Eq. 4 was used with  $D_j$  in Eq. 5 replaced by the liquid sheet thickness. Also, the coefficient  $\epsilon^{1/2}$  was re-evaluated from the high-speed photographs and data obtained by Squire (Ref. 7) with centrifugal nozzles, and was found to be about 9.3.

The effect of the gases on spray from centrifugal nozzles was handled by considering that the gases caused secondary breakup of the initial spray. This was necessary because the correlations used (Ref. 6) do not consider injection into a moving gas stream.

#### Gas Velocity Profile

The equations describing atomization rates, mean droplet sizes, and breakup distances all contain the relative gas-to-liquid velocity. Thus an adequate description of the gas velocity profile is essential to a successful description of the atomization process. The gas velocity will be attenuated primarily by spreading and entrainment of stagnant or recirculating gas and by momentum exchange with the LOX spray. In discussing the axial gas velocity profile, the primary interest for these analyses was in the velocity of the gas within the streamlines acting to atomize the LOX. Thus the description of this velocity profile was handled differently for different types of injector elements.

Showerhead LOX Jet Atomized by Shear of a Surrounding Gas Stream. This is analogous to the conventional LOX/GH<sub>2</sub> coaxial injector element. The gas velocity profile was assumed to be similar to that observed during another Rocketdyne program, and is described in Appendix A. This model applies to element types 1B, 1D, and with some modifications to 1C and 6A.

Annular LOX Jet Atomization by Shear of the Gas Stream Within the Annulus. This is applicable to 1A, 5A, and 1C. Frictional drag by the liquid annulus was found to have negligible effect on the gas momentum. Therefore assumption of constant static pressure (upstream of the flame zone) made it possible to assume constant momentum for the gas-plus-entrained-spray at any axial position within the annulus. Initially, for a conservative estimate of the gas velocity, a stepwise atomization calculation was performed in which it was assumed that the droplets formed over all previous increments were moving at the gas velocity. Cooling of the gas by droplet evaporation was initially neglected. Subsequent calculations where the acceleration of representative droplet sizes was calculated by a droplet drag equation indicated that the previously calculated gas velocity profile was satisfactory. Apparently the effects of having some small droplets traveling at higher velocity than the (decelerating) gas while larger droplets had velocities below that of the gas tended to counterbalance each other.

Gas Jets Impinging With LOX Jets. This applies to the impingement elements (Groups 2 and 3) as well as to elements 4A and 7A. The first step was to describe the gas velocity profile as it would be in the absence of the liquid. Subsequently, the interaction of the liquid and gas streams and the resulting alteration of the gas velocity were considered. Schlichting (Ref. 8) describes the velocity along the axis of a turbulent free gas jet by

$$U_m/U_{inj} = 2.11/n \quad (8)$$

where  $n$  is the number of orifice diameters downstream from the point of injection. The equation is valid only where  $n$  is large enough for similarity to hold; i.e., where the stream "appears" to emanate from a point source. There is apparently some contradiction in the appropriate value for the coefficient 2.11. If Schlichting's description is followed for obtaining Eq. 8, by analogy with his derivation for the laminar case, the results is  $2.11\pi$ . Shih-I Pai (Ref. 9) also obtains  $2.11\pi$ . However, Abramovich (Ref. 10), through comparison with experimental data, finds the coefficient to range from about 2 to 5. To be conservative with regard to gas velocities, Eq. 8 would be used as written. A serious problem with trying to use Eq. 8 was that it is obviously invalid within two or three jet diameters of the injector. Furthermore, for many elements in the subject analyses this region is very important.

An alternate solution was suggested by the fact that under a wide range of conditions free gas jets tend to expand at about a 7-degree angle. For these analyses such an expansion was assumed. Application of continuity (assuming constant density) to such an expanding jet provided a "mass flux-mean" velocity profile. Equation 9 was obtained and used to predict the gas velocity profile, subject to subsequent alteration by interaction with spray.

$$U_g/U_{inj} = \frac{1}{1 + x/0.232} \quad (9)$$

Equation 9 predicts lower gas velocities than Eq. 8. This is in accord with the desire to use conservative estimates of gas velocities.

Further attenuation of the gas velocity through momentum exchange with the spray was predicted by first calculating the relative velocity of

the gas,  $U_r$ , as it first contacts the spray and by then estimating the amount of acceleration of the drops at successive positions in the chamber. The droplet drag equation (Eq. 10) was applied to several representative droplet sizes in the spray to aid in the estimation.

$$dU_d/dt = \frac{9 C_D \rho_g U_r |U_r|}{\rho_d D} \quad (10)$$

Two-Stage or Recessed Cup Elements. These elements were treated in a manner similar to those in Group 3 downstream of the injector face. However, continuity was applied to predict the gas velocities within the recessed cup because it was assumed to flow full.

#### Secondary Droplet Breakup

Secondary breakup of droplets was considered upstream of the flame front or combustion region. (Within the combustion region where the performance computer program "CAM" was used, secondary breakup was not considered. This would tend to make performance predictions conservative.) To describe secondary breakup near the injector, models developed by Coultas and Dickerson (Ref. 11), Wolfe and Anderson (Ref. 12), and Morrell (Ref. 13) were considered. All of the models were semiempirical and all predicted the breakup time  $t_B$  for a given droplet size, relative gas velocity, and gas and liquid densities, viscosities, and surface tension.

The model used by Morrell was selected for use in these analyses for the sole reason that it was the most conservative; i.e., it predicted a longer breakup time. This model was used in the following form:

$$t_B = 1.91 \left( \frac{\rho_l}{\rho_g} \right)^{2/3} \left( \frac{\mu_g}{\mu_l} \right)^{1/3} \frac{D_b}{U_r} \frac{Re^{3/4}}{(2 We)^{1/2}} \quad (11)$$

The model was based on atomization by stripping of a liquid boundary layer and was correlated by high-speed streak and framing photographs of a water jet subjected to a transverse shock wave in air. In Eq. 11, the relative gas velocity must be substituted for Morrell's gas velocity because in his experiments the liquid had no velocity component in the direction of the gas velocity.

The major difficulty in applying Eq. 11 is that  $U_r$ , the relative velocity, is continually changing. It was necessary to employ it by iteration with the following steps:

1. The region over which breakup was expected to occur was estimated
2. The arithmetic average  $U_r$  over the region was calculated and inserted in Eq. 11 to calculate  $t_B$
3. The droplet velocity and  $t_B$  was used to check the estimated breakup location
4. The previous steps were repeated until the predicted and calculated breakup locations converged.

To aid in these calculations, curves were generated by Eq. 11 and breakup distance (for given droplet velocities) were plotted against the average  $U_r$  with initial droplet size as a parameter. For fixed liquid and gas densities, viscosities, and surface tension, the breakup time varies as  $(D_b^{1.25}/U_r^{0.75})$ .

To determine the size of the droplets resulting from secondary breakup, Coultas and Dickerson (Ref. 11) used the criteria:

$$We/\sqrt{Re} \leq 1 \quad (12)$$

Wolfe and Anderson (Ref. 12) used:

$$D_{30} = \left( \frac{136 \mu_l \sigma^{3/2}}{\rho_l} \right)^{1/3} \frac{D_b^{1/6}}{(\rho_g U_r^2)^{4/3}} \quad (13)$$

Both equations predicted droplet sizes of 1 micron or less for the conditions found in the subject analyses, so for all practical purposes the droplets that undergo secondary breakup could be considered to be vaporized.

#### Droplet Vaporization

Acceleration, heating, and vaporization of droplets upstream of the combustion zone were considered by using a computer program "DAV."\* This program is mathematically based on a spherically symmetric liquid droplet immersed in combustion gas. The liquid temperature is uniform throughout the droplet and the gas stream is large enough not to be affected by the droplet. The descriptive equations are similar to those previously used by Priem (Ref. 14). The droplet acceleration is described in Eq. 10 with the drag coefficient depending on the Reynolds number according to

$$\begin{aligned} C_D &= 27 \operatorname{Re}^{-0.84}, \quad 0 < \operatorname{Re} \leq 80 \\ &= 0.271 \operatorname{Re}^{0.217}, \quad 80 < \operatorname{Re} \leq 10^4 \\ &= 2.0, \quad \operatorname{Re} > 10^4 \end{aligned} \quad (14)$$

The equation used in the "DAV" program to describe simultaneous heat and mass transfer may alternatively be obtained from Bird, Stewart, and

---

\*Droplet acceleration, vaporization, and heating program developed previously at Rocketdyne.

Lightfoot's (Ref. 15) "film theory" wherein there is a net transport of only one component across the film. The equations for the liquid temperature are

$$\frac{dT_\ell}{dt} = \frac{6(144)}{C_{p,\ell} \rho_\ell D_d^2} \left\{ k_m (T_g - T) \left( \frac{z}{e^z - 1} \right) \frac{Nu_h}{3600} - \frac{(144) D_v M_\ell H_v P Nu_m}{RT_m} \ell_n \left( \frac{P}{P - P_v} \right) \right\} \quad (15)$$

where

$$z = \frac{(144) (3600) D_v M_\ell C_{p,v} P Nu_m}{k_m RT_m Nu_h} \ell_n \left( \frac{P}{P - P_v} \right) \quad (16)$$

and the equation for the vaporization rate is

$$\dot{w}_v = \frac{dW}{dt} = \frac{(12) \pi D_v D P M_\ell Nu_m}{RT_m} \ell_n \left( \frac{P}{P - P_v} \right) \quad (17)$$

Equations 10 and 14 through 17 were converted into finite difference form for use in the computer program. A simple step-ahead method was initially used for calculating droplet properties over axial distance increments. A difficulty was encountered in that for small droplets (especially less than 50 microns in diameter) the droplet temperature tended to oscillate after the "wet bulb temperature" was initially reached. The program was changed to use a predictor-corrector method of calculating droplet diameter and temperature changes, but the oscillation was still not completely eliminated. Nevertheless, it is expected that the overall vaporization rates calculated were essentially correct. One other alteration in the program was accomplished to permit insertion of a series of droplets at arbitrary axial locations as input data for use in a single execution of the program.

The DAV program does not consider the gas stream to be affected by the droplets; i.e., the gas stagnation temperature and pressure are considered to be constant and the gas velocity-distance profile is part of the input data. For injector element type 1A a sort of iteration was performed in that the gas stream composition, velocity profile, and "mean" stagnation temperature were altered to reflect the effect of heat, mass, and momentum transfer with the spray for successive reruns of the program. The results obtained differed little from those initially calculated.

#### Location of the Start of the Combustion Zone

According to results of previous Rocketdyne studies the location of the flame front depends on the satisfaction of two criteria:

1. The mixture ratio must be greater than approximately 1.0 for the gases to be flammable.
2. The axial gas velocity must not exceed that of the turbulent flame velocity, which is typically on the order of 250 ft/sec in LOX/GH<sub>2</sub> with a chamber pressure near 500 psia.

Results of a previous hot-gas ignition study were used to predict that spontaneous ignition of H<sub>2</sub> and O<sub>2</sub> will occur when mixtures whose mixture ratio exceeds approximately 1.2 are heated to 1500 R or greater. Although the necessary conditions may be readily satisfied locally, adjacent to LOX droplets or jets, it was previously found that the flame front apparently did not creep upstream (adjacent to the LOX jet) beyond the location where the ignition criteria were satisfied in the bulk gas.

In the subject analyses the combustibility criteria listed above were used as a general guide in predicting the axial location at which the combustion should begin; i.e., the position at which the combustion computer program should be initialized. It is emphasized that these criteria served only as a general guide because the injection of hot gas (1660 R) and the probability of more extensive recirculation of gas from the combustion regions should both be expected to promote earlier ignition. Recirculation effects were considered only qualitatively.

In several cases the performance computer program was initiated slightly upstream of the location where the gas velocity matched the turbulent flame velocity. This is not expected to cause appreciable error because the high-velocity hot gas is essentially as effective as chamber combustion gases in vaporizing the LOX.

#### Combustion Zone

The performance computer program "CAM" was derived specifically for a LOX/GH<sub>2</sub> coaxial injector, so the precombustion zone portion of the program had to be removed. Initial conditions describing the gas composition, velocity, stagnation temperature, etc. and the spray distribution and droplet velocities at the start of the combustion zone were obtained by the calculation procedures described above. The "CAM" program could consider two parallel-flowing gas streams, only one of which could contain spray. Mixing between the streams was simulated by the program, but it was necessary to insert a "mixing length" into the program as data. Estimates of the mixing length of coaxial gas streams were obtained by examination of available results of gas-phase mixing calculations performed during other programs at Rocketdyne.

However, to accurately describe the gas phase mixing it would be necessary to run the "mixing" computer programs specifically for each case in the subject analyses, which was beyond the scope of work in this program.

Complete mixing of the gases was assumed within each of the two gas streams. Within the stream containing spray all the gases were assumed to react locally to maintain "thermodynamic equilibrium stagnation conditions, dependent (for a given range of chamber pressures) only upon the local gaseous propellant mixture ratio". Combustion gas properties were obtained from frozen thermodynamic equilibrium performance calculations using the Rocketdyne n-element program (Ref. 16) and were made available to the computer as tabular arrays. For the gas stream containing no spray, combustion was assumed to occur only if the mixture ratio exceeded 1.0. Otherwise the gas stagnation properties were assumed to be invariant.

The spray was represented by up to 12 distinct size groups. The ballistics of the drops were determined by Eq. 10 and 14, while droplet heating and vaporization were calculated from different equations derived from Eq. 15 through 17. Droplet breakup was not considered in the combustion zone. Oxygen vapor emanating from the LOX droplet was assumed to mix and react with the surrounding gases immediately.

The chamber geometry was presented as input data to the program. The chamber was assumed to "flow full" from the initiation of the combustion zone. The distribution of area between the two streams was obtained by iteration using the perfect gas law, isentropic expansion equations, and continuity and conservation of momentum equations.

### Performance Calculations

Input parameters for each injector included the fixed overall mixture ratio (5.0), total propellant injection rate (60.78 lb/sec), injector end chamber pressure (500 psia), and nozzle contraction ratio (2.0) thereby assuming the combustion efficiency. For a given injector, one of these conditions would be redundant, as exemplified by the calculated local Mach number at the geometric throat being, in general, different from unity. To actually calculate the  $c^*$  efficiency, it would be necessary to iterate, say with the injection rate, until sonic gas velocity was obtained at the throat. For relative comparison of the candidate injector concepts, however, such iteration was avoided by rating the injector element types according to the calculated relative mach number at the throat with the same initial conditions, i.e., a fixed propellant feed rate and injector-end chamber pressure.

### Performance Analysis Results and Discussion

The Task I performance analysis was performed considering the 20K elements only. It was generally assumed that 15 percent of the propellants were to be injected as hot gas. The exceptions were configurations 2C with 10-percent hot gas and configurations 1C, 1D, and 3B with 5-percent hot gas. In these cases equal or better performance was expected with less than 15-percent hot gas.

Table 4 summarizes some of the more significant results of the analysis. The performance index shown is based on relative gas Mach number in the throat with the designed injection rate and chamber pressure. Actual  $c^*$  calculations would require iteration of the injection rate to force sonic velocity at the throat.

TABLE 4

PREDICTED INJECTOR PER

Injector Configuration	Initial LOX Breakup			Location of Complete LOX Vaporization, inches from injector	Nozzle Thro	
	Location From Injector, inches	Percent Atomized	Volume Mean Droplet Diameter ( $D_{30}$ ), microns		Unvaporized LOX, percent	
1A	5.6	100	26.6	10.1	0	
1B	13.2 (Nozzle Start)	11.6	---	---	---	
1C	10.0	76.2	41.7	---	---	
1D	---	---	---	---	---	
2A	8.9	100	50.1	---	0.27	
2B	---	---	---	---	---	
2C	8.9	100	20.1	9.5	0	
3A	3.8	100	10.7	3.9	0	
3B	---	---	---	---	---	
3C	---	---	---	---	---	
3D	---	---	---	---	---	
4A	4.9	100	538*	---	59.9*	
5B	2.8	100	26.6	6.0	0	
6A	5.0	38.5	20.0**	---	28.1	
7A	1.7	36.7	18.2	---	15.5	
8A	2.0	100	13.8	2.1	0	
9A	2.0	100	13.8	2.1	0	
10A	1.4	100	6.6	5.1	0	
11A	4.8	25.4/74.6***	10.0/59.5***	---	0.14	
12A	---	---	---	---	---	

NOTE: All configurations analysed at the 20K thrust size and 15-percent hot-gas flowrate unl

# PERFORMANCE

Test Conditions		Performance Index	Remarks
Unmixed Fuel, percent	Stagnation Pressure, psia		
59.7	473	0.57	Performance limited by gas-phase mixing
---	---	---	Analysis stopped: 88.4 percent of LOX not atomized at nozzle entrance
---	---	---	Analysis stopped: initial LOX breakup completed in nozzle; 5 percent hot gas used
---	---	---	Analysis stopped: atomization inferior to 1B
0	469	0.95	
---	---	---	Large LOX core similar to 1B; inferior to 2A and 2C
0	470	1.00	Results based on 10 percent hot-gas flowrate
52.7	502	0.75	Performance limited by gas-phase mixing
---	---	---	Hot-gas momentum ineffective in atomizing LOX; 5-percent hot gas used
---	---	---	Large LOX core similar to 1B and 2B; inferior to 3A
---	---	---	Large LOX core similar to 1B and 2B; inferior to 3A
0	483	0.32 to 0.75	*Pre-flame front evaporation of LOX not included (this should raise index to ~0.75)
0	472	0.97	5B similar to 5A except hot gas is used inside LOX in outer jets
45.9	495	0.51	** $D_{\max}/D_{30} \cong 18$ , not Tanasawa-Nukiyama distribution
0	452	0.80	
0	482	0.96	
0	482	0.96	
0	472	0.91	Performance limited by gas-phase mixing
6.5	460	0.94	***25.4 percent of drops shattered by hot gas ( $D_{30} = 10.0$ ), remainder by influence of liquid velocity
---	---	---	Not analysed

Unless otherwise noted

Where initial calculations (e.g., primary atomization calculations) indicated one or more injector types to be significantly inferior to similar elements within the same group, the analysis was discontinued short of the computer performance calculations.

Primary emphasis in the analyses was placed on atomization, evaporation, breakup, and combustion of LOX. Where the high velocity and high temperature of the hot gas were applied effectively, the calculated droplet sizes were quite small (volume mean droplet diameters often on the order of 10 to 20 microns) and evaporation was rapid. Thus, gas-phase mixing was indicated to be the ultimate limiting factor on performance. Notable examples of this are element types 1A and 3A. This possibility was foreseen early in the analysis, and the performance computer program originally proposed was replaced by one which considers mixing between two concentric streams, one of which was allowed to contain a spray. The gas-phase mixing was assumed to occur linearly at the rate established by an estimated "mixing length". The results obtained by the subject analyses for the various injector element types illustrated in Table 1 are discussed below.

Tricentric injector elements 1B and 1D have a central cylindrical LOX jet in the core which is atomized primarily by shear of surrounding gas streams. The atomization rate was insufficient to accomplish complete breakup of the large (1.6-inch diameter) jet upstream of the chamber exhaust nozzle. For instance, with element 1B the jet diameter was predicted to still be in excess of 1 inch at the nozzle entrance. On the other hand, the annular LOX jet of element 1A was expected to be completely atomized (primarily by the central hot gas jet) within 6 inches of the injector face. The same stripping (atomization) mechanism was assumed in each of these cases. The advantages of element 1A over 1B and 1D can be understood qualitatively as follows:

1. The initial gas/liquid interface area is greater.

2. The gas is partially confined by the liquid and thus its velocity is maintained for a greater distance.
3. Decay of the gas velocity is almost entirely due to momentum exchange with the spray it produces (i.e., it is not expended by mixing with and accelerating surrounding "stagnant" gas).
4. As the gas velocity decreases, the annulus inside diameter increases, thus increasing the gas/liquid interface area.
5. The gas/liquid interface area for the central LOX core elements decreases as LOX is stripped from the surface.

Element 1C also has an annular LOX jet; however, the cool, lower-velocity  $\text{GH}_2$  inside the LOX is less effective than the hot gas as an atomizing agent. The hot gas in this case (outside the LOX) loses much of its momentum by expanding and mixing with surrounding "stagnant" gases. As a result of 5 to 10 percent of the LOX was calculated to be still "unatomized" at the nozzle entrance.

On the basis of the atomization comparison, element 1A was clearly indicated to be the superior tricentric element. The LOX droplets formed by this element were expected to be quite small, with a mean diameter of 26.6 microns and a maximum diameter of only 116 microns. Performance calculations indicate that these drops would be completely evaporated within the chamber. Performance is limited, however, by relatively poor gas-phase mixing between the LOX-rich central combustion gas stream and the surrounding mantle of  $\text{GH}_2$ . It should be noted that the gas-phase mixing analysis was less quantitative than the atomization, vaporization, and combustion analyses so the predicted relative performance index for element 1A (57 percent) may be too conservative. Consideration should be given to minor injector modifications that could force the  $\text{GH}_2$  to

mix more effectively with the spray-bearing gases in the center of the element and therefore make this element more attractive from a performance standpoint.

Although the atomization mechanism was not the same for the impingement elements and the tricentric element, preliminary estimates indicated again that those with a large, single, showerhead LOX jet would not be effectively atomized. This included elements 2B, 3C, and 3D. With elements 2A and 2C, complete atomization should take place within the chamber and the mean droplet sizes should be quite small (50 and 20 microns, respectively), however, it should be remembered that alignment of the liquid and gas jets is quite critical for these elements. Even a very slight misalignment could cause some of the liquid to "miss" the high-velocity gas streams, leaving some very large droplets or ligaments. For element 2C it was found necessary to limit the hot gas to 10 percent, thus giving it a lower injection velocity to permit impingement of the two LOX jets. In comparing this element with 2A it should be noted that a smaller percentage of the propellants are "precombusted". Gas-phase mixing, although more difficult to estimate, should be considerably better for 2A and 2C than for element 1A.

Element 3B was eliminated by qualitative considerations; it is evident by inspection that this concept makes very little use of the hot-gas stream.

Element 3A was the only one of Group 3 to merit serious quantitative consideration. It should be quite effective from the standpoint of atomization, breaking the LOX into spray within approximately 4 inches of the injector face. The calculated mean droplet size was extremely small. However, this element suffers (like 1A) from poor gas-phase mixing.

Element 4A is one of the more complex elements. Initial observations of the design lead to some optimism with regards to atomization and mixing, but a three-dimensional model pointed out some severe disadvantages which subsequently were verified in the calculations. The LOX doublets impinge in a very low gas velocity region, so that very large droplets are formed in the primary atomization. Some of the spray enters the cold  $\text{GH}_2$  stream directly. The remaining spray passes briefly into the hot-gas stream but does not remain there long enough for secondary breakup to occur. As a result the predicted performance for element 4A was low. However, it should not be quite as low as indicated in Table 4 because LOX vaporization upstream of the flame zone and secondary breakup within the combustion zone were not considered. Nevertheless, comparison with analyses of other elements indicated that its performance would be significantly lower than the best six or seven concepts.

In the analyses, element 5A shown in Table 1 was replaced by the more promising "5B" with LOX in the four annular orifices surrounding hot-gas jets. These annular streams impinge over the central showerhead  $\text{GH}_2$  jet. Atomization occurs primarily by the same mechanism as tricentric element 1A, but because of the smaller orifices it occurs more rapidly; i.e., within 3 inches of the injector face. Gas-phase mixing with the fuel should be no problem. The relative performance index calculated for element 5B was 97 percent.

Element 6A contains three relatively large showerhead LOX jets (each approximately 0.6 inch in diameter) in addition to the LOX injected between the hot-gas tubes. The LOX injected between the tubes should react rapidly, but the atomization of the three showerhead jets was calculated to be incomplete at the start of convergence (nozzle entrance). The atomization mechanism of these jets was considered to be analogous to that of element 1B.

The relative performance index of element 7A was 80 percent. The many LOX jets were quite small; however, the problem was that they passed through the hot-gas stream too rapidly to permit complete atomization. It is possible that redesign to keep the liquid within the gas stream for a longer time would significantly improve the performance.

The recessed elements 8A and 9A were essentially indistinguishable as far as the analysis was concerned. A possible difference was that local ignition around individual droplets is more probable with 8A. The analysis treated ignition as occurring at a certain "flame front". This is probably of no serious concern as regards performance because excellent atomization, mixing, and combustion were predicted for these elements even in the absence of localized burning within the recessed cup. The relative performance indexes were 96 percent. The LOX jets were recessed in element 10A (although less than for 8A and 9A), but the fuel orifices were in the injector face. Gas-phase mixing and LOX vaporization occurred more slowly than for 8A and 9A. The relative performance index was 91 percent. The gas/liquid momentum ratio for all three of the recessed cup elements (8A, 9A, and 10A) was high enough to make it somewhat questionable as to whether the liquid jets would actually impinge. If this proves to be true it may be necessary to drop the hot gas from 15 to 10 percent, in which case performance should still be high.

The commercial nozzle (11A) was calculated to yield a bimodal distribution of drops. Approximately 25 percent are expected to be obtained via shear stripping of very small droplets from the liquid sheets (which emanate from the nozzle) by the hot gas, resulting in a very fine spray (mean diameter  $\sim 10$  microns). The remainder was considered to undergo breakup primarily under the influence of the liquid velocity (hydraulic atomization), but was still calculated to give a moderately fine spray ( $D_{30} \sim 60$  microns). Approximately 10 to 12 percent of the fuel was predicted to be unmixed at the nozzle

entrance and this limited the calculated relative performance index to 94 percent, which is still quite high.

The splash plate injector (12A) was rejected because of potential fabrication and cooling disadvantages, therefore it was not quantitatively analyzed for performance.

## INJECTOR RATING AND SELECTION

Injector rating procedures were generated to aid in selecting the four most promising injector concepts for Task II cold-flow studies. The 20 injector concepts initially selected (depicted in Table 1) were rated first with regard to characteristics listed in the rating category column of Table 5. This table also lists the primary tools which were available to guide the injector ratings. A weighting factor was assigned to each of the rating categories so those categories which were more "important" and more "confidently" rated would carry more influence.

Rating results, based on the categories listed in Table 5 (without performance), are shown in the composite rating column of Table 6. These ratings were accomplished by individuals closely associated with the program. The numbers listed are the sum of each individual's rating. The larger numbers represent the best injector concepts.

Performance was the most important aspect of the program and was evaluated (rated) independent of the categories listed in Table 5. Thus, low-performing injector concepts could be weeded out even though other features of the concepts might be outstanding. The performance ratings were based on the results of the previously discussed spray and performance analyses; i.e., the performance rating is the performance index shown in Table 4.

The final rating shown in Table 6 is the product of the performance index (from Table 4) and the composite rating. The highest numbers represent the best injector concepts. No final rating was computed if no performance index was available (previously discussed in the Performance Analysis section of this report). The last column in Table 6 shows the ranking of the most promising injector configurations. The injector with the highest final rating was ranked No. 1, the next highest No. 2, etc. Concept selections for subsequent cold-flow studies were based to a large degree on these rankings.

TABLE 5

## INJECTOR PERFORMANCE RATING CRITERIA

Category	Tools	Weighting Factor, percent
Ease of Fabrication	Sketches and layouts, cost estimates	100
Scalability	Sketches and layouts	15
Packaging	1000K thrust injector layouts	40
Effective Use of Hot Gas	Sketches, vector and spray analyses, judgment	90
Stability	Stability analysis, judgment, experience	15
Cooling	Sketches, experience	50

TABLE 6

## INJECTOR RATINGS

Injector Configuration	Composite Rating	Performance Index	Final Rating	Ranking
<u>Group 1</u>				
1A	225.6	0.57	128.6	8
1B	199.2	--	---	
1C	189.9	--	---	
1D	170.4	--	---	
<u>Group 2</u>				
2A	213.6	0.95	202.9	1
2B	186.0	--	--	2
2C	202.6	1.00	202.6	
<u>Group 3</u>				
3A	169.8	0.75	127.4	9
3B	115.3	--	---	
3C	106.3	--	---	
3D	144.6	--	---	
4A	139.7	0.75	104.8	11
5A, 5B	171.1	0.97	166.0	6
6A	138.3	0.51	70.5	12
7A	159.3	0.80	127.4	9
8A	175.4	0.96	168.4	5
9A	160.4	0.96	154.0	7
10A	185.5	0.91	168.8	4
11A	183.3	0.94	172.3	3
12A	130.9	--	---	

Results of the ranking singled out two concepts: (1) the impinging jet concept (2A-2C) containing two oxidizer jets and two gas jets (hot gas or fuel) impinging on one central gas jet (fuel or hot gas), and (2) the 11A concept employing a commercial nozzle for atomization of a central oxidizer stream. The Bete "Tu-Cone" nozzle (previously discussed in the Design Analysis section of this report) was selected over the other commercial nozzles for the 11A concept because it exhibited good atomization, a consistent spray angle throughout the flowrate range, and because the nozzle size was smaller and more attractive from the fabrication standpoint.

A third injector concept selected was the tricentric configuration 1A containing a central hot-gas jet surrounded by annuli of oxidizer and fuel. Even though low performance was indicated for this concept it was selected because of the vast amount of past experience accumulated with this basic type of injector and because of superior fabrication advantages.

The fourth concept selected was the recessed cup 9A configuration containing four coaxial oxygen/hydrogen jets impinging on a central hot-gas jet. The 9A concept was selected over other recessed cup concepts (8A and 10A) mainly because its potential cup-cooling characteristics were more attractive and the computed performance was relatively high. Also, the 9A concept was selected over the similar flat-face 5A concept because of the potential performance advantages of the recessed cup.

Table 7 shows some of the potentially good and bad features of the four concepts selected. The factors listed are based on comparisons between the selected concepts and others in a particular grouping and/or between all of the remaining candidate concepts. Each of these four concepts was subjected to further evaluation during the Task II cold-flow studies as discussed in the following sections.

TABLE 7

MAJOR CHARACTERISTICS OF FOUR INJECTOR CONCEPTS  
SELECTED FOR COLD-FLOW STUDIES

Configuration	Plus Factors	Minus Factors
Tricentric 1A	Fabrication Simplicity Packaging (1000K) Hot-gas expansion into liquid Best manifolding arrangement Injector/chamber cooling	Liquid atomized by shear Mixing
Impinging Jet 2A, 2C	Fabrication simplicity Atomization by impingement Secondary atomization from biplanar impingement Mixing	Cooling Gas momentum control
Impinging Jet (Recessed Cup) 9A	Atomization by impingement Hot-gas atomization Mixing	Cup cooling Fabrication
Commercial Spray Nozzle 11A	Fabrication Packaging Spray nozzle atomization Forced mixing of liquid and hot gas	Spray nozzle cooling Liquid core

## TASK II

### COLD-FLOW STUDIES

Four selected injector concepts were evaluated during the cold-flow studies. Two models, a single element simulating 5000 pounds of thrust and one simulating 20,000 pounds of thrust, were generated for each of the four concepts, giving a total of eight models. The objective was to cold-flow test each of these models at varying flow conditions and select the two most promising concepts for the hot-firing tests. This screening process was accomplished by comparing high-speed motion pictures of the spray atomization patterns. The individual spray patterns were visually compared to a calibrated flow field designed to provide known spray characteristics. These photographs were not intended to yield quantitative spray droplet size distribution information. A limited number of tests, however, were made with a sampling probe photographic technique in an effort to obtain some quantitative droplet data. In addition, liquid mass distributions were obtained and the results were used as an evaluation index.

As originally planned, approximately 68 tests were required to obtain flow records for each of the eight injector models over the range of conditions shown in Table 8. This table illustrates the flow requirements for three general conditions: (1) all liquid flow (no gases), (2) full propellant flow (liquid + gases), and (3) cold gas-liquid flow (without gas generator-type gases).

All the experiments were conducted using water, gaseous nitrogen, and helium simulating the liquid oxygen, hydrogen, and gas generator hot gases, respectively. As the cold flow program progressed, additional testing was also

accomplished to evaluate modified injector concepts and to investigate observed flow phenomena not predicted by the previous analytical study.

The results of Task II cold-flow testing obtained from mid-December 1966 through mid-March 1967 are presented in the following pages.

TABLE 8

COLD-FLOW TEST MATRIX

- I. ATOMIZATION CHARACTERISTICS (HIGH-SPEED PHOTOS)
  - A. ONE VIEW OF WATER ONLY
  - B. ONE VIEW WITHOUT GAS GENERATOR GASES ( $H_e$ )
  - C. TWO VIEWS OF WATER + ALL GASES
  
- II. LIQUID MASS COLLECTION
  - A. WATER + ALL GASES

## COLD-FLOW APPARATUS

### Injector Elements

The four injector concepts selected for further screening during the cold-flow studies were as follows:

1. Tricentric elements which extend the coaxial injector concept to include hot gas (Type I)
2. Pentad impinging elements with a central gas stream (Types 2 and 9)
3. An element using a commercial centrifugal pressure nozzle (Type 11).

A prime objective of each concept was to utilize the high momentum of the hot gas to effectively atomize the LOX. Each of the four configurations were cold-flow-tested at two different thrust-per-element sizes (5K and 20K). A brief description of each injector type follows.

Tricentric Model 1A Injector. As shown in Table 1, four different tricentric concepts (Type 1) were originally proposed. On the basis of the analytical results (Task I), superior atomization characteristics were clearly indicated for the 1A concept. The LOX droplets formed by this element were expected to be small; i.e., a mean diameter of 26.6 microns.

Detailed designs were created for both the 5K and 20K cold-flow test models to represent the 1A tricentric injector concept. Basically, each model consists of three tubes of different diameters positioned coaxially. The resultant injection areas were identical to those selected for the hot-firing models (see Table 1).

Provisions were made for adjusting the exit position or recess depth of the tubes with respect to each other. The basic material for these cold-flow models was 6061-T6 aluminum. Photographs of the model 1A tricentric injector are given in Fig. 8 and 9 showing the propellant orientation from two different views. The LOX, hot gas, and gaseous hydrogen manifolds were each fed by a single manifold inlet connection. In general, photographs are presented for only the 20K size models because the 5K configurations were identical except for scaling differences.

Various modifications were made to the tricentric 1A configuration during the program. The first modification consisted of varying the relative exist positions of the injector elements. The modified configurations tested are shown schematically in Fig. 10.

Figure 10a represents the original concept with all elements flush. This was the configuration studied during the Task I analysis. The second configuration (Fig. 10b) shows the inner two elements recessed an equal distance from the injector face. Next, the inner two elements were recessed in step increments as shown in Fig. 10c. The last configuration (Fig. 10d) shows the center hot-gas tube extended beyond the face.

Plugs were also inserted into the water (LOX) injection annulus. Figures 11 and 12 show the installation of three 1-inch and six 1/4-inch plugs in the 20K configuration. Similar modifications were made to the 5K injection models representing the same percent flow area reductions.

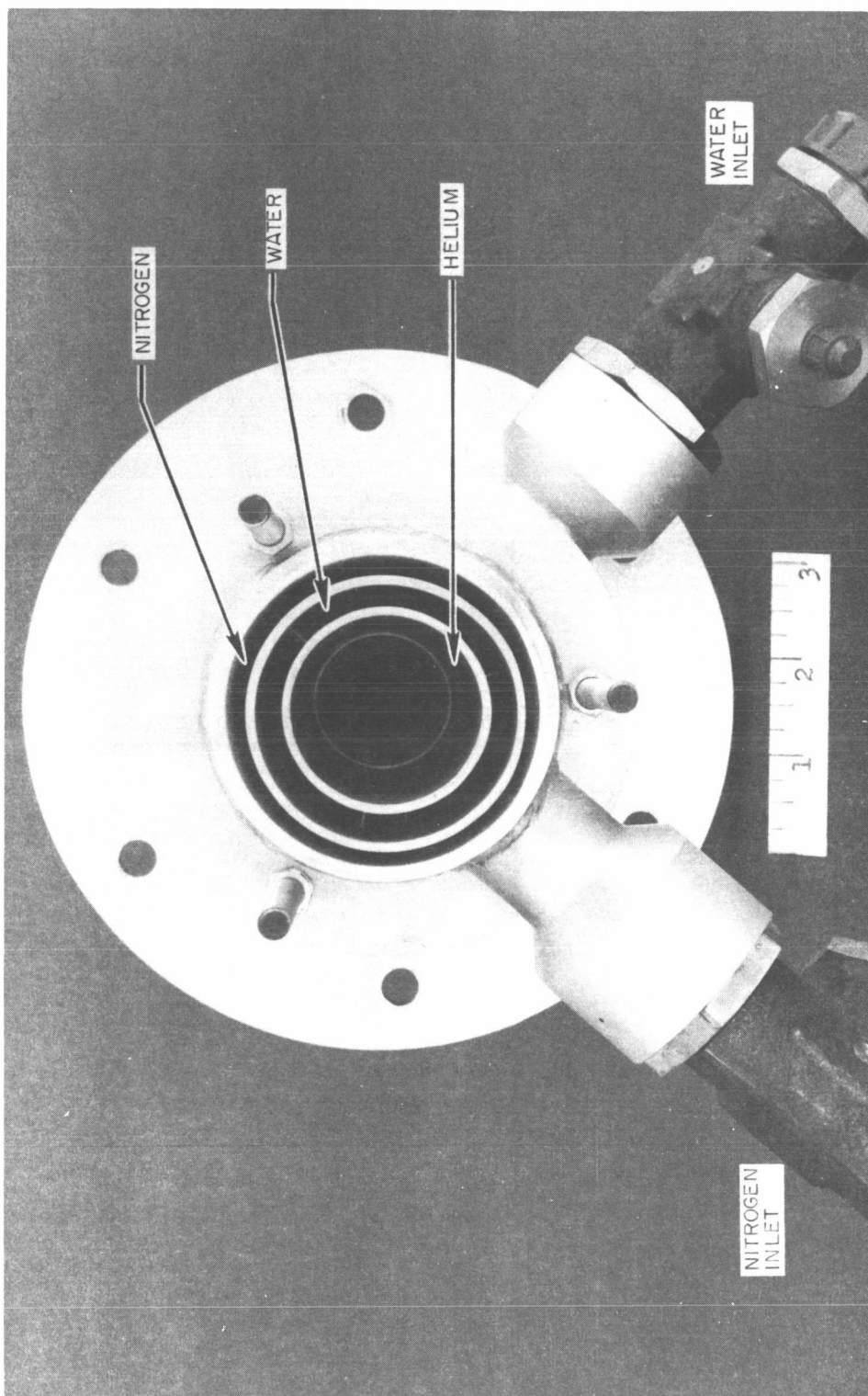


Figure 8. Front View of 20K Tricentric Injector Configuration 1A

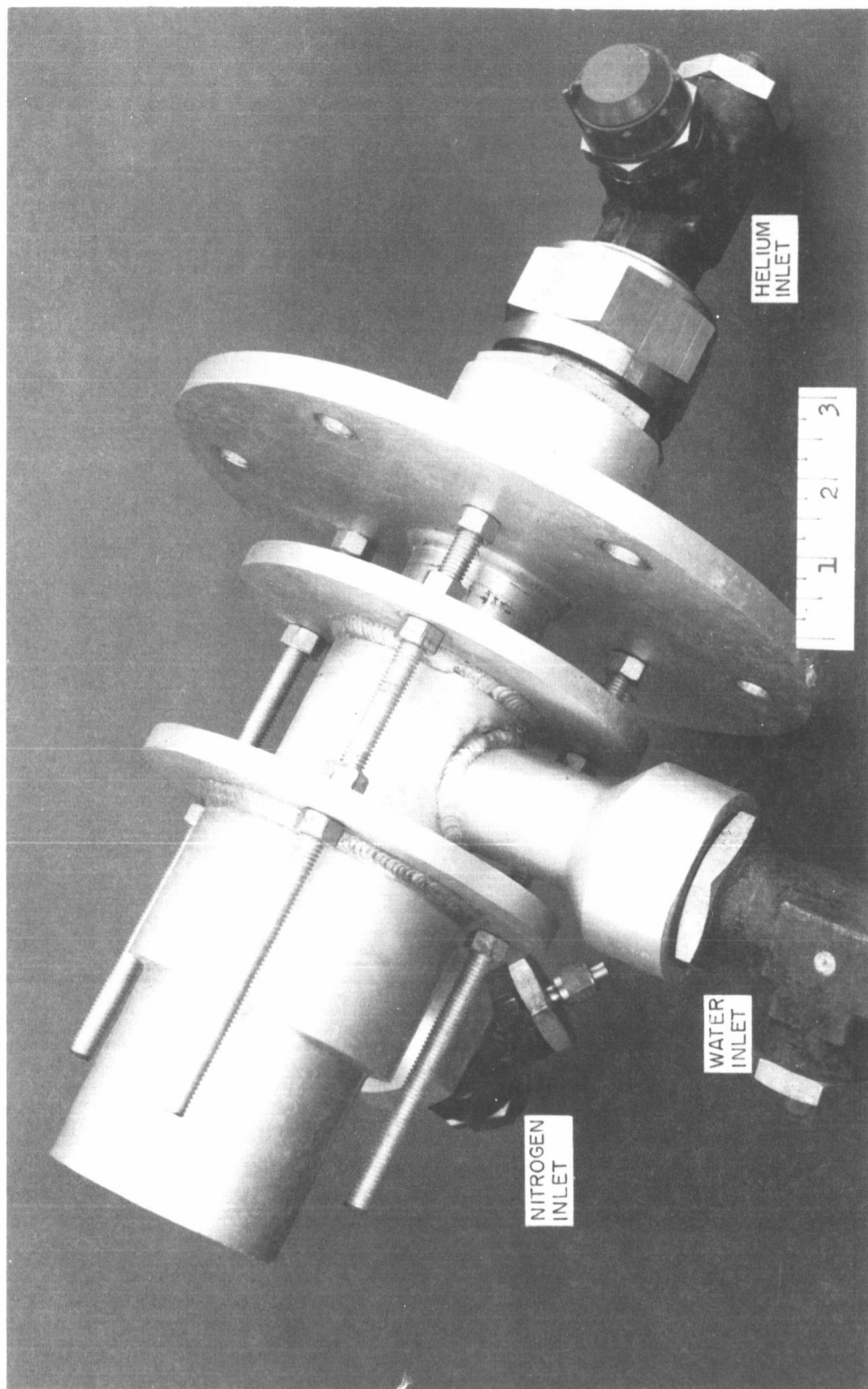


Figure 9. Side View of 20K Tricentric Injector Configuration 1A

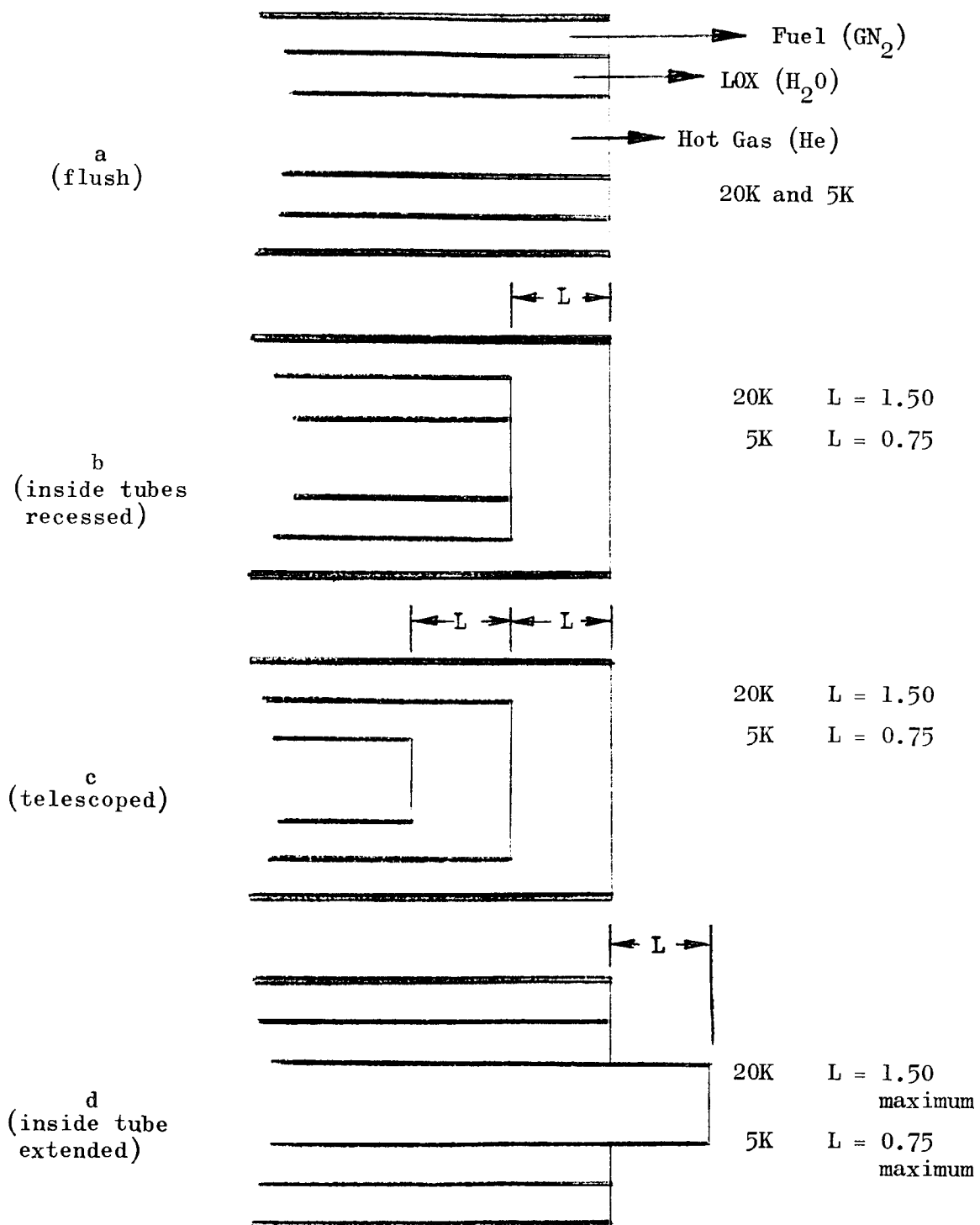


Figure 10. Tricentric Injector Exit Configurations

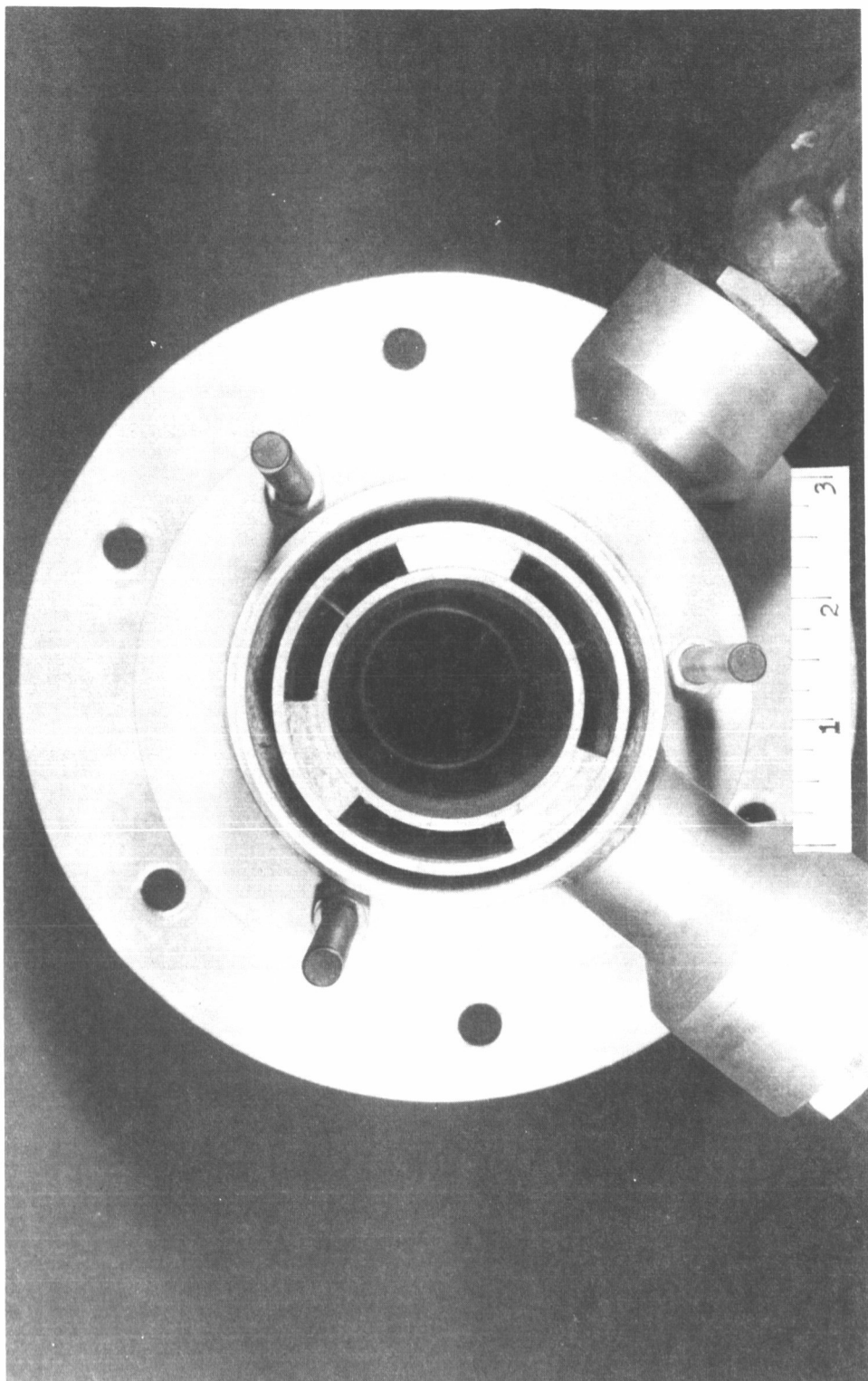


Figure 11. 20K Tricentric Injector Configuration 1A With Three  
1-Inch Plugs Installed in Water Annulus

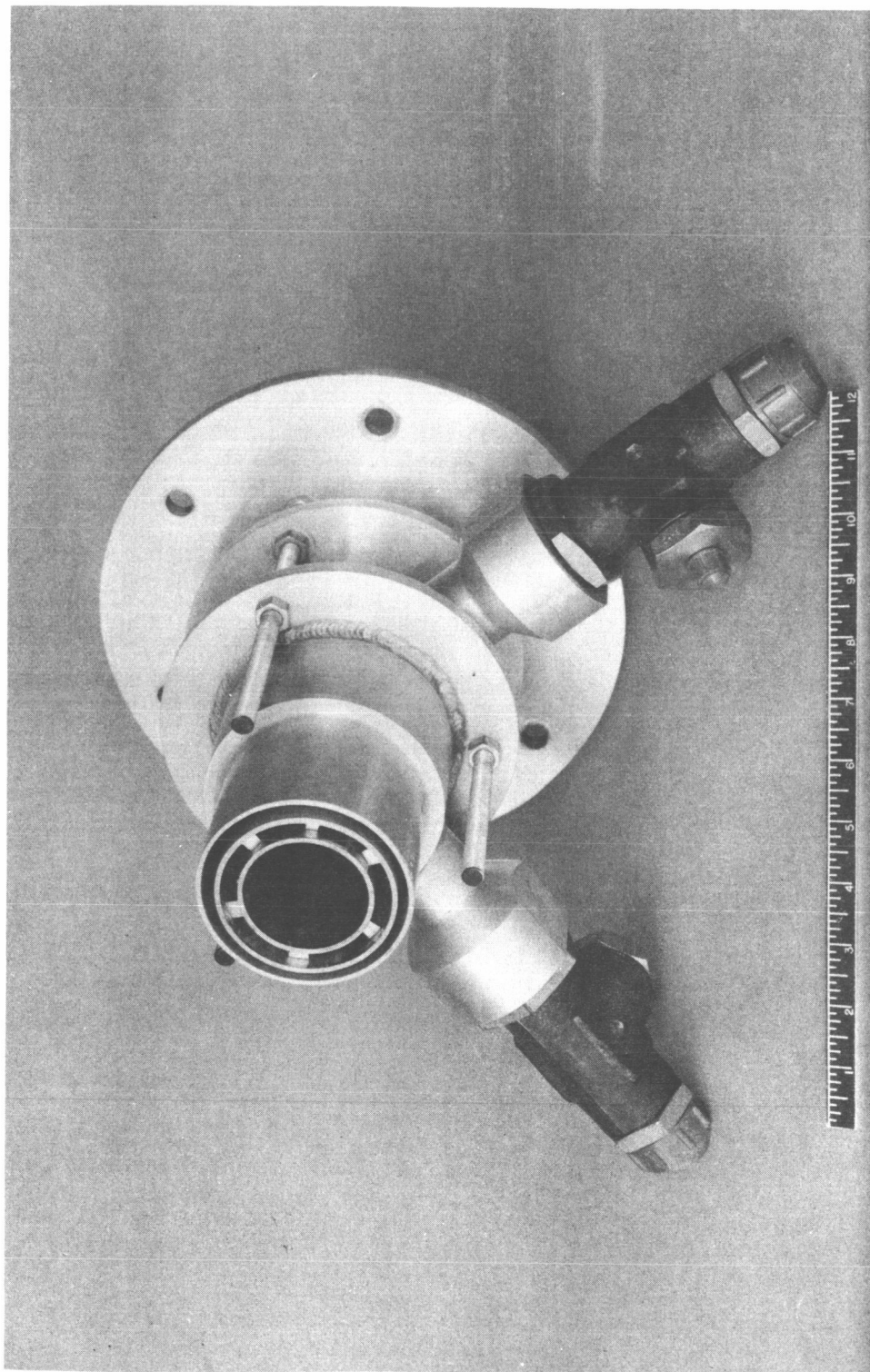


Figure 12. 20K Tricentric Injector Configuration 1A With Six  
1/4-Inch Plugs Installed in Water Annulus and  
Recessed 1/4-Inch From Injector Face

Biplanar Impingement Model 2A Injector. The Model 2A injector configuration (Fig. 13) consisted of two self-impinging doublet elements, each containing LOX and hot gas, respectively, directed on a central showerhead hydrogen fuel orifice. The centerline impingement distances were 2-1/2 inches and 4-1/2 inches, for the water (LOX) and helium (hot gas) streams, respectively. Type 6061-T6 aluminum was used to construct both the 5K and the 20K models. Complete atomization was predicted by the analysis (Task I) to occur with element 2A within the chamber combustion zone. The mean drop sizes were 50 microns.

During the cold-flow experiments with this configuration, it was discovered that the momentum of the gas was not effectively utilized and caused separation within the liquid spray field. Therefore, the 20K model of the 2A configuration was modified to the 2C configuration.

Biplanar Impingement Model 2C Injector. This configuration retained the same basic features as model 2A. The difference was in the orientation of the injected propellants. As shown in Fig. 14, self-impinging doublets of LOX (water) and hydrogen (nitrogen) were directed on a showerhead center orifice containing the hot gas. The design impingement angles of the LOX streams were changed, causing them to impinge at very nearly the same location as the fuel. The theoretical analysis predicted that the mean droplet size for the model 2C configuration would be 20 microns.

Impinging Coaxial Model 9A Injector. This configuration consisted of four LOX/hydrogen coaxial elements self-impinging on a central showerhead hot-gas stream. The coaxial elements were recessed and designed to impinge 1.3 inches upstream of the injector face or end of the cup for the 20K model

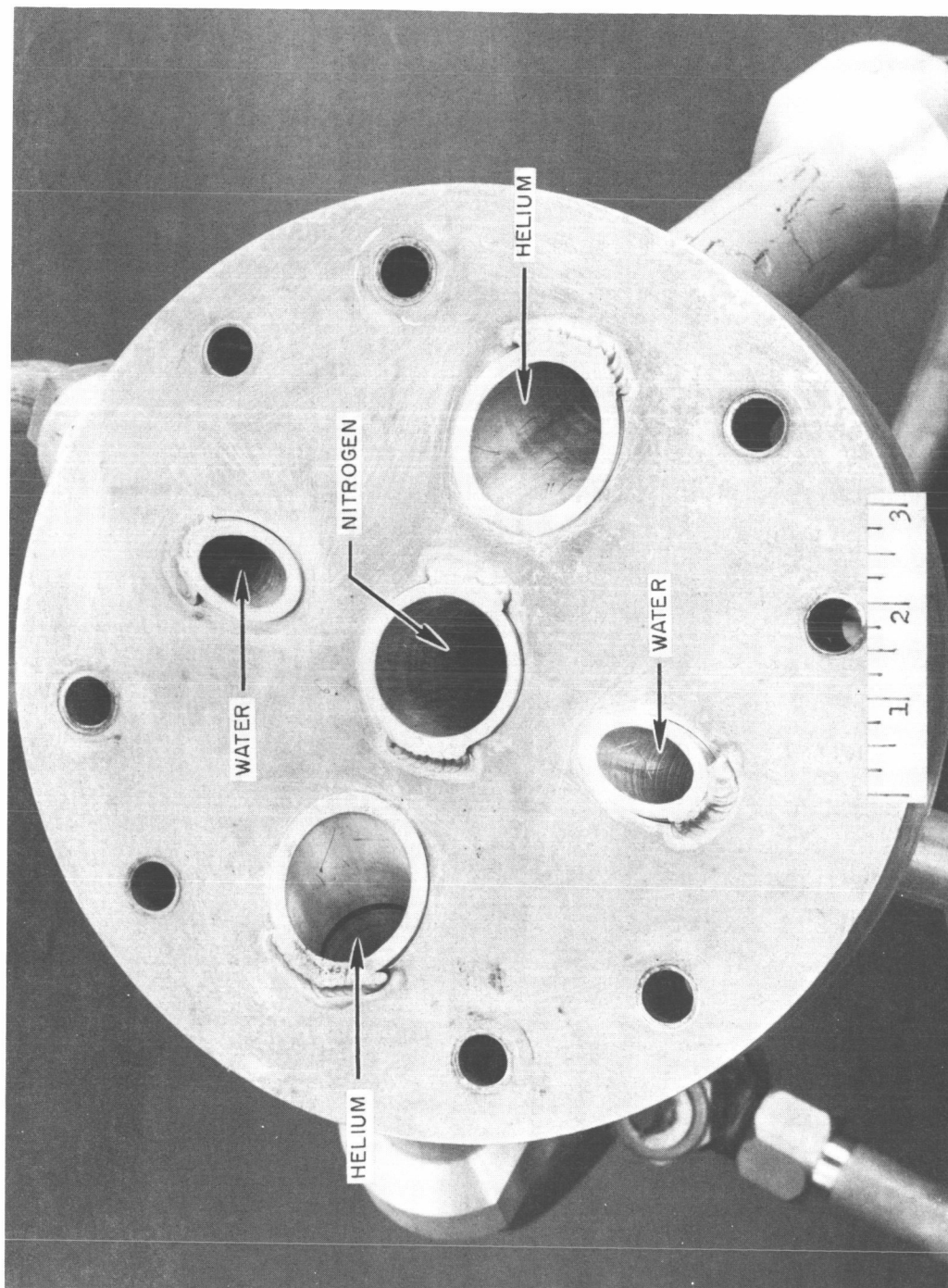


Figure 13. 20K Biplanar Impingement Injector Configuration 2A

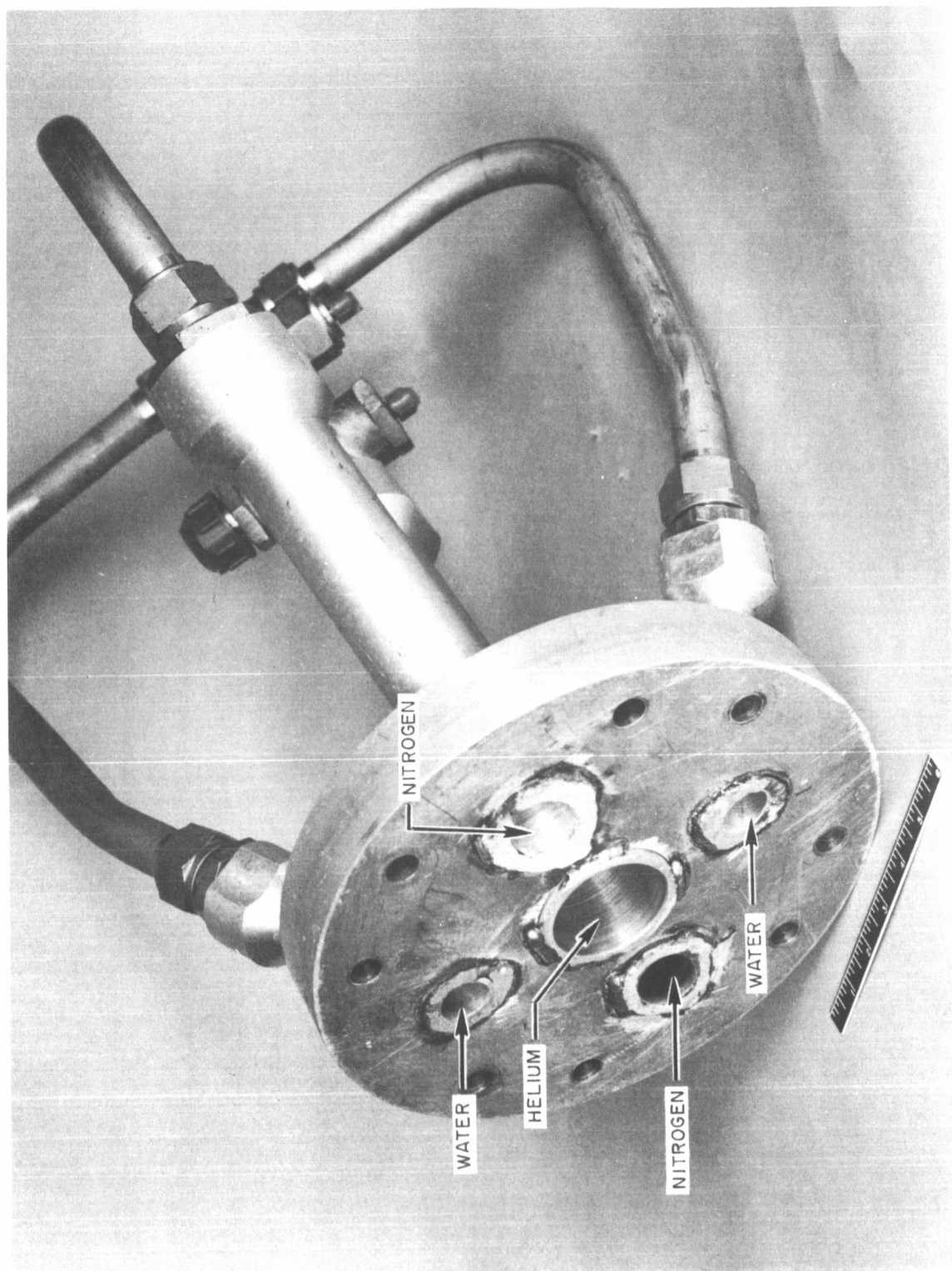


Figure 14. 20K Biplanar Impingement Injector Configuration 2C

containing a cylindrical cup length of 1.43 inches and a diameter of 3.75 inches. The 5K model impinged 0.81 inch upstream of the face, the cup length was 0.75 inch, and the diameter was 2.25 inches. The recessing was done to retain a high hot-gas velocity to ensure adequate LOX atomization. Excellent atomization, mixing, and combustion efficiency were predicted for this configuration.

Because of the possibility of an injector burning problem within the recessed element, the model 9A was modified by removing the cylindrical portion of the recessed cup. Figure 15 is a photograph of the 9A model with the modified cup. Cold-flow experimental data were obtained for both configurations.

Commercial Nozzle Model 11A Injector. Configuration 11A was essentially a tricentric injector with the oxidizer through a commercial spray nozzle in the center surrounded by annulii of hot gas and fuel. The model was designed so the exit position of the injected propellant simulants could be adjusted axially (recessed). The centrifugal nozzle was calculated to yield a bimodal distribution of droplets. Approximately 25 percent were expected to be obtained by shear stripping of small droplets from the liquid sheets by the hot gas, resulting in a very fine spray (mean diameter of 10 microns).

Figure 16 shows the important injector parts and relative propellant injection scheme of the commercial nozzle model 11A concept. Prior to incorporating this particular concept into the cold-flow program, several different commercial spray nozzles were screened during preliminary water flow calibration tests (Task I). The nozzles selected for study were manufactured by the Bete Company of Greenfield, Mass.

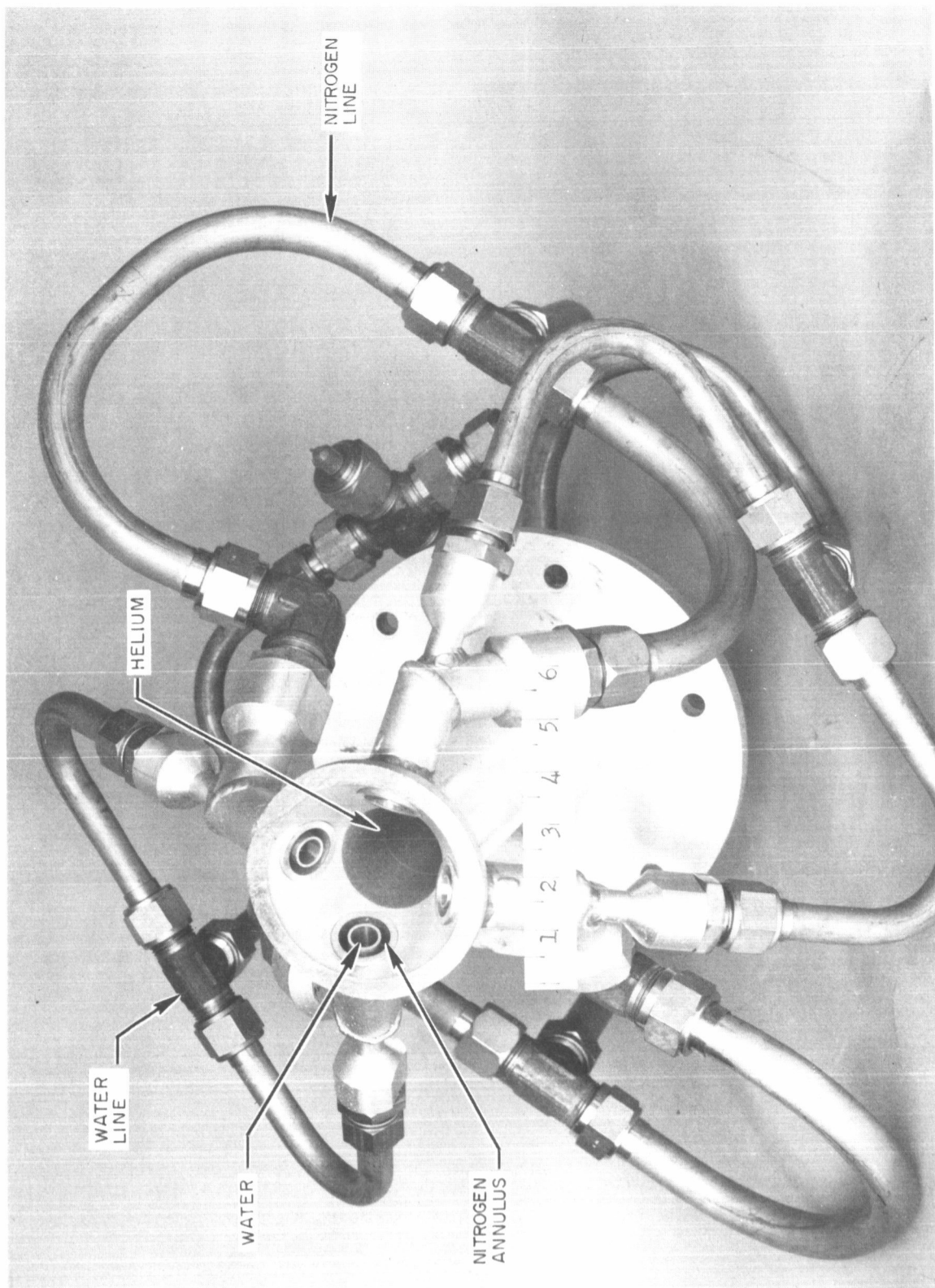


Figure 15. 20K Impinging Coaxial Injector Configuration 9A With  
no Cylindrical Portion on Cup

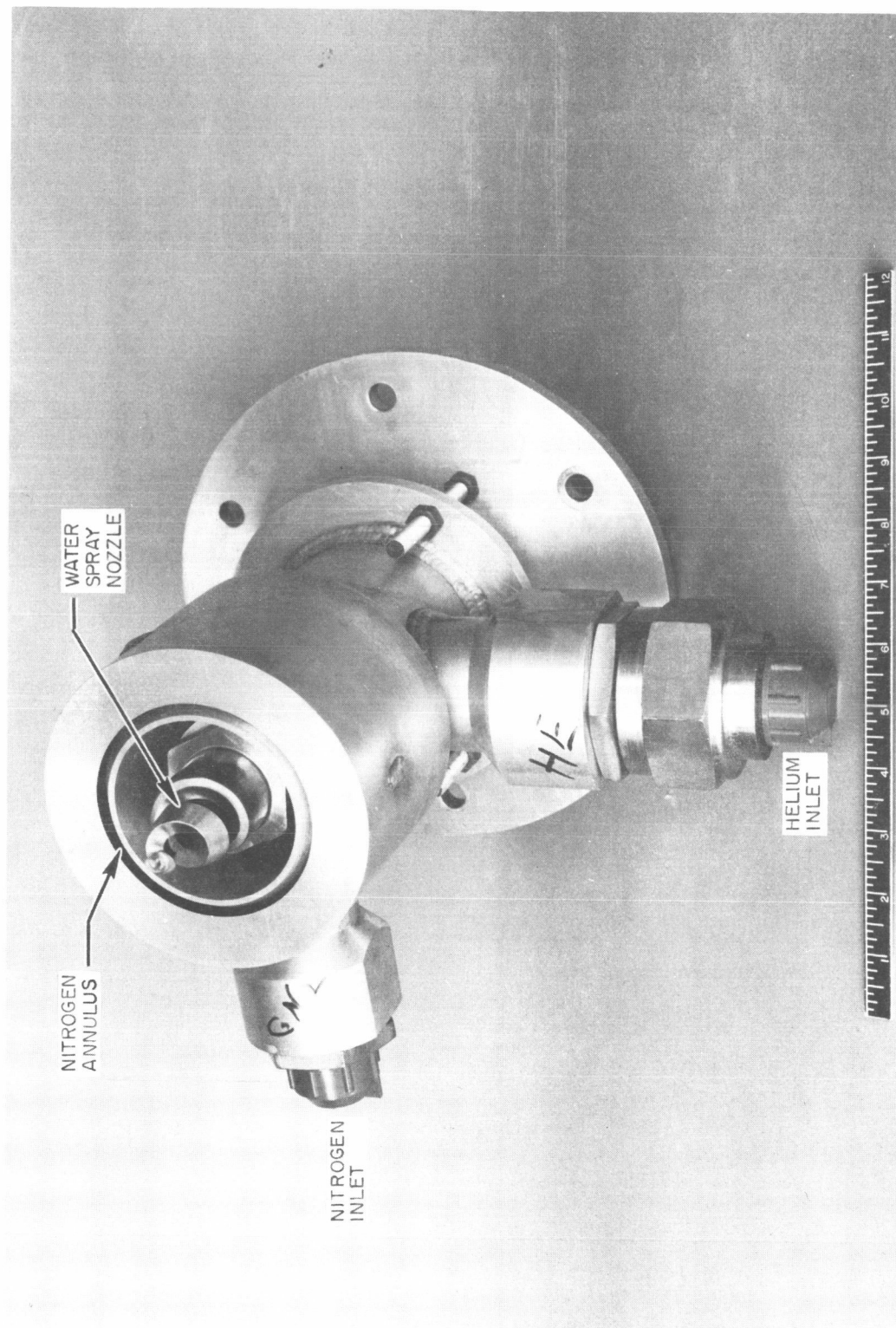


Figure 16. 20K Commercial Nozzle Injector Configuration 11A

## Test Equipment

Spray Pattern Photography. Three types of photographic techniques were investigated to determine which injector gave the best indication of the relative degree of atomization. All employed 16-millimeter Fastax motion pictures (100-foot film rolls) at speeds approaching 5000 frames per second. The field of view was generally from the injector face to 24 inches downstream of the injector face. The first technique used reflected sunlight as backlighting to penetrate the massive spray field. The motion pictures were of satisfactory quality but, as anticipated, did not permit evaluation of the absolute degree of atomization. The second method used the stroboscopic technique, using both front and backlighting. This method proved unsatisfactory because of inability to supply sufficient light to penetrate the spray field. The third method, which was designed to provide more quantitative information, consisted of a sampling probe to isolate and allow photographic coverage of an "element" of the spray field. This device is discussed in Appendix B.

Test Facility. Figure 17 shows the placement of the simulant control valves and model injector mounting in the experimental cold-flow facility. Maximum flexibility was incorporated into the system design to enable testing under a variety of conditions. In particular, the injector mount was adjustable so that a horizontal position could be used when taking high-speed motion pictures, and a vertical position could be used for the mass distribution flow tests. The vertical orientation is shown in Fig. 17. All testing was controlled remotely from a console located within the blockhouse. A schematic of the cold-flow test setup is shown in Fig. 18.

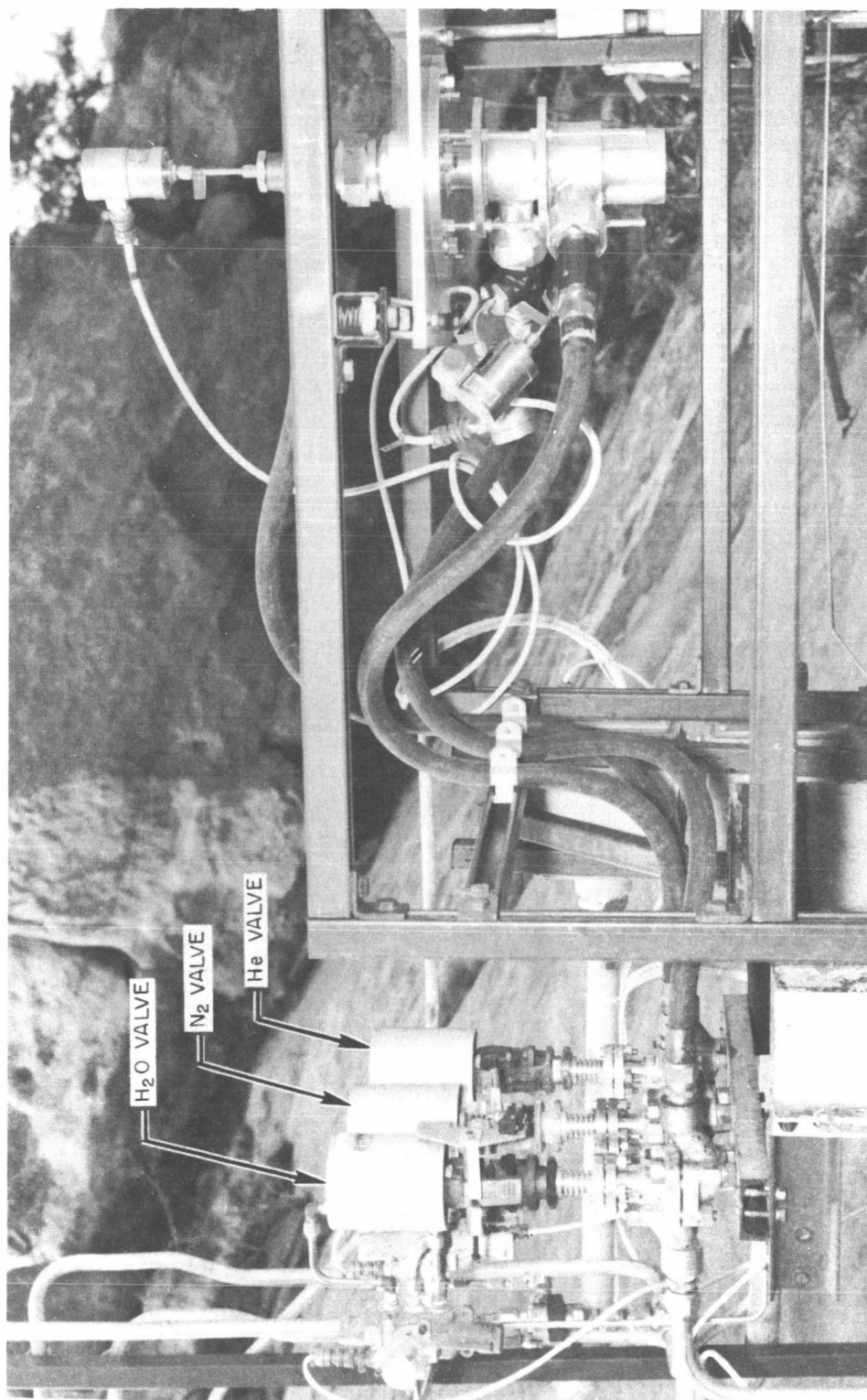


Figure 17. Cold-Flow Test System With Tridentric Injector Configuration 1A in Position for Liquid Mass Distribution Test

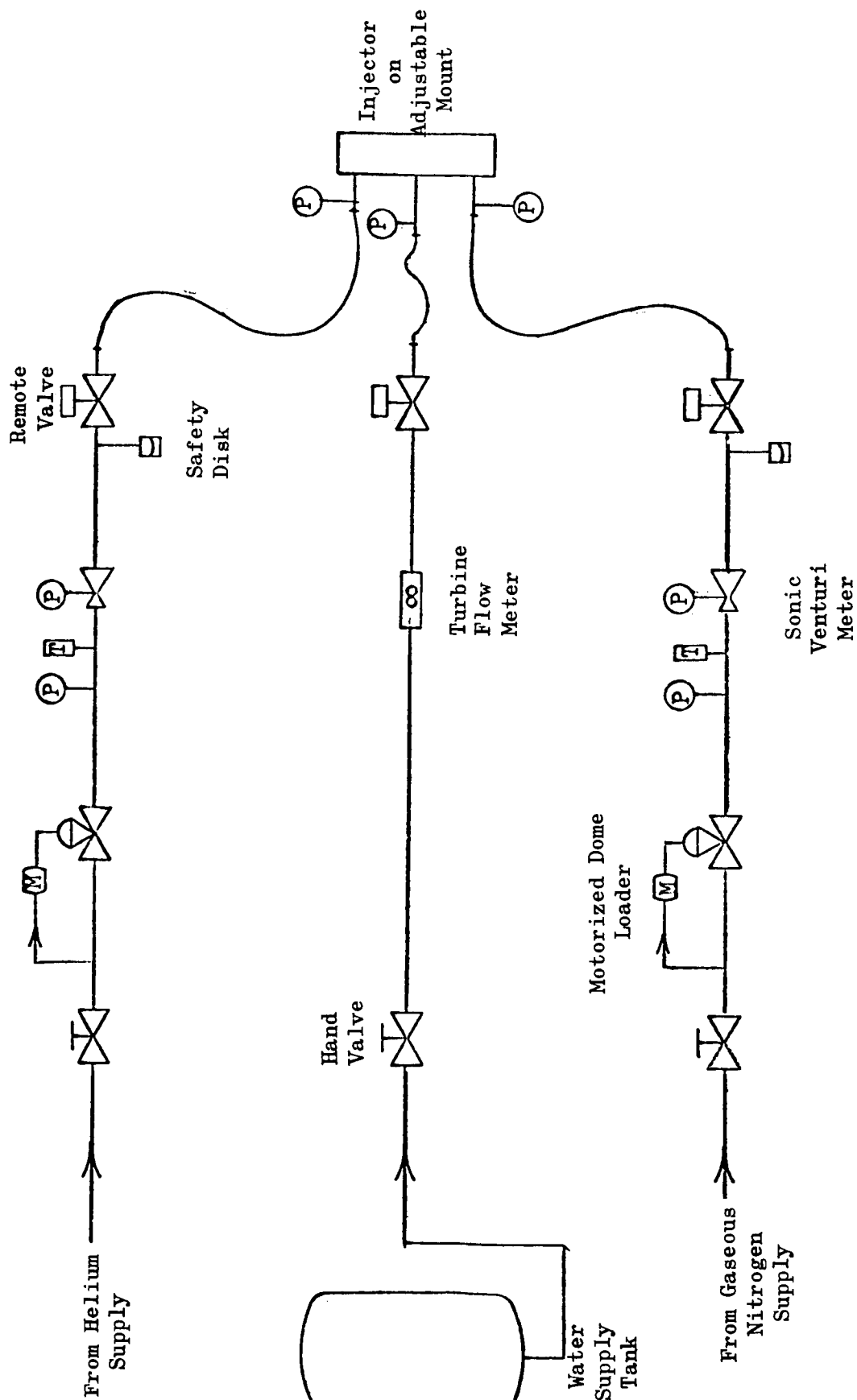


Figure 18. Cold-Flow Test System Schematic

Atomization Standard Injector. A simple impinging doublet was designed with known spray characteristics to obtain a relative comparison of the spray pattern atomization characteristics of the four injector concepts. The standard injector (Fig. 19) was constructed of 1/2-inch tubing with an included impinging angle of 90 degrees. The design operating conditions were selected to provide volume-number-mean droplet diameters ( $D_{30}$ ) of 200 microns according to the following equation developed by Ingebo (Ref. 3):

$$\frac{D_j}{D_{30}} = 2.64 \sqrt{D_j V_j} + 0.97 D_j \Delta V \quad (18)$$

where diameters and velocities are expressed in inches and feet per second, respectively.

Sampling Probe Technique. Quantitative droplet distribution data were difficult to obtain for two reasons: (1) the large quantity of water flowed did not permit adequate penetration of a backlight, and (2) the relatively high velocity of the droplets flowing within the gas stream required extremely fast exposure rates.

The sampling probe was a device inserted in the injected water spray downstream of the model injector. The inlet geometry of the probe could be varied to regulate the amount of water permitted to pass through the photographic field of view. A Fastax camera was installed within the water proofed enclosure to take pictures backlighted by a synchronized 2-microsecond strobe light. Details of the cold-flow probe experiments are given in Appendix B.

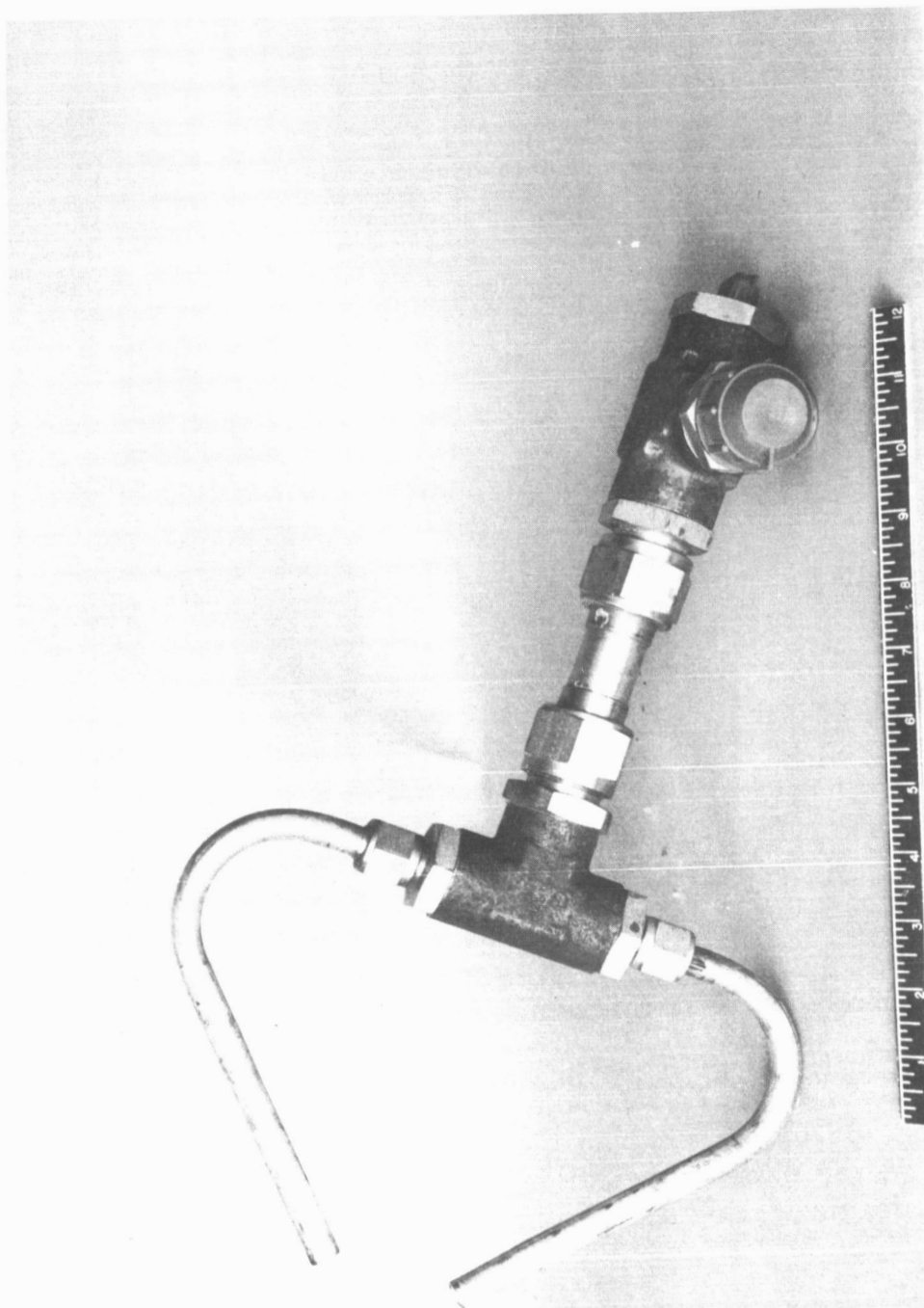


Figure 19. Simple Impinging Doublet Injector Model Used to Produce a Reference Spray Field Characterized by 200-Micron Mean Droplet Size

Mass Distribution. The liquid mass distribution was measured using the apparatus shown in Fig. 20. The collection device consisted of a matrix of 64 individual sampling tubes placed in a square array having a 1-1/2-inch spacing to collect the injected water spray. The distance from the model injector to the collection tubes was varied as appropriate for the test under consideration. Mass distribution plots showing contours of constant mass were obtained for each injector configuration. The data are presented later in this section (Test Results and Discussion).

Instrumentation. The propellant (water, nitrogen, and helium) flows corresponding to the desired simulation ratios were set using direct-recording Dynalog charts. Water flow measurements were made with a Fischer-Porter turbine-type flowmeter and recorded directly on an oscillograph.

The gaseous nitrogen and helium flowrates were established by regulating their supply pressures upstream of sonic venturi meters. The manifold pressures were recorded on an oscillograph during selected tests with the tricentric injector to study the cyclic pressure oscillations associated with its pulsing behavior.

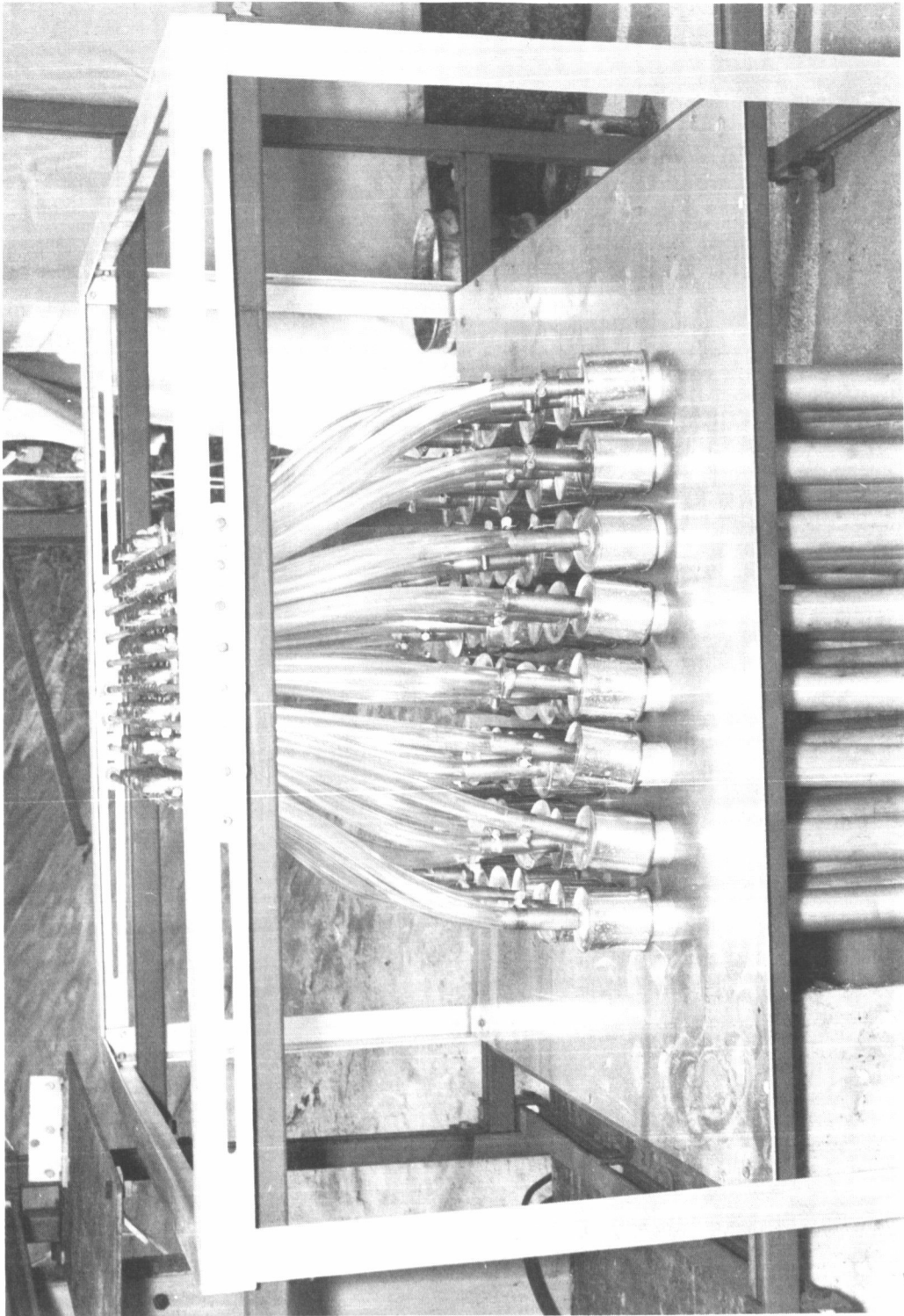


Figure 20. Liquid Mass Distribution Collection Apparatus

## COLD-FLOW SIMULATION

### Analysis of Simulating Conditions

An investigation of the appropriate simulating conditions corresponding to a variety of hot-firing conditions was made to ensure proper cold-flow test coverage. Water, nitrogen, and helium were used to simulate the LOX, hydrogen, and hot gas, respectively. The cold-flow simulation of the hot-firing conditions depended upon the injector concept under consideration.

The size (mean diameter) of droplets formed when liquid jets are subjected to high relative gas velocities can be expressed by the following equation (Eq. 2 of Task I):

$$D = K \left( \frac{\mu_{\ell} \sigma_{\ell}}{\rho_{\ell}} \right)^{1/3} \left( \frac{1}{\rho_g U_r^2} \right)^{2/3} \quad (19)$$

where

- D = droplet size (diameter)
- K = constant
- $\mu_{\ell}$  = liquid viscosity
- $\sigma_{\ell}$  = liquid surface tension
- $\rho_{\ell}$  = liquid density
- $\rho_g$  = gas density
- $U_r$  = relative velocity, gas/liquid

For the cold flow studies the liquid properties remained constant, therefore the most significant variables were  $(\rho_g U_r^2)$ . Because the gas injection velocities were orders of magnitude greater than the liquid, this term could be expressed as  $(\rho U^2)_{\text{gas}}$ , which is the gas momentum per unit area. The development of the above equation assumed no limit upon the amount of gas available to atomize a given quantity of liquid. Under the condition of a finite amount of available gas, a more appropriate consideration was

$$D = f(\dot{w}_g, \dot{w}_{\ell}, \rho_g, U_g) \quad (20)$$

where

$\dot{w}_g$  = gas mass flowrate

$\dot{w}_\ell$  = liquid mass flowrate

$U_g$  = gas velocity

The variables in Eq. 20 were simulated by equating the following ratios:

$$\left( \frac{M_g}{\dot{w}_\ell} \right)_{\text{cold}} = \left( \frac{M_g}{\dot{w}_\ell} \right)_{\text{hot}} \quad (21)$$

where

$M_g$  = gas momentum

Depending upon the particular concept to be evaluated, an alternate simulation approach was also necessary. This involved consideration of the gas-to-liquid momentum ratio. This was important where liquid penetration into the gas flow field was involved. For example, using an impinging stream where liquid streams impinge on a central showerhead gas stream, a sufficient liquid momentum level ( $M_\ell$ ) was required to ensure that the streams were not simply swept aside. Thus, if penetration did not occur only a fraction of the gas would be used to atomize the liquid. Therefore, simulation for impinging injectors was also made on the basis

$$\left( \frac{M_g}{M_\ell} \right)_{\text{cold}} = \left( \frac{M_g}{M_\ell} \right)_{\text{hot}} \quad (22)$$

where

$M_\ell$  = liquid momentum

The water flow required to give liquid penetration to the center of the injector element was determined by the following equation, developed during another program conducted at Rocketdyne:

$$\frac{X}{D_\ell} = 2.5 \left[ \frac{\rho_\ell U_\ell^2}{\rho_g U_g^2} \cos^2 \theta_i \right]^{1/2} \quad (23)$$

where

$X$  = penetration distance

$D_\ell$  = liquid jet diameter

$\theta_i$  = angle between the liquid jet and the injector, expressing the component of the liquid jet velocity normal to the direction of gas flow

$U_\ell$  = liquid velocity

The coefficient 2.5 was experimentally determined for small liquid jets penetrating a gas jet.

In addition to satisfying penetration requirements, test conditions were further restricted by limiting maximum gas flowrates as established by sonic velocities at the injector exit. All the foregoing restrictions made it impossible to match the  $(M_g/\dot{w}_\ell)$  and  $(M_g/M_\ell)$  ratios for both the hot gas/oxidizer and the fuel/oxidizer cases simultaneously. However, the ratios were not of equal importance in simulating each injector model. Accordingly, each injector type was considered from the point of view of which ratio or ratios were the most significant. The cold-flow test conditions were then established to provide a compromise as necessary so that the most significant ratio or ratios were simulated as closely as possible.

In addition to simulating the full-thrust conditions (500-psia chamber pressure) for the injectors, an analysis was made to establish the critical ratios during throttled operation. The throttled conditions of interest were those corresponding to a hot-firing chamber pressure of 200 and 50 psia. When the same criteria were met, namely matching the  $(M_g/\dot{w}_\ell)$  fuel ratio and sonic flow of the simulating helium and nitrogen, it was found that no change was required in the cold-flow condition. In other words, using  $(M_g/\dot{w}_\ell)$  fuel as the critical ratio, atomization was independent of throttling. Accordingly, for the tricentric injectors, a single test condition adequately simulated both full-thrust and throttled conditions. In the case of the impingement injectors, where all of the simulation ratios represented a compromise, a single cold-flow test condition was found to approximate the throttled condition as adequately as the full-thrust conditions.

The simulating ratios, which were used as cold-flow test conditions as they relate to each particular injector model, are given in Tables 9 through 13. In addition to presenting the cold-flow simulation data, the propellant flow-rate and injection areas used for the program are also given. These data are for the 20K models only. For the 5K models, the ratios would remain unchanged but the flowrates and areas would be 1/4 of those listed.

#### Simulation of the Tricentric Model 1A

The  $(M_g/M_\ell)$  ratios were of little importance to the tricentric configurations because there were no impinging streams. It was desirable to match the  $(M_g/\dot{w}_\ell)$  ratios for both the hot gas and fuel cases as nearly as possible. As already indicated, the solution of one ratio predetermined the other because of their interrelationship, so a judicious compromise was required. The compromise selected for the tricentric injector tests is

shown by the data of Table 9. As shown, the cold-flow simulating ratio  $(M_g/\dot{w}_\ell)$  for the fuel was permitted to deviate on the high side by a factor of 2 so that the  $(M_g/\dot{w}_\ell)$  ratio for the hot gas would deviate no more than a factor of 2.5 on the low side.

#### Simulation of Biplanar Impingement Model 2A

Simulating the 2A model required matching the  $(M_g/\dot{w}_\ell)$  fuel ratio because the fuel is the centrally located jet, matching the  $(M_g/\dot{w}_\ell)$  hot-gas ratio as nearly as possible, and ensuring that penetration of the liquid stream into the central gas stream was adequate. It was not possible to completely satisfy all these conditions simultaneously.

As indicated by Table 10, the best compromise was found by matching the  $(M_g/\dot{w}_\ell)$  fuel ratio exactly, approaching the  $(M_g/\dot{w}_\ell)$  hot-gas ratio within a factor of 2, and ensuring that the liquid penetration was greater than one-half the fuel jet diameter. To achieve these conditions with the added restriction of sonic helium flow, the water flowrate had to be established at 5.7 lb/sec. This, in turn, set the nitrogen flowrate at 0.57 lb/sec, which gave subsonic flow conditions at the exit (Mach number of 0.62).

#### Simulation of Biplanar Impingement Model 2C

The model 2C injector was fabricated by modifying the 2A hardware. As a consequence, the 2C model port areas deviated somewhat from the originally proposed design. The simulating ratios shown in Table 11 represent the actual experimental hardware dimensions. The same basic criteria in establishing the ratios was followed as with the 2A model.

TABLE 9

COLD-FLOW SIMULATION OF HOT-FIRING CONDITIONS FOR  
INJECTOR CONFIGURATION 1A AT 15-PERCENT HOT-GAS FLOW

Item	Hot-Firing Conditions	Cold-Flow Simulation
$(M_g/\dot{w}_\ell)$ Hot Gas	25	10
$(M_g/M_\ell)$ Hot Gas	17	40
$(M_g/\dot{w}_\ell)$ Fuel	2.2	4.4
$(M_g/M_\ell)$ Fuel	1.5	18
<u>Total Flow Area, sq in.</u>		
Hot Gas (He)	3.00	3.00
Fuel ( $N_2$ )	1.66	1.66
Oxidizer ( $H_2O$ )	2.03	2.03
<u>Total Flowrate, lb/sec</u>		
Hot Gas (He)	9.13	0.69*
Fuel ( $N_2$ )	5.33	0.92*
Oxidizer ( $H_2O$ )	46.3	7.1

\*Sonic conditions

TABLE 10

COLD-FLOW SIMULATION OF HOT-FIRING CONDITIONS FOR  
INJECTOR CONFIGURATION 2A AT 15-PERCENT HOT-GAS FLOW

Item	Hot-Firing Conditions	Cold-Flow Simulation
$(M_g/\dot{w}_\ell)_{\text{Hot Gas}}$	25	13
$(M_g/M_\ell)_{\text{Hot Gas}}$	7.0	25
$(M_g/\dot{w}_\ell)_{\text{Fuel}}$	2.2	2.2
$(M_g/M_\ell)_{\text{Fuel}}$	0.62	4.5
<u>Total Flow Area, sq in.</u>		
Hot Gas (He)	3.00	3.00
Fuel (N <sub>2</sub> )	1.66	1.66
Oxidizer (H <sub>2</sub> )	0.813	0.813
<u>Flowrate, lb/sec</u>		
Hot Gas (He)	9.13	0.69*
Fuel (N <sub>2</sub> )	5.33	0.57
Oxidizer (H <sub>2</sub> O)	46.3	5.7
Estimated Penetration, inches**	----	0.97

\*Sonic conditions

\*\*Determined by Eq. 23

TABLE 11

COLD-FLOW SIMULATION OF HOT-FIRING CONDITIONS FOR  
INJECTOR CONFIGURATION 2C AT 15-PERCENT HOT-GAS FLOW

Item	Hot-Firing Conditions	Cold-Flow Simulation
$(M_g/\dot{w}_l)_{\text{Hot Gas}}$	25	10
$(M_g/M_l)_{\text{Hot Gas}}$	7.0	13
$(M_g/\dot{w}_l)_{\text{Fuel}}$	2.2	3.8
$(M_g/M_l)_{\text{Fuel}}$	0.62	5.3
<u>Total Flow Area, sq in.</u>		
Hot Gas (He)	3.00	3.14
Fuel (N <sub>2</sub> )	1.66	1.57
Oxidizer (H <sub>2</sub> O)	0.813	0.810
<u>Flowrate, lb/sec</u>		
Hot Gas (He)	9.13	0.73*
Fuel (N <sub>2</sub> )	5.33	0.87
Oxidizer (H <sub>2</sub> O)	46.3	8.1
Estimated Penetration, inches**	----	0.5

\*Sonic conditions

\*\*Determined by Eq. 23

### Simulation of the Impinging Coaxial Model 9A

In the case of the 9A injector model, it was desirous to match both the  $(M_g/\dot{w}_\ell)$  and the  $(M_g/M_\ell)$  ratios of the hot gas. The best compromise was found by letting the  $(M_g/\dot{w})$  ratio come within a factor of 2 on the low side while allowing the  $(M_g/M_\ell)$  ratio deviate by a factor of 3 on the high side. In addition, assurance of penetration of the water stream to the middle of the central helium jet was also necessary. The mass distribution tests, which are discussed in more detail later, verified that this requirement was being met. The simulating ratios for the 9A injector are listed in Table 12.

### Simulation of Commercial Nozzle Model 11A

The model 11A injector, characterized by the commercial spray nozzle, was basically a tricentric design. Accordingly, the  $(M_g/\dot{w}_\ell)$  ratios for both hot gas and fuel were simulated. Again, rather than matching one ratio exactly and allowing the other to deviate widely, a compromise was made. The adapted simulating ratios for this model are shown in Table 13; the  $(M_g/\dot{w}_\ell)$  fuel ratio was allowed to deviate by a factor of 2 on the high side, and the  $(M_g/\dot{w}_\ell)$  hot-gas ratio was allowed to deviate by a factor of 2.5 on the low side.

TABLE 12

COLD-FLOW SIMULATION OF HOT-FIRING CONDITIONS FOR  
INJECTOR CONFIGURATION 9A AT 15-PERCENT HOT-GAS FLOW

Item	Hot-Firing Conditions	Cold-Flow Simulation
$(M_g/\dot{w}_l)_{\text{Hot Gas}}$	22	11
$(M_g/M_l)_{\text{Hot Gas}}$	7.0	21
$(M_g/\dot{w}_l)_{\text{Fuel}}$	1.8	5.8
$(M_g/M_l)_{\text{Fuel}}$	0.56	11
<u>Total Flow Area, sq in.</u>		
Hot Gas (He)	3.20	3.20
Fuel (N <sub>2</sub> )	1.94	1.94
Oxidizer (H <sub>2</sub> O)	0.91	0.91
<u>Flowrate, lb/sec</u>		
Hot Gas (He)	9.13	0.73*
Fuel (N <sub>2</sub> )	5.33	1.07*
Oxidizer (H <sub>2</sub> O)	46.3	6.7
Estimated Penetration, inches**	----	0.85

\*Sonic conditions

\*\*Determined by Eq. 23 (atomizing effect of N<sub>2</sub> neglected)

TABLE 13

COLD-FLOW SIMULATION OF HOT-FIRING CONDITIONS FOR  
INJECTOR CONFIGURATION 11A AT 15-PERCENT HOT-GAS FLOW

Item	Hot-Firing Conditions	Cold-Flow Simulation
$(M_g/\dot{w}_\ell)_{\text{Hot Gas}}$	25	10
$(M_g/M_\ell)_{\text{Hot Gas}}$	6.7	16
$(M_g/\dot{w}_\ell)_{\text{Fuel}}$	2.2	4.6
$(M_g/M_\ell)_{\text{Fuel}}$	0.59	7.1
<u>Total Flow Area, sq in.</u>		
Hot Gas (He)	3.00	3.00
Fuel (N <sub>2</sub> )	1.66	1.66
Oxidizer (H <sub>2</sub> O)	0.785	0.785
<u>Total Flowrate, lb/sec</u>		
Hot Gas (He)	9.13	0.69*
Fuel (N <sub>2</sub> )	5.33	0.92*
Oxidizer (H <sub>2</sub> O)	46.3	7.1

\*Sonic conditions

## TEST RESULTS AND DISCUSSION

Four injector configurations previously screened by theoretical analysis of 20 original concepts were cold-flow tested to select two candidates for the hot-firing program. The cold-flow experiments were designed to provide additional qualitative injector screening information through visual interpretation of the flow spray patterns and analysis of the liquid mass distributions.

An indication of the relative degree of spray atomization was made by comparing the various test photographs to a spray field of known droplet sizes. This standard spray field was generated during two tests by a special self-impinging doublet injector (Fig. 19) designed to produce 200-micron ( $D_{30}$ ) droplets. The resulting liquid spray field pattern is presented in Fig. 21. All other injector spray photographs were compared with this pattern to obtain a qualitative indication of the atomization characteristics and relative spray behavior. Most of the photographs were obtained with high-speed motion picture coverage using reflected-sun backlight for spray penetration. Fifteen photographic tests were conducted with the sampling probe in an effort to obtain additional quantitative droplet size information. A discussion of the results with the probe is given in Appendix B.

The measurement of the liquid mass distribution was accomplished by the collection apparatus previously described and illustrated in Fig. 20. These data provided additional screening information to assist in the injector concept selection.

One hundred forty tests were conducted during the Task II cold-flow studies. Table 14 presents a summary of 102 of these tests related to the basic injector screening experiments. As previously mentioned, 15 other tests were conducted with the sampling probe, and 2 other tests were conducted with

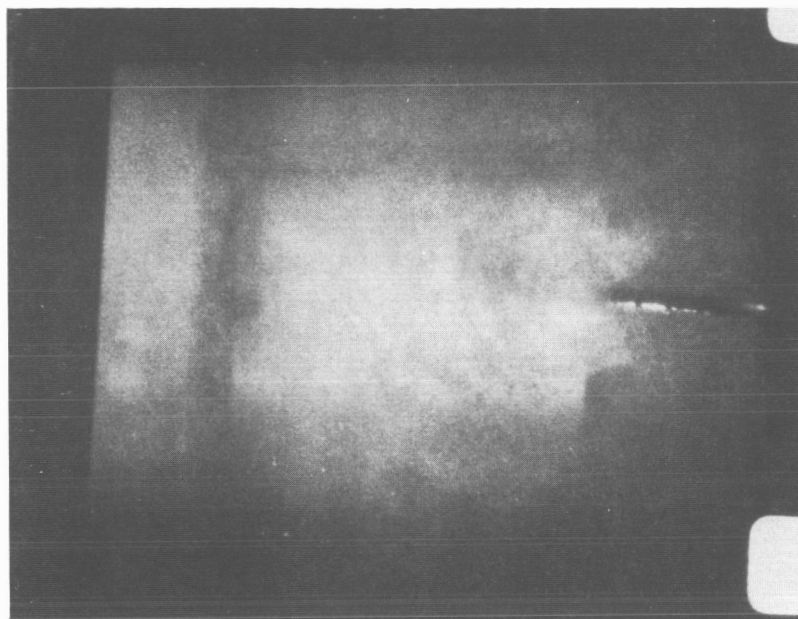


Figure 21. Spray Field Characteristics of  
Standard Doublet Injector

TABLE 14

## SUMMARY OF INJECTOR COLD-FLOW TEST RESULTS

Injector Configuration	Injector Size	Number of Tests	Type of Test	Flow Conditions	Remarks
1A	20K	4	Photo	H <sub>2</sub> O, H <sub>2</sub> O-N <sub>2</sub> , H <sub>2</sub> O-N <sub>2</sub> -He, H <sub>2</sub> O-He	Good photos, but difficult to evaluate degree of atomization; severe pulsing
		3	Photo	He-H <sub>2</sub> O, N <sub>2</sub> -H <sub>2</sub> O, H <sub>2</sub> O only	Helium caused spray pattern to change from conical to paraboloid
		2	Photo	H <sub>2</sub> O-N <sub>2</sub> -He with flowrates reduced to 1/3 and 30 percent of normal rate	Pulsing not reduced by threefold decrease in gas flows
		1	Photo	H <sub>2</sub> O-N <sub>2</sub> -He	Pulsing reduced; inner and middle tubes recessed
		3	Photo	H <sub>2</sub> O, H <sub>2</sub> O-N <sub>2</sub> , H <sub>2</sub> O-N <sub>2</sub> -He	Outside tube extended 1-1/2 inch
		1	Photo	H <sub>2</sub> O-N <sub>2</sub> -He	Telescoped in 1-1/2 inch steps
		3	Mass Distribution	H <sub>2</sub> O-N <sub>2</sub> -He	Outside tube extended 1-1/2 inch
		6	Photo	H <sub>2</sub> O, H <sub>2</sub> O-N <sub>2</sub> , H <sub>2</sub> O-N <sub>2</sub> -He	Three 1-inch-wide plugs in H <sub>2</sub> O annulus
		1	Mass Distribution	H <sub>2</sub> O-N <sub>2</sub> -He	Three 1-inch-wide plugs in H <sub>2</sub> O annulus
		3	Photo	H <sub>2</sub> O, H <sub>2</sub> O-N <sub>2</sub> , H <sub>2</sub> O-N <sub>2</sub> -He	Six 1/4-inch-wide plugs in H <sub>2</sub> O annulus
1A	5K	1	Photo	H <sub>2</sub> O-N <sub>2</sub> -He	Pulsing as severe as with 20K size; frequency faster
		3	Photo	H <sub>2</sub> O, H <sub>2</sub> O-N <sub>2</sub> , H <sub>2</sub> O-N <sub>2</sub> -He	Outside tube extended 3/4 inch
		1	Photo	H <sub>2</sub> O-N <sub>2</sub> -He	Telescoped in 3/4 inch steps
		1	Photo	H <sub>2</sub> O-N <sub>2</sub> -He	Inside tube extended 3/4 inch
		2	Mass Distribution	H <sub>2</sub> O-N <sub>2</sub> -He	Outside tube extended 3/4 inch
		3	Photo	H <sub>2</sub> O-N <sub>2</sub> -He	Inside tube extended 0, 1/8, 1/4, 1/2, and 3/4 inch
		3	Photo	H <sub>2</sub> O, H <sub>2</sub> O-N <sub>2</sub> , H <sub>2</sub> O-N <sub>2</sub> -He	Three 1/2-inch-wide plugs in H <sub>2</sub> O annulus; pulsed
		1	Mass Distribution	H <sub>2</sub> O-N <sub>2</sub> -He	Three 1/2-inch-wide plugs in H <sub>2</sub> O annulus
2A	20K	3	Photo	H <sub>2</sub> O, H <sub>2</sub> O-N <sub>2</sub> , H <sub>2</sub> O-N <sub>2</sub> -He	Fan view
		3	Photo	H <sub>2</sub> O, H <sub>2</sub> O-N <sub>2</sub> , H <sub>2</sub> O-N <sub>2</sub> -He	Edge view
		3	Photo	H <sub>2</sub> O-N <sub>2</sub> , H <sub>2</sub> O-N <sub>2</sub> -He, H <sub>2</sub> O-He	Fan view; increased nitrogen flow
		1	Photo	H <sub>2</sub> O-N <sub>2</sub> -H <sub>2</sub> O	Between fan and edge view
		4	Mass Distribution	H <sub>2</sub> O, H <sub>2</sub> O-N <sub>2</sub> , H <sub>2</sub> O-N <sub>2</sub> -He	4-1/2, 6-1/2, and 9 inch distances to collector
2A	5K	3	Photo	H <sub>2</sub> O, H <sub>2</sub> O-N <sub>2</sub> , H <sub>2</sub> O-N <sub>2</sub> -He	Fan view
		3	Photo	H <sub>2</sub> O, H <sub>2</sub> O-N <sub>2</sub> , H <sub>2</sub> O-N <sub>2</sub> -He	Edge view
		2	Photo	H <sub>2</sub> O-N <sub>2</sub> , H <sub>2</sub> O-N <sub>2</sub> -He	Fan view; threefold increase in N <sub>2</sub>
		3	Mass Distribution	H <sub>2</sub> O-N <sub>2</sub> -He	3-1/2 and 6 inch distances to collector
2C*	20K	4	Photo	H <sub>2</sub> O, H <sub>2</sub> O-N <sub>2</sub> , H <sub>2</sub> O-N <sub>2</sub> -He	Edge view
		4	Photo	H <sub>2</sub> O, H <sub>2</sub> O-N <sub>2</sub> , H <sub>2</sub> O-N <sub>2</sub> -He	Fan view
		1	Mass Distribution	H <sub>2</sub> O-N <sub>2</sub> -He	
9A	20K	3	Photo	H <sub>2</sub> O, H <sub>2</sub> O-N <sub>2</sub> , H <sub>2</sub> O-N <sub>2</sub> -He	Double normal water flowrate
		3	Photo	H <sub>2</sub> O, H <sub>2</sub> O-N <sub>2</sub> , H <sub>2</sub> O-N <sub>2</sub> -He	
		2	Mass Distribution	H <sub>2</sub> O-N <sub>2</sub> -He	
		3	Photo	H <sub>2</sub> O, H <sub>2</sub> O-N <sub>2</sub> , H <sub>2</sub> O-N <sub>2</sub> -He	Cylindrical portion of cup eliminated
		1	Mass Distribution	H <sub>2</sub> O-N <sub>2</sub> -He	Cylindrical portion of cup eliminated
9A	5K	3	Photo	H <sub>2</sub> O, H <sub>2</sub> O-N <sub>2</sub> , H <sub>2</sub> O-N <sub>2</sub> -He	Cylindrical portion of cup eliminated
		1	Mass Distribution	H <sub>2</sub> O-N <sub>2</sub> -He	Cylindrical portion of cup eliminated
11A	20K	3	Photo	H <sub>2</sub> O, H <sub>2</sub> O-N <sub>2</sub> , H <sub>2</sub> O-N <sub>2</sub> -He	Double normal water flowrate
		1	Mass Distribution	H <sub>2</sub> O-N <sub>2</sub> -He	
		3	Photo	H <sub>2</sub> O, H <sub>2</sub> O-N <sub>2</sub> , H <sub>2</sub> O-N <sub>2</sub> -He	
		1	Mass Distribution	H <sub>2</sub> O-N <sub>2</sub> -He	

\*Modified from configuration 2A

the standard 200-micron droplet size injector. The remaining 21 tests were visual experiments of an exploratory nature where no photographs or mass distribution data were obtained.

### Tricentric Model LA Injector

The tricentric LA configuration contained a LOX annulus with hot gas injected through the center core and hydrogen fuel around the periphery. The original injector concept was designed and fabricated to provide injection of all propellants at the same axial position within the chamber; i.e., through elements flush with the injector face.

Experimental results obtained during the cold-flow studies indicated the existence of a severe flow-pulsing phenomenon which was believed to be associated with the reduced velocity of sound propagation through the homogeneous two-phase mixture of water and gas. Both gaseous simulants were injected at sonic velocity during the cold-flow tests. The calculated sonic velocity through the water was approximately 5000 ft/sec. The sound velocity for helium was 3260 ft/sec at the existing cold-flow conditions. For a two-phase mixture of water and helium the velocity of sound propagation can be calculated by the equation

$$c = \left[ \frac{1}{\rho^2} \frac{1}{1-x/\rho_\ell^2 c_\ell^2 + x/\rho_g^2 c_g^2} \right]^{1/2} \quad (23)$$

where

$c$  = acoustic velocity

$\rho$  = density

$x$  = quality (gas to liquid mass ratio)

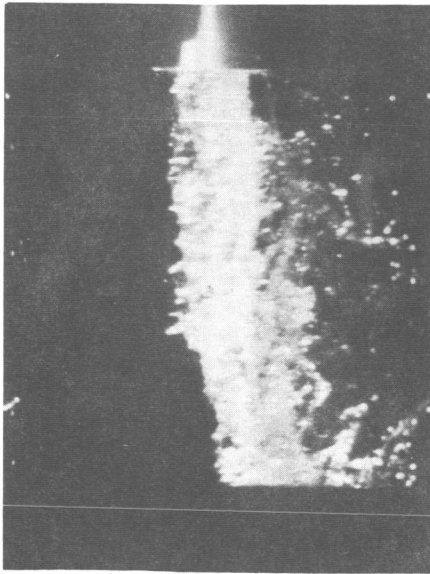
This equation assumes that for the two-phase mixture, the pressure changes do not effect the atomization rates. Using this expression, the velocity of sound propagation in the water-helium mixture at the exit of the tricentric

injector was calculated to be 975 ft/sec. To satisfy the conditions of continuity, the change in exit velocity caused a corresponding change in gas density within the helium manifold, and thereby generated unsteady flow conditions.

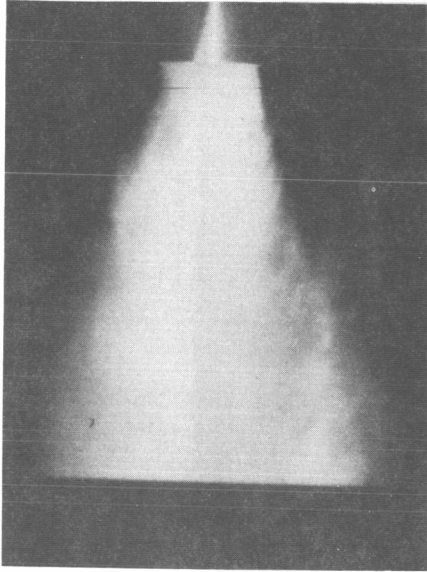
A series of tests was conducted with modified tricentric configurations to study the pulsing behavior. The modifications consisted of altering the exit geometry of the basic flush-mounted elements. The first modified configuration tested contained recessed water and helium injector elements as illustrated in Fig. 10b. Figure 22a illustrates the typical spray pattern with only the injected water flowing; relatively large ligaments of unatomized water can be seen. The nitrogen gas is additionally flowing through the outer annulus for Fig. 22b. Comparison of these two photographs illustrates that there is a considerable enhancement of the atomization as a result of the gas/liquid interaction. Particular details of the sprays are not distinguishable; however, it is obvious that these photographs do provide a qualitative indication of the gas/liquid interaction.

The spray field can be seen to broaden further in Fig. 22c during the introduction of the helium flow. The pulsing phenomena was usually associated with the water/helium flow combination. Although the pulsing was readily apparent when viewing the projected 16-millimeter motion pictures, it is difficult to illustrate graphically with a single-frame enlargement.

The liquid mass distribution obtained for this same tricentric configuration is shown in Fig. 23. The numbered contour lines represent regions of constant mass flowrate expressed in milliliters of collected water. The data were obtained with the collection apparatus placed 9 inches below the injector face. Two observations were made. First, a region of relatively high mass concentration can be seen diminishing slightly at the



a.  $H_2O$  (Test No. 71)



b.  $H_2O$  and  $N_2$  (Test No. 72)



c.  $H_2O$ ,  $N_2$ , and He  
(Test No. 73)

Figure 22. Spray Field Characteristics of 20K Tricentric Injector Configuration 1A With Outside Tube Extended 1-1/2 Inches (see Fig. 10b)

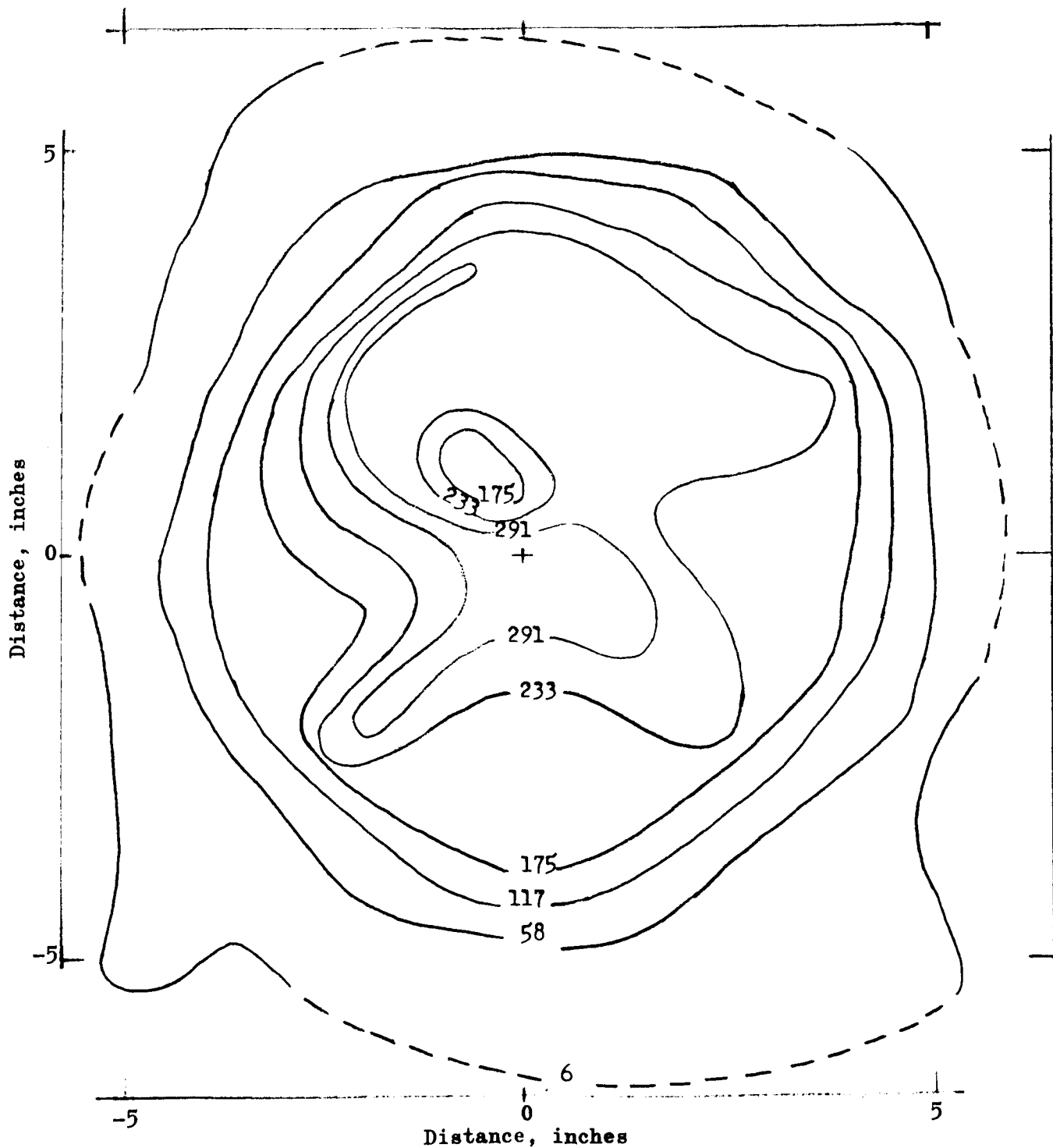


Figure 23. Liquid Mass Distribution of 20K Tricentric Injector Configuration 1A (Contours are in milliliters of water normalized to a total water discharge of 200 pounds. Collector was 9 inches from injector face. Test No. 78.)

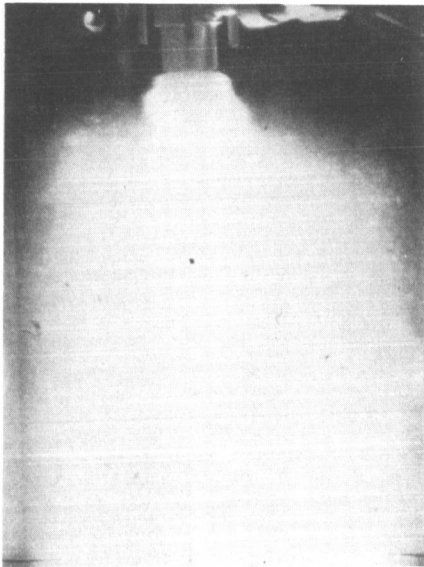
distribution center. This mass concentration suggests fairly good liquid penetration into the region of relatively high momentum helium gas. Second, the mass is shown to be unsymmetrically distributed. This is probably a result of unbalanced pressure distributions within the simulant propellant manifolds.

In addition, tests were conducted with two other exit configurations; internal telescoping (Fig. 10c) and extension of the helium center tube (Fig. 10d). All these variations were done in 1.50-inch step increments on the 20K size injector and 0.75-inch increments on the 5K size injector.

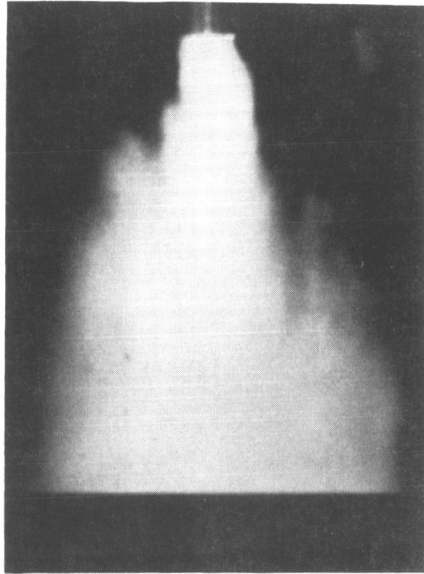
Typical flow-pulsing conditions with the 5K tricentric configurations are illustrated in Fig. 24a and 24b. A maximum flow-pulsing condition is indicated in Fig. 24a and a minimum flow-pulsing condition is shown in Fig. 24b.

Extension of the helium tube (Fig. 10d) effectively isolated the water and helium streams, thereby preventing the two-phase mixture confinement and the associated unsteady-flow phenomena. To determine the minimum extension distance necessary to stop the pulsing, a series of tests were conducted on the 5K size of the model 1A at extension distances of  $1/8$ ,  $1/4$ ,  $1/2$ , and  $3/4$  inch. Evaluation of the Fastax films show that no threshold pulsing condition existed but generally there was an inverse linear relationship between extension distance and pulsing severity. The pulsing was virtually eliminated with an extension distance of  $3/4$  inch. This condition is illustrated in Fig. 24c for the 5K model tricentric.

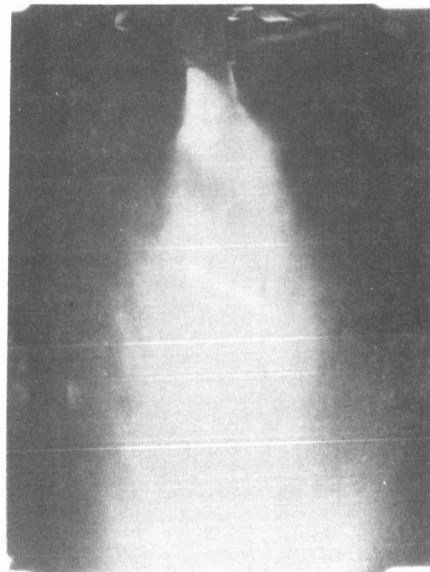
Another approach to the pulsing problem was to insert plugs in the water annulus to block off a portion of the water injection region, thus allowing the helium stream to be less confined by the water stream. With



a. All Tubes Flush  
(Test No. 105)



b. Outside Tube Extended  
(Test No. 60)



c. Inside Tube Extended  
(Test No. 108)

Figure 24. Spray Field Pattern of 5K Tricentric Injector Configuration LA  
With Three Exit Nozzle Configurations

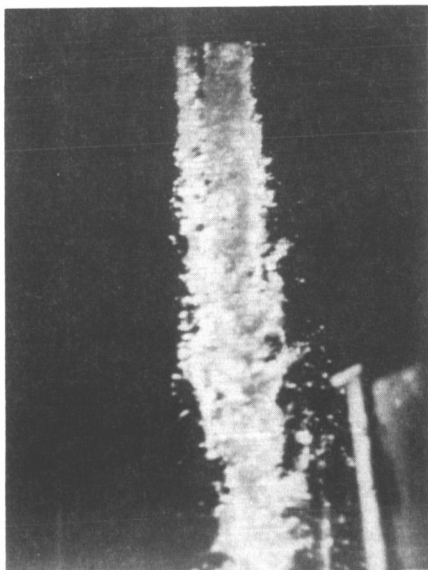
the inclusion of three 1-inch-wide plugs in the 20K size injector (which reduced the water flow area by approximately 40 percent), the pulsing characteristic was virtually eliminated. The water flowrate was held constant, causing a corresponding increase in the injection velocity.

The next series of tests employed six 1/4-inch-wide plugs, blocking off only 20 percent of the water flow area. In addition, these plugs were recessed 1/4-inch from the exit of the injector. The Fastax films of this series showed that the injector pulsed as badly as the original tricentric model 1A.

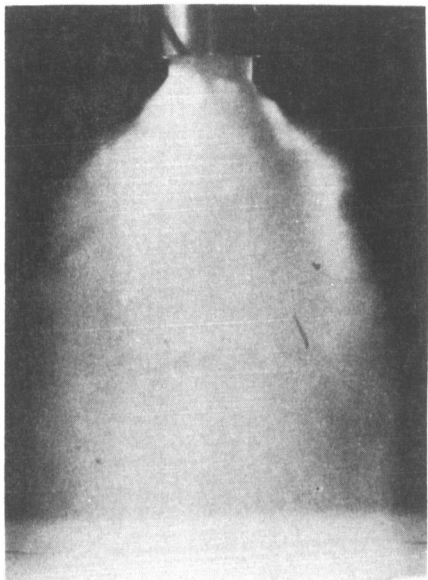
A water-only test with three plugs installed is shown in Fig. 25a. A void in the liquid spray field can be seen corresponding to the position of a plug. A stable test with the 20K configuration is shown in Fig. 25b with all simulants flowing. However, the instability persisted with the equivalent area reduction for the 5K model. This 5K model with the three plugs is graphically illustrated in Fig. 25c. These data suggest that the width of the plug may affect stability more than the percent of area blocked.

The mass distribution collected during a steady-flow run with the 20K three-plug configuration is shown in Fig. 26. Although the distribution is similar to that shown in Fig. 23, the lower concentration of flow in the center is more pronounced for the steady-flow case. The mass distribution data obtained during the pulsing condition (Fig. 23) represent an integrated average with the flowrate varying from maximum to minimum values during the collection period.

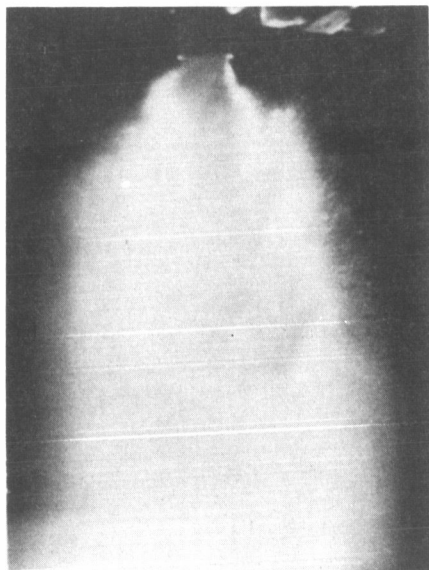
In general, the injectors could not be differentiated on the basis of atomization characteristics.



a.  $H_2O$ ; 20K Size  
(Test No. 122)



b.  $H_2O$ ,  $N_2$ , and He; 20K Size  
(Test No. 124)



c.  $H_2O$ ,  $N_2$ , He; 5K Size  
(Test No. 136)

Figure 25. Spray Fields of 5K and 20K Tricentric Injector Configuration 1A  
Modified With Three Plugs in the Water Annulus

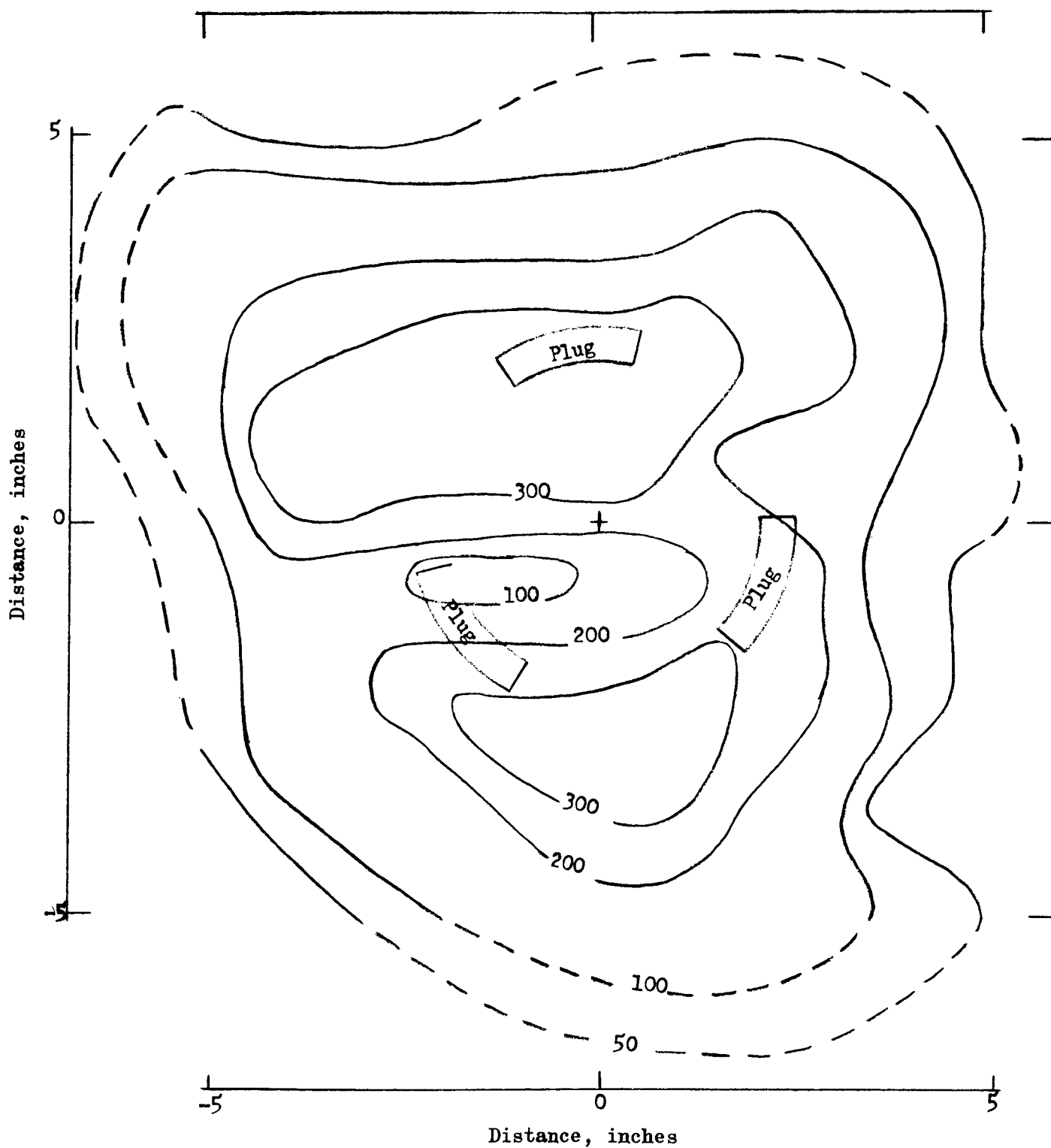


Figure 26. Liquid Mass Distribution Modified 20K Injector Configuration 1A (Modification included three 1-inch plugs inserted in the annular water passage. Contours are in milliliters of water normalized to a total water discharge of 200 pounds. Collector was 9 inches from injector face. Test No. 112.)

### Biplanar Impingement Model 2A Injector

The model 2A configuration consisted of two different pairs of like doublets impinging upon a central showerhead fuel (nitrogen) orifice. One doublet pair contained water and the other contained helium. The center-line impingement distances from the face were  $2\frac{1}{2}$  and  $4\frac{1}{2}$  inches, respectively. The photographs shown in Fig. 27 were taken with the camera field of view aligned with the edge of the water fan formed by the self-impinging water streams. The first view (Fig. 27a) shows the resulting fan formed in the absence of any secondary gas flow. The showerhead nitrogen gas stream was flowing for Fig. 27b. The gas/liquid interaction greatly enhanced the atomization process as evidenced by relative size of the formed droplets and broadening of the overall spray pattern.

Figure 27c shows the spray pattern with just the four impinging (water and helium) streams flowing. Considerable liquid splashback can be observed from the injector face. All propellant simulants were injected for Fig. 27d. Both figures (27c and 27d) graphically illustrate the existence of a void region centrally located within the liquid spray field. The void was caused by the displacement of the spray by the helium injected through one of the doublet elements. These results are further substantiated by the mass distribution plot shown in Fig. 28 through 30.

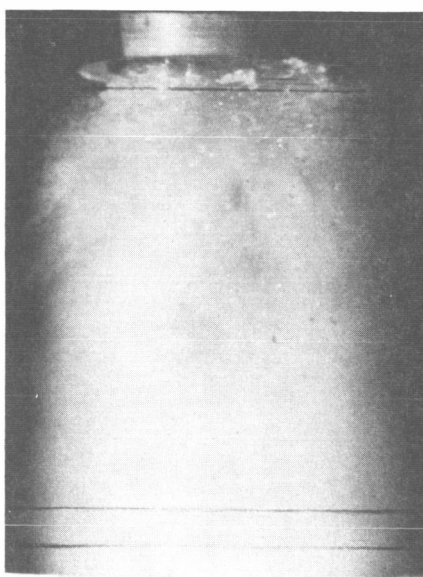
The typically expected fan-shaped pattern is presented in Fig. 28. The somewhat-distorted portion of the fan was probably caused by a slight mismatch in either the momentum of the water streams or in the impingement location. Both water and the showerhead nitrogen stream were flowing for Fig. 29. As expected, the injected gas flow broadened the spray field. The void region caused by the high momentum of the doublet helium streams is graphically illustrated by the distribution pattern of Fig. 30. In this



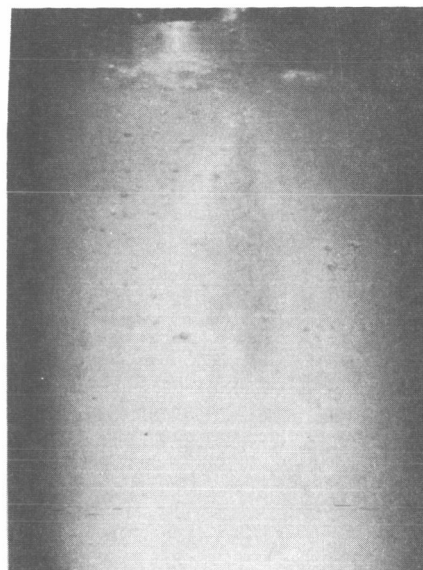
a.  $H_2O$  (Test No. 67)



b.  $H_2O$  and  $N_2$  (Test No. 68)



c.  $H_2O$  and He (Test No. 70)



d.  $H_2O$ ,  $N_2$ , and He (Test No. 69)

Figure 27. Fan-Edge View of Spray From 20K Biplanar Impingement  
Injector Configuration 2A

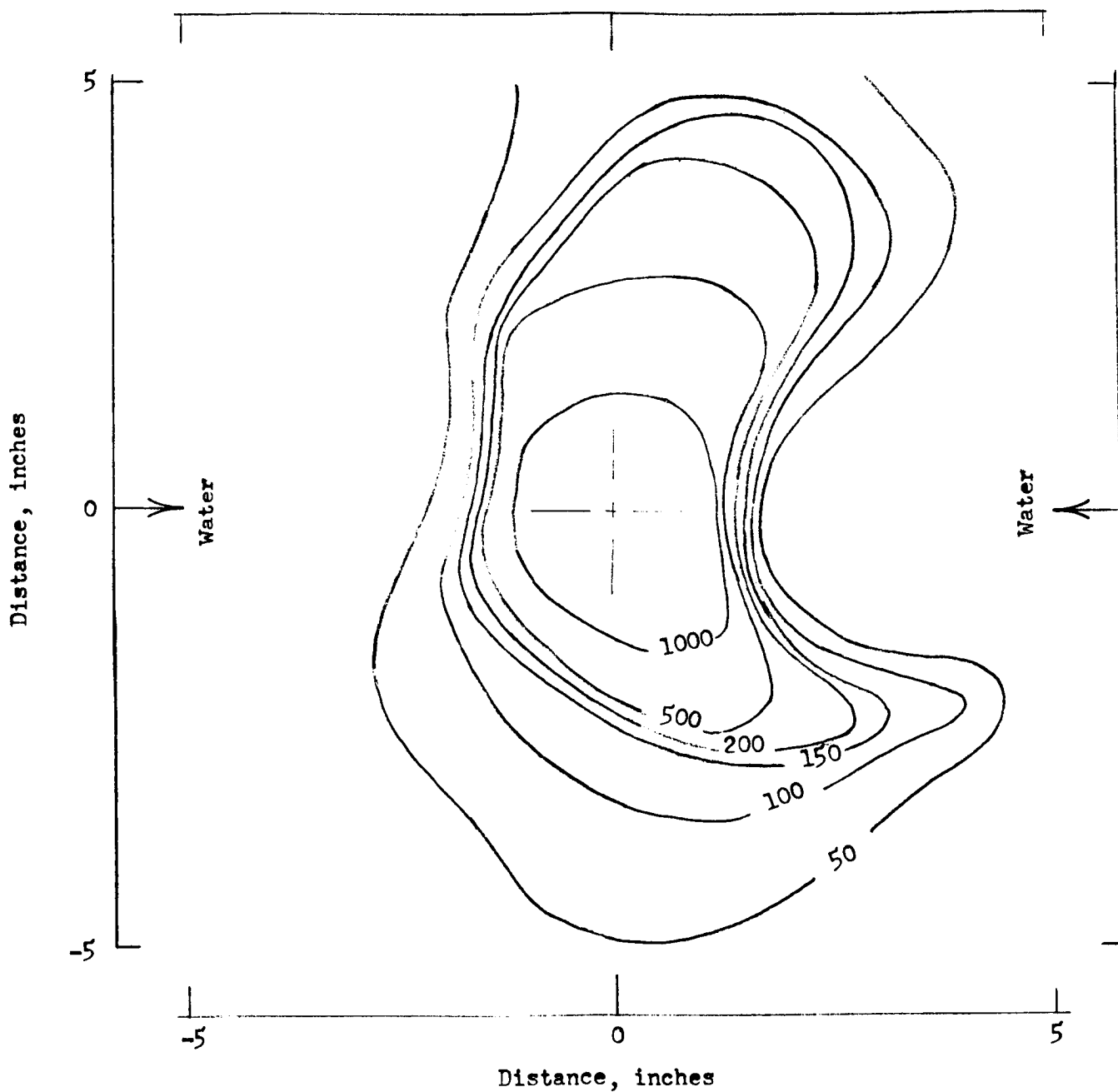


Figure 28. Liquid Mass Distribution of 20K Biplanar Impingement Injector Configuration 2A With Water Only Flowing (Contours are in milliliters of water normalized to a total water discharge of 200 pounds. Collector was located 4-1/2 inches from injector face, at helium impingement location. Test No. 34.)

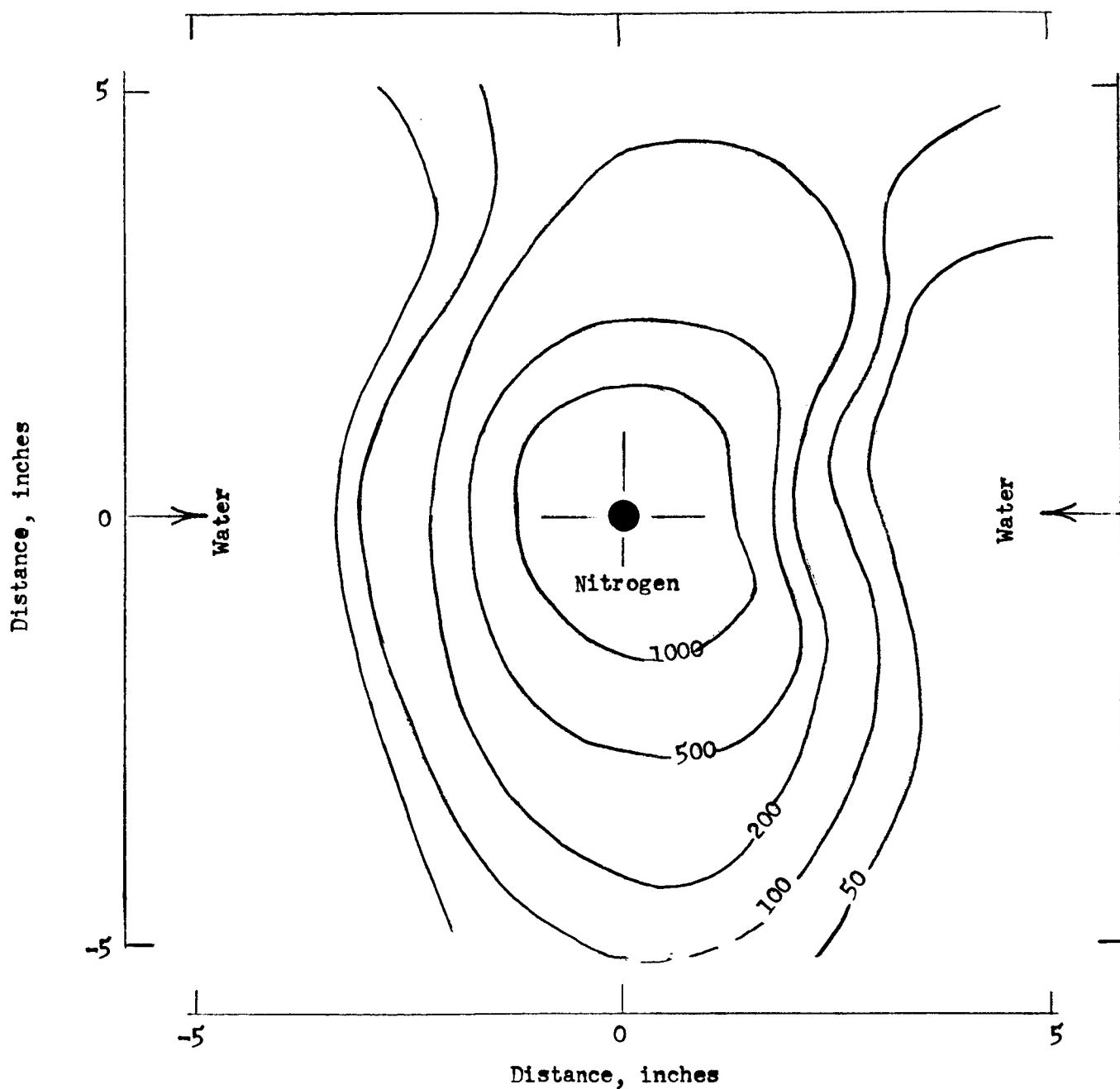


Figure 29. Liquid Mass Distribution for 20K Biplanar Impingement Injector Configuration 2A With Water and Nitrogen Flowing (Contours are in milliliters of water normalized to a total water discharge of 200 pounds. Collector was 4-1/2 inches from injector face. Test No. 35.)

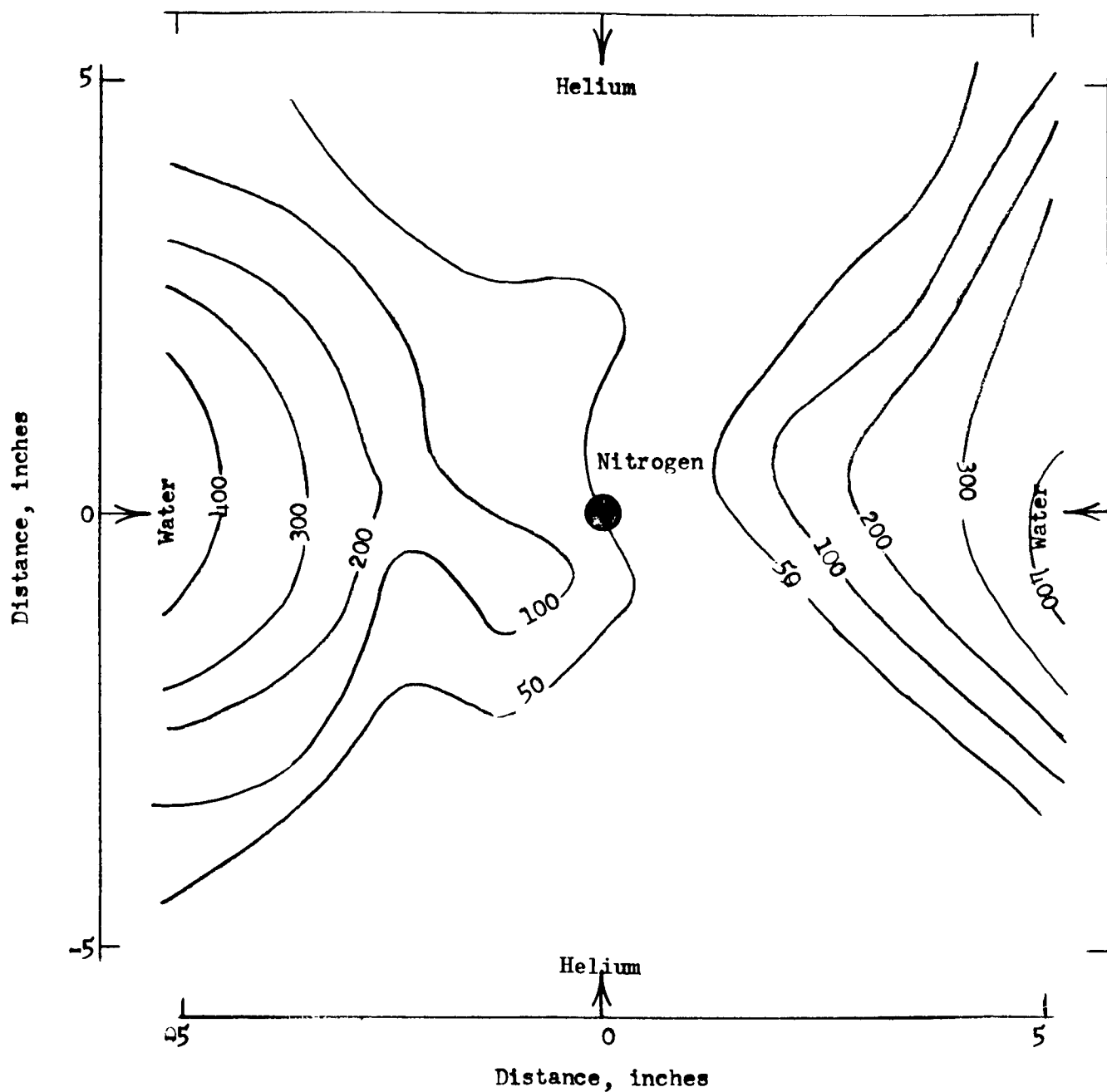


Figure 30. Liquid Mass Distribution for 20K Biplanar Impingement Injector Configuration 2A With All Simulants Flowing (Contours are in milliliters of water normalized to a total water discharge of 200 pounds. Collector was 6-1/2 inches from injector face. Test No. 36.)

case the majority of the injected water was accumulated at the periphery of the collection apparatus. Similar trends were obtained with the 5K model. The mass distribution plot shown in Fig. 31 with all propellants flowing shows that a similar void in the spray pattern occurred. Thus, with the model 2A injector concept, the momentum of the hot-gas simulant was not effectively being utilized.

#### Biplanar Impingement Model 2C Injector

The relatively poor mass distribution data obtained with model 2A suggested that a reversal in the gaseous propellants would more effectively utilize the high momentum of the hot-gas stream. A better placement for the hot-gas energy was considered to be through the central showerhead orifice. Accordingly, the 2A model was modified into the 2C configuration by interchanging the nitrogen and the helium streams, adjusting the injector port sizes, and changing the impingement angle of the water streams causing them to impinge at very nearly the same location as the nitrogen.

The four different flow conditions tested with the model 2C injector are shown in Fig. 32. A fan-edge view showing the impingement of only the water streams is shown in Fig. 32a. The self-impinging nitrogen streams were additionally injected in Fig. 32b and resulted in a relatively coarse atomized injector spray pattern. As shown in Fig. 32c, a finer spray resulted with the water showerhead helium combination. With all simulants flowing, a void region again resulted within the spray pattern, as indicated by Fig. 32d. This pattern is quite similar to that obtained previously with all simulants flowing with the 2A configuration (Fig. 27d). It is rather apparent that injecting the second gas through the doublet elements causes flow separation within the liquid spray field. This is

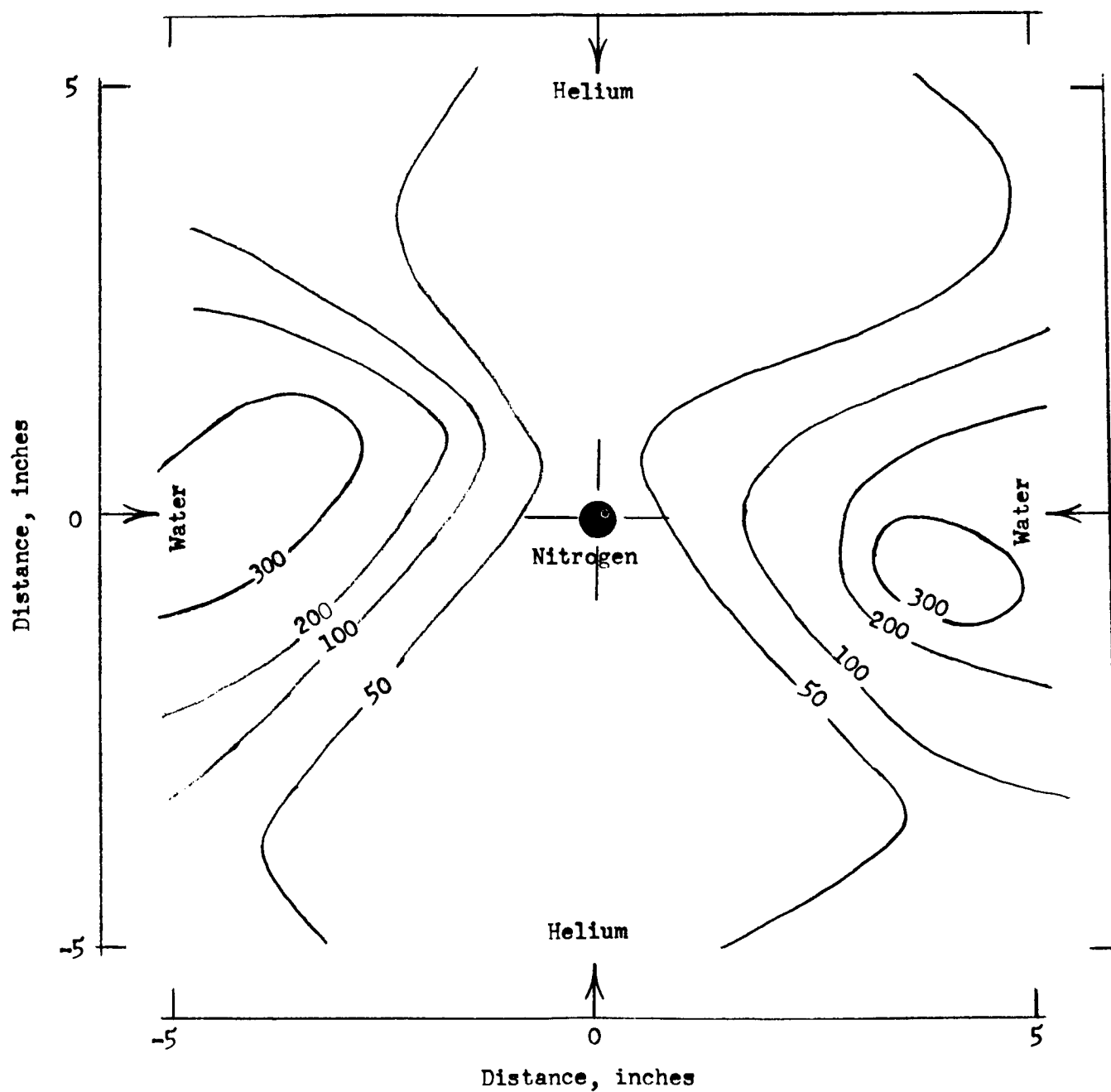
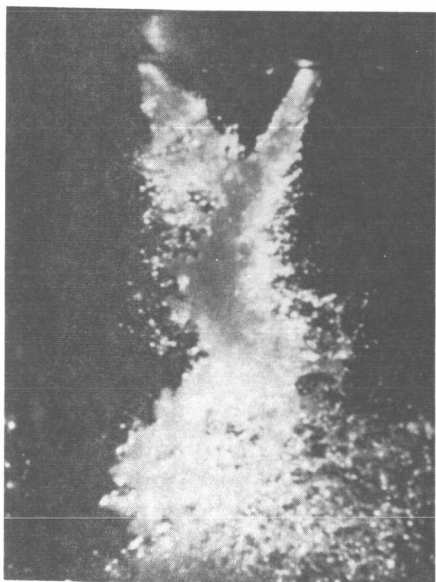


Figure 31. Liquid Mass Distribution of 5K Injector Configuration 2A With all Simulants Flowing (Contours are milliliters of water normalized to a total water discharge of 200 pounds. Collector was 6 inches from injector face. Test No. 81.)



a.  $H_2O$  (Test No. 113)



b.  $H_2O$  and  $N_2$  (Test No. 114)



c.  $H_2O$  and He (Test No. 116)



d.  $H_2O$ ,  $N_2$ , and He (Test No. 115)

Figure 32. Fan-Edge View of Spray From 20K Biplanar Impingement Injector Configuration 2C

further substantiated by the liquid mass distribution data of Fig. 33. Again the central injection region is completely void of liquid.

Although the biplanar impingement injector as designed for the model 2A and 2C configurations gave poor liquid mass distributions, a satisfactory combination of the physical injection parameter could probably provide the desired distribution by further consideration of the secondary impinging gas momentum level and impingement orientation.

#### Impinging Coaxial Model 9A Injector

The model 9A consisted of four coaxial elements impinging upon a large central helium stream. Each coaxial element contained a water core surrounded by a nitrogen mantle. The coaxial elements were designed to impinge 1.3 inches upstream from the injector face with a "recessed cup". The purpose of the cup was to maintain a high relative velocity between the helium and water and thereby accelerate the liquid atomization process.

Three sequential photographs of the 20K model with the recessed cup are shown in Fig. 34 with different simulant combinations. The first (Fig. 34a) shows the injection pattern with water only through the core of each impinging coaxial element. The four impinging streams cause some initial breakup of the injected water. The addition of nitrogen injection around each coaxial water core results in the atomization pattern indicated in Fig. 34b. Although the spray pattern appears good, relatively large droplets can be seen around the spray periphery. Finally, with all simulants flowing, an improved spray pattern results as shown in Fig. 34c. The mass distribution contour map for the configuration with all simulants flowing is shown in Fig. 35. It contains four small regions of relatively high liquid concentration as might be expected with its four symmetrically located impinging streams.

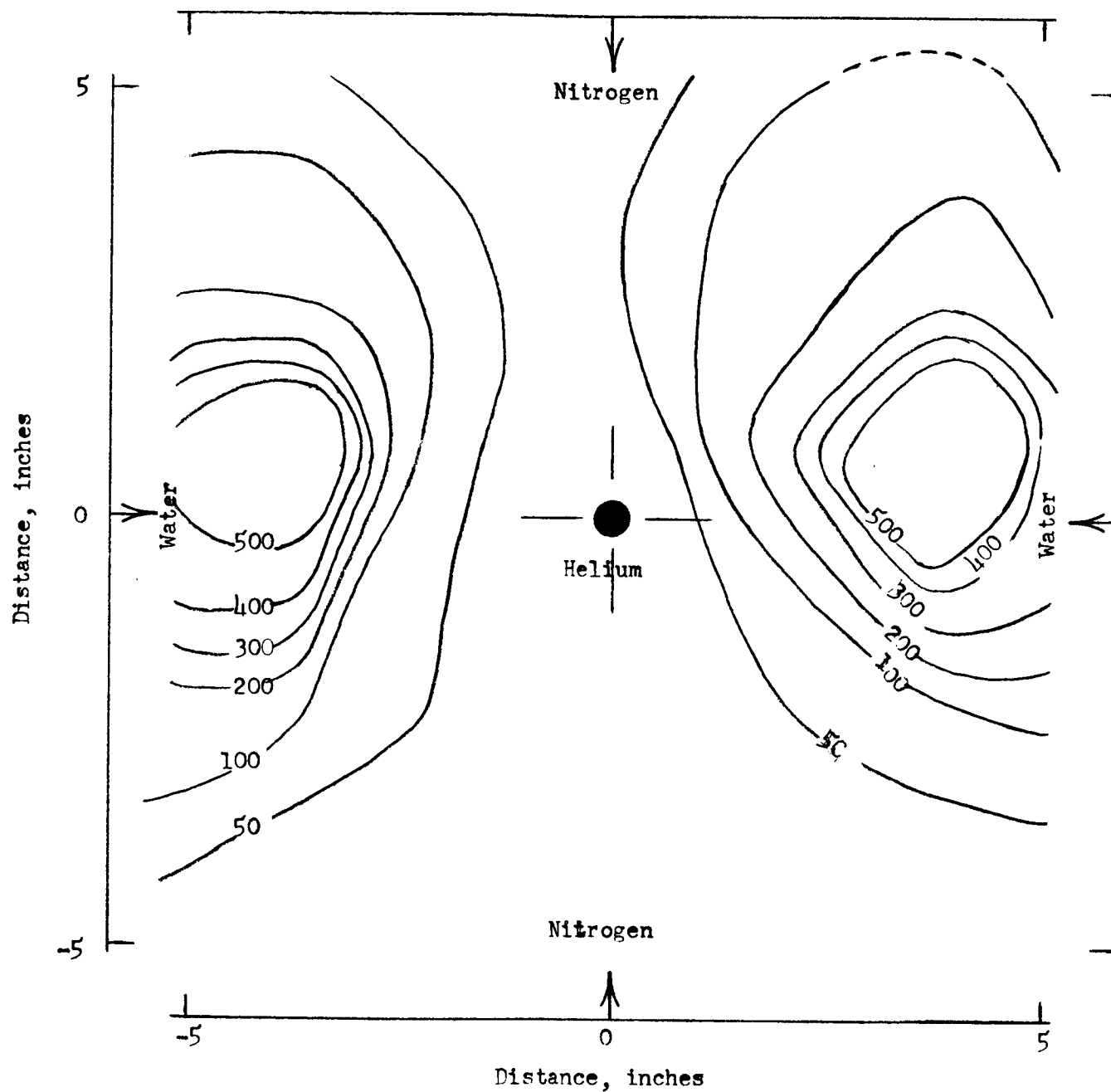
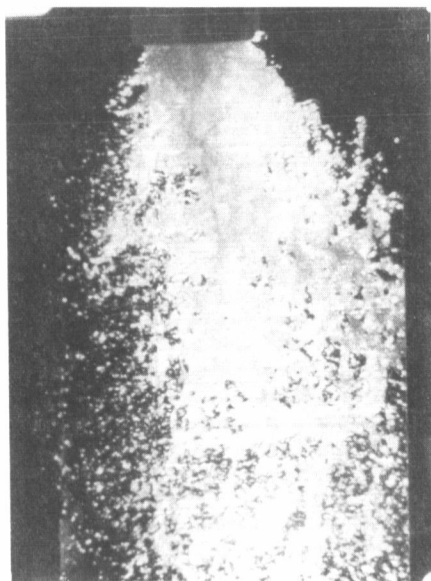
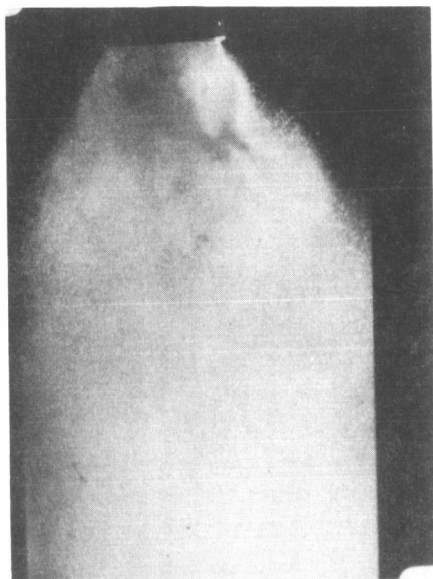


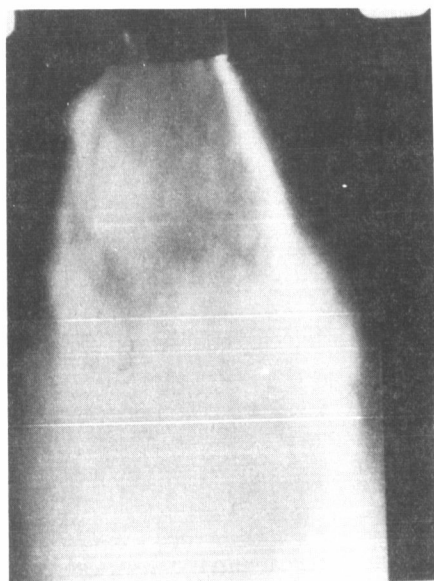
Figure 33. Liquid Mass Distribution of 20K Biplanar Impingement Injector Configuration 2C With All Simulants Flowing. (Contours are in milliliters of water normalized to a total water discharge of 200 pounds. Collector was 9 inches from injector face. Test No. 121.)



a. H<sub>2</sub>O (Test No. 91)



b. H<sub>2</sub>O and N<sub>2</sub> (Test No. 92)



c. H<sub>2</sub>O, N<sub>2</sub>, and He  
(Test No. 93)

Figure 34. Spray Field Characteristics of 20K Impinging Coaxial  
Injector Configuration 9A With Recessed Cup

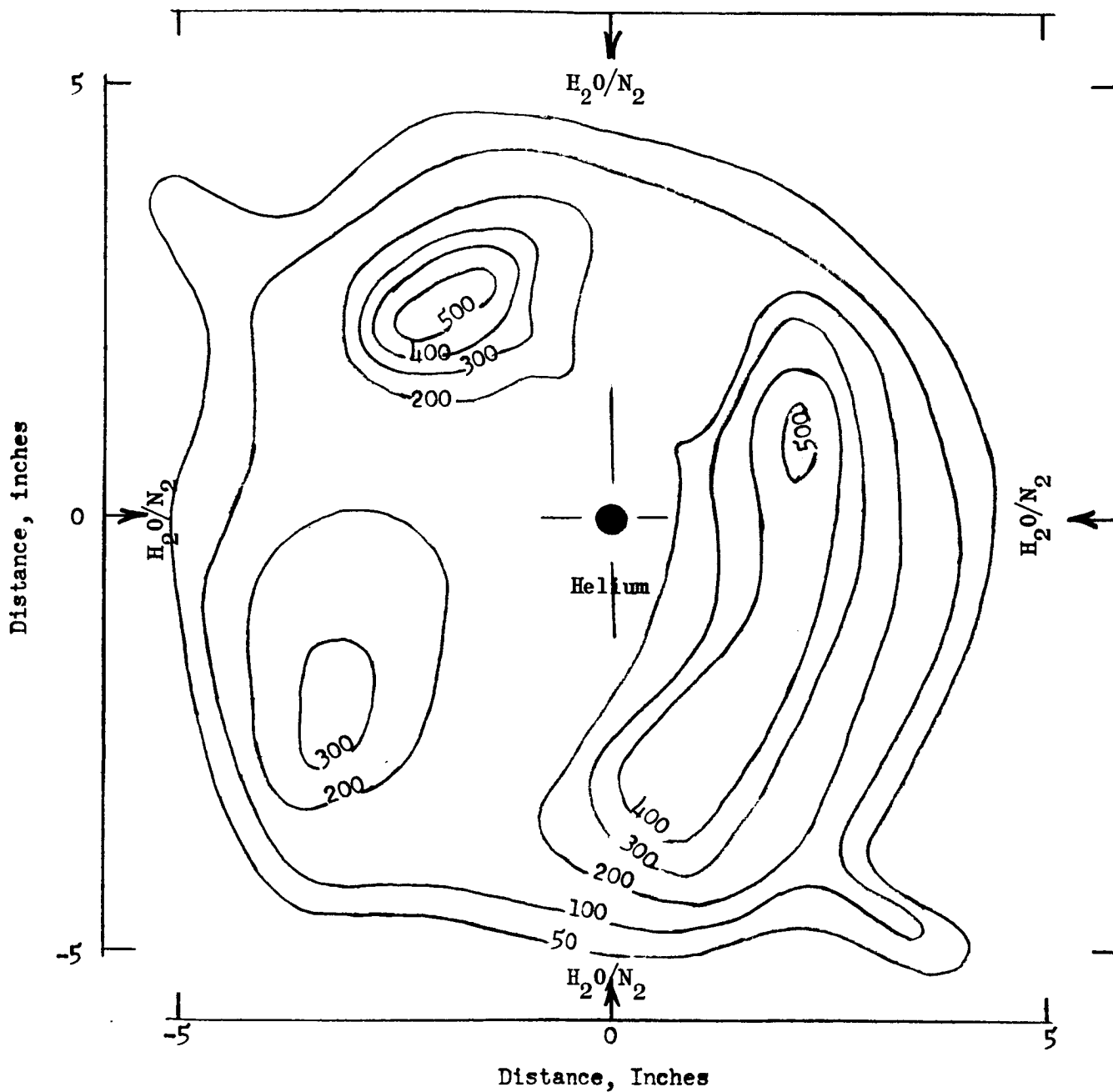


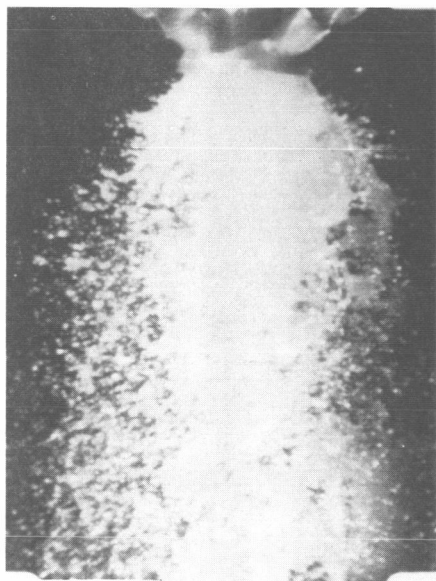
Figure 35. Liquid Mass Distribution of 20K Impinging Coaxial Injector Configuration 9A (Contours are in milliliters of water normalized to a total water discharge of 200 pounds. Collector was 9 inches from injector face. Test No. 95.)

Because the recessed cup design could prove undesirable if burning occurred during the hot-firing tests, an additional series of cold-flow tests was conducted after removing the cylindrical portion of the cup. Qualitative judgment of the Fastax movies indicate better spray characteristics with the shortened cup than with the original test unit. This is illustrated in Fig. 36. Increased droplet atomization is indicated in Fig. 36a and 36b, compared with the similar water/nitrogen flow conditions of Fig. 34. This can be attributed to possible splashback within the longer cup portion of the injector. The relative atomization characteristics appear similar with all simulants flowing; however, a broader spray field results with the modified injector (see Fig. 36c). This fact is further evidenced by the mass distribution plot of Fig. 37. The contour map shows that the mass distribution approaches a more uniform profile without discrete regions of extremely high concentrations.

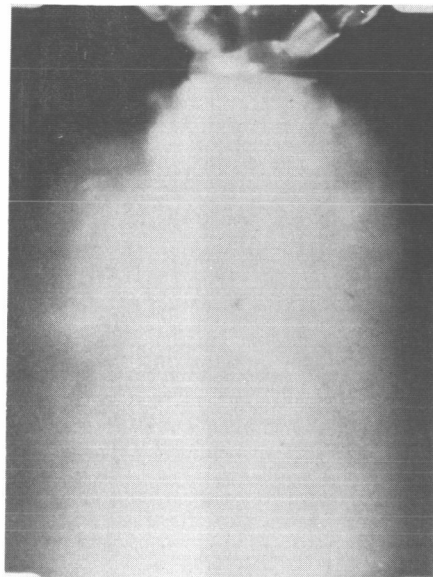
Although not illustrated by spray pattern photographs, similar qualitative results were obtained with the 5K configuration. There was no evidence of any flow instabilities with either 9A model.

#### Commercial Nozzle Model 11A Injector

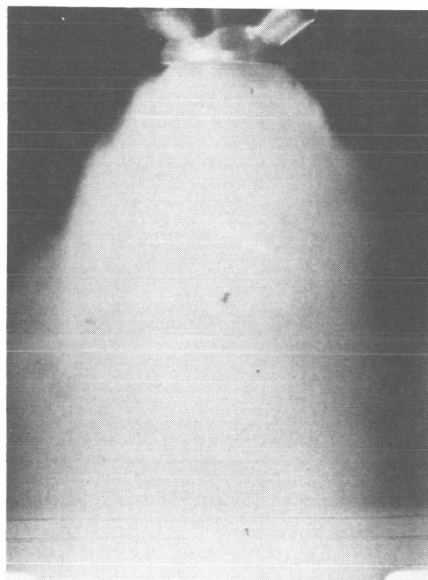
The last injector configuration to be tested was the 11A model. The significant design characteristics of this injector was a commercially available centrifugal pressure-spray nozzle centrally mounted for LOX injection. During cold-flow tests with water only, the nozzle produced a very uniform, cone-shape, coarsely atomized, spray field as shown in Fig. 38a. The helical spray pattern is readily discernible in this photograph for successive convolutions of the flow field. Figure 38b shows the spray pattern collapsing to a narrow field with the addition of the nitrogen flow. With the



a. H<sub>2</sub>O (Test No. 125)



b. H<sub>2</sub>O and N<sub>2</sub> (Test No. 127)



c. H<sub>2</sub>O, N<sub>2</sub>, and He  
(Test No. 128)

Figure 36. Spray Field Characteristics of Modified 20K Impinging Coaxial Injector Configuration 9A (Modified by Removing the Cylindrical Portion of the Cup)

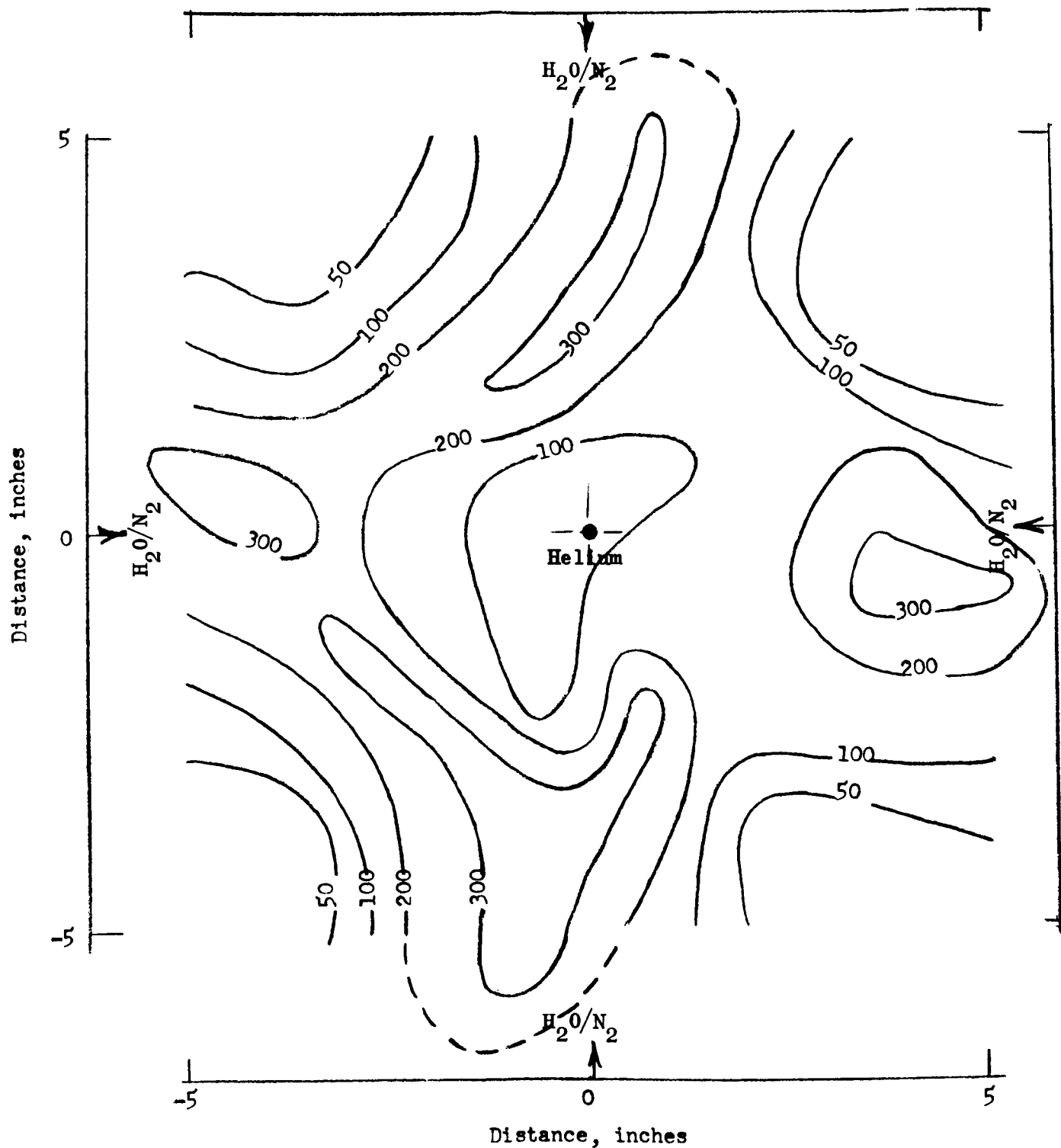
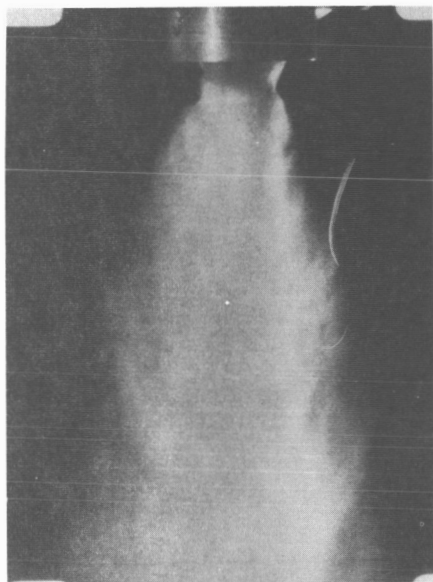


Figure 37. Liquid Mass Distribution of Modified 20K Impinging Coaxial Injector Configuration 9A (Modification was by severing the cylindrical portion of the cup. Contours are in milliliters of water normalized to a total water discharge of 200 pounds. Collector was 9 inches from injector face. Test No. 129.)



a.  $H_2O$  (Test No. 98)



b.  $H_2O$  and  $N_2$  (Test No. 99)



c.  $H_2O$ ,  $N_2$ , and He  
(Test No. 100)

Figure 38. Spray Field Characteristics of 20K Commercial Nozzle  
Injector Configuration 11A With Normal Water Flowrate

introduction of helium flow, which was injected in the annulus immediately surrounding the spray nozzle, the liquid spray field was reduced even further as shown in Fig. 38c. This narrow spray pattern is graphically illustrated by the contour map of the mass distribution test as shown in Fig. 39. To determine how sensitive the distribution pattern was to liquid flowrate, the water flowrate was doubled in a second series of tests. There was some broadening of the spray field as shown in Fig. 40, and the appearance of a depleted region in the middle of the field as evidenced by the mass distribution plot of Fig. 41. The latter would normally be expected by the helical spray nozzle. The questionable improvement in the spray field pattern is still far from satisfactory. Furthermore, the slight improvement that was gained by increasing the water flowrate is offset by the unacceptable deviation in the simulation ratios ( $M_g/\dot{w}_l$ ) and ( $M_g/M_l$ ). The data show quite clearly that the mass distribution of the model 11A is unsatisfactory.

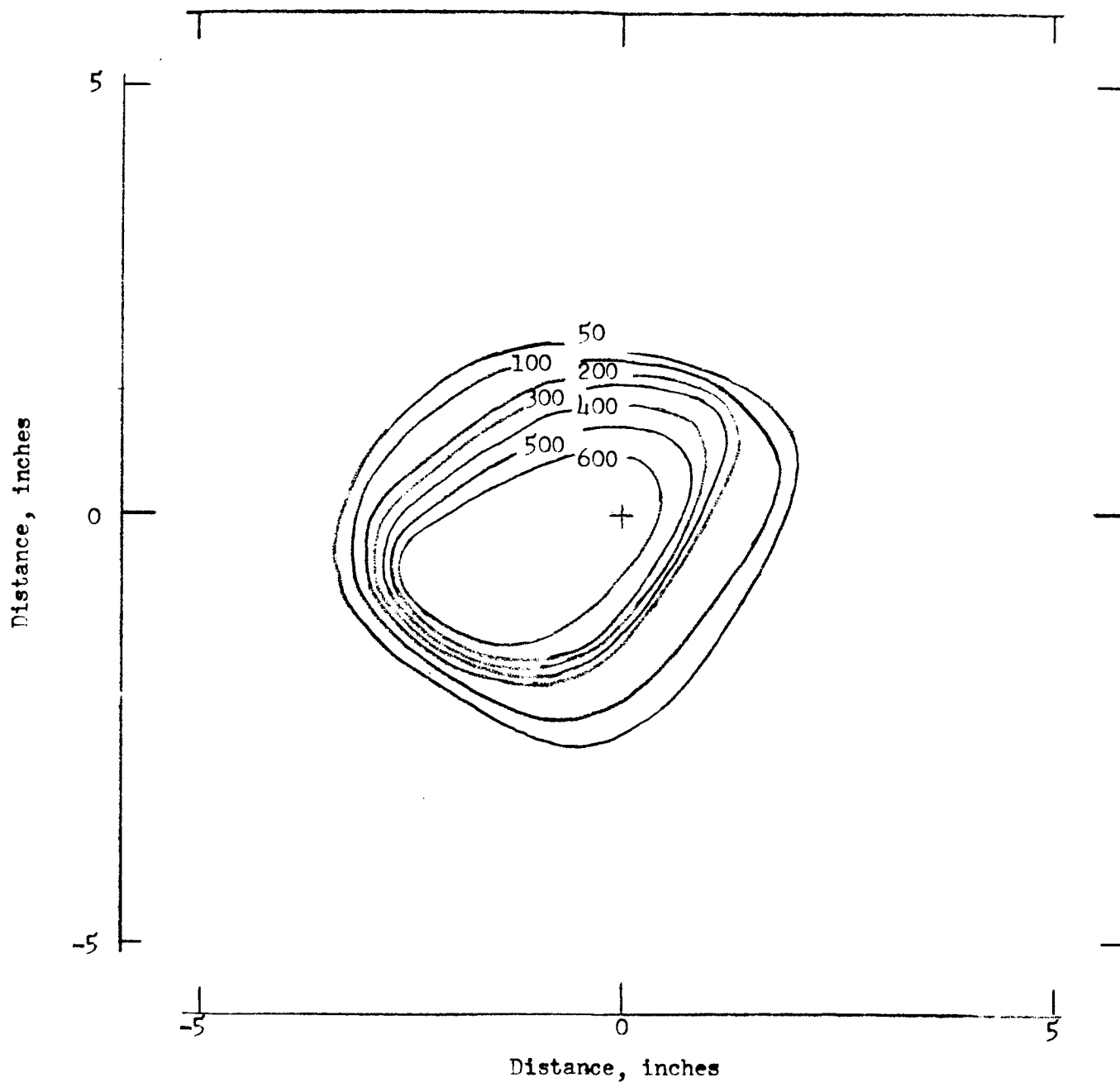
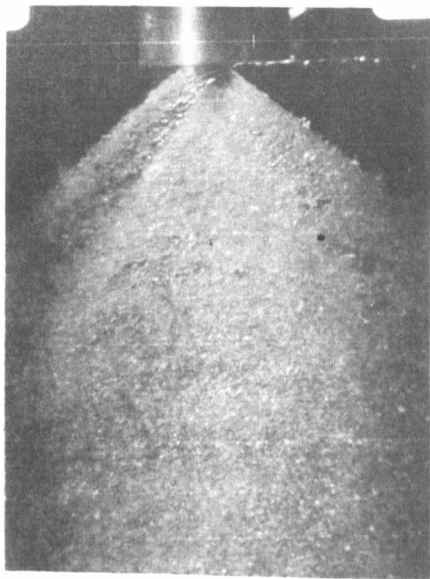
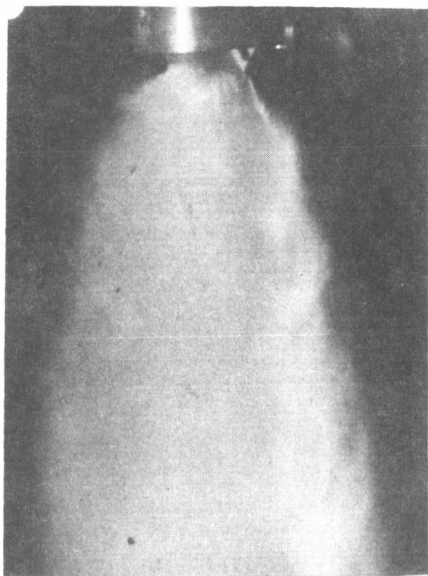


Figure 39. Liquid Mass Distribution of 20K Commercial Nozzle Injector Configuration 11A With Normal Water Flow-rate (Contours are in milliliters of water normalized to a total water discharge of 200 pounds. Collector was 9 inches from injector face. Test No. 96.)



a.  $H_2O$  (Test No. 101)



b.  $H_2O$  and  $N_2$  (Test No. 102)



c.  $H_2O$ ,  $N_2$ , and He  
(Test No. 103)

Figure 40. Spray Field Characteristics of 20K Commercial Nozzle  
Injector Configuration 11A at Twofold Increase in  
Water Flowrate

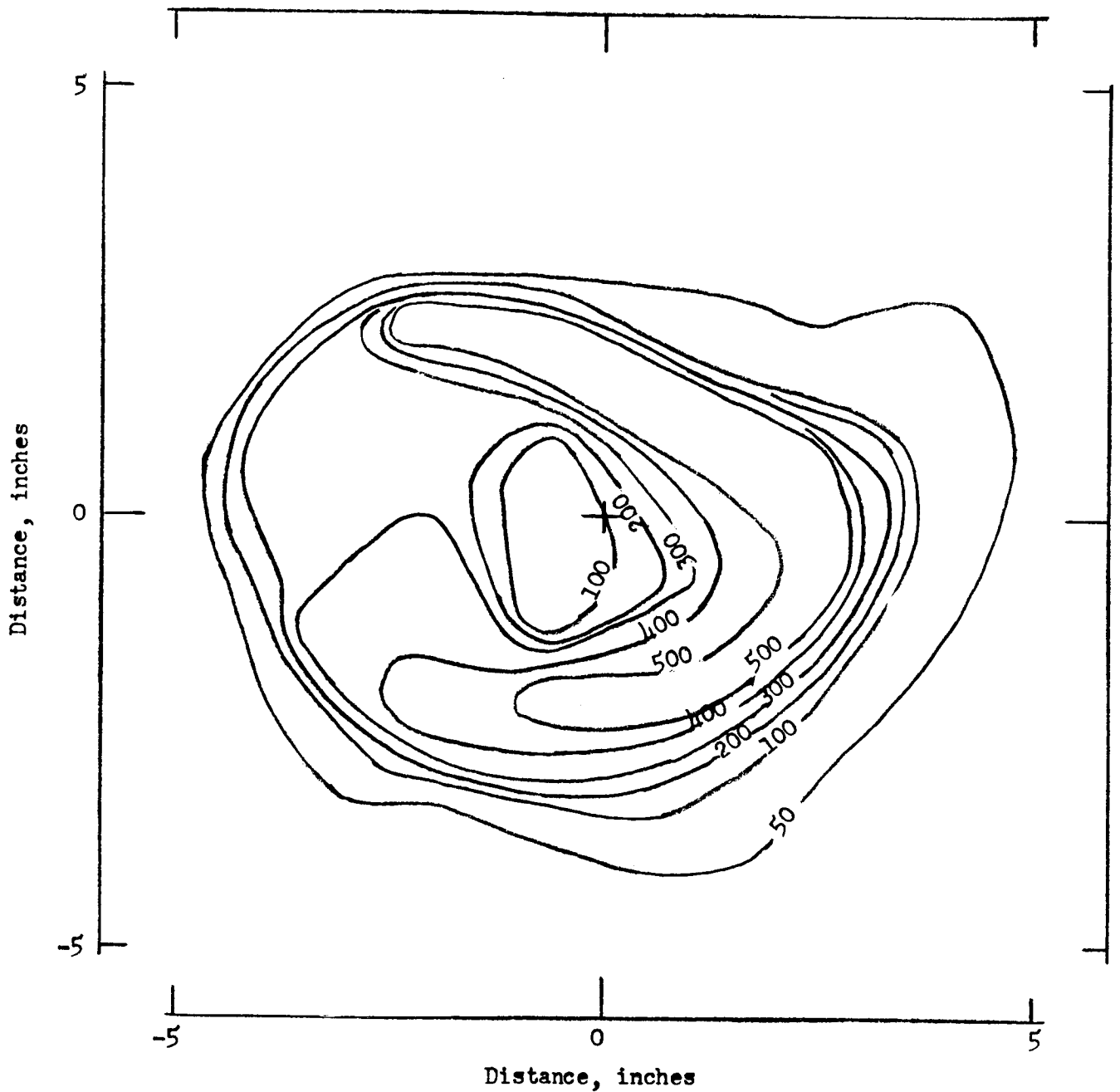


Figure 41. Liquid Mass Distribution of 20K Commercial Nozzle Injector Configuration 11A at Twofold Increase in Water Flowrate (Contours are in milliliters of water normalized to a total water discharge of 200 pounds. Collector was located 9 inches from injector face. Test No. 97.)

## SUMMARY OF COLD-FLOW RESULTS

In general, the experimental results obtained during the Task II cold-flow tests yielded information not predicted by the preliminary theoretical analysis. For example, the analysis did not predict the tricentric model 1A pulsing behavior or the mass distribution problems associated with the biplanar impingement models 2A and 2C. Thus, the cold-flow studies complemented the theoretical analysis to provide useful screening information which permitted the final selection of the modified 1A and 9A injector concepts.

Specific observations made during the program relative to each injector configurations tested are presented below.

### Tricentric Model 1A Injector

1. The tricentric injector models were characterized by a pulsating flow phenomena (~100 cps) with the exit geometry flush-mounted (Fig. 10a).
2. The pulsating flow was virtually eliminated by modifications to the exit geometry; i.e., by extension of the inner (hot-gas) tube of both 5K and 20K models or by partial restriction of the oxidizer annulus of the 20K model.
3. Liquid atomization characteristics appeared satisfactory.
4. Liquid mass distribution characteristics were satisfactory.

The pulsating flow phenomena of the tricentric injector models appears to be related to reduced velocity of sound propagation through the two-phase flow mixture of liquid and gas. Additional study is required to better define the pulsating flow characteristics associated with this type of injector model. The limited results reported herein have shown that the "fixes" are not directly scalable (on an area basis) between different-size models.

### Biplanar Impingement Model 2A and 2C Injectors

1. The high momentum of the injected gases was not effectively utilized.
2. The liquid atomization characteristics appeared satisfactory except for some splashback from the injector face.
3. The liquid mass distribution was not satisfactory with all simulated propellants flowing.

It was apparent during the testing of the 2A and 2C models that the introduction of either gas through the doublet elements caused flow separation within the injected liquid spray. However, an improved spray pattern and liquid mass distribution was obtained when either gas was injected alone through the central showerhead orifice. It follows that a logical location for the injection of both gases is through a central coaxial element or, for one gas species, through a single element.

### Impinging Coaxial Model 9A Injector

1. The liquid mass distribution was satisfactory with the original and shortened cup depths.
2. The liquid atomization characteristics appeared satisfactory with both cup configurations.
3. An improved liquid mass distribution was obtained with the shortened cup. Similarly the liquid atomization appeared better with the shortened cup.

### Commercial Nozzle Model 11A Injector

1. A concentrated liquid mass distribution was obtained which was not satisfactory.
2. The liquid atomization characteristics appeared satisfactory.

### TASK III

#### HOT-FIRE TESTING

The hot-fire testing was conducted primarily for performance and stability evaluation of the most promising high-thrust-per-element two-stage injector concepts. Two injector concepts were selected from the Task II cold-flow study and two different thrust-per-element sizes were designed for each concept, giving a total of four injectors. A workhorse thrust chamber and a hot-gas generator were selected to support the injector evaluations. Operating parameters for the main thrust chamber assembly components are shown in Table 15.

The hot-firing test series was conducted for each of the four injector configurations at different hot-gas flowrates while maintaining a relatively constant overall mixture ratio, chamber pressure, and chamber length. The chamber length was increased for stability evaluation purposes, in selected tests, and the chamber pressure was reduced in selected tests to evaluate the throttling capability. Performance measurements included characteristic exhaust velocity ( $c^*$ ) and specific impulse. Characteristic exhaust velocity was determined independently from measurements of thrust and chamber pressure.

TABLE 15

## MAIN THRUST CHAMBER OPERATING PARAMETERS USING 5K AND 20K INJECTORS

Component	Value
<u>Chamber</u>	
Propellants	Hydrogen (50 to 250 R temperature) and LOX
Maximum Thrust Level, pounds	20,000 (sea level)
Mixture Ratio, oxidizer/fuel	5.0 (includes hot-gas flow)
Chamber Pressure, psia	50 to 500
Characteristic Length ( $L^*$ ), inches	30 to 70
<u>Gas Generator</u>	
Propellants	Liquid Hydrogen and LOX
Exhaust Temperature, F	1200
Flowrate	Up to 15 percent of total flow

## TEST HARDWARE

Each of the four injectors was designed for a nominal thrust level of 20,000 pounds. These injector designs were started during the design studies of Task I and were completed during the hot-firing portion of the program. A workhorse thrust chamber was designed and fabricated to support the injector evaluations. In addition to the basic 30-inch characteristic length ( $L^*$ ) chamber, a combustion chamber extension section (for a 70-inch  $L^*$ ) and a spare nozzle liner were used. The hot gas was supplied by an existing J-2 gas generator.

### 20K Tricentric Injector Configuration 1A

The 20K configuration 1A injector consisted of a single tricentric element positioned in the center of a circular injector plate. The injector element contained three different-diameter tubes positioned coaxially. Hot (1200 F) gas generator gas passed through the center tube and was surrounded by an annulus of LOX and then an outer annulus of hydrogen fuel. The three tubes were welded together with the exit ends flush mounted, and the tubes (tube assembly) were welded to a flat face or mounting plate. (The inner two tubes can be recessed or extended by simple modification,)

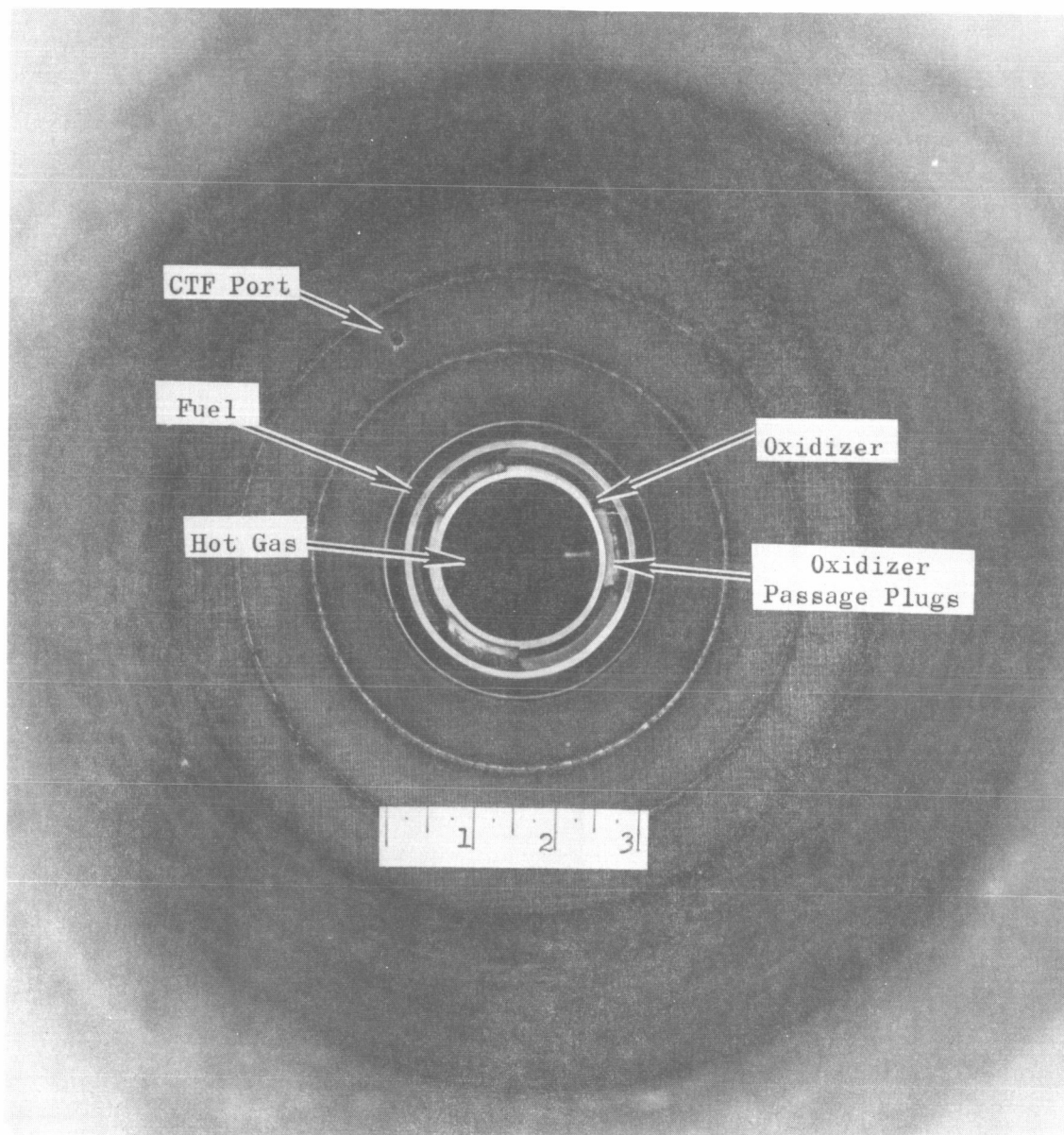
The injector face plate was transpiration cooled with hydrogen passing through a porous Rigimesh material. Hot gas was supplied to the injector through a straight line from a gas generator mounted directly behind the injector. The oxidizer entered the injector from an annular manifold which was fed from a single line located at the back and to one side of the injector element. The fuel was also supplied from the back and to

one side of the injector element. Two lines were used to feed the annular manifold, thus minimizing potential maldistribution. Injector orifice areas and other related operating characteristics are listed in Table 1. Type 347 CRES material was used for fabricating most of the injector components.

Pulsing was noted with the flush-mounted geometrical orifice arrangement during the cold-flow studies; however, the pulsing was virtually eliminated by inserting three 1-inch-wide plugs or interruptions equally spaced in the oxidizer annulus. This three-plug modification was incorporated into the hot-firing injector. The plugs were fabricated from copper, equally spaced and recessed 1/4 inch inside the oxidizer annulus, and then brazed in place.

A photograph of the injector (from the exit end of the thrust chamber) is shown in Fig. 42. Also shown is the end of a small tube midway between the injector element and the chamber wall. This tube was used to inject CTF into the chamber for ignition. Provisions were made on the oxidizer, fuel, and hot-gas injector manifolds to measure the injection temperatures and pressures.

The injector face heat flux was assumed to be the same as the combustion zone maximum (12 Btu/in.<sup>2</sup>-sec). A film-coolant mass flowrate of 0.7 lb/sec was computed (Appendix C) as necessary to cool the face at a 500-psia combustion chamber pressure ( $P_c$ ). Coolant flows at reduced chamber pressures would vary by approximately  $P_c^{0.8}$  power from the design point flowrate. However, to allow for maldistribution of coolant flow and potential high local heat fluxes, more than the computed flowrate was planned for this and each of the other injectors at the nominal design condition.



1XX42-5/15/67-S1

Figure 42. 20K Tricentric Injector Configuration 1a  
Mounted in Thrust Chamber

### 5K Tricentric Injector Configuration 1A

The 5K injector configuration 1A consisted of four elements uniformly spaced and attached to a flat circular faceplate. Each element was similar to the 20K element used for the first injector although the 5K elements were smaller; (one-fourth the injection area of the 20K element). As with the 20K element, three tubes of different diameters were coaxially positioned; however, the exit end of the outer two 5K element tubes were flush mounted to the injector face and the inner tube extended  $3/4$  inch outward (into the chamber). The extension of the inner tube eliminated pulsing during the cold-flow testing as discussed in the Task II section of this report. The plugs, or interruptions, used in the 20K element did not eliminate the pulsing in the 5K element.

Manifolding for the injector was uniformly arranged so each element was supplied with an equal amount of propellant. The hot gas was supplied to the elements from a point directly behind the injector. The oxidizer and fuel entered annular manifolds around each injector element through a series of symmetrically formed tubes. Like the first injector, the face plate was transpiration cooled with hydrogen passing through a porous Rigimesh material. Type 347 CRES was used as the basic material for constructing the injector.

The face of the 5K injector is shown in Fig. 43. The symmetrical manifolding for each of the three propellants is shown in Fig. 44. The fuel enters from the right, the hot gas from the center, and the oxidizer from the left. A portion of the fuel manifolding was removed for this photo to give a better view of the internal plumbing. Injection pressure and temperature pickup ports are in the fuel and oxidizer manifold "TEE's" of this injector (Fig. 44). The hot-gas pressure and temperature pickup ports are in the feedline from the gas generator to the injector.

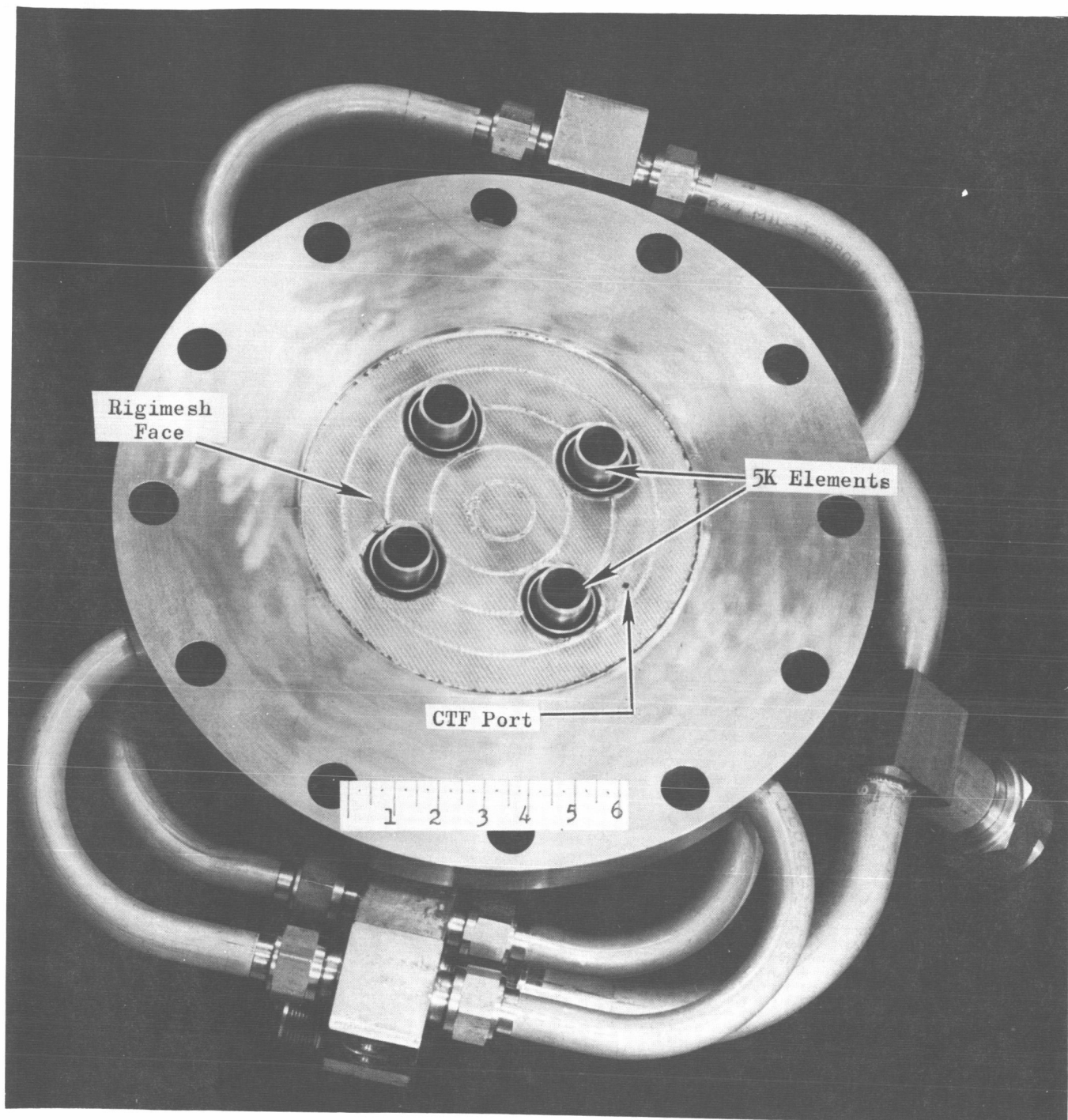


Figure 43. Front View of 5K Tricentric  
Injector Configuration 1a

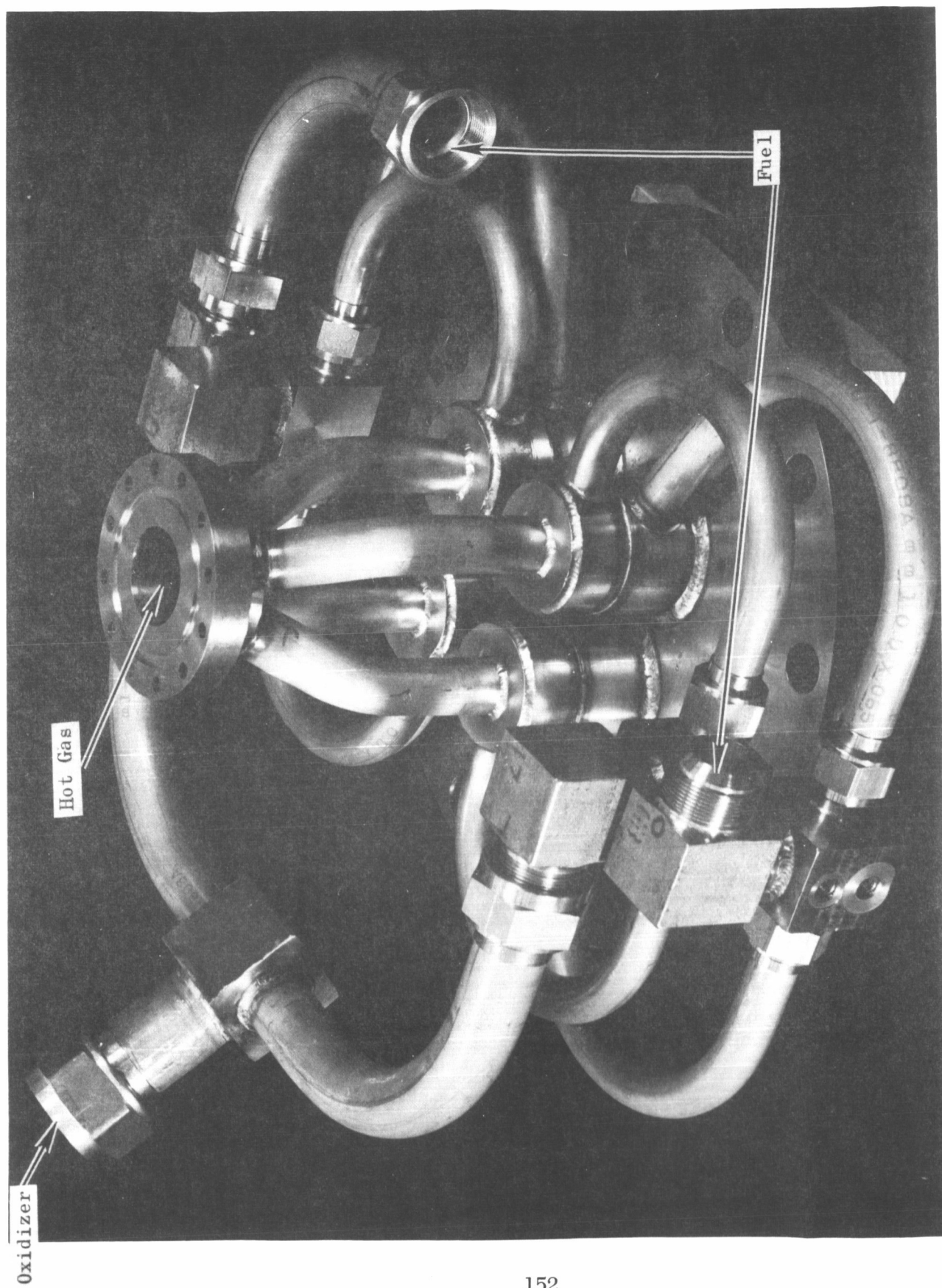


Figure 44. Rear View of 5K Tricentric Injector Configuration 1A

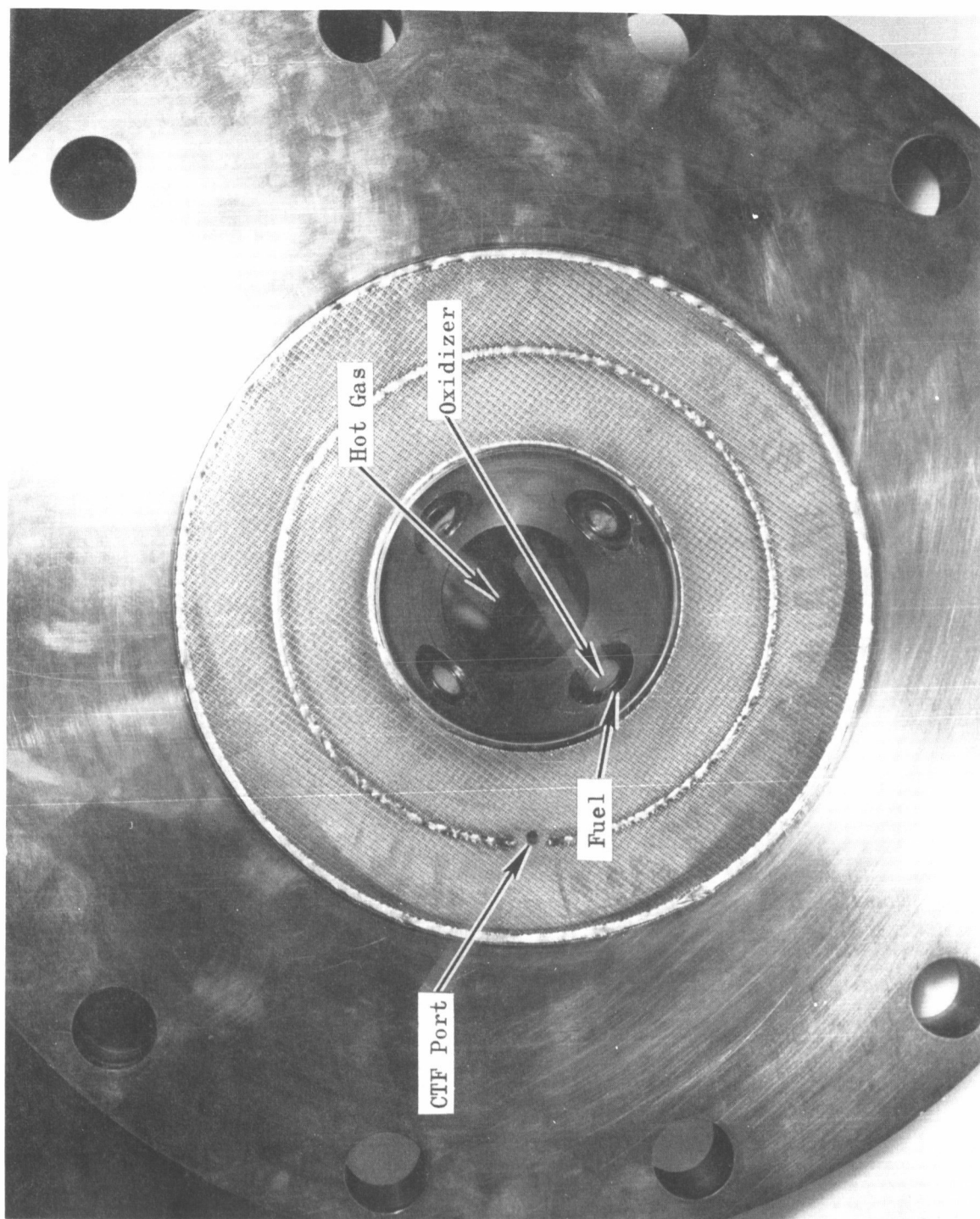
20K Impinging Coaxial Injector Configuration 9A  
(Recessed Cup)

The 20K injector configuration 9A consisted of a central hot-gas jet surrounded by and impinging with four equally spaced coaxial oxidizer/fuel jets. All the jets or injector orifices were inside a shallow recessed cup, thus the centerline impingement point of the jets was near (0.130 inch downstream) the plane of the injector face. The included angle of the coaxial impinging jets was 120 degrees.

Hot gas was supplied to the central injector orifice through a straight line from directly behind the injector. The oxidizer was manifolded into the recessed cup through four tubes which served as the impinging oxidizer orifices. The four tubes were symmetrically manifolded together from a common point at one side and to the back of the injector. The fuel passed into the recessed cup through an annulus around each of the oxidizer tubes. These four annular fuel passages were supplied from an annular manifold which, like the oxidizer, was supplied from the back and to one side of the injector element.

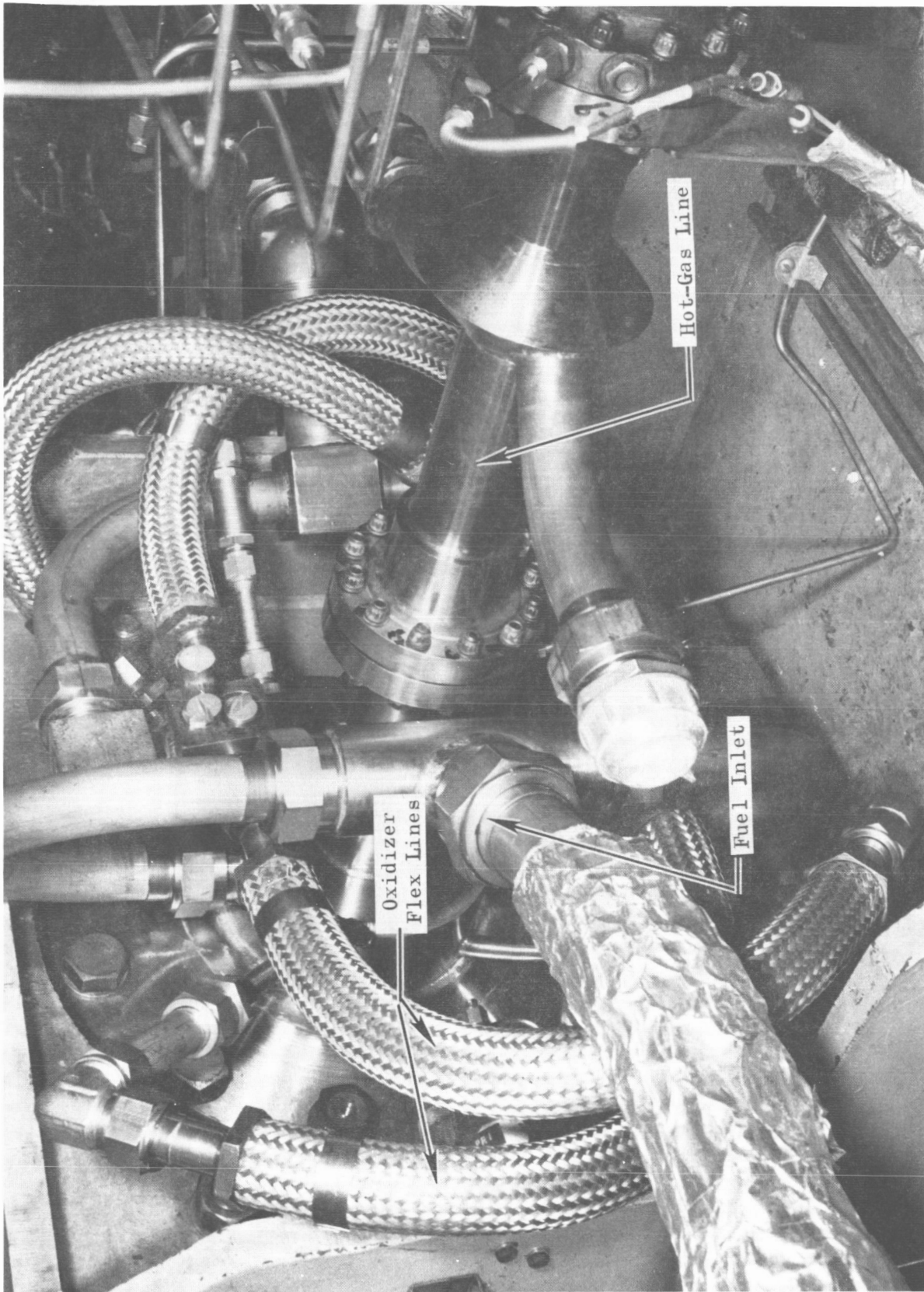
The 20K element was mounted in the center of a flat circular injector faceplate. Hydrogen (fuel) transpiration cooling was used to protect the faceplate. Type 347 CRES material was used to construct the injector components.

A photo of the injector face is shown in Fig. 45. Figure 46 shows the back side of the same injector mounted in place on the test stand. Flex lines were used to manifold the oxidizer to the injector. The oxidizer inlet is at the left, the fuel inlet at the right and the hot-gas duct is in the center.



LXX53-6/3/67-SLA

Figure 45. Front View of 20K Impinging Coaxial Injector Configuration 9A



LXX53-6/7/67-SLB

Figure 46. Rear View of 20K Impinging Coaxial Injector Configuration 9A

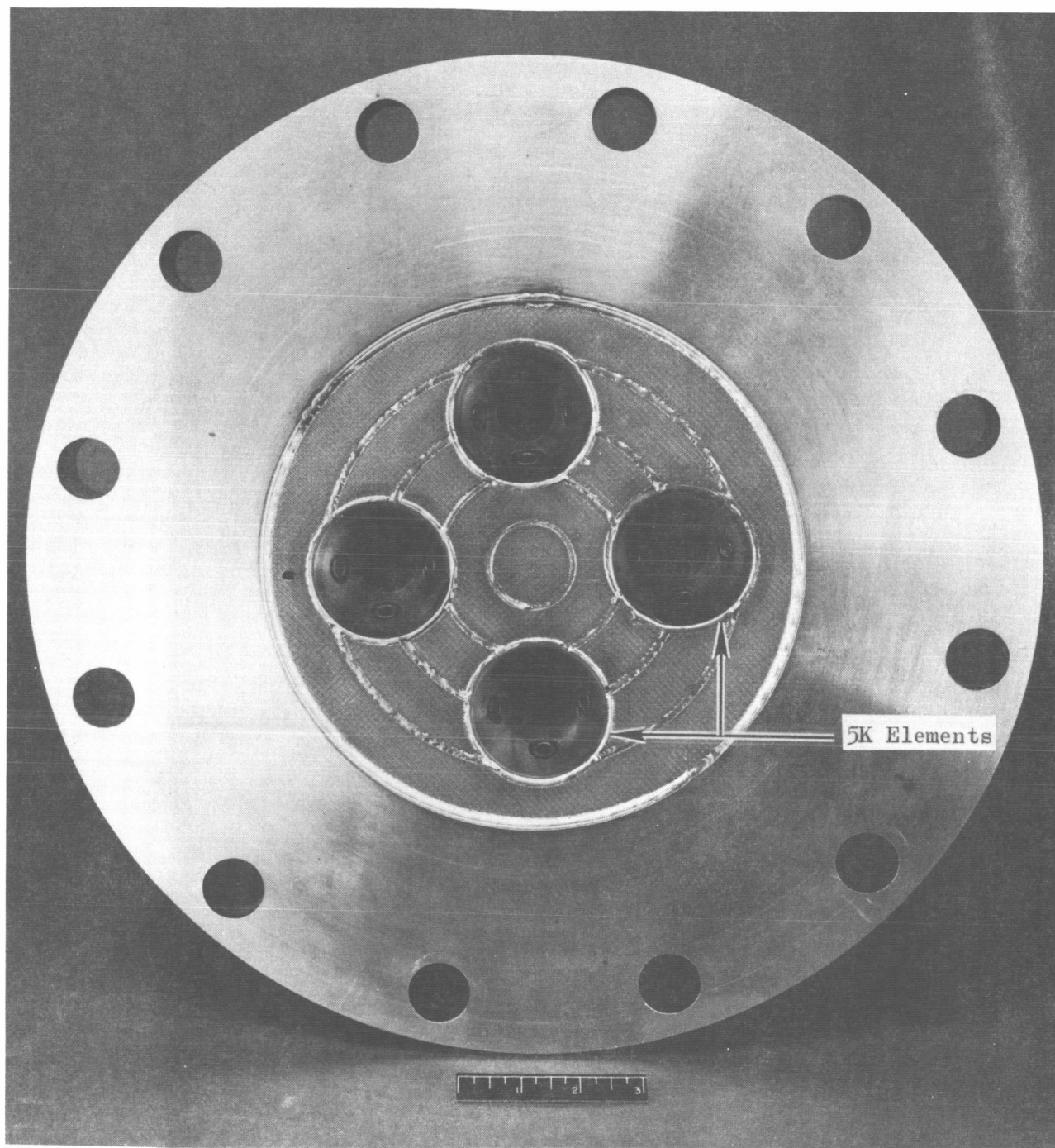
### 5K Impinging Coaxial Injector Configuration 9A (Recessed Cup)

The 5K configuration 9A contained four elements uniformly spaced and attached to a flat circular faceplate. Each element was similar to, but smaller than, the 20K element described previously. As in the 20K configuration, each element consisted of a central hot-gas jet surrounded by and impinging with four equally-spaced coaxial oxidizer/fuel jets. All the jets or orifices were confined inside a shallow recessed cup. The centerline impingement point of the jets was slightly upstream of (0.250 inch) the injector face plane, and the impingement angle (included angle) of the coaxial jets was 120 degrees.

Hot gas was supplied to the center of each of the four elements from a point directly behind the injector. The oxidizer was injected into the recessed cup of each element through four tubes which served as the impinging oxidizer orifices. All the oxidizer tubes for each element were supplied by a common manifold which was supplied by tubing from the back and to one side of the injector.

The fuel passed into each recessed cup through annulii around each of the four oxidizer tubes. The four annulii were supplied from an annular manifold around each element, and these annular manifolds were symmetrically manifolded together at the back and to one side of the injector. Like the other three injectors, the faceplate was transpiration cooled by the fuel passing through a porous Rigimesh material and 347 CRES was used for construction.

Figure 47 shows the face view of this injector. As shown, only one CTF igniter port was used. Plumbing for the injector was similar to that shown in Fig. 46.



IXX42-6/2/67-C1A

Figure 47. Front View of 5K Impinging Coaxial  
Injector Configuration 9a

### Workhorse Thrust Chamber

A workhorse thrust chamber was designed and fabricated for use as the injector test bed during the hot-firing phase of the program (Fig. 48). The chamber design consisted of an uncooled copper combustion zone and a water-cooled copper nozzle. The combustion zone section of the chamber consisted of a 1-inch-thick copper liner inside a 3/8-inch-thick steel jacket. Flanges were provided at both ends of the jacket for attaching the injector and nozzle.

Temperature and pressure instrumentation ports were located at select positions in the combustion zone as shown in Fig. 48. Two combustion zone sections (spools) were fabricated; one was 13.23 inches long giving an  $L^*$  of 30 inches, and one was 20 inches long to increase the  $L^*$  to 70 inches.

The nominal combustion chamber  $L^*$  was established at 30 inches; however, the capability of increased combustion chamber length was required for a more complete evaluation of stability. A chamber length was selected which could produce a longitudinal acoustic frequency equivalent to the first tangential mode of a 1-million-pound-thrust engine. The first tangential acoustic frequency of a 42-inch-diameter 1-million-pound-thrust engine was calculated to be 930 cps from the following equation.

$$f_T = 0.586 \frac{c}{D}$$

where  $c$  is the acoustic velocity in the chamber and  $D$  is the combustion chamber diameter. The longitudinal frequency of the constructed combustion chamber is given by

$$f_L = \frac{c}{2L}$$

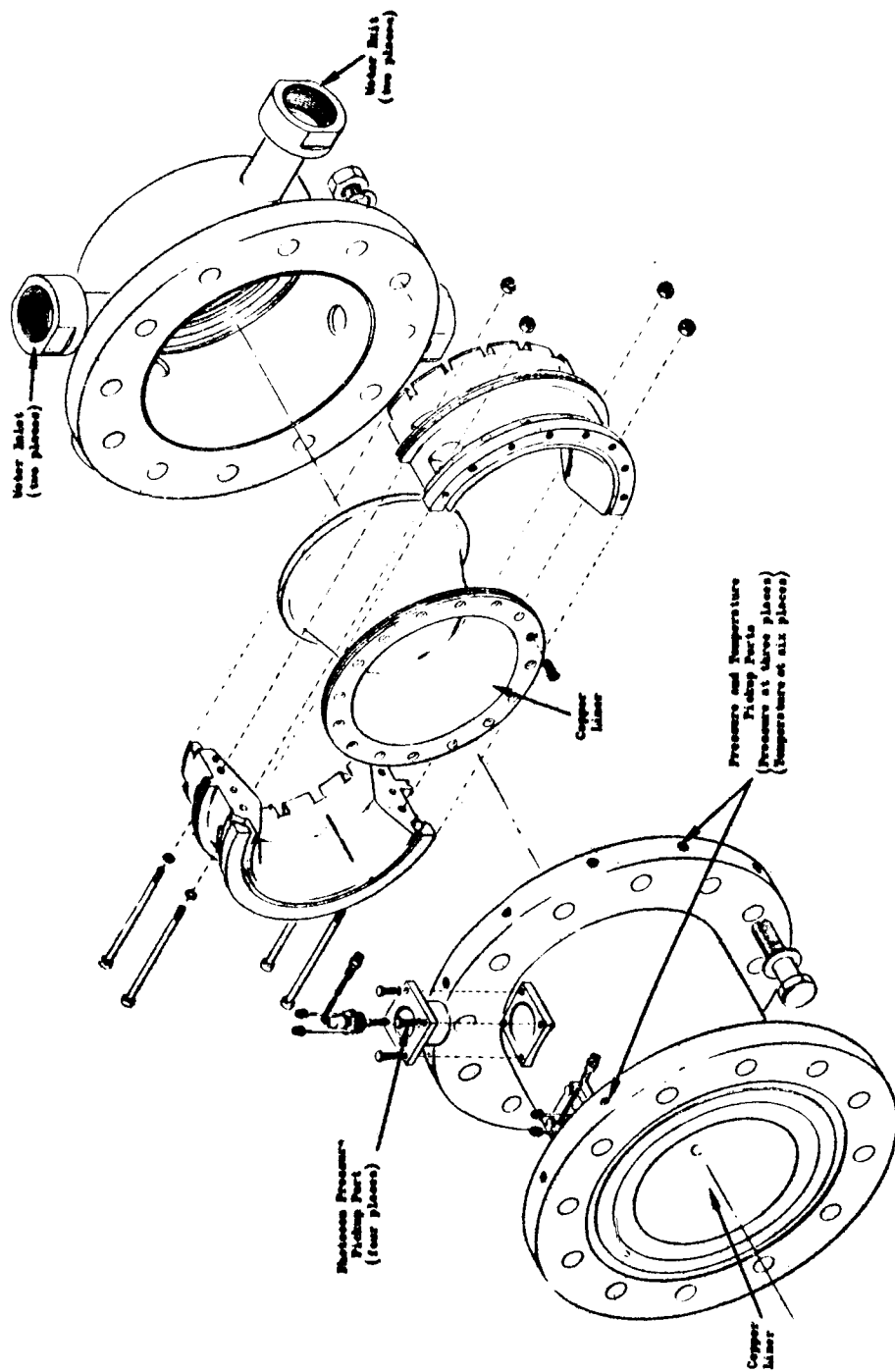


Figure 48. Isometric View of Workhorse Thrust Chamber Used for Hot-Firing Tests

where  $L$  is the distance from the injector to a plane near the chamber throat. The length ( $L$ ) to achieve a 930-cps frequency was calculated to be 35.5 inches, or approximately 20 inches longer than the nominal combustion chamber.

The thrust chamber nozzle section contained a water-cooled copper liner adjacent to the hot gas, and a steel jacket as the outside wall. The initial step in the design of the thrust chamber cooling system was to evaluate the hot-gas film coefficient. The point of maximum heat flux occurs at the throat, which tends to dictate the wall thickness at that location. The hot-gas film coefficients were computed (Eq. C-1 of Appendix C), and the resulting maximum values for the throat and combustion zone ( $\epsilon_c = 2$ ) are listed in Appendix C along with the nominal design conditions. Virtually the same throat film coefficient was obtained when available experimental data were adjusted to expected conditions.

The heat fluxes in the throat and the convergence and expansion sections require water cooling to allow for a reasonable test duration, while the combustion zone was constructed as a copper heat sink. The necessary wall thickness at the throat was determined by considering the heat flux capability of the wall and the material strength. The design heat transfer equation is listed as Eq. C-2 in Appendix C. The point selected for the nominal design conditions was a wall thickness of 0.2 inch, which provides for a 50-percent margin in the heat flux before the melting point is reached. The design wall temperature at the throat of the chamber was computed to be 1350 F, which corresponds with a heat flux of approximately 21 Btu/in.<sup>2</sup>-sec.

The minimum coolant velocity required to avoid the film boiling regime of water was determined to be 50 ft/sec. The saturation temperature of water at 250 psia is 400 F, which provides subcooling ( $T_{wc} = T_B$ ) of about 300 F at the throat of the cooling system. The resulting water mass flowrate to the model with a 0.1 inch annulus is 45 lb/sec, and the bulk temperature rise, as computed with Eq. C-3, was approximately 56 F. Therefore, the subcooling at the exit of the nozzle was still approximately 300 F. During hot-firing tests the coolant velocity was increased to about 67 ft/sec to provide for an additional cooling margin. Correspondingly, the water coolant flowrate increased to about 60 lb/sec and the bulk temperature rise was reduced to 42 F. An increase in the coolant pressure would also increase the cooling margin; however, material strength considerations limited this pressure to about 250 psi at the throat.

A transient analysis was utilized to yield parametric wall temperature curves (Fig. 49) for the combustion zone. The analysis assumes a step function rise in adiabatic wall temperature at time zero, a uniform initial wall-temperature distribution, and an insulated back wall. The design equation is Eq. C-4 of Appendix C. The maximum allowable duration was 3 seconds at the most severe heat transfer condition before melting of the wall would occur at the hot-gas surface. A wall thickness of 1 inch was selected to maintain a somewhat cooler region at the back wall for structural support. Longer durations could be achieved by coating the combustion zone with a thermally insulating layer.

The water-cooled nozzle section was supplied by two inlet lines located 180 degrees apart. From the inlets, the water coolant was distributed into a common manifold cavity inside a carbon steel nozzle shell. The coolant then passed from the manifold through a single constant-width

# COMBUSTION ZONE ( $O_2/H_2$ PROPELLANTS)

$h_g = 0.003 \text{ Btu/in.}^2\text{-sec-F}$      $\alpha = 0.1565 \text{ in.}^2\text{/sec}$   
 $T_{aw} = 5420 \text{ F}$      $k = 4.63 \times 10^{-3} \text{ Btu/in.}^2\text{-sec-F}$   
 $P_c = 500 \text{ psia}$      $\rho = 0.323 \text{ lbm/in.}^3$   
 $MR = 5.0$      $T_{wi} = 80 \text{ F}$   
 $\epsilon_c = 2.0$

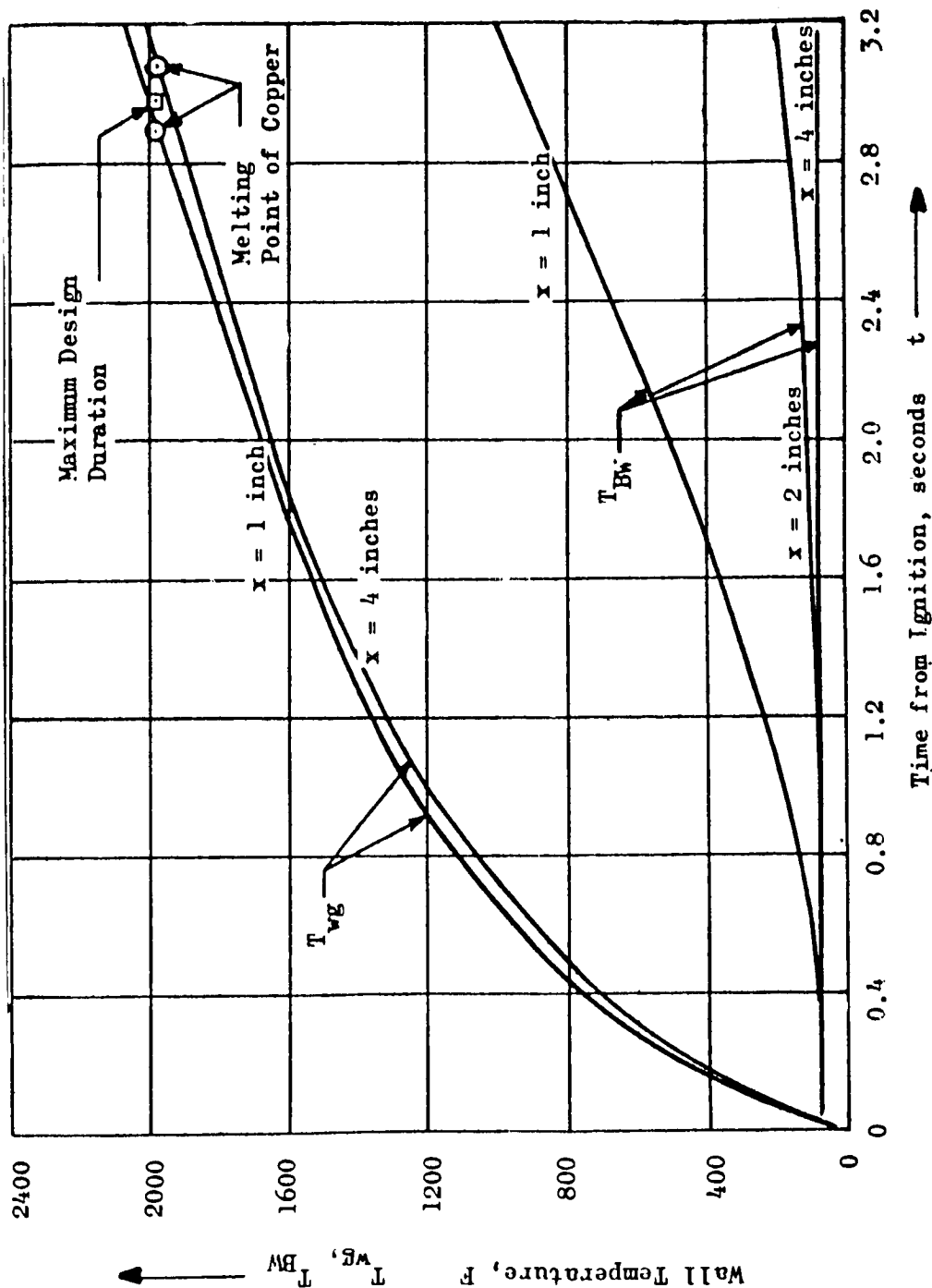


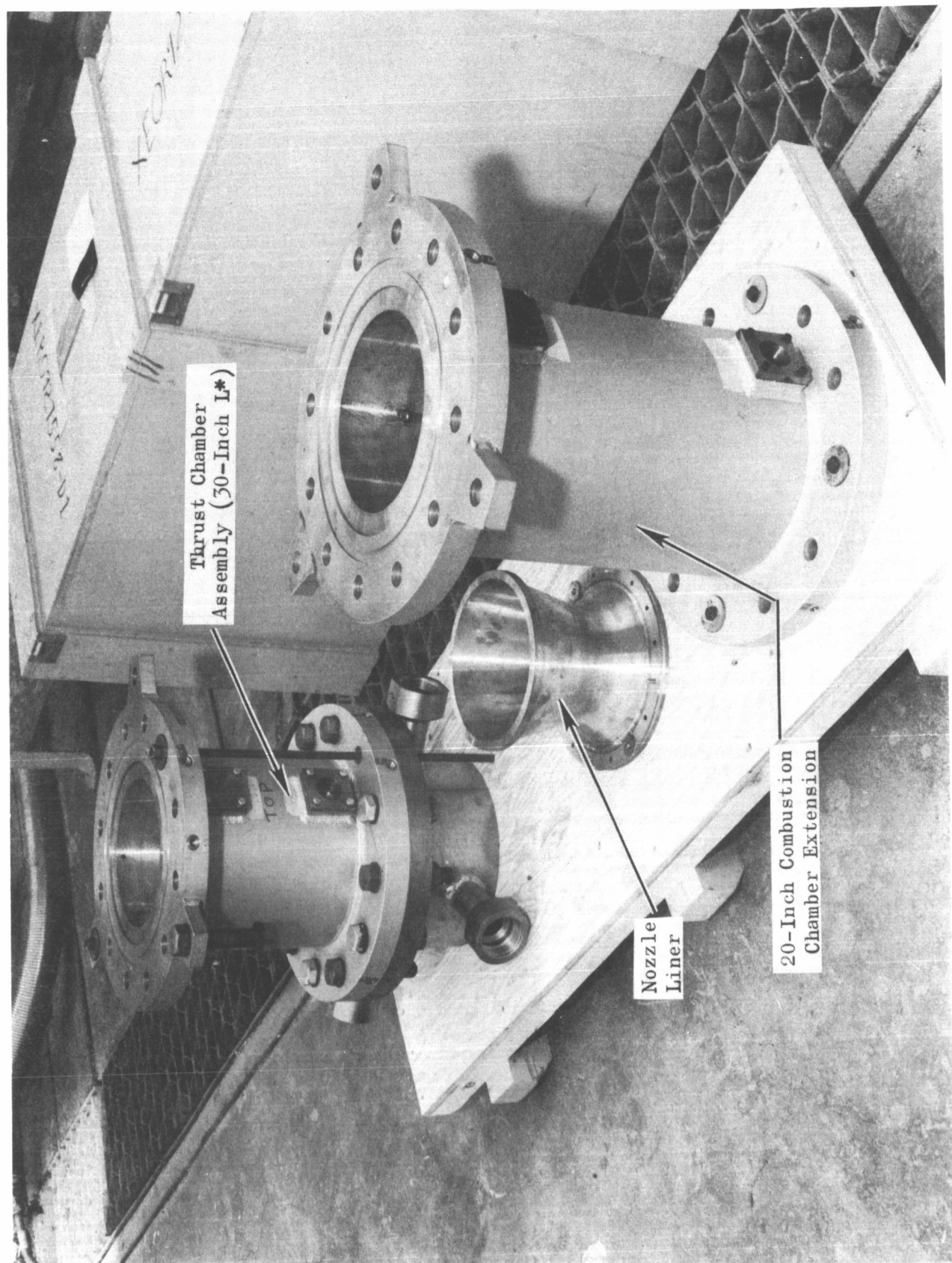
Figure 49. Transient Heating of a Solid Copper Wall Without Convective Cooling

(0.1 inch) passage behind the nozzle contoured wall into a common exit manifold at the nozzle exit and then out through two exit passages 180 degrees apart and 90 degrees from the inlet passages. An isometric drawing of the nozzle and related cooling passages was shown in Fig. 48. A photograph of the chamber assembly (30-inch  $L^*$ ) is shown in Fig. 50 along with a spare copper nozzle liner and the 20-inch combustion chamber extension section.

Pertinent thrust chamber design geometry was as follows:

Combustion chamber diameter, inches	8.55
Nozzle throat diameter, inches	6.05
Nozzle throat area, inches	28.75
Contraction area ratio ( $\epsilon_c$ )	2
Expansion area ratio ( $\epsilon_e$ )	2
Nozzle convergence angle, degrees	60
Nozzle divergence angle, degrees	30
Injector-to-throat length, inches (30-inch $L^*$ )	15.77
Injector-to-throat length, inches (70-inch $L^*$ )	35.77

Provisions were made for installing chamber wall heat flux probes at several (six) axial and circumferential locations within the combustion chamber. Two of the six ports for the probes were in the flange adjacent to the injector, and the remaining four ports were in the flange just upstream of the nozzle converging section as previously shown in Fig. 48. Analysis of temperature data from these heat flux probes was used to provide qualitative mixing and performance comparisons between the various injectors.



1XX32-3/9/67-S1

Figure 50. Workhorse Thrust Chamber Assembly and Spare Parts

Three pressure pickup ports were also located in the chamber flanges, one at the injector end and two adjacent to the nozzle. Four photocon pressure transducer ports were positioned in the combustion zone as indicated in Fig. 48. Three of these ports were located 3 inches downstream from the injector face at 0, 120, and 225 degrees from the top centerline looking aft. The fourth photocon port was 3 inches upstream from the nozzle converging section on the top centerline (0 degrees). These photocon pressure pickup ports were for fast-responding and wide-frequency-range instrumentation to be used for stability evaluation.

#### Gas Generator

A J-2 engine gas generator assembly (Fig. 51) was selected to provide the hot-gas flow requirements of the hot-firing injector evaluation phase of the program. Operational reliability and performance of the gas generator had been previously established and it was readily available. This unit was capable of providing the required exhaust temperatures (1200 F) and discharge pressures over a propellant weight flowrate range of 4 to 9 lb/sec.

Potential hot-gas flow requirements for the two-stage injector tests were as low as 0.3 lb/sec. The means for accomplishing this low-flow condition was to employ hot-gas bypass ducts and fixed orifices to divert the excess gas generator flow. Two discharge ducts were used; these were positioned to prevent an undesirable thrust component. The gas generator system installation made use of standard flanges, tubing, and fittings for installation of the gas generator assembly, its associated components, and propellant and control lines. Gas generator ignition was accomplished by pyrotechnic igniters.

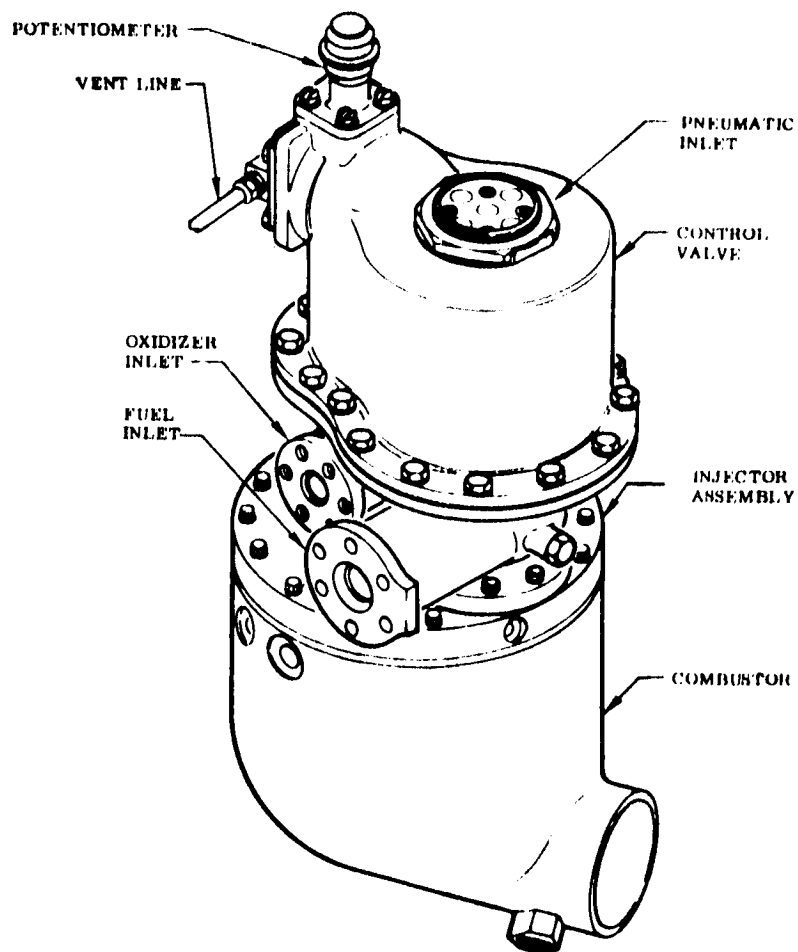


Figure 51. Gas Generator Assembly for J-2 Engine

## TEST FACILITY

The injector performance and stability tests were conducted at CTL-3, Cell 18B, of the Rocketdyne Santa Susana Field Laboratory. CTL-3 is a multiposition test complex containing four multicell test modules with a central control and recording center. Complete buildup of the test facility was accomplished to support the hot-firing phase of this program.

The test facility consisted of a thrust mount attached to a concrete pad, plumbing for the main propellants, plumbing for water coolant, and the electrical and control systems. A 20,000-pound-thrust load cell was used to measure the main thrust component from the chamber firing in a horizontal position. The main propellant lines and water coolant lines tied into the plumbing for the adjacent Test Cell 18A. Therefore, the tanks, many of the valves, controls, and much of the instrumentation were common to both test positions. For the sake of economy, the thrust stand, many of the valves, and other equipment were utilized from other currently inactive test facilities.

A single LOX run tank supplied oxidizer to the main thrust chamber and the gas generator. A turbine-type flowmeter was used to measure the total LOX flow from the tank. A portion of this flow was then split off for the gas generator and was measured by a turbine-type flowmeter. An orifice was used to control the flow in the main LOX line, and a cavitating venturi was used as a control in the gas generator line.

The hydrogen fuel system was designed to deliver liquid or gas to the injector and liquid to the gas generator. An  $\text{LH}_2/\text{GH}_2$  mixer (conditioner) and servosystem were used to control and to vary the injector fuel inlet temperature from 250 to 50 R in less than 1 second during any given test.

A venturi meter was used downstream of the mixer to measure the fuel flowrate to the chamber.  $\text{LH}_2$  for the gas generator was tapped off the  $\text{LH}_2$  line upstream of the mixer. This flow was measured with a cavitating venturi meter.

A gas generator was used to provide the 1200 F, fuel-rich hot gas to the injector. The unit was capable of providing 15 percent of total injector flow at 500 psia. Under these conditions the gas generator delivered approximately 9 lb/sec. At the low hot-gas flowrates required during some of the testing, the excess portion of the hot gas was dumped overboard. Orifices in the hot-gas line and sonic flow nozzles in the dump lines were used to control and to measure the quantity of hot gas.

Water was used as the coolant for the thrust chamber nozzle section. A turbine-type flowmeter and orifices (upstream and downstream of the nozzle) were used to measure and control the flow.

High-pressure helium,  $\text{GN}_2$ , and  $\text{GH}_2$  systems were used for pressurizing the propellant tanks, purging, and for valve operation.

A schematic of the test system is shown in Fig. 52, along with valves, flowmeters, and the primary control orifices relative to the main propellants and coolant. Also shown are some of the basic chamber assembly temperature and pressure measurements recorded during the testing.

Several measuring devices and control systems were used throughout the test program. Chamber pressures, thrust chamber injection pressures, hot gas and fuel injection temperatures, and the main chamber flowrate parameters were recorded on an oscillograph for transient response and

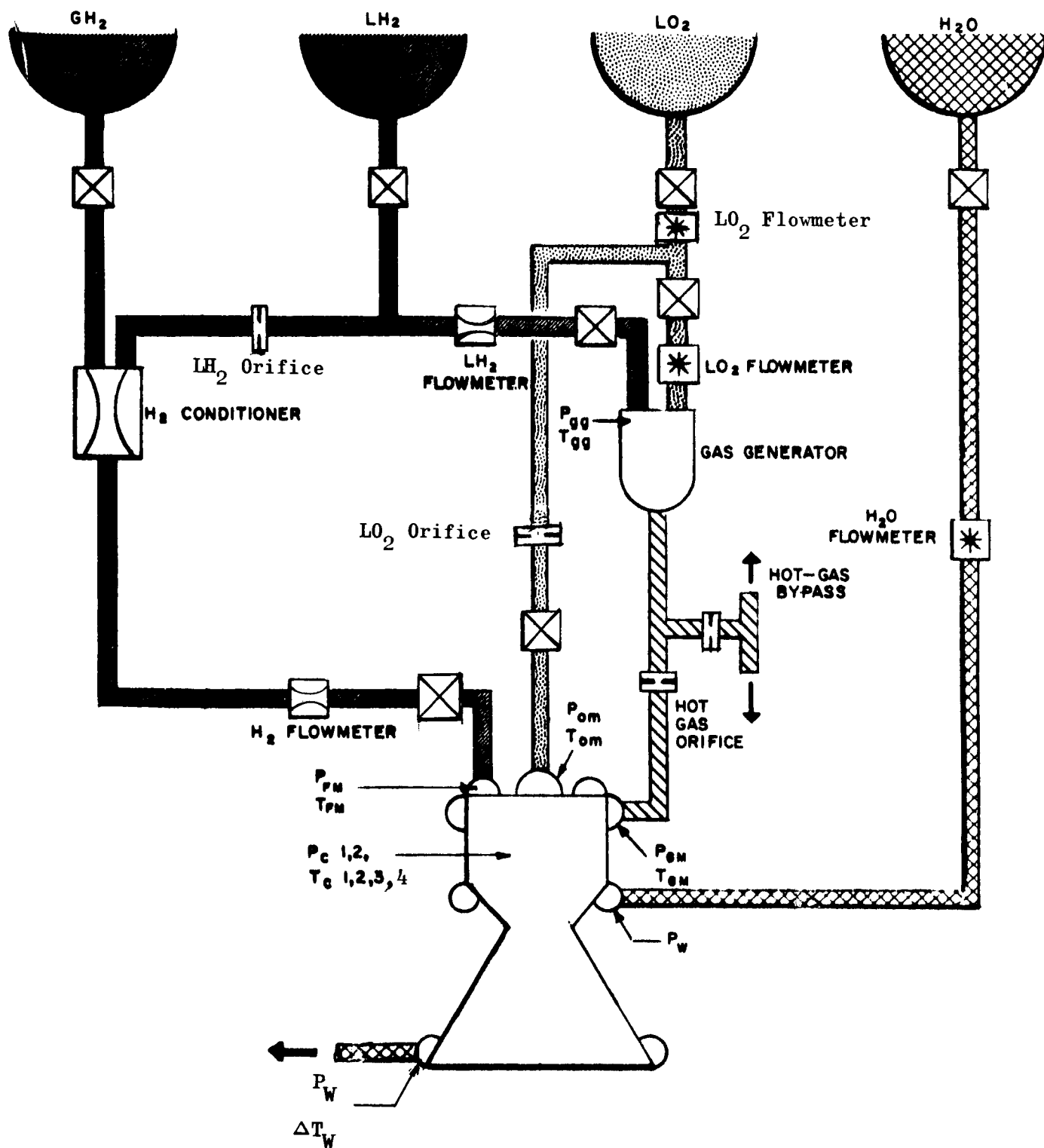


Figure 52. Schematic of Two-Stage Injector Test System

on direct-inking graphic recorders (DIGR's) for precision of stabilized data. Other DIGR parameters included tank pressures, gas generator injection pressures and temperatures, water coolant pressures and temperatures, and in general all parameters where response time was not critical. Chamber wall temperatures were recorded on the oscillograph to achieve rapid response. Table 16 shows the main parameters recorded during the bulk of the testing, the type of recording used, and the range of the pickups used.

Response from high-frequency instrumentation, consisting of three chamber pressure Photocons, one oxidizer injection pressure Photocon, and an axial accelerometer, were recorded on tape. This high-frequency instrumentation was primarily for monitoring and analysis of combustion stability. The accelerometer was monitored by a vibration safety circuit device with a variable delay time and "g" cutoff loading.

Event recorders, sequence timers, etc., were employed throughout the program for proper test setup and control. Motion picture coverage of all firings was used to aid test analysis and provide test documentation.

TABLE 16

## PRIMARY INSTRUMENTATION USED DURING HOT-FIRE TESTS

Parameter	Range	Recorder
<u>Oxidizer System</u>		
Hypergol Upstream Pressure, psig	0/2000	DIGR
Hypergol Downstream Pressure, psig	0/2000	DIGR
LOX Tank Temperature, F	-325/+175	DIGR
LOX Tank Pressure, psig	0/3000	DIGR
LOX Temperature at 2 inches Flowmeter (Main Flow), F	-300/-200	DIGR
LOX Temperature at Gas Generator Flowmeter, F	-300/-200	DIGR
LOX Pressure at Gas Generator Inlet, psig	0/2000	DIGR
LOX Injector Pressure, psig	0/2000	DIGR and Oscillograph Tape
LOX Injector Upstream Pressure (Photocon), psig	0/2000	
LOX Injector Temperature, F	-325/+175	DIGR
Main LOX Flowrate, lb/sec	0/60	DIGR and Oscillograph
Gas Generator LOX Flowrate, lb/sec	0/10	DIGR and Oscillograph
<u>Fuel System</u>		
Liquid Hydrogen Tank Pressure, psig	0/3000	DIGR
Liquid Hydrogen Upstream Pressure and $\Delta P$ , psig and psi	0/5000 and 0/200	DIGR
Gas Generator Venturi Upstream Pressure, psig	0/3000	DIGR
Gas Generator Venturi Upstream Temperature, F	-425/-350	DIGR
Gas Generator Fuel Inlet Pressure, psig	0/2000	DIGR
Gaseous Nitrogen Bottle Bank Downstream Pressure, psig	0/5000	DIGR
Gaseous Nitrogen Servo Upstream Pressure, psig	0/5000	DIGR

NOTE: DIGR = Direct Inking Graphic Recorder

TABLE 16  
(Concluded)

Parameter	Range	Recorder
<u>Fuel System</u>		
Injector Venturi Upstream Pressure, psig	0/3000	DIGR and Oscillograph
Injector Venturi Upstream Temperature, F	-425/-150	DIGR and Oscillograph
Fuel Injection Temperature, F	-425/-150	DIGR
Fuel Injection Pressure, psig	0/2000	DIGR and Oscillograph
<u>Hot Gas System</u>		
<u>Gas Generator</u>		
Chamber Pressure, psig	0/1000	DIGR and Oscillograph
Bypass Upstream Temperature (2), F	0/2000	DIGR
Bypass Upstream Pressure (2), psig	0/1000	DIGR
Upstream Injector Temperature, F	0/2000	DIGR and Oscillograph
Upstream Injector Pressure, psig	0/2000	DIGR and Oscillograph
<u>Thrust Chamber</u>		
Chamber Pressure (3) (Photocon), psig	0/1000	Tape
Chamber Pressure (2), psig	0/1000	DIGR and Oscillograph
Chamber Temperature (Nanmac) (4), F	0/2000	Oscillograph
Accelerometer* (Axial), g	0/300	Tape
Thrust (Axial), pounds	0/25,000	DIGR and Oscillograph
<u>Water Coolant System</u>		
Flowrate, lb/sec	0/80	DIGR and Oscillograph
Inlet Pressure (2), psig	0/1000	DIGR
Outlet Pressure (2), psig	0/1000	DIGR
Outlet Temperature (2), F	0/+300	DIGR
Tank Pressure, psig	0/2000	DIGR

Note: DIGR = Direct-Inking Graphic Recorder

\*Accelerometer used in conjunction with vibration safety cutoff device

## TEST PROCEDURES

Following buildup of the test facility, a series of blowdowns was conducted consisting of one fuel, two oxidizer, two hot gas, and one water blowdown. These blowdowns were performed to calibrate the various propellant and coolant systems, to establish appropriate orifice sizes, and to determine other pertinent operating characteristics of the systems such as valve opening times, etc. Sequence checks were also performed to ensure proper start and cutoff procedures.

The same basic start and cutoff sequence was used for all of the main-stage tests. First, gas generator and main chamber purges (helium and  $\text{GN}_2$ ) for the propellant lines were "on" prior to the start of the test. These purges were checked and/or sequenced off as the propellants entered. Prior to "start", the water coolant for the chamber nozzle was turned on. The gas generator start followed the water coolant. This start began with the pyrotechnic igniter firing, followed by fuel and then oxidizer. The hot (approximately 1200 F) gas generator gases flowed into the main chamber through the injector for about 2 seconds. The main chamber fuel was then sequenced on and both the hot gas and fuel continued through the chamber for 5 to 10 seconds until the fuel temperature reached a predetermined value. At this time a CTF hypergol slug entered the chamber followed by igniter oxidizer flow (GOX) to sustain ignition. Approximately 0.6 second later the main oxidizer flow entered the chamber with subsequent pressure buildup and mainstage.

The cutoff sequence was essentially the reverse of the start sequence; i.e., oxidizer off first, then fuel off, followed by hot gas and then water coolant. Purges were initiated as the propellant flows decayed. The basic operating sequence is shown in Fig. 53.

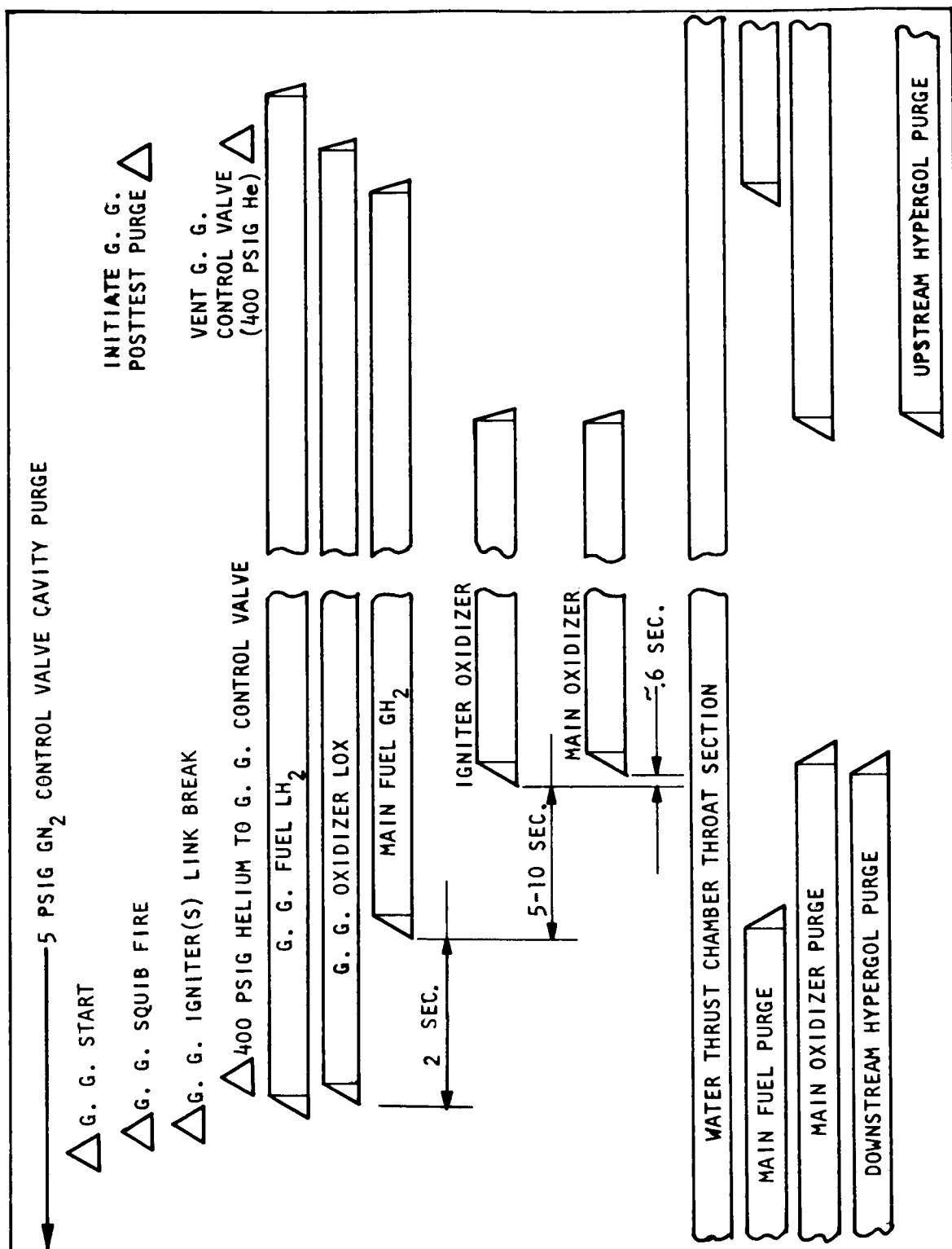


Figure 53. Test Operating Sequence

Twenty mainstage tests were conducted to evaluate the four different hot-firing injectors. Each injector along with the corresponding number of mainstage tests is listed below and the operating parameters for each of the tests are shown in Table 17.

<u>Injector Type</u>	<u>Number of Mainstage Tests</u>
20K Tricentric 1A	5
5K Tricentric 1A	2
20K Impinging Coaxial 9A (Recessed Cup)	10
5K Impinging Coaxial 9A (Recessed Cup)	3

The test program was organized so that each of the four injectors was subjected to a minimum number of mainstage tests to characterize its performance and stability. During these characterization tests (Tests 001 through 014) the quantity of hot gas was the prime variable while chamber pressure, mixture ratio, hot-gas temperature, etc., were maintained at or near the nominal design values. Also, during the characterization tests, the fuel temperature was varied to a limited degree to determine its effect on performance and stability.

After completion of the checkout tests, two injectors were selected for further evaluation testing. The 20K tricentric injector configuration 1A was subjected to two additional tests (Tests 015 and 016) to evaluate a performance improvement modification. The 20K impinging coaxial injector configuration 9A was subjected to additional tests (Tests 017 through 024) to evaluate off-design conditions which included low chamber pressure, low fuel temperature and long  $L^*$ . A brief description of each mainstage test is given in the following paragraphs. Four additional tests which did not reach mainstage were also conducted.

TABLE 17

## SUMMARY OF HOT-FIRE TEST RESULTS

Test Number	Test Date	Injector Configuration	Characteristic Length (L*), inches	Mainstage Duration, seconds	Site Thrust, pounds	Nozzle Chamber Pressure, psia	Total <sup>(1)</sup> Oxidizer Weight Flowrate, lb/sec	Total Fuel Weight Flowrate, lb/sec	Mixture Ratio, Oxidizer/Fuel	Hot-Gas Weight Flowrate, Percent of Total Propellant Flowrate	Hot-Gas Temperature, F	Fuel Temperature to Inject, F
001	5/25/67	1A (20K)	30	0.00	--	--	--	--	--	--	--	--
002	5/26/67	↓	↓	0.40	14,807	396.7	51.06	10.33	4.94	13.1	1048	257
003	6/1/67	↓	↓	2.51	16,658	427.6	53.02	11.32	4.68	13.4	1159	256
		↓	↓		15,727	411.3	53.16	11.55	4.60	13.3	1159	45
004	6/2/67	↓	↓	2.93	15,984	432.3	53.08	12.31	4.31	10.1	1283	255
005	6/8/67	9A (20K)	↓	0.67	17,937	473.7	48.44	10.60	4.57	9.0	1214	253
006	6/8/67	↓	↓	3.35	18,041	473.3	48.52	10.46	4.64	8.8	1228	260
		↓	↓		18,083	475.4	47.59	11.48	4.15	8.8	1242	118
007	6/13/67	↓	43.5	0.96	19,765	498.1	51.05	10.35	4.93	14.2	1310	255
008	6/14/67	↓	43.5	1.69	18,357	479.6	47.70	10.91	4.38	6.6	1227	253
009	6/20/67	1A (5K)	30	1.08	19,219	502.3	56.15	10.73	5.23	6.1	1352	253
010	6/20/67	1A (5K)	↓	0.96	20,464	522.5	59.91	10.20	5.87	12.4	1352	253
011	6/26/67	9A (5K)	↓	0.71	20,432	512.7	55.75	10.27	5.43	13.2	1365	258
012	6/27/67	↓	↓	1.36	18,432	473.7	52.48	9.74	5.39	8.2	1310	258
013	6/28/67	↓	↓	0.00	--	--	--	--	--	--	--	--
014	6/30/67	↓	↓	1.17	16,443	421.8	51.69	8.68	5.96	0.0	--	256
015	7/6/67	1A Mod (20K)	↓	1.32	17,171	435.0	50.21	10.78	4.66	6.1	1241	255
016	7/7/67	1A Mod (20K)	↓	1.23	17,392	445.0	52.18	10.87	4.80	6.1	1255	259
017	7/11/67	9A (20K)	↓	1.15	17,359	450.0	55.26	9.75	5.67	8.5	1310	49
018	7/12/67	↓	↓	0.00	--	--	--	--	--	--	--	--
019	7/12/67	↓	↓	1.25	7,868	213.5	24.90	4.35	5.72	11.0	1460	205
020	7/13/67	↓	↓	0.00	--	--	--	--	--	--	--	--
021	7/17/67	↓	↓	1.12	7,930	212.9	24.16	5.13	4.71	7.3	1380	260
022	7/18/67	↓	↓	2.58	1,075	45.8	4.39	1.42	3.09	23.1	1145	257
023	7/19/67	↓	70	1.04	19,858	505.4	53.26	10.27	5.19	13.7	1283	261
024	7/19/67	↓	70	0.78	18,850	486.1	57.03	9.51	6.00	8.4	1448	50

(1) Adjusted for impurities

FOLDOUT FRAME 2

FOLDOUT FRAME 1

re or,	Throat Area, sq in.	Remarks
28.94	28.94	Cut off before mainstage due to facility error Observer cutoff due to igniter line fire
28.97	28.97	Minor injector erosion near oxidizer plugs,
28.97	28.97	fuel ramped to 45 R Temperature
29.00	29.00	Slight increase in injector erosion, fuel ramped to 60 R temperature
29.15	29.15	
29.18	29.18	Chamber erosion in four places, fuel ramped
29.18	29.18	to 118 R temperature
29.21	29.21	Minor chamber erosion
29.24	29.24	Minor chamber erosion
29.25	29.25	Minor chamber erosion
29.28	29.28	Minor chamber erosion
29.35	29.35	Injector erosion in three of the four cups, minor chamber erosion
29.36	29.36	Minor chamber erosion
--	--	Cut off before mainstage due to gas generator overpressure
29.33	29.33	
29.35	29.35	Injector hot-gas swirler eroded, minor chamber erosion
29.36	29.36	Minor chamber erosion
29.41	29.41	Minor chamber erosion
--	--	Cut off before mainstage due to gas generator overtemperature
29.35	29.35	Low-frequency fuel temperature cycling throughout test
--	--	Cut off before mainstage due to gas generator overtemperature and fuel cycling
29.37	29.37	
29.31	29.31	
29.48	29.48	Minor chamber erosion
29.50	29.50	Minor chamber erosion

#### Tests 001 Through 004

The 20K tricentric injector configuration 1A and the 30-inch L\* thrust chamber were used for this test series. Primary test objectives were to establish the performance and stability characteristics of the hardware at the specific operating conditions.

Test 001, the first attempted mainstage test was terminated before mainstage was achieved.

The first successful mainstage test, Test 002, was conducted on 26 May 1967. The test was programmed for 1 second of mainstage at 450-psia chamber pressure using 15 percent of the total flow as hot-gas flow and using 250 R hydrogen to the main chamber.

Testing was terminated after 0.40 second of stabilized mainstage when a fire was observed in the area behind the injector. Posttest inspection revealed a damaged CTF (igniter fuel) line and check valve plus minor damage to the injector main oxidizer inlet line. Probable cause of damage was contamination in the CTF system (check valve).

Test 002 began with 2.2 seconds of gas generator (hot-gas) operation followed by 7.6 seconds of main fuel and hot-gas flow, then CTF ignition, main oxidizer flow, and mainstage. The chamber pressure buildup into mainstage appeared to be smooth, although the fast-responding photocon pressure pickups suggested a high-pressure surge at start; i.e., ignition may have originated from an external source if the CTF line was damaged prior to main propellant ignition. At cutoff, the oxidizer flow was sequenced off first, followed by main fuel and hot-gas flows.

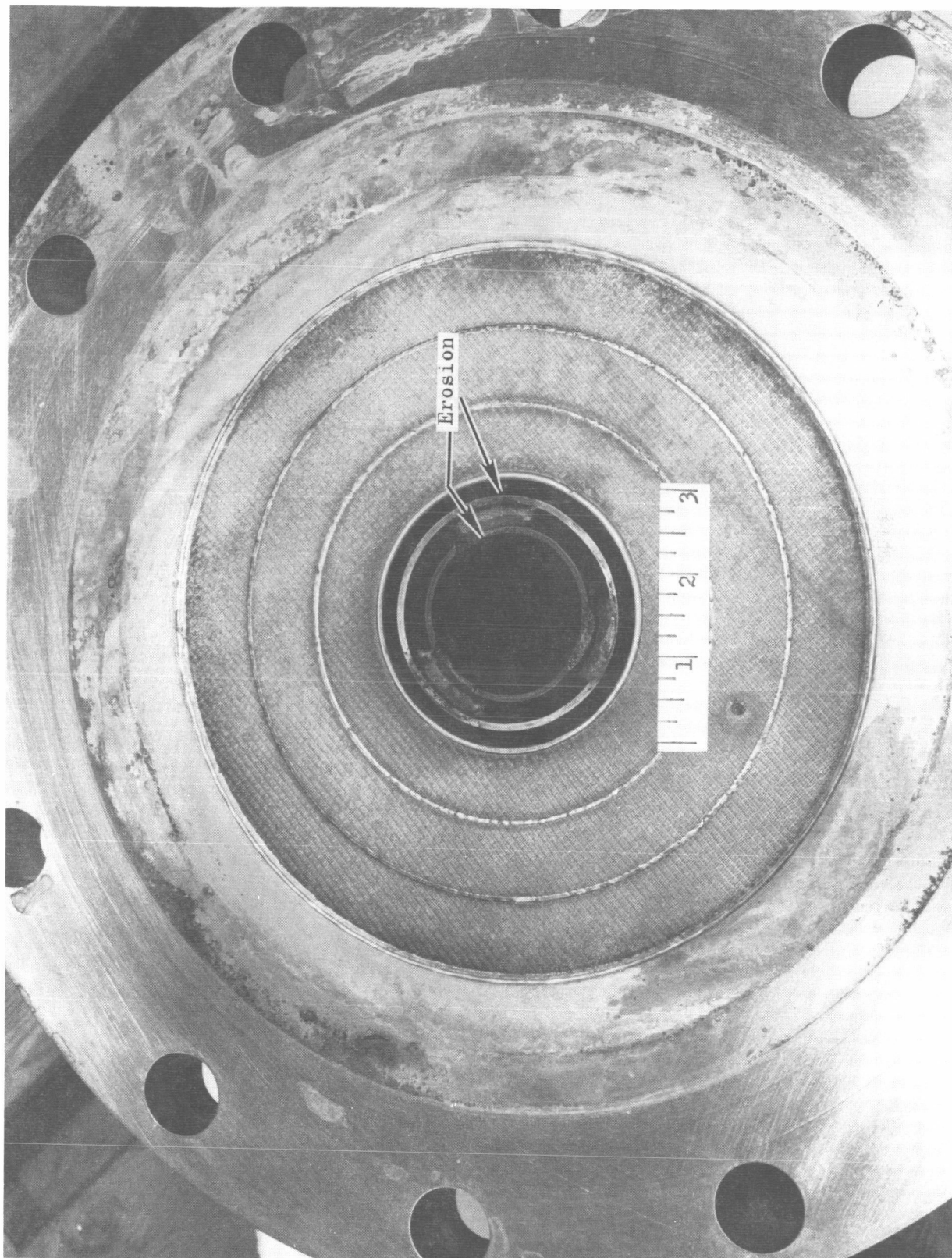
Operating parameters for this and each of the other tests are shown in Table 17. During Test 002 stabilized data were not obtained from the more accurate direct-inking graphic recorders (DIGR's); however, the oscillograph data were stabilized. The oscillograph data were used to determine chamber pressure and thrust for Test 002, adjusted to correspond with the DIGR values by factors determined from subsequent tests.

Test 003 was conducted with the same hardware, and the operating conditions were the same as those of Test 002 except that the test duration was increased to approximately 2.5 seconds and the fuel temperature was "ramped" from 256 to 45 R in 1.1 seconds. The start, cutoff, and mainstage characteristics of the test were satisfactory and stable over the entire fuel temperature range. Following the test, minor injector erosion was noted on the lip of the tubes downstream of the three oxidizer passage plugs. This erosion was apparently caused by recirculation in the void areas.

The hardware and operating conditions for Test 004 were essentially the same as for Test 003 except the goal for Test 004 was to decrease the quantity of hot-gas flow to the injector. Test objectives were accomplished; the fuel temperature ramped from 255 R to 60 R, and the quantity of hot-gas flow was 10 percent. The hardware condition was satisfactory following the test. A slight increase in injector erosion occurred downstream of the three oxidizer plugs (Fig. 54). The preliminary evaluation of the 20K tricentric injector configuration 1A was completed with this test, so a new injector was installed.

#### Tests 005 Through 008

This series of tests was conducted to determine the operating characteristics of the 20K impinging coaxial injector configuration 9A (recessed cup). A 30-inch  $L^*$  chamber was used for Tests 005 and 006 and a 43.5-inch  $L^*$  chamber for Tests 007 and 008.



LXX53-6/3/67-SLC

Figure 54. 20K Tricentric Injector Configuration 1A After Test 004

The primary goals for Test 005 were to check the operating characteristics of the injector during a short mainstage test using approximately 10-percent hot-gas flow and 250 R fuel to the main chamber. All test objectives were successfully accomplished.

Test 006 was conducted with the same hardware as used during the previous test. The goals for this test were to evaluate the injector using the same basic operating conditions as Test 005 except that the test duration was increased and the fuel temperature was ramped from 260 to 118 R. Test objectives were satisfactorily accomplished and the condition of the injector was satisfactory following the test. Erosion (streaking) was observed, however, at four locations 90 degrees apart on the uncooled combustion chamber walls. The erosions were of varying depths located at 0, 90, 180, and 270 degrees from the top centerline and they were in line with the zones between the four impinging injector streams (i.e., the streams were at 45, 135, 225, and 315 degrees from the top centerline). The erosions began about 6 inches above the nozzle converging section, extending down to the water-cooled nozzle converging section. The maximum width of the erosions was about 2 inches, and the maximum depth varied from about 1/32 inch at the 90-degree location up to 1/4 inch at the 0-degree location. One of the chamber erosions was aggravated by an instrumentation (Photocon) port in the chamber, necessitating removal of the combustion chamber section for repair.

A new, longer combustion chamber section was installed for Test 007, resulting in a 43.5-inch  $L^*$  chamber. Test conditions were set to give 14.2-percent hot-gas flow, and 255 R fuel to the chamber. The test objectives were successfully accomplished and injector condition was satisfactory following the test. Minor chamber erosion was observed on the uncooled combustion chamber wall around two instrumentation (Photocon) ports. This type of chamber erosion was repeated during several subsequent tests. It did not, however, affect the test results; it only resulted in limiting test durations so chamber life could be prolonged.

The hardware and targeted mainstage conditions for Test 008 were the same as those for Test 007, except that the goal was to evaluate the effects of reduced hot-gas flow (reduced to 6.6 percent). The test objectives were successfully accomplished and the injector condition was satisfactory. With this test, the preliminary evaluation of the 20K impinging coaxial injector configuration 9A was completed.

#### Tests 009 and 010

The 5K tricentric injector configuration 1A and the 30-inch  $L^*$  chamber were employed for this test series. The objectives of Test 009 were to evaluate the injector performance and stability using a hot-gas flow of 6.1 percent and 253 R fuel to the main chamber. The test results were successfully accomplished and the injector condition was satisfactory following the test.

Hardware for Test 010 was the same as for Test 009. The test goals were to evaluate the injector at an increased hot-gas flowrate (12.4 percent) and to ramp the fuel temperature from 250 to 100 R during approximately 2.5 seconds of mainstage. This test was terminated prematurely after approximately 1 second because of excessive pressure in the hot-gas generator. All test objectives were satisfactorily accomplished except for the fuel temperature ramp. Like the previous test, the injector condition was satisfactory. Hot firing evaluation of the 5K tricentric injector configuration 1A was concluded with this test.

#### Tests 011 Through 014

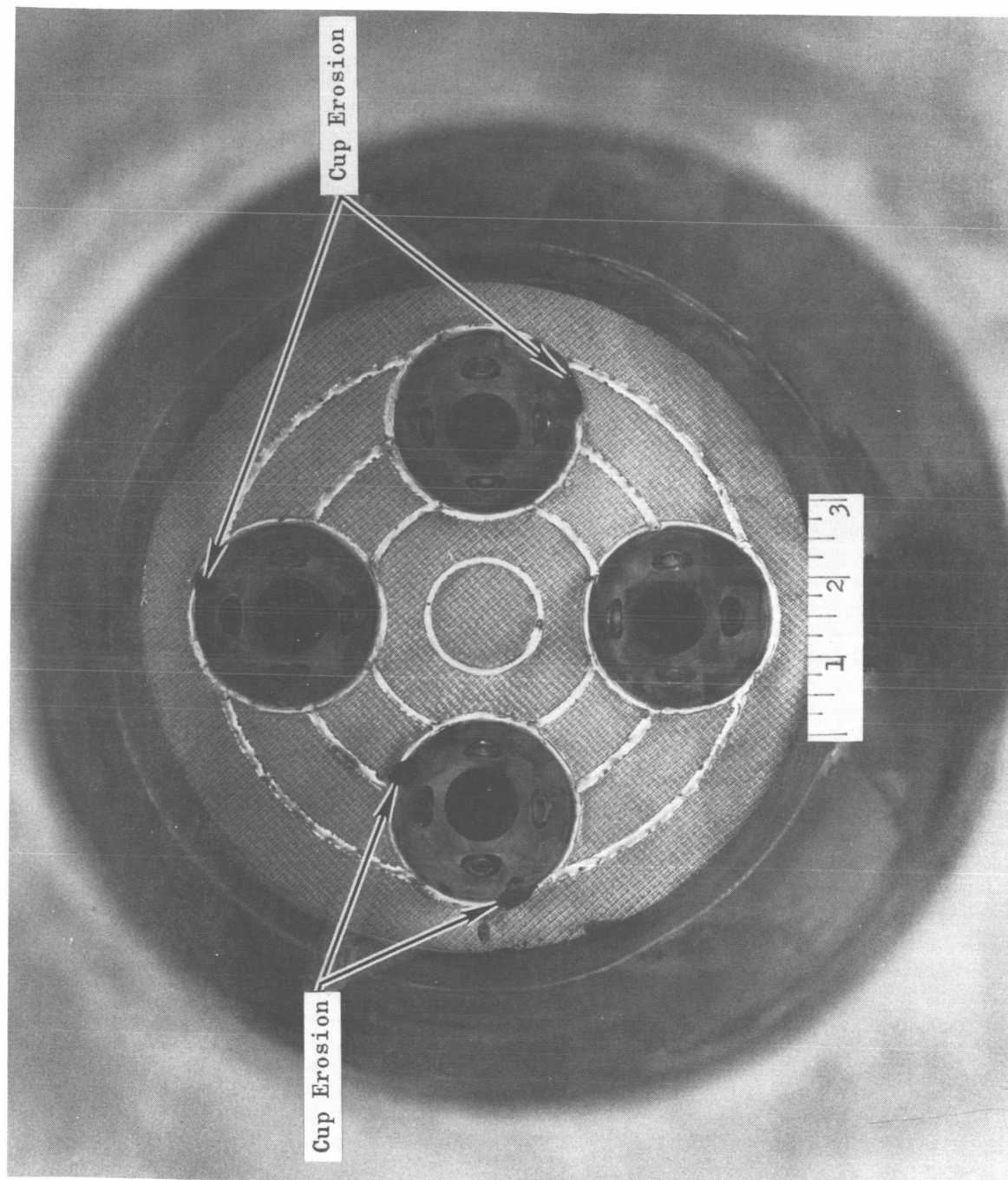
The 5K impinging coaxial injector configuration 9A (recessed cup) and the 30-inch  $L^*$  chamber were employed for this test series. Test objectives

were to characterize the performance and operating characteristics of the injector. For Test 011, the quantity of hot gas was set at 13.2 percent, and the fuel temperature to the chamber at 258 R. Test objectives were achieved. Following the test, injector erosion was noted at four places in three of four cups, near the downstream edge beginning near an impinging jet and extending about  $1/4$  of the way around toward the next jet (Fig. 55). Depth of the erosions was approximately  $1/8$  to  $1/4$  inch and width of the erosion was about  $1/2$  inch to 1 inch. The cause of the injector erosion was unknown, although a logical contributing factor could be slight maldistribution of propellants. High-speed motion picture films of the test indicated that the erosion began about 0.2 second after start of mainstage and ended after about 0.6 second of mainstage and prior to cutoff. Prior to the next test, the abrupt discontinuities in each of the injector cup erosions were ground smooth.

Test 012 was initiated to evaluate the 5K 9A injector using a hot-gas flowrate of 8.2 percent and a main fuel temperature of 258 R. Test objectives were satisfactorily accomplished and no further injector erosion was observed.

The primary objective of Test 013 was to evaluate the injector with 0-percent hot-gas flow. This test was terminated prior to mainstage.

Test 014 used the same hardware and was programmed for the same operating conditions as Test 013. The test objectives were satisfactorily accomplished, and the hardware condition remained essentially unchanged. The evaluations of the 5K impinging coaxial injector configuration 9A were concluded with this test.



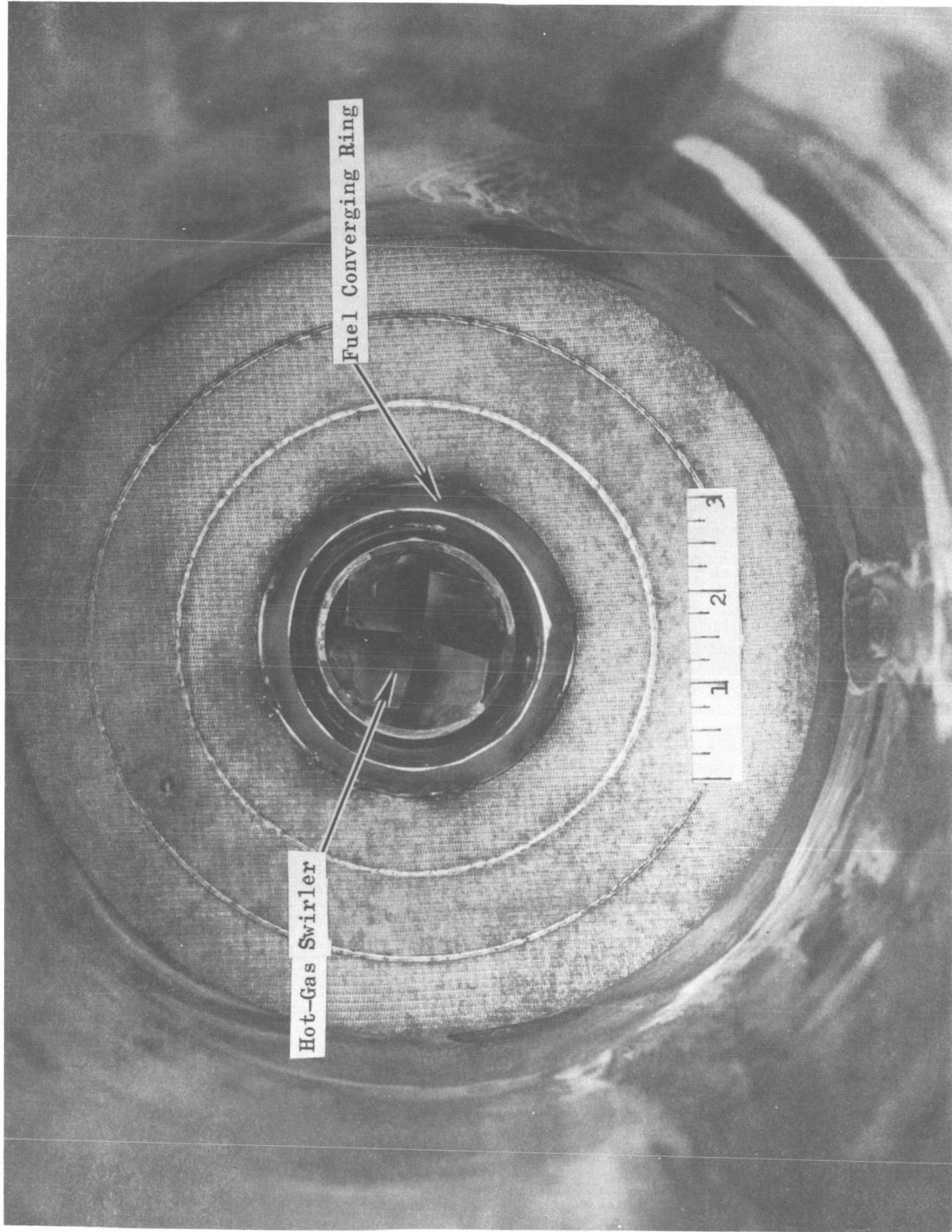
LXX43-6/26/67-S1B

Figure 55. 5K Impinging Coaxial Injector Configuration 9A After Test 011

### Tests 015 and 016

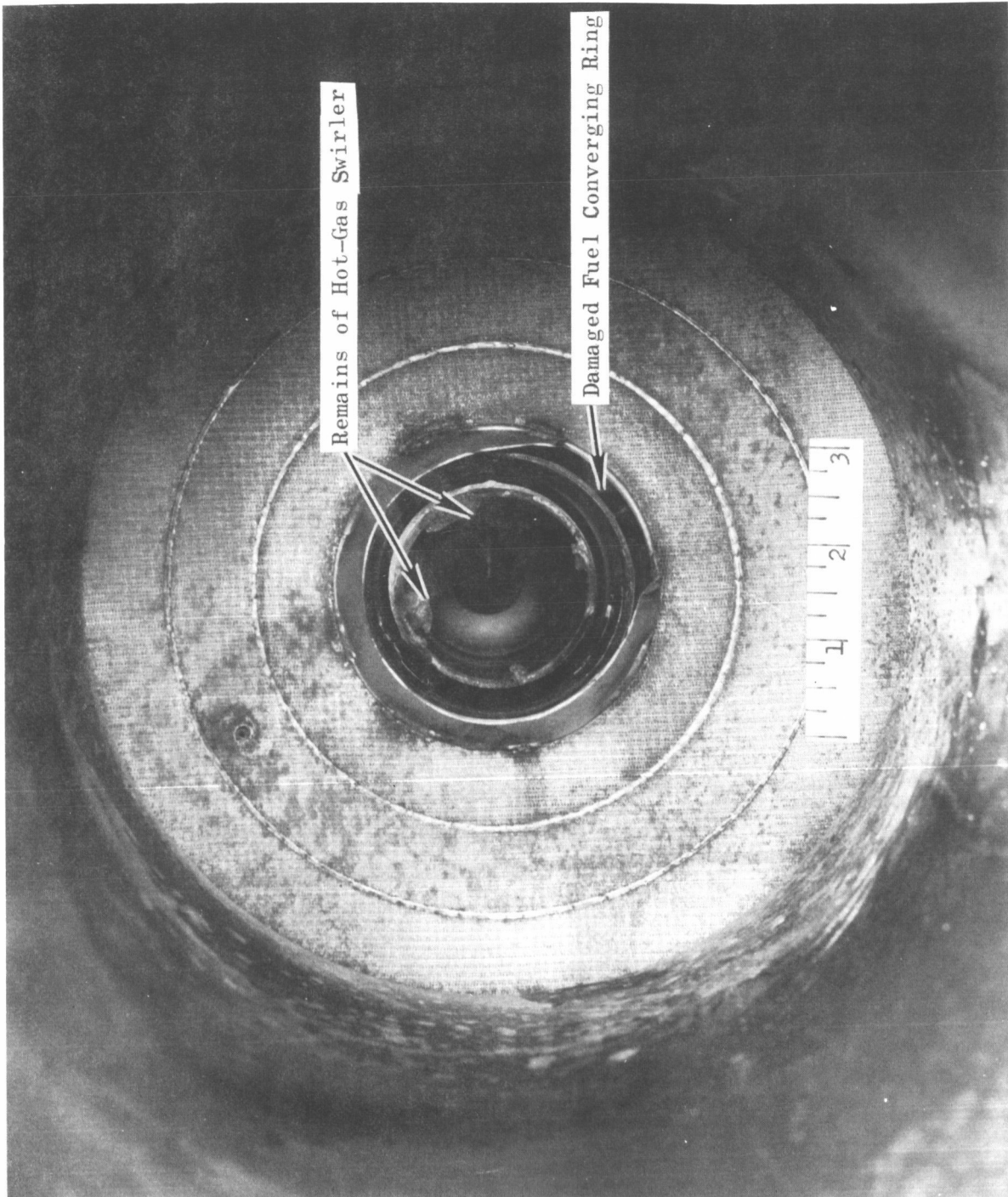
The 30-inch L\* chamber and a modified 20K tricentric injector configuration 1A were used for these tests. As previously mentioned, the analytical studies conducted in Task I suggested that the performance of this injector would be limited by mixing of the fuel with the oxidizer/hot-gas combination. In addition, the oxidizer atomization would be somewhat degraded by the increased velocity due to the three plugs in the oxidizer passage. Low performance was evident during Tests 002 through 004, so in an attempt to improve performance the injector was modified by (1) removing the three plugs, (2) installing a converging ring outside the annulus to direct the fuel inward and force it to mix with the oxidizer and hot gas, and (3) installing a swirl device in the central hot-gas passage to force the hot gas outward toward the oxidizer and fuel and at the same time decrease the axial velocity component in favor of more hot-gas "stay time." A photograph of the modified injector is shown in Fig. 56.

Operating conditions for Test 015 were programmed to give 1 to 1.5 seconds of mainstage with 6.1-percent hot-gas flow and 255 R fuel. The test proceeded as scheduled, however, after the test the hot-gas swirl device was almost completely burned away as shown in Fig. 57. Also, an approximate 1.5-inch (15 percent) portion of the fuel converging ring was hanging loose. A review of the high-speed motion picture for this test showed that the swirl device began burning away at the start of mainstage and that most of it was gone halfway through the test. Thus, the performance results produced by this test were probably without the swirler. Swirler burning was most likely caused by recirculating gas. The damage to the fuel converging ring was the result of insufficient weld in the damaged area.



IXX42-7/5/67-SIA

Figure 56. Modified 20K Tricentric Injector Configuration 1A Prior to Test 015



LXX43-7/7/67-S1

Figure 57. Modified 20K Tricentric Injector Configuration 1A After Test 015

Test 016 used the same test hardware and was programmed for the same operating conditions as Test 015. The main test objective was to determine the performance of the modified injector without the swirler and to compare these results with those of the previous test (015) where there was uncertainty whether the swirler was functioning. The test objectives were successfully accomplished, and the injector condition was unchanged following the test. Evaluation of the modified 20K tricentric injector configuration 1A was concluded with this test.

#### Test 017

Test 017 was conducted with the 20K impinging coaxial injector configuration 9A (recessed cup) and the 30-inch L\* chamber. This injector was selected over the other concepts for further evaluation because of its high performance during the initial series of checkout tests (005 through 008). The primary goal of Test 017 was to evaluate the injector performance and stability at a main chamber fuel temperature of 49 R. The quantity of hot gas for the test was 8.5 percent. Test objectives were successfully accomplished and the injector condition was satisfactory.

#### Tests 018 and 019

Test 018 was terminated prior to mainstage.

Test 019 was conducted with the same hardware used for Test 017. Like Test 018, the primary objectives of Test 019 were to evaluate injector performance and stability at a reduced (200 vs 500 psia) chamber pressure, while using approximately 11-percent hot-gas flow. Basically, the test

results were accomplished as scheduled. However, during the test the fuel temperature cycled from 343 R to 68 R at approximately 3 cps. As a result, the main chamber fuel flowrate, chamber pressure, thrust, etc. also cycled. The hardware condition was satisfactory following the test.

The main chamber operating parameters (Table 17) are the average values obtained during the cycling and as such create some doubt about their validity. The cycling was the result of insufficient pressure and  $\Delta P$  (resistance) in the liquid hydrogen system.

#### Tests 020 and 021

The test hardware and targeted operating conditions for these tests were the same as those for Test 019 (~200 psia chamber pressure) except the main goal was to evaluate a reduced quantity of hot gas at the reduced chamber pressure. Test 020 was terminated prior to mainstage. During Test 021, the objectives were successfully accomplished, and the previously experienced fuel temperature cycling was eliminated. The condition of the hardware was essentially unchanged by the test.

#### Test 022

This test was programmed for about 2.5 seconds of mainstage at 50-psia chamber pressure, 15-percent hot-gas flow, and 250 R hydrogen to the main chamber. The test hardware was the same as for Test 021. The main test objectives were to evaluate the injector performance and stability at 50-psia chamber pressure; a 10-to-1 reduction in the nominal design conditions. Results of this test were satisfactory and the hardware condition was unchanged.

#### Test 023

Test 023 was conducted with the 20K impinging coaxial injector configuration 9A (recessed cup); however, the combustion chamber length was increased to give a 70-inch  $L^*$ . The test utilized 13.7-percent hot-gas flow and 261 R fuel to the main chamber. Primary test objectives were to determine the effects of the increased  $L^*$  on performance and stability. The results of this test were satisfactory, and the condition of the injector remained unchanged.

#### Test 024

Test 024 used the same hardware as Test 023. Test 024 was basically a repeat of Test 017 using 50 R fuel. The primary goal of the test was to evaluate the effects of the increased  $L^*$  in conjunction with the cold fuel. The test objectives were successfully accomplished and the injector condition was satisfactory.

The hot-firing test program was completed following this test.

## TEST RESULTS

### Performance Data

The primary objective of the Two-Stage Bipropellant Injection System Program was to evaluate performance of the select injector concepts. Thus, injector (or combustion) efficiency was the performance parameter which received the most attention during the course of the hot firing program. Characteristic exhaust velocity (or combustion) efficiency ( $\eta_{c*}$ ) was determined in two ways: from the chamber pressure and flowrate data, and from the thrust and flowrate data. Specific impulse efficiency was also determined in conjunction with the program requirements. The test data used for computing the performance and the procedures followed are discussed herein. A summary of these data is presented in Table 18. (For viewing convenience, this table is located on page 223).

Flowrates. As previously mentioned, the total oxidizer flowrate and the gas generator oxidizer flowrate were measured by turbine-type flowmeters. The fuel flows to the gas generator and to the main chamber were measured by venturi meters. When a portion of the hot-gas flow was dumped, this flow was measured by sonic flow nozzles and subtracted from the total flow to the chamber.

The propellant flowrates as measured were adjusted for impurities present in the propellants. This adjustment was for the density change due to impurities and the corrected flowrates were computed as:

$$\dot{w}_{\text{corrected}} = \dot{w}_{\text{measured}} \frac{\rho_{\text{impure}}}{\rho_{\text{pure}}}$$

where

$\rho$  = density

Samples of the hydrogen fuel were taken on numerous occasions prior to this test program and the results showed very little (negligible) impurity. Thus, the fuel flowrate was not corrected. The LOX was sampled four times during the hot-firing test program and purity ranged from 98.0 to 99.05 percent by volume. Most of the impurity was nitrogen. These oxidizer samples were taken from the LOX storage tanks under low-pressure static conditions and, as such, do not reflect the additional quantities of nitrogen (used as the pressurant) which are normally entrained in the oxygen during transfer to the run tank and during the high-pressure dynamic conditions of a test.

Based on the sampling results, the oxidizer flowrates were adjusted for all of the tests. A conservative approach was taken and only 1-percent nitrogen impurity by volume was assumed for each test. The net result was

$$\frac{\rho_{\text{corrected}}}{\rho_{\text{pure}}} = 0.9965$$

or a constant 0.35-percent adjustment was applied to all oxidizer flowrates. Table 18 shows the adjusted flowrates.

Chamber Pressure. The static chamber pressure during each test was measured at two locations in the cylindrical portion of the chamber; i.e., upstream of the nozzle contraction section. These pressure pickups were about 13, 20, and 33 inches downstream from the injector face for the 30-, 43.5- and 70-inch L\* chambers. The two static pressure measurements, generally within  $\pm 5$  psi (1 percent) of the average, were averaged together to give a single value for each test. The perfect gas relationship was used to

obtain the stagnation pressure from the static pressure at start of contraction.

$$P_c = P_{soc} \left[ 1 + \frac{\gamma - 1}{2} M_{soc}^2 \right]^{\frac{\gamma}{\gamma - 1}}$$

where soc signifies start of contraction. For the contraction ratio and chamber conditions of interest  $P_c = 1.0538 P_{soc}$ .

This relationship was essentially true for the entire pressure and temperature range experienced during the testing. Therefore, the chamber pressures listed in Table 18 are the nozzle stagnation pressures computed from  $1.0538 P_{soc}$ .

Thrust. The thrust was measured during each test by a dual-bridge load cell with the output recorded on both the oscillograph and the DIGR. The more accurate DIGR value was used for the performance calculations. The measured thrust then was converted to vacuum thrust for all tests by the following relationship:

$$F_{vac} = F_{site} + P_a A_e$$

where

$$P_a = \text{ambient pressure}$$

$$A_e = \text{chamber exit area}$$

For this test program the  $P_a A_e$  was very nearly constant and equal to 800 pounds.

The main propellant lines to the test hardware and other stand equipment were mounted (Fig. 58) so as to minimize interference (resistance) with the thrust measurements, however, some interference was obvious. Therefore, an "in position" calibration was required. Following the last test a thrust calibration fixture was constructed and installed in front (at the exit end) of the thrust chamber assembly with a calibration load cell and a hydraulic loading device attached. The thrust system was calibrated and the calibration factor was used to determine each of the thrust values shown in Table 18. The accuracy of these thrust values is subject to some error because the calibration took place under static, ambient-temperature conditions. During actual testing the main propellant and water coolant lines were flowing full and the line temperatures, particularly the oxidizer and fuel line temperatures were cold, rather than ambient.

Specific Impulse and Impulse Efficiency. The specific impulse shown in Table 18 is computed as follows:

$$I_{s \text{ vac}} = \frac{F_{\text{vac}}}{\dot{w}_{\text{total}}}$$

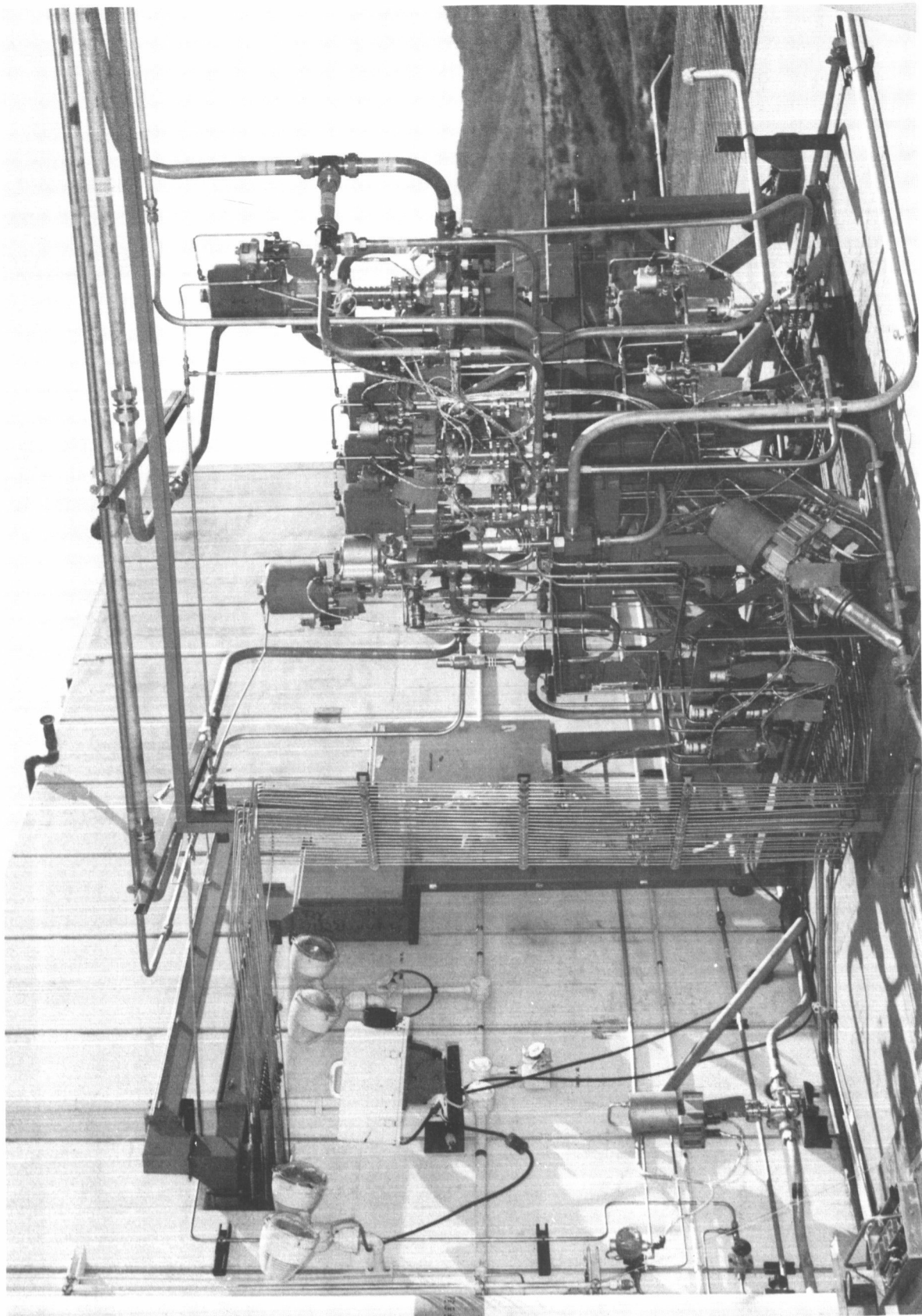
where

$$F_{\text{vac}} = \text{vacuum thrust}$$

$$\dot{w}_{\text{total}} = \text{the sum of the fuel and oxidizer flowrates entering the chamber}$$

The specific impulse efficiency was computed as follows:

$$\eta_{I_s} = \frac{I_{s \text{ vac}}}{I_{s \text{ vac. ideal}}}$$



1XX41-4/25/67-SIB

Figure 58. Rear View of Test Facility

where  $I_{s_{vac_{ideal}}}$  is the vacuum ideal chemical equilibrium specific impulse for the specific chamber, chamber pressure, mixture ratio, propellant temperatures, etc.

Combustion Efficiency from Thrust. The characteristic velocity was calculated from the thrust and flowrate by the relationship:

$$c^*_{\text{uncorrected}} = \frac{g I_{\text{vac}}}{C_{F_{\text{vac}_{ideal}}}} = \frac{g F_{\text{vac}} / \dot{w}_{\text{total}}}{C_{F_{\text{vac}_{ideal}}}}$$

and this value was corrected by:

$$c^*_{\text{corrected}} = \frac{c^*_{\text{uncorrected}}}{\eta_{\text{T.C.}}}$$

where the sum of the thrust chamber losses

$$\eta_{\text{T.C.}} = 1 - (1 - \eta_K) - (1 - \eta_G) - (1 - \eta_D) - (\eta_{\text{HL}} - 1) - (\eta_{\text{Imp}} - 1)$$

and

$\eta_K$  = kinetic efficiency

$\eta_G$  = divergence efficiency

$\eta_D$  = boundary layer efficiency

$\eta_{\text{HL}}$  = specific impulse heat loss correction

$\eta_{\text{Imp}}$  = specific impulse impurity correction

The reaction kinetic efficiency  $\eta_K$  is defined as

$$\eta_K = 1 - \left( \frac{\Delta C_F}{C_F} \right)_{\text{reaction kinetics}}$$

For this test program  $\eta_K = 1.0$  for all chamber pressures and mixture ratios of interest.

The geometric or divergence efficiency  $\eta_G$  is defined as

$$\eta_G = 1 - \left( \frac{\Delta C_F}{C_F} \right)_{\text{divergency}}$$

For the test nozzle the divergence efficiency, calculated by the method of characteristics with  $\gamma = 1.165$ , was  $\eta_G = 0.9849$

The boundary layer efficiency  $\eta_D$  is defined as

$$\eta_D = 1 - \left( \frac{\Delta C_F}{C_F} \right)_{\text{boundary layer}}$$

and represents the loss of thrust caused by wall shear and wall heat loss in the boundary layer. The boundary layer losses are shown in Fig. 59 as a function of chamber length before start of contraction. These values are nearly independent of mixture ratio and hydrogen injection temperature.

The specific impulse correction,  $\eta_{HL}$  is defined as:

$$\eta_{HL} = 1 + \left( \frac{\Delta I_s}{I_s} \right)_{\text{heat loss}}$$

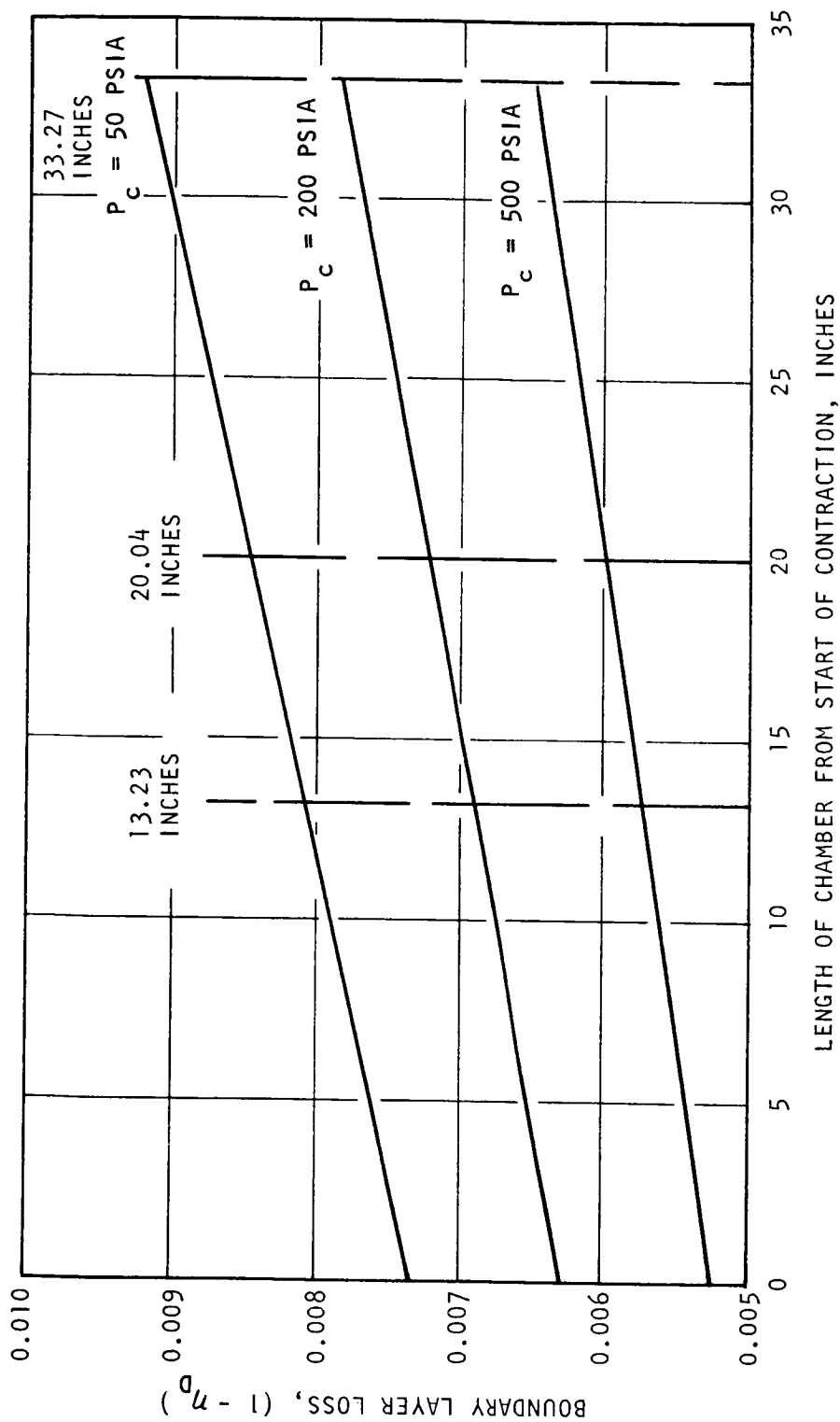


Figure 59. Boundary Layer Losses vs Chamber Length

Heat loss correction factors were computed for each test by the following equation (Ref. 17):

$$\eta_{HL} = 1 + \frac{1}{2} \left[ \frac{\sum_i (Q/A_i) A_i}{\dot{w}} \right] \left[ \frac{1 - (T_e/T_c)}{h_c - h_e} \right]$$

where

$Q/A$  = heat flux

$A_i$  = area through which heat is transferred

$\dot{w}$  = total propellant flowrate

$T_e$  = theoretical nozzle exit temperature

$T_c$  = theoretical chamber temperature

$h_c$  = theoretical chamber enthalpy

$h_e$  = theoretical nozzle exit enthalpy

The heat transfer losses ( $Q$ ) were computed for each test based on the quantity of heat transferred to the water-cooled nozzle section. The water coolant bulk temperature rise  $\Delta T$  was measured for each test and used to compute the nozzle heat losses as follows:

$$Q_{noz} = \dot{w} C_p \Delta T$$

The  $Q_{noz}$  experimental was assumed directly proportioned to the  $Q_{noz}$  ideal at each station in the nozzle thus:

$$\text{experimental } \sum_i \left( \frac{Q}{A_i} \right) A_i = \text{theoretical } \sum_i \left( \frac{Q}{A_i} \right) A_i \times \frac{Q_{noz\_exp}}{Q_{noz\_ideal}}$$

This same ratio,  $Q_{noz\_exp} / Q_{noz\_ideal}$ , was used to compute the uncooled combustion zone heat transfer, assuming again that the combustion zone heat transfer was proportioned to the theoretical heat transfer at each station.

The computed specific impulse heat loss correction factors ranged from a low of 1.0027 (0.27-percent change) for low-performing Tests 002-004 to a high of 1.0166 (1.66-percent change) for Test 023 with high performance and extra chamber surface area; i.e., 70-inch  $L^*$  chamber.

The specific impulse impurity correction  $\eta_{imp}$  is defined as:

$$\eta_{imp} = 1 + \left( \frac{\Delta I_s}{I_s} \right)_{impurity}$$

As previously discussed, samples of the oxidizer were taken and 1-percent nitrogen impurity was used to adjust the oxidizer density and flowrates. This same 1 percent was used as the basis for determining the impurity correction factor. Theoretical thermochemical performance calculations were employed (with and without nitrogen) to compute the impurity corrections. The resultant change in the specific impulse was approximately 0.2 percent, giving a correction factor  $\eta_{imp} = 1.002$ . This factor varies slightly with chamber pressure and mixture ratio, however, it was assumed constant for all tests. Once the correction factors have been applied to the uncorrected  $c^*$ , the combustion efficiency was computed by:

$$\eta_{c^*} = \frac{c^*_{corrected}}{c^*_{ideal}}$$

where the  $c^*_{ideal}$  is the theoretical chemical equilibrium characteristic velocity at the correct chamber pressure, mixture ratio, and injection temperature.

Combustion Efficiency from Chamber Pressure. The characteristic velocity was calculated from the chamber pressure and flowrate by the relationship:

$$c^*_{uncorrected} = \frac{P_c A_t g}{\dot{w}_{total}}$$

The measured  $c^*$  was then corrected for chamber heat loss, impurities and changes in throat area during the test.

$$c^*_{\text{corrected}} = c^*_{\text{uncorrected}} (C_D \times \eta_{\text{HL}} \times \eta_{\text{Imp}} \times \eta_{\text{T.E.}})$$

where

$C_D$  = discharge coefficient

$\eta_{\text{HL}}$  =  $c^*$  heat loss correction

$\eta_{\text{Imp}}$  =  $c^*$  impurity correction

$\eta_{\text{T.E.}}$  =  $c^*$  throat expansion correction

The discharge coefficient  $C_D$  is defined as the ratio of the actual flow-rate to that which would be obtained for ideal one-dimensional flow.

$$C_D = \frac{\dot{w}}{\rho^* a^* A_T} = \frac{\rho^* a^* A^*}{\rho^* a^* A_T} = \frac{A^*}{A_T}$$

where  $a^*$  = sonic velocity at the throat

$\rho^*$  = density where velocity is sonic

$A^*$  = stream area where velocity is sonic

The discharge coefficient includes the effects of both nonuniform flow and boundary layer. The overall discharge coefficient is

$$C_D = C_{D_A} C_{D_B}$$

where  $C_{D_A}$  is the discharge coefficient for inviscid flow and  $C_{D_B}$  is the discharge coefficient for the boundary layer flow. For the test nozzle

$$C_{D_A} = 0.99444$$

The discharge coefficient including the boundary layer effect is shown in Fig. 60. These values are, to a good approximation, independent of mixture ratio and hydrogen injection temperature.

The characteristic velocity heat loss correction,  $\eta_{HL}$  is defined as:

$$\eta_{HL} = 1 + \left( \frac{\Delta c^*}{c^*} \right)_{\text{heat loss}}$$

where the heat loss occurs in the combustion chamber. The heat loss correction factors were computed for each test by an equation similar to that used for the specific impulse heat loss correction

$$\eta_{HL} = 1 + \frac{1}{2} \left[ \frac{\sum_i (Q/A_i) A_i}{\dot{w}} \right] \left[ \frac{1 - (T_t/T_c)}{h_c - h_t} \right]$$

where

$T_t$  = theoretical throat temperature

$h_t$  = theoretical throat enthalpy

The heat transfer losses ( $Q$ ) for the characteristic velocity corrections were computed in the same manner as those used for the specific impulse heat loss corrections except only the combustion zone losses were applicable. The resultant characteristic velocity heat loss correction factors ranged from 1.0016 (0.16-percent change) for the lowest performing tests (002 through 004) to a high of 1.0123 (1.23-percent change) for Test 023 with high performance and the 70-inch  $L^*$  chamber.

The  $c^*$  impurity correction factor  $\eta_{Imp}$  is defined as:

$$\eta_{Imp} = 1 + \left( \frac{\Delta c^*}{c^*} \right)_{\text{impurity}}$$

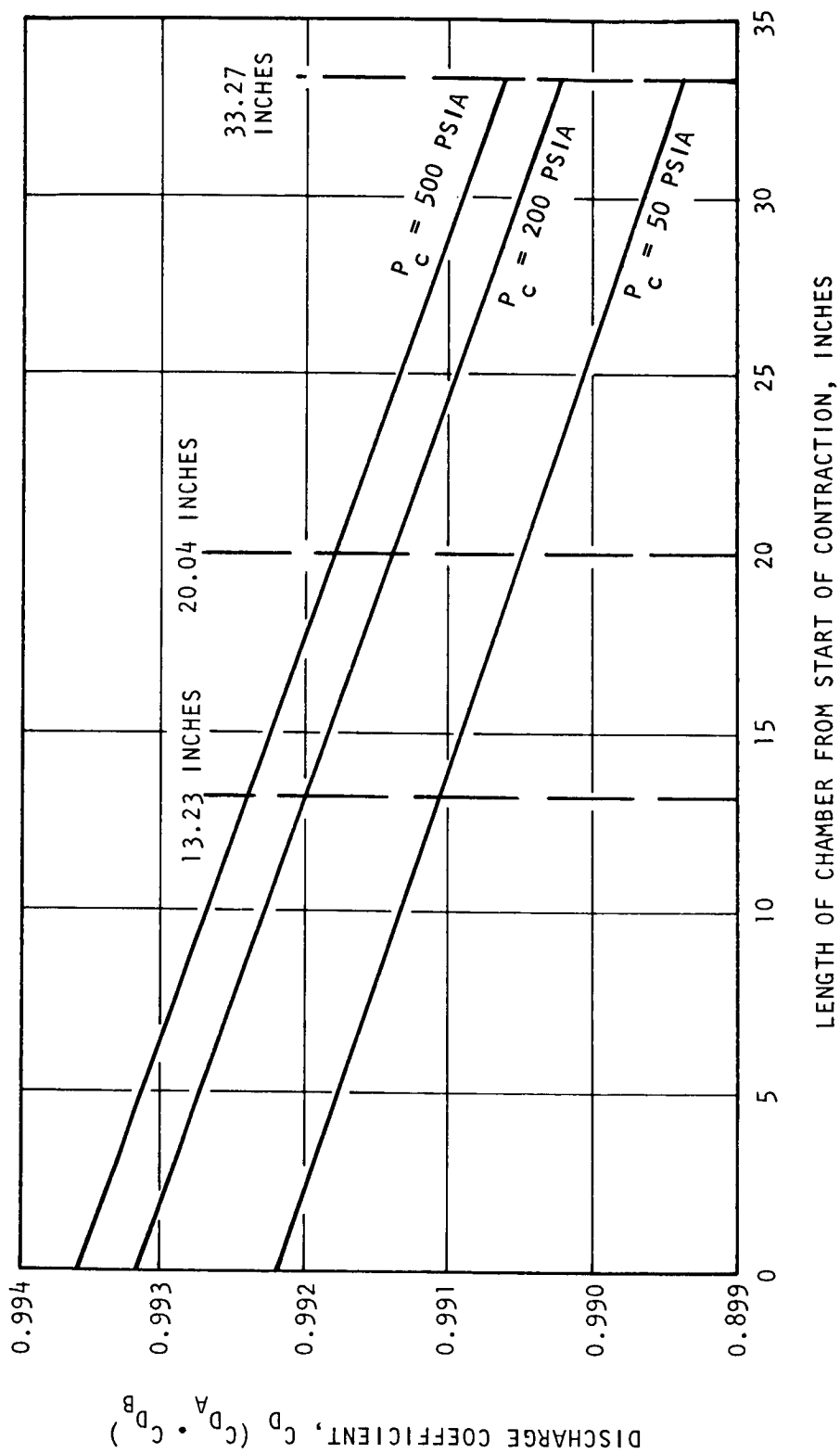


Figure 60. Nozzle Discharge Coefficient vs Chamber Length

This factor was determined in basically the same manner as the specific impulse impurity correction. The changes in the characteristic velocity were slightly less than these for the specific impulse (0.2 percent), however, the characteristic velocity factor was assumed constant and equal to 1.002 for each test.

The throat expansion correction factor,  $\eta_{T.E.}$ , is defined as:

$$\eta_{T.E.} = \frac{A_{T_{hot}}}{A_{T_{cold}}}$$

During the hot-firing tests the thrust chamber throat diameter and area would increase (compared to the ambient dimensions) as a function of the wall temperature. The "hot" throat area was computed for each test as follows:

$$A_{t_{hot}} = \left[ (\alpha \Delta T_{avg} + 1) D_t \right]^2 \pi / 4$$

where

$\alpha$  = thermal expansion coefficient (copper)

$T_{avg}$  = change in average throat wall temperature during the test

During the course of the testing, the "cold" throat diameter  $D_t$  was measured three times; before Test 001, after Test 010, and after Test 024. The corresponding "cold" throat areas were 28.666, 28.933, and 29.124 sq in. A linear throat area change was assumed for the tests where no throat area

(diameter) measurements were taken. The change in the average throat wall temperature was computed from:

$$\left(T_{wg} - T_{wc}\right)_{exp} = \left(T_{wg} - T_{wc}\right)_{theo} \times \frac{\Delta T_{B_{exp}}}{\Delta T_{B_{theo}}}$$

where

$\Delta T_B$  = water coolant bulk temperature change

$T_{wg} - T_{wc}$  = gas to coolant wall temperature change at the throat

The  $\Delta T_{avg}$  term, then, is the change in the wall temperature (cold to hot) at the midpoint between the gas and coolant throat walls, computed for each test.

After all corrections were applied the combustion efficiency was computed from the corrected characteristic velocity in the same manner as the combustion efficiency from thrust, i.e.,

$$\eta_{c*} = \frac{c^*_{corrected}}{c^*_{ideal}}$$

Performance Calculations. A computer program was used throughout the test program to compute some of the correction factors and performance numbers. This computer program was developed during previous Rocketdyne studies. Table 18 gave the performance and operating parameters for each test with the appropriate corrections applied.

#### Stability Data

Stability evaluation of the various hot firing injectors was one of the program goals which received significant attention during the hot-fire

testing. Wide-frequency-range, fast-responding instrumentation was used to aid the stability evaluation. As previously mentioned, this instrumentation consisted of one axial accelerometer, one oxidizer injection pressure photocon, and three chamber pressure photocons (two near the injector and one just upstream of the nozzle converging section). In addition, provisions were made for adding one additional chamber pressure photocon and, in some injectors, fuel and hot-gas injection pressure photocons. A tape recorder was used to monitor all the photocon and accelerometer outputs.

The tape (stability) data from each test was transcribed onto an oscillograph-type record. These records were subsequently reviewed to determine if any high amplitude instabilities were evident. None were observed.

In addition to the oscillograph transcriptions, tape data from four tests (004, 006, 009, and 011; one test for each type injector), were transcribed onto Brush records where the time base and the amplitudes were highly expanded. A typical mainstage portion of the Brush record from Test 004 is given in Fig. 61. The fuel temperature was ramped but no change was observed in the traces during the test. This record is typical of all tests. Indication of low-amplitude oscillations can be seen in the photocon pressure traces. High-frequency oscillations (10,000 cps and above) appeared in the accelerometer trace, however, this high frequency was attributed to instrumentation noise because (1) the high-frequency indications were present before the start of the test, (2) the pressure traces indicated that high-frequency oscillations were no problem, and (3) these high frequencies were beyond the realm of the normally experienced chamber frequencies.

In most cases the actual oscillation frequencies cannot be determined from the direct transcription on to the Brush-type records without

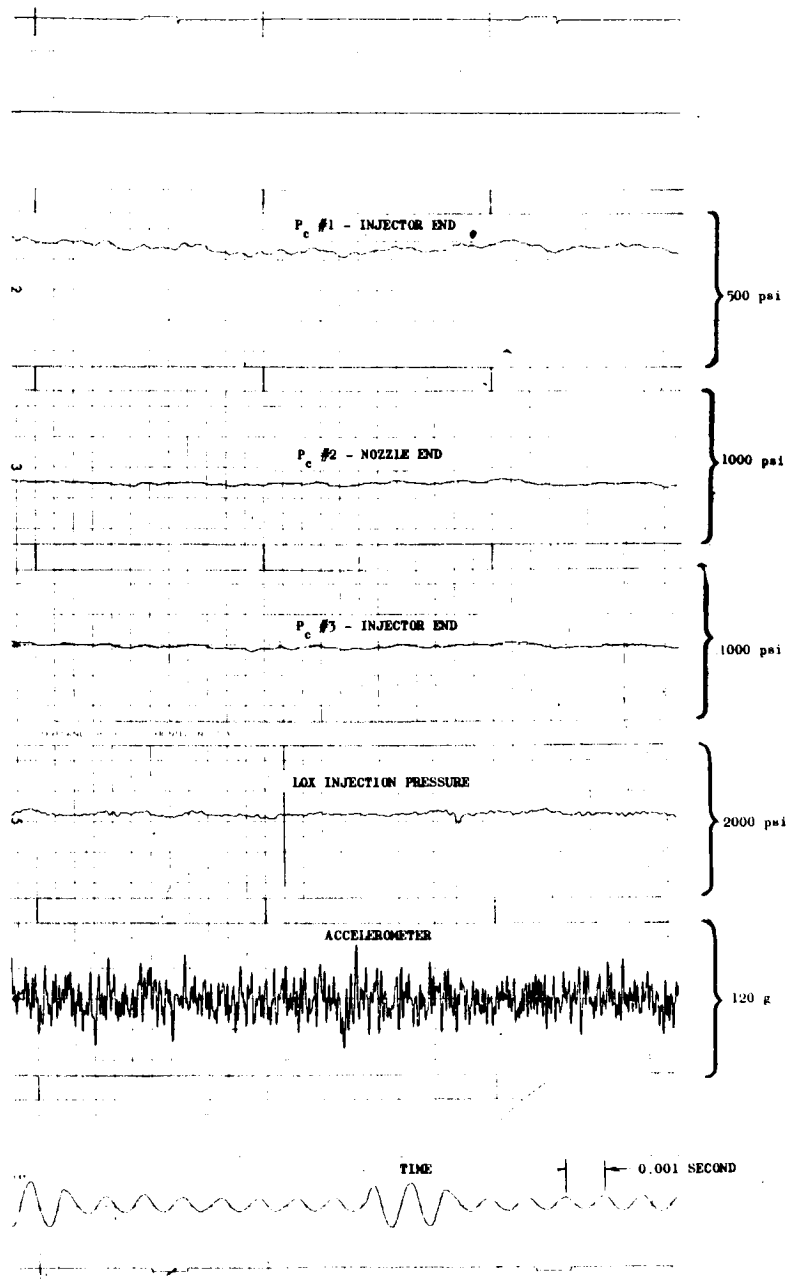


Figure 61. Brush Recording of Photocon and Accelerometer Data From Test 004

"filtering out" the unwanted frequencies. To isolate the various frequencies, "sonics" were made from the tape data for selected tests. The "sonics" gave a picture of the different frequencies experienced and they showed the amplitudes, primarily the peak amplitudes at the various frequencies. The "sonics" were made for the mainstage portion of the tests because this was the primary area of interest. Tests were selected for "sonics" which represented a good cross-section of all tests; i.e , injector type, chamber pressure, fuel temperature and  $L^*$  were the main variables studied in conjunction with the "sonics". Like the brush records, the "sonics" showed traces of many different low and high frequency oscillations but predominant frequencies were lacking. The lower frequencies experiences are most likely the chug or buzz modes associated with the feed system and chamber. The higher frequencies may be associated with the acoustic type frequencies of the chamber. The acoustic frequencies for the tested chamber are approximately as shown below.

<u>Acoustic Frequency</u>	<u>Value, cps</u>
First Tangential	4500 cps
Second Tangential	7500 cps
First Radial	9500 cps
Longitudinal (30-inch $L^*$ )	2300 cps
Longitudinal (70-inch $L^*$ )	950 cps

Many of these acoustic frequencies were detectable but the indicated resonant oscillations at these frequencies were not dominant and they were of low amplitude.

In general, the energy level of all frequencies combined produced pressure (chamber or LOX manifold) oscillation amplitudes less than  $\pm 5$  percent of

the operating pressure during periods of maximum activity. The amplitudes of the individual frequencies would be even less. Because of the low amplitudes experiences and because of a lack of predominant frequencies, stability problems proved to be nonexistent.

### Heat Transfer Data

A water-cooled copper nozzle was used for each test with a water-coolant flowrate of approximately 60 lb/sec and a corresponding throat coolant velocity of 67 ft/sec. The water-coolant bulk temperature rise was monitored during each test. The bulk temperature measurement was used to approximate the nozzle throat heat flux and to give a qualitative indication of the injector performance. The throat heat flux was computed as follows:

$$Q/A_{\text{exp}} = Q/A_{\text{theo}} \times \frac{\Delta T_{B_{\text{exp}}}}{\Delta T_{B_{\text{theo}}}}$$

The bulk temperature change data and heat transfer calculation results are presented for each test in Table 19. Also, the performance efficiency ( $\eta_{c^*}$  based on  $P_c$ ) is shown for comparison with the heat flux. In almost all cases the heat flux and the performance compliment each other; i.e., as the heat flux increases, so does the performance for a given injector. Adjustments are required for differences in chamber pressure; i.e., for Tests 019, 021, and 022 in particular.

An uncooled (heat sink) copper combustion chamber was used for each test. Four copper Nanmac heat flux probes were installed in the chamber to measure the hot-gas wall temperature. Three of these probes were located in a plane just upstream of the water-cooled nozzle and one was located

TABLE 19

## NOZZLE HEAT TRANSFER RESULTS

Test Number	Coolant Bulk Temperature Change, F	Throat Heat Flux, Btu/in. <sup>2</sup> -sec	Characteristic Velocity Efficiency From Chamber Pressure, percent
002	NS	---	76.6
003	12.5	6.0	78.5
004	10	4.8	77.4
005	NS	---	95.1
006	34.5	16.8	95.2
007	35.5	17.0	97.4
008	34.5	16.5	96.9
009	30.5	14.6	90.6
010	32	15.4	92.2
011	38	17.7	94.8
012	36.5	17.4	92.8
014	28	12.7	86.6
015	27.5	13.1	85.2
016	25	12.0	84.5
017	30	14.2	85.8
019*	14	6.7	90.8
021*	16.5	7.9	87.4
022*	5	2.4	93.9
023	36	16.8	97.6
024	34	15.9	92.4

\*Low chamber pressure test

just downstream from the injector. The purpose of the temperature probes was to give a qualitative indication of mixing and performance for the various injectors.

The operating characteristics of the heat flux probes were influenced to a large degree by the injector tested, the test duration, and the type of tests conducted. The probe behavior appeared to be very sensitive to immersion depth, and the service life was limited to only a few tests before rework was required. The probe behavior often was erratic at the high temperatures. Because of these unstabilizing factors only gross qualitative results were obtained from the heat flux probes. Some of the results were as follows:

1. The unmodified 20K tricentric injector configuration 1A produced the lowest chamber wall temperatures.
  - a. The wall temperatures of this injector decreased as the fuel temperature was ramped down.
  - b. Modification to this injector produced higher wall temperatures than the unmodified version.
2. The 5K tricentric injector configuration 1A produced chamber wall temperatures higher than the 20K tricentric 1A.
3. Chamber wall temperatures for the 20K impinging coaxial injector configuration 9A (recessed cup) decreased with a fuel temperature decrease and with chamber pressure.
4. The 5K impinging coaxial injector configuration 9A (recessed cup) produced the highest chamber wall temperatures in line with the elements compared to the areas between elements. The temperature probes were not in the right position to show this "streaking" with the other injectors (5K tricentric 1A and 20K impinging coaxial 9A).

Actual chamber wall erosion occurred during several tests; however, this erosion was primarily due to disturbance in the gas flow caused by the Photocon pressure pickup ports. Erosion did occur outside of the instrumentation port areas during Test 006.

Each of the four injectors contained a porous face material which was film cooled with hydrogen during each of the tests. This type of face cooling appeared to be satisfactory because no injector damage was experienced. The quantity of fuel film cooling used was not measured during the testing, although it was approximated for each test from the pressure and flowrate data. The quantity of fuel film coolant ranged from about 7 to 17 percent of the total fuel flow. The highest film coolant flowrates were produced when the hot-gas flowrates were the lowest.

## DISCUSSION OF TEST RESULTS

Twenty mainstage tests were conducted as planned during the hot-firing injector evaluation phase of the program. Each of the four injectors was tested to characterize its performance with respect to the quantity of hot gas used. During these initial characterization tests, most of the operating parameters (chamber pressure, mixture ratio, hot-gas temperature, etc.) were held at or near the nominal design values. The fuel temperature was varied to a limited degree (Tests 003, 004, and 006) to determine its effect on performance and stability.

Upon completion of the initial characterization tests, two injectors were selected for further evaluation; namely, the 20K tricentric 1A and the 20K impinging coaxial 9A. The 20K tricentric injector configuration 1A was modified to improve performance and then was subjected to two evaluation tests. The 20K impinging coaxial injector configuration 9A (recessed cup) gave the highest performance and was subjected to performance and stability evaluations at off-design conditions.

Table 20 shows the tests conducted with each injector, the quantity of hot gas used, and the combustion efficiency. The quantity of hot gas used was the prime variable during the test program although other parameters were varied as shown in the off-design column of Table 20. The combustion efficiency listed is the efficiency based on chamber pressure. This efficiency was judged to be more accurate than the combustion efficiency based on thrust because the thrust calibration was subject to possible error as previously mentioned. Also two separate chamber pressure measurements were used for computing efficiency, compared to only one thrust measurement. Thus the combustion efficiencies referred to in this discussion are based on chamber pressure. The efficiencies based on thrust averaged about 2 percent (from 0.2 to 4.3 percent) less than that based on chamber pressure; however, the general trends were the same for both efficiencies.

TABLE 20  
SUMMARY OF SELECT HOT-FIRE TEST RESULTS

Injector Configuration	Test Number	Hot-Gas Weight Flowrate, percent of total propellant	Characteristic Velocity Efficiency from Chamber Pressure, percent	Off-Design Conditions
20K Tricentric 1A	002	13.1	76.6	Thrust Chamber Fuel Temperature = 45 R
	003	13.4	78.5	
	003	13.3	75.2	
	004	10.1	77.4	
20K Tricentric 1A (Modified)	015	6.1	85.2	
	016	6.1	84.5	
5K Tricentric 1A	009	6.1	90.6	
	010	12.4	92.2	
20K Impinging Coaxial 9A (Recessed Cup)	005	9.0	95.1	Thrust Chamber Fuel Temperature = 118 R Characteristic Length (L*) = 43.5 inches Characteristic Length (L*) = 43.5 inches Thrust Chamber Fuel Temperature = 49 R Chamber Pressure = 213.5 psia Chamber Pressure = 212.9 psia Chamber Pressure = 45.8 psia Characteristic Length (L*) = 70 inches Characteristic Length (L*) = 70 inches; Thrust Chamber Fuel Temperature = 50 R
	006	8.8	95.4	
	006	8.8	95.0	
	007	14.2	97.4	
	008	6.6	96.9	
	017	8.5	85.8	
	019	11.0	90.8	
	021	7.3	87.4	
	022	23.1	93.9	
	023	13.7	97.6	
	024	8.4	92.4	
5K Impinging Coaxial 9A (Recessed Cup)	011	13.2	94.8	
	012	8.2	92.8	
	014	0.0	86.6	

NOTE: Nominal operation was

1. Chamber Pressure = 400 to 500 psia
2. Characteristic Length (L\*) = 30 inches
3. Thrust Chamber Fuel Temperature = ~ 250 R

### 20K Tricentric Injector Configuration 1A

Performance of the 20K tricentric injector configuration 1A was relatively low (in the 77-percent range). No significant change in performance was observed with a change in the quantity of hot gas; i.e., Tests 002 and 003 vs Test 004. Analytical studies (Task 1) suggested that performance of this injector was probably limited by poor mixing of the fuel with the oxidizer/hot-gas combination. Also, the oxidizer atomization of the tested injector was somewhat degraded compared to the originally conceived concept because of the three plugs installed in the oxidizer annulus (for stability reasons); i.e., the oxidizer velocity would be higher and the exposed area less.

As previously mentioned, this injector was modified by adding a hot-gas swirler and a fuel converging ring and by removing the three oxidizer passage plugs. Performance of the modified injector was about 8-percent greater than the unmodified injector. All the increase appears to be due to the fuel converging ring (improved mixing) and to the removal of the three plugs, thereby supporting the analysis predictions. The hot-gas swirler was lost early in the first test (015), so its potential remains unknown.

### 20K Impinging Coaxial Injector Configuration 9A (Recessed Cup)

The 20K impinging coaxial injector configuration 9A produced very good performance (in the 95- to 97.5-percent range). When comparing Tests 007 and 008, the performance fell off slightly with the smaller quantity of hot gas. Also, the increased  $L^*$  (43.5 vs 30 inches) appeared to affect the performance slightly as evidenced by Tests 005 and 006 vs Test 008. However,

when the  $L^*$  was increased from 43.5 to 70 inches (Tests 007 and 023) no significant change was observed, implying that the longer (70-inch)  $L^*$  was not required at the particular test conditions. The  $L^*$  did make a significant difference in the performance when 50 R fuel was used; i.e., the performance increased about 7 percent when the  $L^*$  was increased from 30 to 70 inches.

Off-design chamber pressures of 200 and 50 psia and also 50 R fuel produced lower performance with this injector as shown in Table 20. (During Test 003, where the fuel was ramped to 45 R, the performance also fell off slightly with the 20K tricentric injector configuration 1A.) Performance at these off-design conditions could be improved by tailoring the injectors to operate over a wider range of test conditions. During this program the injector designs were slanted toward the use of gaseous hydrogen and high-chamber-pressure operation with little attention paid to optimizing the designs for cold hydrogen or for low chamber pressures. Although combustion efficiency decayed at the low chamber pressures, it appeared higher at 50 than at 200 psia. This higher performance was attributed to the higher quantity (23 percent) of hot gas at 50 psia; however, accuracy of the test data is questionable at this low instrumentation operating range.

#### 5K Tricentric Injector Configuration 1A

Performance of the 5K tricentric injector configuration 1A was approximately 14 percent higher than the 20K tricentric injector configuration 1A, thereby implying that element size has a significant influence on performance of the tricentric injector concept. Again, with this 5K injector, the performance increased slightly with increased hot gas flow.

### 5K Impinging Coaxial Injector Configuration 9A (Recessed Cup)

The 5K impinging coaxial injector configuration 9A performed in the 95-percent range during Test 011 with 13-percent hot-gas flow. Like the other configurations, as the quantity of hot gas decreased, the performance also decreased. When no hot gas was used (Test 014), a very noticeable performance loss occurred, thus highlighting the value of the hot gas; i.e., highlighting the two-stage injection principle.

Contrary to expectations, this injector was lower performing than the 20K impinging coaxial injector configuration 9A, even though both contained the same basic design features. No explanation was found for this performance difference.

### Gas Momentum vs Performance

Performance for each of the injectors was plotted against the ratio of oxidizer flow to total gas momentum (fuel plus hot gas momentum) as indicated in Fig. 62. Each injector is represented in Fig. 62 by a curve or curves showing the general performance trend as a function of gas momentum. As shown, all of the curves tend to fall off as the ratio of oxidizer flow to gas momentum increases; i.e., as the actual total gas momentum decreases. Peak or optimum performance values seem to be approached at the lower ratios for both 5K injector configurations and for the 20K configuration 9A. In all cases these low ratios were produced when the hot-gas flows were 12 to 14 percent of the total and the main fuel entering the injector was about 250 R.

As the fuel temperature and momentum decreased (momentum ratio increased) so did the performance. Likewise, as the hot-gas quantity and momentum

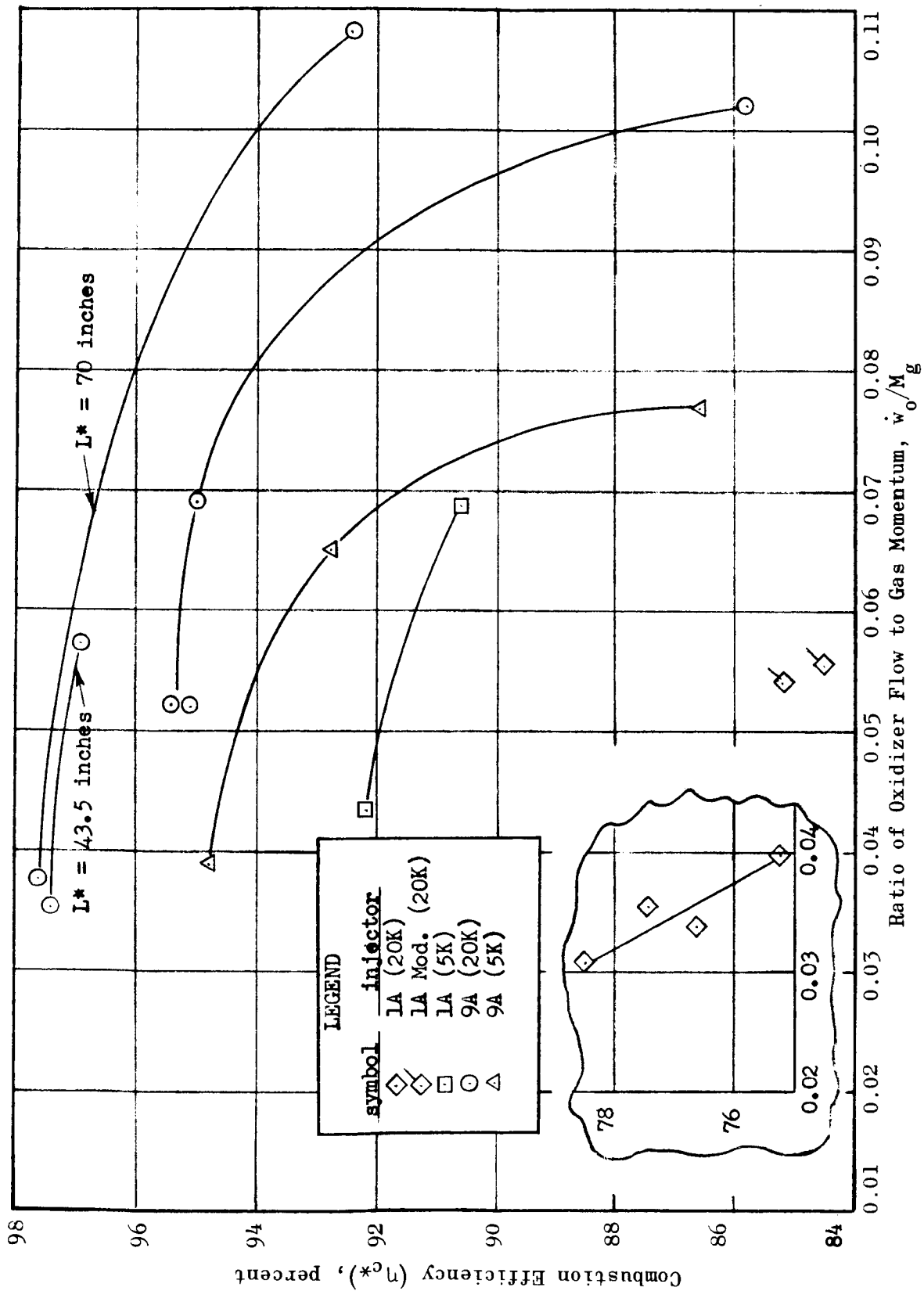


Figure 62. Total Gas Momentum Effect on Injector Performance (Chamber Pressure approx. 400 to 500 psia; Characteristic Length 30 inches unless otherwise noted)

decreased so did the performance. Thus, both types of gases seem to influence the performance, implying that they could possibly be combined into one gas species.

The relative value of one gas over the other (hot gas vs fuel) could not be singled out from this study although the hot gas produced the highest momentum for a given quantity of flow.

The total gas momentum vs performance relationships (Fig. 62) best describe the behavior of the different injectors. Fuel momentum, hot gas momentum, or the actual quantity of hot gas variables, by themselves, did not give consistent trends. For example: when the quantity of hot gas was reduced the performance was reduced; however, when the fuel temperature was reduced the performance was reduced even though the hot gas was essentially unchanged; i.e., in Tests 006 vs 017 and in the two data slices from Test 003. Thus the cold-temperature hydrogen tests did not conform to the set pattern unless the total gas momentum was considered.

Figure 62 shows the general performance vs flow-to-momentum-ratio trend for each injector. These trends appear representative from the interpretations of available data but should not be taken as absolute for injector design point selections. Additional data points are required to truly define these curves. Data shown on Fig. 62 also lumps a relatively wide range of chamber pressures (397 to 523 psia) and mixture ratios (4.15 to 6.0). It is expected that these variations may influence observed trends. The low-chamber-pressure tests (50 to 200 psia) were not included.

### Injector Cooling

The face of each injector was cooled with fuel passing through a porous face material during the testing. The quantity of fuel coolant ranged from about 7 to 17 percent of the total fuel and from about 1 to 3 percent of the total propellant. Conservative heat transfer calculations suggest that 1 percent of the total was more than enough to cool the face. Thus, some performance improvement is possible if the quantity of film coolant were reduced. The quantity of coolant might be reduced to 0 if regenerative cooling were used and/or if the unused portion of the injector face were eliminated. For a single injector element the chamber tubes could be contoured inward to meet the edge of the element, thereby eliminating the "injector face."

### Combustion Stability

The stability of each injector tested was considered normal and presented no problem. Minor insignificant oscillations were recorded for each injector. These oscillations occurred at many different frequencies although none were predominant. No change (decrease) in stability was observed with a decrease in fuel temperature to approximately 50 R, with increased  $L^*$  to 70 inches, or with reduced chamber pressures to approximately 50 psia.

High-speed motion picture films of certain tests revealed some pulsing tendencies in the flame pattern; however, photocon and accelerometer instrumentation data showed that the pulsing was insignificant.

### Hardware Integrity

The durability of each injector was very good throughout the hot-firing test program. Minor erosions were noted on 20K injector configuration 1A and 5K injector configuration 9A; however, these erosions proved to be insignificant and of the type which could be prevented with minor modifications. During Test 006, erosion occurred on the uncooled chamber walls in the vicinity of instrumentation ports and in other areas. These erosions were related to the long test duration (3.35 seconds) and to the higher performing injector. To minimize chamber erosions and thereby prolong chamber life, subsequent tests (after Test 006) were limited to about 1 to 2 seconds duration. With this reduced duration, stabilized data were obtained and the chamber erosions were minor and isolated to the areas around the instrumentation ports.

Test Number	Injector Configuration	Characteristic Length (L*), inches	Vacuum Thrust, pounds	Nozzle Chamber Pressure, psia	Total* Oxidizer Weight Flowrate, lb/sec	Total Fuel Weight Flowrate, lb/sec
002	1A (20K)	30	15,607	396.7	51.06	10.33
003	↓	↓	17,458	427.6	53.02	11.32
004	↓	↓	16,527	411.3	53.16	11.55
005	9A (20K)	↓	16,784	432.3	53.08	12.31
006	↓	↓	18,737	473.7	48.44	10.60
007	↓	↓	18,841	473.3	48.52	10.46
008	↓	43.5	18,883	475.4	47.59	11.48
009	1A (5K)	43.5	20,565	498.1	51.05	10.35
010	1A (5K)	30	19,157	479.6	47.79	10.91
011	9A (5K)	↓	20,019	502.3	56.15	10.73
012	↓	↓	21,264	522.5	59.91	10.20
014	↓	↓	21,232	512.7	55.75	10.27
015	1A Mod (20K)	↓	19,232	473.7	52.48	9.74
016	1A Mod (20K)	↓	17,243	421.8	51.69	8.68
017	9A (20K)	↓	17,971	435.0	50.21	10.78
019	↓	↓	18,192	445.0	52.18	10.87
021	↓	↓	18,159	450.0	55.26	9.75
022	↓	↓	8,668	213.5	24.90	4.35
023	↓	↓	8,730	212.9	24.16	5.13
024	↓	70	1,875	45.8	4.39	1.42
		70	20,658	505.4	53.26	10.27
		70	19,650	486.1	57.03	9.51

\* Adjusted for impurities

FOLDOUT FRAME /

TABLE 18

## SUMMARY OF PERFORMANCE RESULTS

	Mixture Ratio, Oxidizer/ Fuel	Hot-Gas Weight Flowrate, Percent of Total Propellant Flow	Hot-Gas Temperature, F	Fuel Temperature to Injector, R	Throat Area, sq in.	Delivered Vacuum Specific Impulse, seconds	Delivered Vacuum Specific Impulse Efficiency, percent	Characteristic Velocity, ft/sec	Characteristic Velocity Efficiency From Thrust, percent	Characteristic Velocity Efficiency From Chamber Pressure, percent	Test Number
	4.94	13.1	1048	257	28.94	254.2	71.4	5986	73.3	76.6	002
	4.68	13.4	1159	256	28.97	271.3	75.9	6163	77.9	78.5	003
	4.60	13.3	1159	45	28.97	255.4	71.6	5894	73.5	75.2	
	4.31	10.1	1283	255	29.00	256.7	71.2	6137	73.1	77.4	004
	4.57	9.0	1214	253	29.15	317.4	88.4	7510	91.2	95.1	005
	4.64	8.8	1228	260	29.18	319.6	89.0	7519	91.9	95.4	006
	4.15	8.8	1242	118	29.18	319.7	88.7	7541	91.6	95.0	
	4.93	14.2	1310	255	29.21	334.9	94.0	7623	97.2	97.4	007
	4.38	6.6	1227	253	29.24	326.4	90.4	7691	93.6	96.9	008
	5.23	6.1	1352	253	29.25	299.3	84.5	7045	87.0	90.6	009
	5.87	12.4	1352	253	29.28	303.3	87.4	6997	90.0	92.2	010
	5.43	13.2	1365	258	29.35	321.6	91.3	7317	94.2	94.8	011
	5.39	8.2	1310	258	29.36	309.1	87.6	7177	90.4	92.8	012
	5.96	0.0	—	256	29.33	285.6	82.4	6572	84.8	86.6	014
	4.66	6.1	1241	255	29.35	294.7	82.1	6716	84.7	85.2	015
	4.80	6.1	1255	259	29.36	288.5	80.6	6644	83.0	84.5	016
	5.67	8.5	1310	49	29.41	279.3	80.4	6529	82.8	85.8	017
	5.72	11.0	1460	205	29.35	296.2	85.7	6873	88.3	90.8	019
	4.71	7.3	1380	260	29.37	297.9	83.4	6854	86.1	87.4	021
	3.09	23.1	1145	257	29.31	322.2	89.0	7431	92.5	93.9	022
	5.19	13.7	1283	261	29.48	325.2	91.8	7581	95.5	97.6	023
	6.00	8.4	1448	50	29.50	295.3	85.9	6953	89.1	92.4	024

FOLDOUT FRAME

2

223/224

FOLDOUT FRAME

3

## REFERENCES

1. Mayer, E.: "Theory of Liquid Atomization in High Velocity Gas Streams," ARS Journal, Vol. 31, No. 12, December 1961.
2. Dickerson, R. A. and M. D. Schuman: "Atomization Rates of Droplets and Jets," AIAA Preprint No. 63-498, AIAA Heterogeneous Combustion Conference, Palm Beach, Florida, December 1963.
3. Ingebo, R. D.: "Drop-Size Distribution for Impinging-Jet Breakup in Air-streams Simulating the Velocity Conditions in Rocket Combustors," NASA TN 4222, 1958.
4. Tanasawa and Tesima, J.S.M.E., Vol. 1, No. 1, 1958.
5. Clarke, B. J.: "Breakup of a Liquid Jet in a Transverse Flow of Gas," NASA TN D-2424, August 1964.
6. Nelson, P. and W. Stevens: "Size Distribution of Droplets from Centrifugal Spray Nozzles," AIChE Journal, Vol. 7, No. 1, March 1961.
7. Squire, H. B.: British J. App. Phys., Vol. 4, June 1953.
8. Schlichting, H.: "Boundary Layer Theory," 4th ed., McGraw-Hill Book Co., Inc., New York, N.Y., 1962.
9. Shi-I Pai: "Fluid Dynamics of Jets," Van Nostrand Co., Inc., New York, N.Y., 1954.
10. Abramovich, G. N.: "The Theory of Turbulent Jets," MIT Press, Massachusetts Institute of Technology, Cambridge, Massachusetts, 1963.
11. Dickerson, R. A. and T. A. Coultas: "Breakup of Droplets in an Accelerating Gas Flow," AIAA Paper No. 66-611, AIAA Second Propulsion Joint Specialist Conference, Colorado Springs, Colorado, June 1966.
12. Wolfe, H. E. and W. H. Anderson: "Kinetics Mechanism and Resultant Droplet Sizes of the Aerodynamic Breakup of Liquid Drops," Aerojet-General Corp., Report 0395-04 (18) SP., April 1964.

13. Morrell, G.: "Rate of Liquid Jet Breakup By a Transverse Shock Wave," NASA TN D-1728, May 1963.
14. Priem, R. J. and Heidmann: "Propellant Vaporization as a Design Criteria for Rocket Engine Combustion Chambers," NASA TR-67, 1960.
15. Bird, R. B., W. E. Stewart and E. N. Lightfoot: "Transport Phenomena," John Wiley & Sons, New York, N.Y., 1960.
16. Gerhouser, J. M. and R. J. Thompson, Jr.: "Theoretical Performance Evaluation of Rocket Propellants," Report No. R-5802, Rocketdyne, a Division of NAA, Inc., August 1964.
17. R-6597P-1: Two State Bi-Propellant Injection, Rocketdyne, a Division of North American Aviation, Inc., Canoga Park, California, 8 June 1966.

# NOMENCLATURE

$A_s$	= Surface area of liquid jet
$c$	= Acoustic velocity
$C_a$	= Coefficient of proportionality for atomization rate
$c_D$	= Drag coefficient
$C_p$	= Specific heat
$D$	= Diameter
$D_a$	= Air core diameter (for centrifugal nozzles)
$D_b$	= Droplet diameter before secondary breakup, used only in equation (11) applied to secondary breakup
$D_j$	= Diameter of jet
$D_\ell$	= Liquid jet diameter
$D_o$	= Orifice diameter
$D_f$	= Molecular diffusivity
$h_g$	= Gas side heat transfer coefficient
$H_v$	= Latent heat of vaporization
$k$	= Thermal conductivity
$M_g$	= Gas momentum
$M_\ell$	= Molecular weight of liquid propellant and liquid momentum
$n$	= $x/D_o$
$Nu_h$	= Nusselt number for heat transfer
$Nu_m$	= Nusselt number for mass transfer
$P$	= Static pressure
$P_v$	= Vapor pressure

$Q/A$	= Heat flux
$Re$	= Reynold's number
$s$	= Standard deviation for the log normal distribution
$t$	= Time
$t_B$	= Breakup time
$T$	= Temperature
$T_B$	= Coolant bulk temperature
$T_g$	= Gas temperature
$T_{hg}$	= Hot gas temperature
$T_\ell$	= Liquid (or drop) temperature
$T_m$	= Average (film) temperature = $1/2 (T_g + T_\ell)$
$T_{wc}$	= Coolant side wall temperature
$T_{wg}$	= Gas side wall temperature
$T_{wi}$	= Initial wall temperature
$U_d$	= Drop velocity
$U_g$	= Gas velocity
$\vec{U}_g$	= Gas velocity vector
$U_{inj}$	= Injection velocity
$U_j$	= Jet velocity
$U_\ell$	= Liquid (or drop) velocity
$\vec{U}_\ell$	= Liquid velocity vector
$\bar{U}_{\ell,x}$	= Average axial component of liquid velocity
$U_m$	= Maximum gas velocity, or velocity along the jet axis
$U_r$	= Relative velocity between the gas and liquid (or drop)

$V$	= $ \vec{U}_g - \vec{U}_l $ , see reference 5
$\dot{w}$	= Flowrate
$We$	= Weber number, $D \rho U^2 / \sigma$
$\dot{w}_{hg}$	= Hot gas flowrate
$\dot{w}_v$	= Vaporization rate
$x$	= Distance (parallel to the axis of the engine) and gas to liquid mass ratio
$\alpha$	= Thermal diffusivity and thermal expansion coefficient
$\epsilon$	= Measure of liquid jet distortion, see reference 5
$\theta$	= Angle relative to chamber axis
$\theta_i$	= Angle relative to injector face
$\mu_g$	= Gas viscosity
$\mu_l$	= Liquid viscosity
$\rho$	= Density
$\rho_g$	= Gas density
$\rho_l$	= Liquid density
$\sigma$	= Surface tension
$\sigma_l$	= Liquid surface tension
$\phi_m$	= Maximum included angle of spray cone

## APPENDIX A

### TRICENTRIC INJECTOR ATOMIZATION ANALYSES

This appendix describes the atomization analysis performed for the tricentric injector elements. The elements are characterized by (a) a LOX jet core surrounded by hot gas or by  $\text{GH}_2$  or (b) a LOX annulus atomized by hot gas or by  $\text{GH}_2$  inside the annulus. The atomization rate equation was obtained from Mayer (Ref. 1) and is basically the same as used in Ref. 2 and 11. It expresses the atomization rate per unit area,  $\dot{w}_A/A_s$  as:

$$\dot{w}_A/A_s = C_A \left( \frac{\mu_l \rho_l}{\sigma} \right)^{1/3} (\rho_g U_r^2)^{2/3} = K_A (\rho_g U_r^2)^{2/3} \quad (\text{A-1})$$

The term  $K_A$  depends only on liquid properties.  $U_r$  is the gas velocity relative to the liquid jet velocity. The constant  $K_A$  was obtained from a previous Rocketdyne study which was a combined experimental/analytical investigation of coaxial LOX/ $\text{GH}_2$  injection simulating J-2 injectors. Operating conditions included 457 psia chamber pressure and a mixture ratio of 4.93 with the  $\text{GH}_2$  at 465 R and the LOX at 185 R. The calculated gas and droplet velocity vs distance (from the injector) profiles were verified experimentally by streak photographs of a transparent two-dimensional chamber. To obtain  $K_A$  from their atomization vs distance curves, Eq. A-1 was integrated using  $U_r$  as the gas velocity at the spray zone boundary.  $K_A$  thus obtained from two experimental runs under quite different run conditions agreed within  $\pm 1.70$  percent.

#### LOX CENTRAL CORE

To predict the atomization rate of the 20K tricentric injector configuration 1A using LOX in the center, Eq. A-1 was integrated using a gas velocity

profile developed under similar run conditions (457 psia, mixture ratio = 4.93). This velocity profile is closely fit by:

$$U_r = \frac{U_{ri}}{(1 + x/0.232)} \quad (A-2)$$

where  $U_{ri}$  is the initial relative velocity and  $x$  is the distance downstream of the injector (in inches). Gas density was assumed constant. The two cases examined are with LOX surrounded by (1)  $\text{GH}_2$  injected at 1230 ft/sec and (2) hot gas injected at 4125 ft/sec. Figure A-1 shows the results of these calculations in terms of the resulting mixture ratio as a function of axial distance. During another program it was found that 50 percent of the atomized LOX had vaporized upstream of the flame front. Assuming a similar degree of vaporization, gas phase mixture ratios are also shown in Fig. A-1. Previously it was found that the "flame front" did not penetrate upstream of where the mixture ratio was 0.84 or lower.

The tentative conclusion is that for  $\text{GH}_2$  surrounding a central core of LOX in a 20K tricentric configuration 1A the gas will not atomize sufficient LOX to support a flame front. Attainment of a flame would depend on vaporization of the remaining LOX jet with its relatively low surface/volume ratio. One reservation is that scaling of the velocity profile (Eq. A-2) from the small (0.132-inch diameter) LOX jet to the 1.61-inch diameter size should cause the gas velocity to decay more slowly. On the other hand, however, the 200 R hydrogen is colder than that in the previously mentioned experimental studies (305 to 465 R), so the percent of LOX vaporized would be considerably less than that assumed in Fig. A-1. These two effects may be expected to roughly cancel one another.

For the case of hot gas surrounding a central core of LOX the rate of LOX vaporization may produce a more favorable gas phase mixture ratio than shown

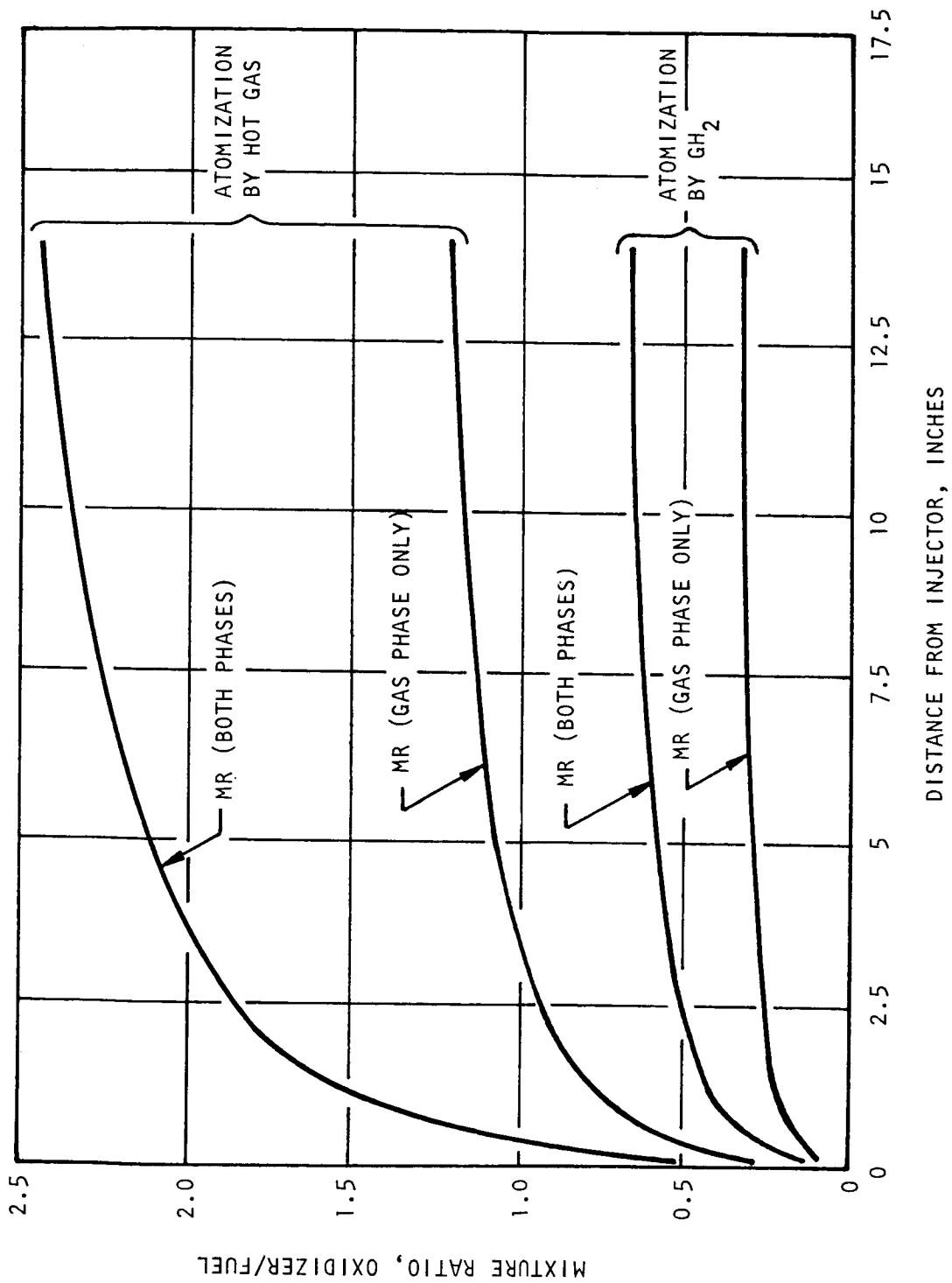


Figure A-1. Atomization of Lox Jet by Surrounding Gas

in Fig. A-1. In this case a flame front could be obtained at perhaps 3 inches downstream of the injector. At this point about 18 percent of the LOX will have been atomized. With the design contraction ratio of 2.0, the combustion gas velocity upstream of the nozzle will not exceed 1700 ft/sec. Using this velocity in Eq. A-1 an additional 12.6 inches would be required to atomize the entire LOX jet. Even if scaling to the larger diameter causes a slower decrease in gas velocity upstream of the flame front the LOX jet is expected to persist 15 or more inches downstream of the injector. This would place it in the nozzle for the motor with an  $L^*$  of 30.

#### LOX ANNULUS

No experimental data were available to describe the velocity profile for the case of hot gas of  $\text{GH}_2$  inside an annular LOX jet. However, available experimental data with LOX/ $\text{GH}_2$  do indicate very nearly constant pressure upstream of the flame front. Therefore, assuming constant pressure, a simple momentum balance was used to obtain the gas velocity profile within the LOX annulus. Frictional drag along the "wall" of LOX was found to have negligible effect. Therefore gas velocity was assumed to be degraded only via momentum exchange with the atomized droplets. At the end of each axial increment the atomized LOX was assumed to have attained gas velocity. As the gas velocity decreased, the inside diameter of the annulus had to increase to maintain continuity. Converting Eq. A-1 to finite difference form and replacing the annular inside diameter by its value obtained from continuity, the following equation was obtained expressing the weight/second of LOX atomized in the distance  $\Delta x$ :

$$\Delta \dot{w} = 4 \dot{w}_{g,i}(\Delta x) K_A \frac{\left( \frac{\rho_g U_r^{-2}}{\rho_g (\bar{U}_r + U_j)} \right)^{2/3}}{\rho_g (\bar{U}_r + U_j)} \quad (\text{A-3})$$

$U_j$  is the LOX jet velocity (assumed constant) and  $\dot{w}_{g,i}$  is the hot gas (or  $\text{GH}_2$ ) injection rate.  $K_A$  was obtained as described above.  $U_r$  is the arithmetic average relative velocity across  $\Delta x$ .  $U_r$  was calculated by the momentum balance:

$$U_r(x) = \frac{\dot{w}_{g,i} U_{r,i}}{\dot{w}_{g,i} + \dot{w}_a} \quad (\text{A-4})$$

where  $\dot{w}_a$  is the flowrate of atomized LOX at the position  $\Delta x$ . Equations A-3 and A-4 were solved by iteration to obtain the atomization rate and gas velocity over successive increments  $\Delta x$ . Figure A-2 shows the percent of the LOX stream atomized by (1)  $\text{GH}_2$  injected at 1230 ft/sec, and (2) hot gas injected at 4125 ft/sec inside a LOX annulus sized for a 20K element. Atomization on the outside of the LOX was not included. Velocity profiles had the form:

$$U_r = \frac{U_{r,i}}{(1 + x/b)^{1/2}} \quad (\text{A-5})$$

where  $b$  is a constant.

For  $\text{GH}_2$  the mixture ratio criteria for flame front penetration would be satisfactory at 2.0 inches if 50 percent of the atomized LOX vaporized, however, due to the low  $\text{GH}_2$  temperature, the flame front is expected to be further downstream.

In the case of hot gas the complete atomization of the LOX jet is predicted to occur within 6 inches of the injector. This configuration obviously makes effective use of the hot-gas momentum. Because of this favorable result initial conditions were estimated for this element type in order

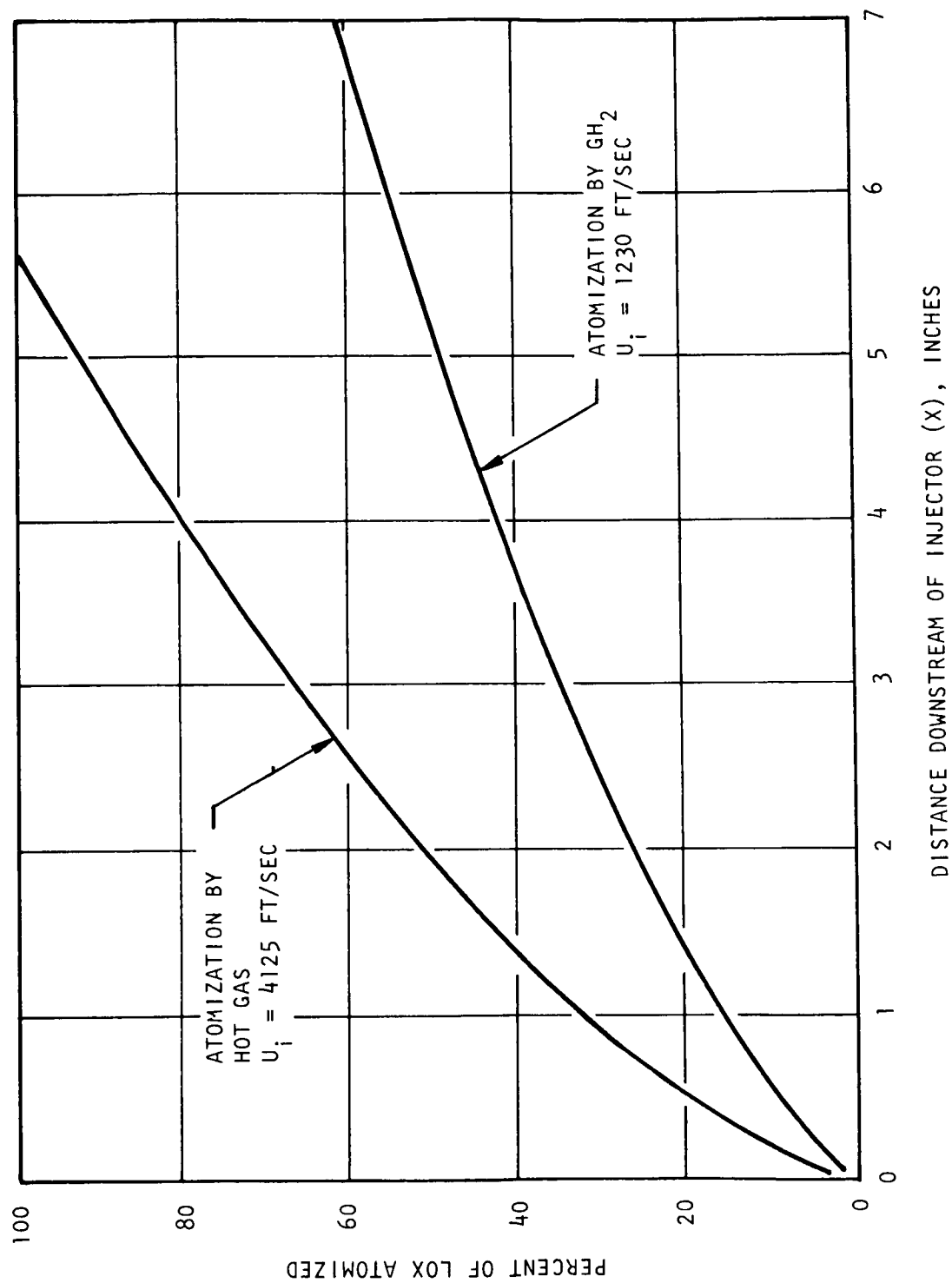


Figure A-2. Atomization of Annular LOX Jet

to run the one-dimensional computer program and predict performance. Atomized droplet diameters were obtained by the equation

$$D \text{ (microns)} = 2.07 \times 10^9 \frac{(\mu_{\sigma}^2)}{\rho_l}^{1/3} (\rho_g U_r^2)^{-2/3} \quad (\text{A-6})$$

Minimum and maximum diameters indicated that

$$11.0 < D \text{ (microns)} < 116.3 \quad (\text{A-7})$$

The volume mean diameter of the droplets formed,  $D_{30}$ , was 26.6 microns. Although the gas-phase mixture ratio would certainly exceed 0.84 within the first 1/2 inch from the injector, the gas velocity is so much higher than the estimated turbulent flame velocity (about 250 ft/sec) that a "flame front" should occur further downstream. For purposes of calculation it was presumed to occur at  $x = 6$  inches.

The prediction of rapid atomization of the annular LOX jet is strengthened by the observation that most of the assumptions used in the calculation were conservative. Some of these are discussed as follows:

1. Assumption of constant pressure: If the pressure drops within the annulus, gas velocities will fall still more slowly, leading to more rapid atomization.
2. Assumption that droplets attain gas velocity at the end of each increment,  $x$ : The failure of droplets to reach gas velocity will mean that the gas velocity will attenuate more slowly than that used in the calculations so this assumption is conservative with regard to the atomization rate.

3. Neglect of droplet evaporation: Evaporation of LOX droplets would force the LOX annulus to expand more rapidly, increasing the gas/liquid contact area and thus increasing the atomization rate.
4. Neglect of heat transfer from gas to LOX: Cooling of the gas by heating LOX droplets would tend to reduce the LOX annulus diameter and counteract assumption 3.
5. Determining atomization rate by means of the "momentum mean" gas velocity: The rate constant  $K_A$  was empirically obtained to describe the atomization rate as a function of gas velocity at the spray rate as a function of gas velocity at the spray zone outer boundary. It is reasonable to assume that the mean velocity within the annulus would similarly affect atomization.

## DISCUSSION

The calculations clearly indicate that gas is much more effective at atomizing the LOX if it is injected within an annular jet of the liquid rather than around a liquid core. Qualitatively this can be attributed to: (1) no gas momentum is lost to external stagnant gas, (2) the initial contact area is greater, and (3) the area of contact grows as the gas velocity is attenuated.

The tricentric element with hot gas inside an annular LOX jet appeared to be the most promising.

## APPENDIX B

### COLD FLOW SAMPLING PROBE RESULTS

A limited effort was made to obtain some quantitative spray distribution data. The large physical size of the injected water spray fields prevented complete backlighting penetration necessary for meaningful droplet photography. For this reason a flow sampling probe was designed (Fig. B-1) to limit the amount of water permitted to pass through the photographic field of view. An additional problem encountered with droplet photography was associated with the relatively high droplet velocities caused by the sonic injector flows.

Fifteen tests were conducted with the sampling probe in an effort to obtain droplet size information. The most significant test was obtained with water only. In this test, some of the droplets were sharply focused so that their size and velocity could be determined. The smallest droplets that could be resolved were about 500 microns. The velocity of all the droplets were 15 to 20 ft/sec, corresponding closely to the water injection velocity. A photographic enlargement obtained with the probe is shown in Fig. B-2. By contrast, when the gas streams were flowing with the liquid, no material was sharply focused except a few droplets in secondary flow streams (rising rather than falling).

After analysis of the photographs and the experimental system, it was concluded that in order to see and measure droplets by this method, increased magnification was necessary and a much faster photographic speed needed than that supplied by the 2-microsecond stroboscope unit.

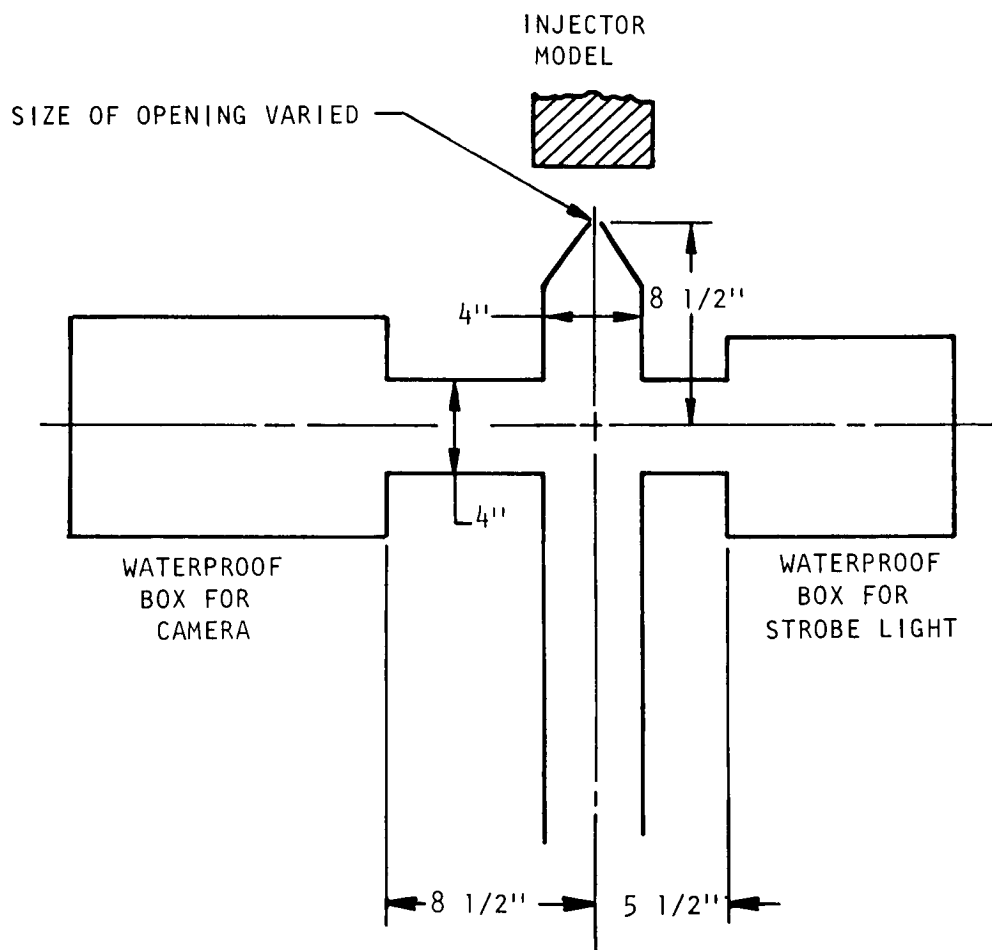


Figure B-1. Schematic of Sampling Probe

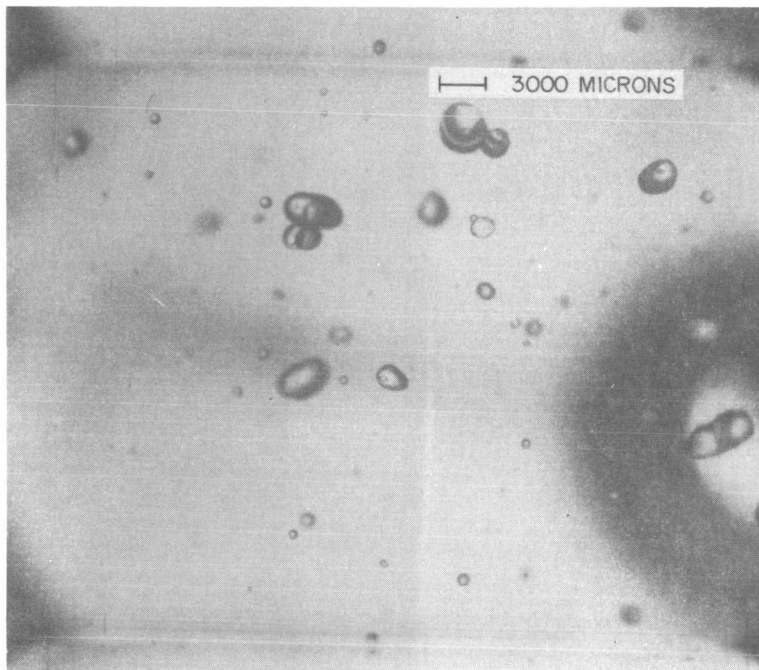


Figure B-2. Droplet Photograph Obtained With Sampling Probe

## APPENDIX C

### HEAT TRANSFER OPERATING CONDITIONS, PROPERTIES, AND DESIGN EQUATIONS FOR HARDWARE DESIGN

#### LOW-MIXTURE-RATIO GASES TO INJECTOR

$$\begin{aligned} \text{MR} &= 1.0 \\ C_p &= 1.8 \text{ Btu/lbm-F} \\ \dot{w}_g &= 9 \text{ lbm/sec} \\ P_c &= 500 \text{ psia} \\ k &= 1.5 \times 10^{-6} \text{ Btu/in.-sec-F} \end{aligned}$$

#### PROPERTIES FOR COPPER

$$\begin{aligned} \alpha &= 0.1565 \text{ in.}^2/\text{sec} \\ \rho &= 0.323 \text{ lbm/in.}^3 \\ k &= 4.63 \times 10^{-3} \text{ Btu/in.-sec-F} \\ T_{\text{melt}} &= 1980 \text{ F} \\ T_{\text{wi}} &= 80 \text{ F (combustion zone)} \end{aligned}$$

#### NOMINAL CHAMBER CONDITIONS USED FOR THERMAL DESIGN

$$\begin{aligned} P_c &= 500 \text{ psia} \\ \text{MR} &= 5.0 \\ T_{\text{aw}} &= 5420 \text{ F} \\ h_g &= 0.0052 \text{ Btu/in.}^2\text{-sec (throat)} \\ h_g &= 0.00299 \text{ Btu/in.}^2\text{-sec (combustion zone)} \end{aligned}$$

## EQUATIONS

### Hot-Gas Film Coefficient, Bartz Simplified Equation

$$h_g = \frac{0.026}{d^{0.2}} \frac{\mu^{0.2} C_p}{Pr^{0.6}} G^{0.8} \sigma \quad (C-1)$$

where

$$\sigma = \left\{ \frac{T_{wg}}{2 T_{aw}} \left( 1 + \frac{\gamma-1}{2} M^2 \right) + 1/2 \right\}^{0.68} \left\{ 1 + \left( \frac{\gamma-1}{2} \right) M^2 \right\}^{-0.12}$$

### Heat Conduction Through the Wall

$$Q/A = \frac{k}{\Delta x} (T_{wg} - T_{wc}) \quad (C-2)$$

$$T_{wc} = T_{sat} + 20^\circ \text{ (nucleate boiling)}$$

### Coolant Bulk Temperature

$$Q/A = \frac{\dot{w}_c}{A_S} C_p \Delta T_B \quad (C-3)$$

### Transient Heat Conduction in a Slab, Combustion Zone

$$\frac{T_w - T_{aw}}{T_{wi} - T_{aw}} = \sum_{n=1}^{\sigma} \frac{e^{-\delta_n^2 (\alpha t/L^2)} 2 \sin \delta_n \cos (\delta_n X/L)}{\delta_n + \sin \delta_n \cos \delta_n} \quad (C-4)$$

where

$$\delta_n \tan \delta_n = (h_g L/k)$$

Injector Film Cooling

$$Q/A = \frac{\dot{w}_{FC}}{A} C_p (T_{wg} - T_w) \quad (C-5)$$

APPENDIX D

REPORT DISTRIBUTION LIST FOR  
CONTRACT NO. NAS3-7962

National Aeronautics and Space Administration (1)  
Lewis Research Center  
21000 Brookpark Road  
Cleveland, Ohio 44135  
Attention: Contracting Officer, MS 500-210

National Aeronautics and Space Administration (8)  
Lewis Research Center  
21000 Brookpark Road  
Cleveland, Ohio 44135  
Attention: Liquid Rocket Technology Branch, MS 500-209

National Aeronautics and Space Administration (1)  
Lewis Research Center  
21000 Brookpark Road  
Cleveland, Ohio 44135  
Attention: Technical Report Control Office, MS 5-5

National Aeronautics and Space Administration (1)  
Lewis Research Center  
21000 Brookpark Road  
Cleveland, Ohio 44135  
Attention: Technology Utilization Office, MS 3-16

National Aeronautics and Space Administration (2)  
Lewis Research Center  
21000 Brookpark Road  
Cleveland, Ohio 44135  
Attention: AFSC Liaison Office, MS 4-1

National Aeronautics and Space Administration (2)  
Lewis Research Center  
21000 Brookpark Road  
Cleveland, Ohio 44135  
Attention: Library

National Aeronautics and Space Administration (1)  
Lewis Research Center  
21000 Brookpark Road  
Cleveland, Ohio 44135  
Office of Reliability and Quality Assurance, MS 500-203

National Aeronautics and Space Administration (1)  
Lewis Research Center  
21000 Brookpark Road  
Cleveland, Ohio 44135  
Attention: R. J. Priem, MS 7-1

National Aeronautics and Space Administration (1)  
Lewis Research Center  
21000 Brookpark Road  
Cleveland, Ohio 44135  
Attention: E. W. Conrad, MS 100-1

National Aeronautics and Space Administration (1)  
Lewis Research Center  
21000 Brookpark Road  
Cleveland, Ohio 44135  
Attention: D. L. Nored, MS 500-209

National Aeronautics and Space Administration (1)  
Lewis Research Center  
21000 Brookpark Road  
Cleveland, Ohio 44135  
Attention: W. E. Roberts, MS 3-17

National Aeronautics and Space Administration (1)  
Washington, D.C. 20546  
Attention: Code MT

National Aeronautics and Space Administration (2)  
Washington, D.C. 20546  
Attention: Code RPX

National Aeronautics and Space Administration (2)  
Washington, D.C. 20546  
Attention: Code RPL

National Aeronautics and Space Administration (1)  
Washington, D.C. 20546  
Attention: Code SV

National Aeronautics and Space Administration (1)  
Washington, D.C. 20546  
Attention: R. Levine

Scientific and Technical Information Facility (6)  
P. O. Box 33  
College Park, Maryland 20740  
Attention: NASA Representative  
Code CRT

National Aeronautics and Space Administration (1)  
Ames Research Center  
Moffett Field, California 94035  
Attention: Library

National Aeronautics and Space Administration (1)  
Flight Research Center  
P. O. Box 273  
Edwards, California 93523  
Attention: Library

National Aeronautics and Space Administration (1)  
Goddard Space Flight Center  
Greenbelt, Maryland 20771  
Attention: Library

National Aeronautics and Space Administration (1)  
John F. Kennedy Space Center  
Cocoa Beach, Florida 32931  
Attention: Library

National Aeronautics and Space Administration (1)  
Langley Research Center  
Langley Station  
Hampton, Virginia 23365  
Attention: Library

National Aeronautics and Space Administration (1)  
Manned Spacecraft Center  
Houston, Texas 77001  
Attention: Library

National Aeronautics and Space Administration (1)  
George C. Marshall Space Flight Center  
Huntsville, Alabama 35812  
Attention: Library

National Aeronautics and Space Administration (1)  
George C. Marshall Space Flight Center  
Huntsville, Alabama 35812  
Attention: Keith Chandler, R-P&VE-PA

National Aeronautics and Space Administration (1)  
Western Operations Office  
150 Pico Boulevard  
Santa Monica, California 90406  
Attention: Library

Jet Propulsion Laboratory (1)  
4800 Oak Grove Drive  
Pasadena, California 91103  
Attention: Library

Office of the Director of Defense Research & Engineering (1)  
Washington, D. C. 20301  
Attention: Dr. H. W. Schulz, Office of Asst. Dir.  
(Chem. Technology)

Defense Documentation Center (1)  
Cameron Station  
Alexandria, Virginia 22314

Arnold Engineering Development Center (1)  
Air Force Systems Command  
Tullahoma, Tennessee 37389  
Attention: AE01M

Advanced Research Projects Agency (1)  
Washington, D. C. 20525  
Attention: D. E. Mock

Aeronautical Systems Division (1)  
Air Force Systems Command  
Wright-Patterson Air Force Base, Ohio  
Attention: D. L. Schmidt, Code ASRCNC-2

Air Force Rocket Propulsion Laboratory (RPR) (1)  
Edwards, California 93523

Air Force Rocket Propulsion Laboratory (RPM) (1)  
Edwards, California 93523

Air Force FTC (FTAT-2) (1)  
Edwards Air Force Base, California 93523  
Attention: Library

Air Force Office of Scientific Research (1)  
Washington, D. C. 20333  
Attention: SREP, Dr. J. F. Masi

Office of Research Analyses (OAR) (1)  
Holloman Air Force Base, New Mexico 88330  
Attention: RRRT

Office of Research Analyses (OAR) (1)  
Holloman Air Force Base, New Mexico 88330  
Attention: Maj. R. E. Brocken, Code MDGRT

U. S. Air Force (1)  
Washington, D. C.  
Attention: Col. C. K. Stambaugh, Code AFRST

Commanding Officer (1)  
U. S. Army Research Office (Durham)  
Box CM, Duke Station  
Durham, North Carolina 27706

U. S. Army Missile Command (1)  
Redstone Scientific Information Center  
Redstone Arsenal, Alabama 35808  
Attention: Chief, Document Section

Commander (1)  
U. S. Naval Missile Center  
Point Mugu, California 93041  
Attention: Technical Library

Commander (1)  
U. S. Naval Ordnance Test Station  
China Lake, California 93557  
Attention: Library

Commanding Officer (1)  
Office of Naval Research  
1030 East Green Street  
Pasadena, California 91101

Director (Code 6180) (1)  
U. S. Naval Research Laboratory  
Washington, D. C. 20390  
Attention: H. W. Carhart

Picatinny Arsenal (1)  
Dover, New Jersey  
Attention: I. Forsten, Chief  
Liquid Propulsion Laboratory

Air Force Aero Propulsion Laboratory (1)  
Research & Technology Division  
Air Force Systems Command  
United States Air Force  
Wright-Patterson AFB, Ohio 45433  
Attention: APRP (C. M. Donaldson)

Aerojet-General Corporation (1)  
P. O. Box 296  
Azusa, California 91703  
Attention: Librarian

Aerojet-General Corporation (1)  
11711 South Woodruff Avenue  
Downey, California 90241  
Attention: F. M. West, Chief Librarian

Aerojet-General Corporation (1)  
P. O. Box 1947  
Sacramento, California 95809  
Attention: Technical Library 2484-2015A

Aeronutronic Division of Philco Corp. (1)  
Ford Road  
Newport Beach, California 92600  
Attention: Technical Information Dept.

Aeroprojects, Inc. (1)  
310 East Rosedale Avenue  
West Chester, Pennsylvania 19380  
Attention: C. D. McKinney

Aerospace Corporation (1)  
P. O. Box 95085  
Los Angeles, California 90045  
Attention: Library-Documents

Arthur D. Little, Inc. (1)  
Acorn Park  
Cambridge 40, Massachusetts  
Attention: A. C. Tobey

Astropower, Inc. (1)  
Subs. of Douglas Aircraft Company  
2968 Randolph Avenue  
Costa Mesa, California  
Attention: Dr. George Moc  
Director, Research

Astrosystems, Inc. (1)  
1275 Bloomfield Avenue  
Caldwell Township, New Jersey  
Attention: A. Mendenhall

ARO, Inc. (1)  
Arnold Engineering Development Center  
Arnold AF Station, Tennessee 37389  
Attention: Dr. B. H. Goethert  
Chief Scientist

Atlantic Research Corporation (1)  
Shirley Highway & Edsall Road  
Alexandria, Virginia 22314  
Attention; Security Office for Library

Battelle Memorial Institute (1)  
505 King Avenue  
Columbus, Ohio 43201  
Attention: Report Library, Room 6A

Beech Aircraft Corporation (1)  
Boulder Facility  
Box 631  
Boulder, Colorado  
Attention: J. H. Rodgers

Bell Aerosystems, Inc. (1)  
P. O. Box 1  
Buffalo, New York 14205

Bendix Systems Division (1)  
Bendix Corporation  
Ann Arbor, Michigan  
Attention: John M. Bureger

The Boeing Company (1)  
Aerospace Division  
P. O. Box 3707  
Seattle, Washington 98124  
Attention: Library

Chemical Propulsion Information Agency (1)  
Applied Physics Laboratory  
8621 Georgia Avenue  
Silver Springs, Maryland 20910

Chrysler Corporation (1)  
Missile Division  
Warren, Michigan  
Attention: John Gates

Chrysler Corporation (1)  
Space Division  
New Orleans, Louisiana  
Attention: Librarian

Curtiss-Wright Corporation (1)  
Wright Aeronautical Division  
Woodridge, New Jersey  
Attention: G. Kelley

University of Denver (1)  
Denver Research Institute  
P. O. Box 10127  
Denver, Colorado 80210  
Attention: Security Office

Douglas Aircraft Company, Inc. (1)  
Santa Monica Division  
3000 Ocean Park Boulevard  
Santa Monica, California 90405  
Attention: Library

Fairchild Stratos Corporation (1)  
Aircraft Missiles Division  
Hagerstown, Maryland  
Attention: J. S. Kerr

General Dynamics/Astronautics (1)  
P. O. Box 1128  
San Diego, California 92112  
Attention: Library & Info. Services (128-00)

Convair Division (1)  
General Dynamics Corporation  
P. O. Box 1128  
San Diego, California 92112  
Attention: Mr. W. Fenning  
Centaur Resident Project Office

General Electric Company (1)  
Flight Propulsion Lab. Department  
Cincinnati 15, Ohio  
Attention: D. Suichu

Grumman Aircraft Engineering Corporation (1)  
Bethpage, Long Island, New York  
Attention: Joseph Gavin

IIT Research Institute (1)  
Technology Center  
Chicago, Illinois 60616  
Attention: C. K. Hersch, Chemistry Division

Kidde-Aerospace Division (1)  
Walter Kidde & Company, Inc.  
675 Main Street  
Belleville 9, New Jersey  
Attention: R. J. Hanville,  
Director of Research Engineering

Lockheed Missiles & Space Company (1)  
P. O. Box 504  
Sunnyvale, California  
Attention: Technical Information Center

Lockheed-California Company (1)  
10445 Glen Oaks Boulevard  
Pacoima, California  
Attention: G. D. Brewer

Lockheed Propulsion Company (1)  
P. O. Box 111  
Redlands, California 92374  
Attention: Miss Belle Berlad, Librarian

Lockheed Missiles & Space Company (1)  
Propulsion Engineering Division (D.55-11)  
1111 Lockheed Way  
Sunnyvale, California 94087

Marquardt Corporation (1)  
16555 Satcoy Street  
Box 2013-South Annex  
Van Nuys, California 91404  
Attention: Librarian

Martin-Marietta Corporation (1)  
Martin Division  
Baltimore 3, Maryland  
Attention: John Calathes (3214)

McDonnell Aircraft Corporation (1)  
P. O. Box 6101  
Lambert Field, Missouri  
Attention: R. A. Herzmark

North American Rockwell Corporation (1)  
Space & Information Systems Division  
12214 Lakewood Boulevard  
Downey, California 90242  
Attention: Technical Information Center  
D/096-722 (AJ01)

Northrop Space Laboratories (1)  
1001 East Broadway  
Hawthorne, California  
Attention: Dr. William Howard

Purdue University (1)  
Lafayette, Indiana 47097  
Attention: Technical Librarian

Republic Aviation Corporation (1)  
Farmingdale, Long Island, New York  
Attention: Dr. William O'Donnell

Rocket Research Corporation (1)  
520 South Portland Street  
Seattle, Washington 98108

Rocketdyne Division (1)  
North American Rockwell Corporation  
6633 Canoga Avenue  
Canoga Park, California 91304  
Attention: Library, Dept. 596-306

Rohm and Haas Company (1)  
Redstone Arsenal Research Division  
Huntsville, Alabama 35808  
Attention: Librarian

Space-General Corporation (1)  
777 Flower Street  
Glendale, California  
Attention: C. E. Roth

Stanford Research Institute (1)  
333 Ravenswood Avenue  
Menlo Park, California 94025  
Attention: Thor Smith

Texaco Experiment, Inc. (1)  
P. O. Box 1-T  
Richmond, Virginia 23202  
Attention: Librarian

Thiokol Chemical Corporation (1)  
Alpha Division, Huntsville, Plant  
Huntsville, Alabama 35800  
Attention: Technical Director

Thiokol Chemical Corporation (1)  
Reaction Motors Division  
Denville, New Jersey 07834  
Attention: Librarian

Thiokol Chemical Corporation (1)  
Redstone Division  
Huntsville, Alabama  
Attention: John Goodloe

TRW Systems, Inc. (1)  
1 Space Park  
Redondo Beach, California 90200  
Attention: STL Tech. Lib. Doc. Acquisitions

TRW Systems, Inc. (1)  
1 Space Park  
Redondo Beach, California 90200  
Attention: H. Burge

United Aircraft Corporation (1)  
Corporation Library  
400 Main Street  
East Hartford, Connecticut 06118  
Attention: Library

United Aircraft Corporation (1)  
Pratt & Whitney Division  
Florida Research & Development Center  
P. O. Box 2691  
West Palm Beach, Florida 33402  
Attention: Library

United Aircraft Corporation (1)  
United Technology Center  
P. O. Box 358  
Sunnyvale, California 94088  
Attention: Librarian

Vought Astronautics (1)  
P. O. Box 5907  
Dallas 22, Texas  
Attention: Warren C. Trent

UNCLASSIFIED

Security Classification

## DOCUMENT CONTROL DATA - R &amp; D

2. (Security classification of title, body of abstract and indexing annotation must be entered when the overall report is classified)		
1. ORIGINATING ACTIVITY (Corporate author) Rocketdyne, a Division of North American Rockwell Corporation, 6633 Canoga Avenue, Canoga Park, California 91304		2a. REPORT SECURITY CLASSIFICATION UNCLASSIFIED
3. REPORT TITLE  TWO-STAGE BIPROPELLANT INJECTION SYSTEM STUDIES		2b. GROUP
4. DESCRIPTIVE NOTES (Type of report and inclusive dates)		
5. AUTHOR(S) (First name, middle initial, last name)  Paul F. Mehegan		
6. REPORT DATE 19 April 1968	7a. TOTAL NO. OF PAGES 258	7b. NO. OF REFS 17
8a. CONTRACT OR GRANT NO. NAS3-7962	9a. ORIGINATOR'S REPORT NUMBER(S) R-7199	
b. PROJECT NO.	9b. OTHER REPORT NO(S) (Any other numbers that may be assigned this report) NASA CR-72303	
c.		
d.		
10. DISTRIBUTION STATEMENT		
11. SUPPLEMENTARY NOTES		12. SPONSORING MILITARY ACTIVITY
13. ABSTRACT  The Two-Stage Bipropellant Injection System Program was initiated to investigate hot-gas injection in combination with large-thrust-per-element injector concepts. Analyses and cold-flow experiments were used to guide the selection of injector concepts to be evaluated during hot-firing tests. Twenty hot-firing tests were conducted to evaluate the performance and stability of four different injectors. The test results proved feasibility of the principle and also demonstrated that stable operation and high combustion efficiencies of at least 97.5 percent were possible with a single-element 20,000-pound-thrust injector.		

14.	KEY WORDS	LINK A		LINK B		LINK C	
		ROLE	WT	ROLE	WT	ROLE	WT
	Tricentric Injector						
	Impinging Jet Injector						
	Coaxial Impinging Recessed-Cap Injector						
	Commercial Nozzle Injector						
	Two-Stage Injection						
	Performance Analysis						
	Stability						
	Design Feasibility						
	Design Analysis						
	Cold-Flow Studies						
	Hot-Fire Testing						
	Test Hardware						
	Heat Transfer						
	Atomization Analyses						
	Thermal Design						